AD_____

Award Number: W81XWH-08-1-0178

TITLE: Understanding and targeting cell growth networks in breast cancer

PRINCIPAL INVESTIGATOR: Jason D. Weber, Ph.D.

CONTRACTING ORGANIZATION:
Washington University School of Medicine
St. Louis, MO 63110

REPORT DATE: April 2013

TYPE OF REPORT: Final

PREPARED FOR: U.S. Army Medical Research and Materiel Command
Fort Detrick, Maryland 21702-5012

DISTRIBUTION STATEMENT: Approved for Public Release;
Distribution Unlimited

The views, opinions and/or findings contained in this report are those of the author(s) and should not be construed as an official Department of the Army position, policy or decision unless so designated by other documentation.

REPORT DOCUMENTATION PAGE

Form Approved
OMB No. 0704-0188

Public reporting burden for this collection of information is estimated to average 1 hour per response, including the time for reviewing instructions, searching existing data sources, gathering and maintaining the data needed, and completing and reviewing this collection of information. Send comments regarding this burden estimate or any other aspect of this collection of information, including suggestions for reducing this burden to Department of Defense, Washington Headquarters Services, Directorate for Information Operations and Reports (0704-0188), 1215 Jefferson Davis Highway, Suite 1204, Arlington, VA 22202-4302. Respondents should be aware that notwithstanding any other provision of law, no person shall be subject to any penalty for failing to comply with a collection of information if it does not display a currently valid OMB control number. **PLEASE DO NOT RETURN YOUR FORM TO THE ABOVE ADDRESS.**

1. REPORT DATE	2. REPORT TYPE	3. DATES COVERED
April 2013	Final	17 March 2008- 16 March 2013

4. TITLE AND SUBTITLE

Understanding and targeting cell growth networks in breast cancer

5a. CONTRACT NUMBER
W81XWH-08-1-0178

5b. GRANT NUMBER
W81XWH-08-1-0178

5c. PROGRAM ELEMENT NUMBER

6. AUTHOR(S)
Jason D. Weber

E-Mail: jweber@dom.wustl.edu

5d. PROJECT NUMBER

5e. TASK NUMBER

5f. WORK UNIT NUMBER

7. PERFORMING ORGANIZATION NAME(S) AND ADDRESS(ES)
Washington University School of Medicine

St. Louis, MO 63110 USA

8. PERFORMING ORGANIZATION REPORT NUMBER

9. SPONSORING / MONITORING AGENCY NAME(S) AND ADDRESS(ES)
U.S. Army Medical Research and Materiel Command
Fort Detrick, Maryland 21702-5012

10. SPONSOR/MONITOR'S ACRONYM(S)

11. SPONSOR/MONITOR'S REPORT NUMBER(S)

12. DISTRIBUTION / AVAILABILITY STATEMENT
Approved for Public Release; Distribution Unlimited

13. SUPPLEMENTARY NOTES

14. ABSTRACT

In this final report, we describe all of the results from the five-year grant. Cancers result from an inability of a cell to control its own growth. Normally, a cell interprets external and internal signals to create a balanced growth schedule. The main interpreters of these signals within a cell are called ARF and p53, and it falls on the shoulders of these two proteins to maintain normal cell growth. In this sense, both ARF and p53 are tumor suppressors that constantly monitor the growth state of the cell. We report that loss of ARF results in tremendous gains in protein synthesis and growth. This phenotype is caused by deregulation of DDX5 and DHX33 RNA helicases. While neither DDX5 nor DHX33 are transforming oncogenes, both are required for RasV12 oncogenic transformation of cells. We also have show that ARF itself is regulated at the level of translation by the mTOR pathway. A common mechanism of translation regulation occurs through the recruitment or loss of RNA biding proteins to specific messages. Two ARF-regulated mRNAs are Drosha and NPM. Both involve proteins bound to and repressing the 3'-UTRs. Loss of ARF relieves this repression and translation of each mRNA ensues. In this manner, selective mRNA translation can be viewed as a necessary process during transformation and that the resulting proteins, while not individually oncogenic, provide activities that are required for the oncogenic phenotype. Thus, these translation pathways could be viewed as targetable moieties in the treatment of breast cancer.

15. SUBJECT TERMS
Cell growth, breast cancer cells, p68DDX5, ribosomes

16. SECURITY CLASSIFICATION OF:			17. LIMITATION OF ABSTRACT	18. NUMBER OF PAGES	19a. NAME OF RESPONSIBLE PERSON
a. REPORT	b. ABSTRACT	c. THIS PAGE			USAMRMC
U	U	U	UU	112	19b. TELEPHONE NUMBER *(include area code)*

Table of Contents

Page

INTRODUCTION

Cancers result from an inability of a cell to control its own growth. Normally, a cell interprets external and internal signals to create a balanced growth schedule. The main interpreters of these signals within a cell are called ARF and p53, and it falls on the shoulders of these two proteins to maintain normal cell growth (1, 2). In this sense, both ARF and p53 are tumor suppressors that constantly monitor the growth state of the cell. In mouse and human cancers, loss of the ARF tumor suppressor is second only to mutation of p53, providing critical evidence of ARF's role in both monitoring and preventing the outbreak of cancer cells. A common target of ARF is the NPM/B23 oncogene, an abundant protein of the nucleolus (3, 4). NPM normally responds to growth factors and, due to its nucleolar localization, is thought to transmit these growth signals to the maturing ribosome machinery (5, 6). Cells lacking *Arf* exhibit tremendous gains in ribosome production and subsequent protein synthesis (7). Moreover, the entirety of this growth phenotype is dependent on NPM and p68DDX5 expression in the nucleolus, with loss of either capable of completely reversing the phenotype back to normal (8). This exciting new finding indicates that ARF is a master regulator of cell growth through its tight control of NPM- or DDX5-directed ribosome production and export. Importantly, we have found NPM overexpressed in nearly 50% of breast carcinomas that we have analyzed, implying that dysregulation of NPM may be a key event in promoting breast cancer development. In effect, tumor cells that require increased protein synthesis might accumulate more NPM or DDX5 in an attempt to increase ribosome output. It is our goal to determine whether NPM directly regulates ribosome maturation to promote breast cancer formation and to establish the importance of ARF in deterring this effect. We propose to now determine the complex roles of ARF, DDX5, and NPM in the nucleolus of breast epithelial cells and how they impact both ribosome biogenesis and cell growth to prevent and/or promote tumorigenesis.

This work has tremendous clinical implications as *Arf* (9p21) and *p68Ddx5* (17q24) reside on loci that are either deleted or amplified in ER+ resistant breast tumors, respectively. This fact makes our basic science on this interesting growth network directly applicable to the breast cancer phenotype/genotype.

BODY

Task 1. Determine the role of ARF in suppressing breast tumor formation (Months 1-30):

a. Establish cultures of mouse mammary epithelial cells (MEC) from wild type and *Arf*-null female virgin mice (Months 1-6). 50 mice per year.
b. Measure ribosome DNA transcription and rRNA processing in *Arf*-/- MEC (Months 6-18).
c. Measure rRNA export and functional polysome content (Months 12-20).
d. Generate and validate polysome microarray profiles for wild type and *Arf*-null MECs (Months 10-30).
e. Determine the influence of ARF on DROSHA-mediated RNA translation (Months 11-16).
f. Identify the signaling pathway(s) responsible for enhanced ARF mRNA translation (Months 12-24)
g. Determine the mechanism for ARF translation (Months 12-30).

We have successfully completed this entire Task. We now have a list of mRNAs that are preferentially loaded or unloaded on polysomes in the presence or absence of ARF. We know that this process is largely controlled by mTOR and that ARF itself is regulated at the level of translation.

We now have immortal *Arf*-/- MMECs that retain a diploid and genomically stable genotype (Task 1a). They are still sensitive to DNA damage pathway activation events such as UV and gamma irradiation. Using these cells, we have now begun our studies of ribosome biogenesis pathway activation in the absence of *Arf*. We have discovered that MMECs lacking *Arf* exhibit extremely high levels of 47S transcription (**Figure 1**, top band). Additionally, *Arf*-null MMECs process rRNA at a considerably higher rate than wild-type counterparts, indicating that rRNA processing rates are elevated in the absence of *Arf* (Figure 1) (Task 1b).

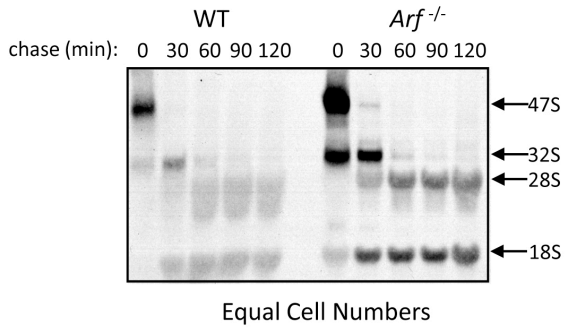

Figure 1. Ribosome DNA transcription and rRNA processing are enhanced in the absence of *Arf*. Primary MMECs harvested from wild-type (WT) and *Arf*-/- littermates were cultured in the presence of [^{3}H-methyl]-methionine for 30 minutes to allow for the labeling of the 47S rRNA transcript. Cells were then washed and cultured in label-free media for the indicated times to chase the label into processed rRNAs as indicated (Task 1b).

For Task 1c & d, this included the challenging job of generating polysome arrays derived from wild-type and *Arf*-deficient cells. In this endeavor, we have been extremely successful. We isolated 2 μg of polysome-associated mRNA from fractions harvested by gradient centrifugation and constant UV monitoring (**Figure 2**). Using this standard technique, it is clear that cells lacking *Arf* contain greater numbers of polysomes actively translating mRNAs (**Figure 2**, compare red and blue lines at the far right end of the sucrose gradient).

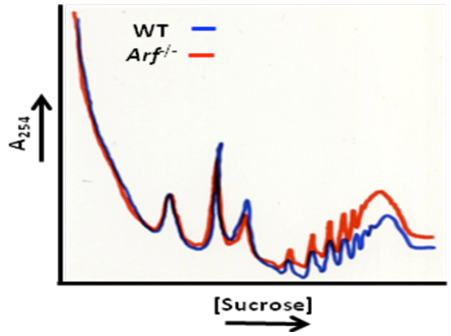

Figure 2. Equal numbers of wild-type (WT) and *Arf*-/- MMECs ($3x10^6$) were isolated and incubated with 50 μg/ml cycloheximide to freeze ribosomes on mRNA. Cells were lysed and separated on continuous sucrose gradients by ultracentrifugation. Fractions were isolated using ISCO constant UV monitoring and plotted as absorbance (254 nm) versus gradient position. The peaks from left to right are 40S, 60S, 80S and polysomes. (Task 1d)

We next isolated mRNA from sucrose gradient fractions taken at 2 ml intervals. Thus, each fraction contained approximately 2 μg of total RNA (mRNA + rRNA). Isolated mRNA was amplified and labeled for microarray analysis. We utilized the mouse 20k gene array from Illumina. We also performed this analysis on identical samples of total mRNA. This allowed us to functionally analyze both the transcriptome (total mRNA) and translatome (polysome mRNA) from wild-type and *Arf*-/- cells. As

shown in **Figure 3**, WT and *Arf*-/- total and polysomes did not cluster together (Task 1d). Rather, replicates from each sample clustered nicely which allowed us to perform broad statistical analyses on each sample.

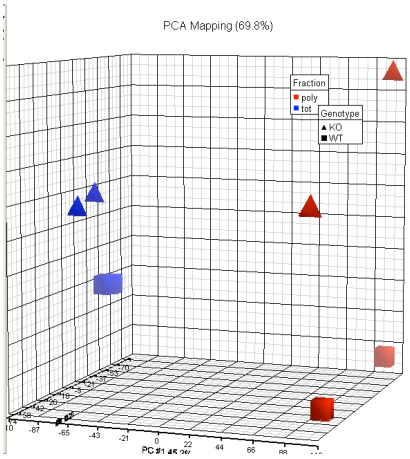

Figure 3. mRNA isolated from polysomes of wild-type (WT) and *Arf*-/- MMECs ($3x10^6$) was hybridized to Illumina bead chips containing mouse mRNA probes spanning over 20,000 genes. Total RNA was also isolated to compare transcriptome to translatome. WT mRNA is depicted as squares and *Arf*-/- as triangles. Total RNA is in blue and polysome RNA is in red. (Task 1d)

One hypothesis that could explain the differences in translation we observed in the absence of *Arf* could be a dysregulation of microRNA biogenesis. To assess this possibility, we first investigated the expression levels of Drosha, a key component of primary microRNA processing in the nucleoplasm. Wild-type and *Arf*-/- MEFs were passaged every three days and harvested for western blot analysis using antibodies recognizing mouse Drosha. We found that indeed Drosha protein expression increased in the absence of *Arf* (**Figure 4**) (Task 1e).

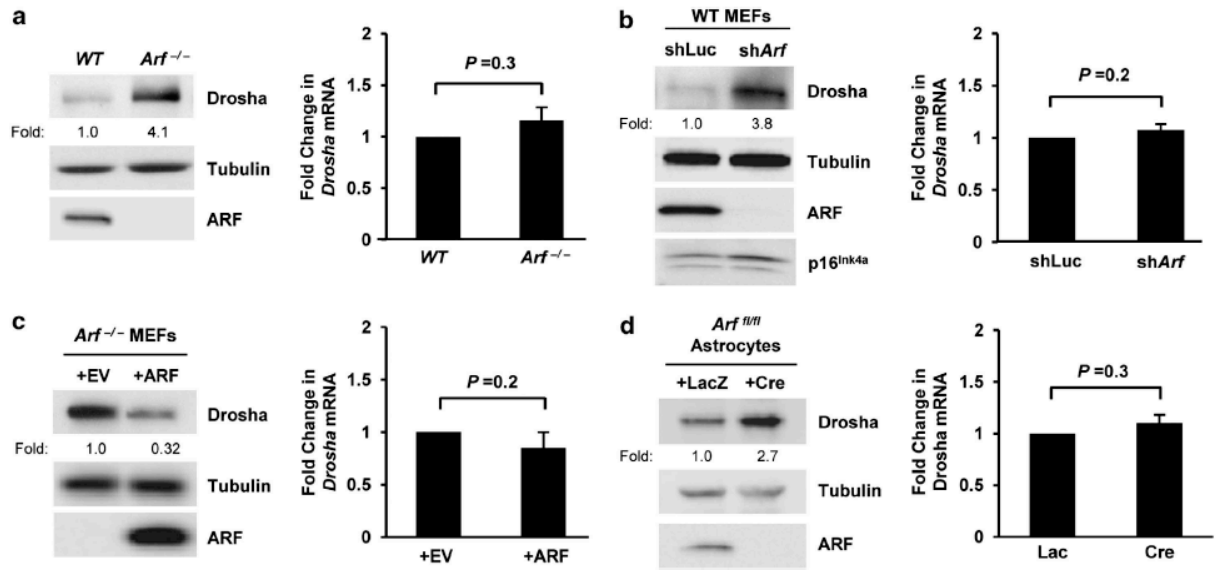

Figure 4. ***Arf*** **negatively regulates Drosha protein expression in a transcriptionally independent manner.** (a-d, left column) Cells of the indicated genotype were lysed, and separated proteins were immunoblotted for the indicated proteins. *Arf* $^{flox/flox}$ astrocytes were infected with adenoviruses encoding β-galactosidase (LacZ) or Cre recombinase and were harvested at 5 days post-infection for gene expression analysis. Drosha expression fold change relative to WT or control infected cells is indicated. (a-d, right column) Quantitative RT-PCR analysis was performed. Drosha mRNA levels were normalized to *Gadph* mRNA levels. Fold change was calculated using the $\Delta\Delta C_T$ method. Data are the mean ± SEM (N=3).

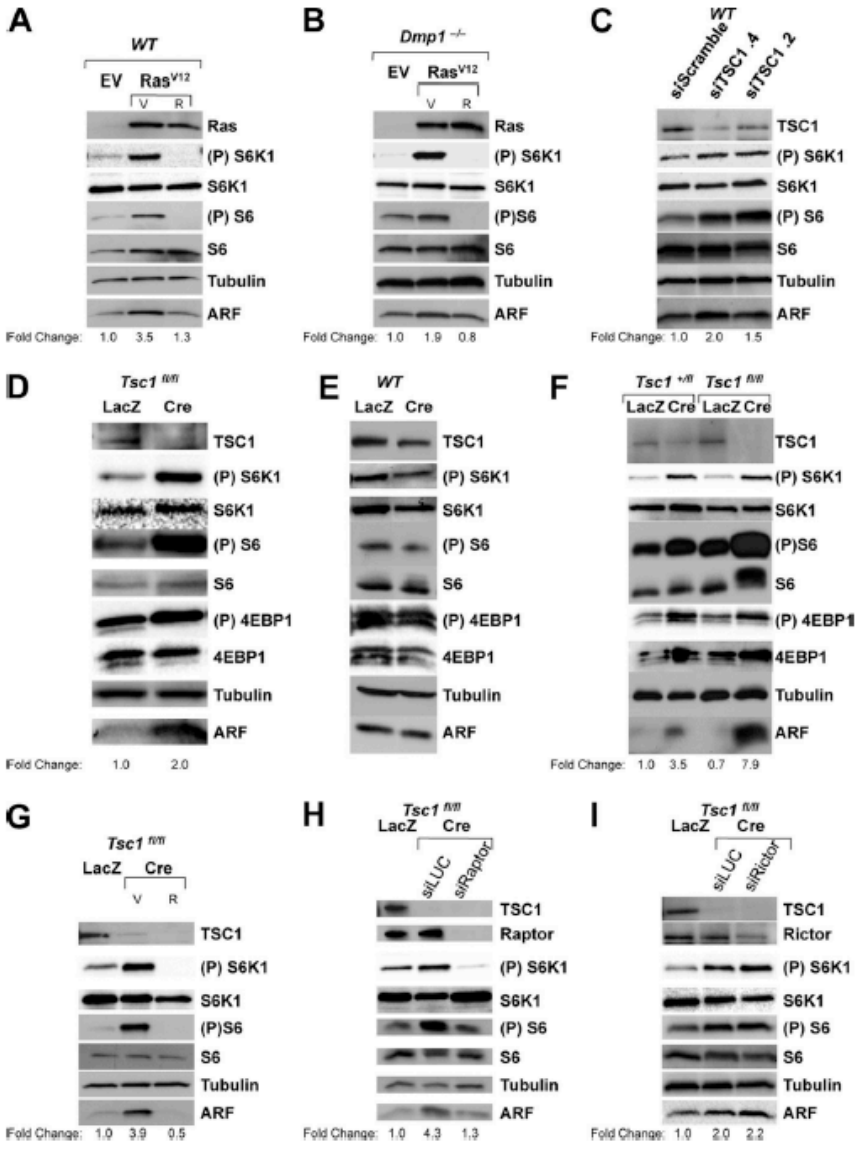

Figure 5. Ras/PI3K/TSC/mTORC1 pathway can regulate ARF. For all panels, infected cells were lysed, and separated proteins were immunobloted for indicated proteins. Expression fold change over EV or LacZ control is indicated. (A) Wild type (WT) MEFs were infected with retroviruses encoding empty vector or Ras^{V12} and were harvested at five days post infection. Cells were treated with LY294002 or vehicle for 24 hours prior to harvesting. (B) WT or *Dmp1*$^{-/-}$ MEFs were infected with retroviruses encoding empty vector or Ras^{V12} and were harvested at five days post infection. Ras^{V12} infected cells were treated with rapamycin or vehicle for 24 hours prior to harvesting. (C) Wild type MEFs were infected with lentiviruses encoding short hairpins against *Tsc1* or siScrambled control and were harvested at seven days post infection. (D-E) *Tsc1*$^{flox/flox}$ or WT MEFs were infected with adenoviruses encoding β-galactosidase (LacZ) or Cre recombinase and were harvested at nine days post infection. (F) *Tsc1*$^{+/flox}$ or *Tsc1*$^{flox/flox}$ MEFs were infected with adenoviruses encoding β-galactosidase (LacZ) or Cre recombinase and were harvested at nine days post infection. (G) *Tsc1*$^{flox/flox}$ MEFs were infected with adenoviruses encoding β-galactosidase (LacZ) or Cre recombinase and harvested at nine days post infection. Cre infected cells were treated with rapamycin or vehicle control for 24 hours prior to harvesting. (H-I) *Tsc1*$^{flox/flox}$ MEFs were infected with adenoviruses encoding β-galactosidase (LacZ) or Cre recombinase. Cre infected cells were then transduced with short hairpins recognizing *Raptor* (H) or *Rictor* (I) or siLUC control at five days post infection, and then harvested at nine days post infection for western blot analysis.

We hypothesized that the phosphatidylinositol-3-kinase/mammalian target of rapamycin (PI3K/mTOR) signal transduction pathway could potentially regulate ARF expression. To begin evaluating this pathway, wild-type MEFs were transduced with Ras^{V12} and then treated with LY294002, a pharmacological inhibitor of PI3K, for 24 hours prior to harvesting. Decreased levels of phospho-S6 (Ser 240/244) demonstrated that downstream mTOR signaling was abrogated following LY294002 treatment (Fig 5A). Ras^{V12} robustly induced ARF protein levels, and this induction was abrogated with LY294002 treatment (Fig. 5A). Furthermore, wild-type and *Dmp1*$^{-/-}$ MEFs were transduced with Ras^{V12} and subsequently treated with rapamycin, the pharmacological inhibitor of mTOR, for 24 hours prior to harvesting. Repressed levels of phospho-S6 (Ser 240/244) revealed that mTOR signaling was disrupted from rapamycin exposure (Fig. 5B). Tuberous sclerosis complex 1 (TSC1) is an upstream member of the mTOR pathway. We hypothesized that activation of the mTOR pathway by acute knockdown of TSC1 would induce ARF protein levels. To test this, wild-type MEFs were infected with lentiviruses encoding siRNAs recognizing *Tsc1*. Two hairpins were used to reduce TSC1 expression (Fig. 5C). ARF protein levels were up-regulated from transient knockdown of TSC1 in a dose dependent manner (Fig. 5C). Also, *Tsc1*$^{flox/flox}$ MEFs were infected with adenoviruses encoding Cre recombinase or a β-galactosidase (LacZ) control. Enhanced levels of phospho-S6 (Ser 240/244) demonstrated that hyper-activation of mTOR signaling occurred from loss of *Tsc1* (Fig. 5D). Genetic ablation of *Tsc1* also caused an increase in ARF protein levels (Fig. 5D), corroborating the results observed from using RNAi against *Tsc1.* Moreover, we infected wild-type MEFs with LacZ or Cre to ensure that this finding was not a nonspecific off-target effect of Cre recombinase or adenoviral infection protocol (Fig. 5E). Additionally, *Tsc1*$^{+/flox}$ and *Tsc1*$^{flox/flox}$ were infected with Cre or LacZ to evaluate a dose dependent loss of *Tsc1* on ARF protein levels (Fig. 5F). Loss of one copy of *Tsc1* was sufficient to induce ARF protein expression, while loss of both copies of *Tsc1* induced ARF protein expression to a greater extent (Fig. 5F). To investigate whether the ARF induction observed from the loss of *Tsc1* is dependent on TSC/mTOR signaling, we infected *Tsc1*$^{flox/flox}$ MEFs with Cre or LacZ control and then treated with rapamycin for 24 hours prior to harvesting. Diminished levels of phospho-S6 (Ser 240/244) demonstrated that rapamycin successfully blocked mTOR signaling (Fig. 5G). As seen before with Ras^{V12} infection (Fig. 5B), ARF protein levels induced from the loss of *Tsc1* were sensitive to rapamycin treatment (Fig. 5G). mTORC1 contains Raptor, LST8, Deptor, PRAS40, and mTOR, and is critical for regulating protein synthesis. RNA interference was used to acutely knockdown *Raptor* or *Rictor* in order to respectively assess the contributions of mTORC1 or mTORC2 following *Tsc1* deletion (Fig. 5H and Fig. 5I). Acute knockdown of *Raptor*, but not *Rictor*, abrogated the induction of ARF expression from the ablation of *Tsc1* (Fig. 5H and Fig. 5I). This suggests that mTORC1, but not mTORC2, is necessary for mediating mTOR induction of ARF (Task 1f).

To further test the hypothesis that translational regulation could be the molecular mechanism responsible for eliciting ARF's induction from mTOR hyperactivation, we assessed the association of *Arf* mRNA with actively translating polyribosomes. To accomplish this task, cytosolic ribosomes were isolated by sucrose gradient centrifugation from equal numbers of *Dmp1*$^{-/-}$ MEFs infected with either Ras^{V12} or an empty vector control (Fig. 6A). Ribosomal RNAs were detected by continuous UV monitoring of cytosolic rRNAs' absorbance [A_{254nm}] (Fig 6B). To assess the distribution of *Arf* mRNA transcripts in individual fractions comprising isolated monosomes, disomes, or polysomes, total RNA was isolated from each sucrose gradient fraction and *Arf* mRNA levels were determined with qRT-PCR. Strikingly, *Arf* mRNA transcripts associated with different polyribosome fractions in Ras^{V12}-infected and empty vector-infected *Dmp1*-null cells (Fig 6C). In Ras^{V12}-infected *Dmp1*$^{-/-}$ MEFs, *Arf* mRNA was pooled to a heavier polyribosome fraction, indicating that there is a greater extent of *Arf* mRNAs being actively translated by multiple ribosomes (more ribosomes associated per mRNA) in these cells (Fig. 6C). These

data support the hypothesis that ARF is translationally regulated in the presence of oncogenic Ras^{V12} signals (Task 1g).

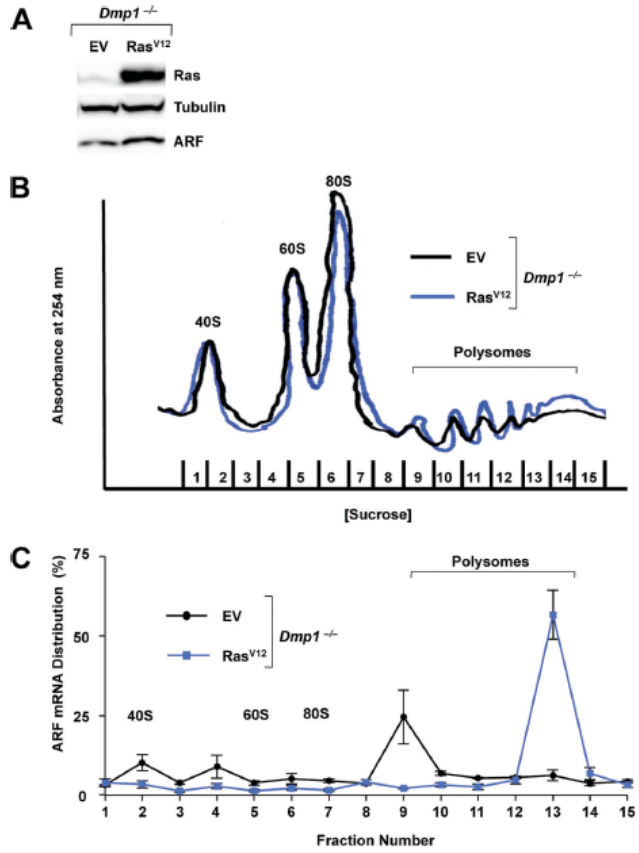

Figure 6: ARF mRNA associatation with actively translating polyribosomes increases with hyper-growth stimuli. *Dmp1*$^{-/-}$ MEFs were transduced with retroviruses encoding empty vector or Ras^{V12} and were harvested at five days post infection (A). Cytosolic extracts from equal number of cells ($3x10^6$) treated for 5 minutes with cycloheximide (10 µg/mL) were separated on 7 – 47% sucrose gradients with constant UV monitoring. (B) The representative graph depicts the A_{254} absorbance of ribosome subunits over increasing sucrose density. (C) Total RNA was isolated from each sucrose gradient fraction. Monosome, disome, and polysome associated *Arf* mRNA were measured with qRT-PCR and were calculated as percentage of total *Arf* mRNA collected in all fractions. Data are the mean +/– S.E.M. of three independent experiments, and *P* values are calculated using Student *t*-test.

Miceli A.P., Saporita A.J., and **Weber J.D.** (2012). Hyper-growth mTORC1 signals translationally activate the ARF tumor suppressor checkpoint. *Molecular and Cellular Biology*, 32: 348-64.

Kuchenreuther M.J. and **Weber J.D.** (2013). The ARF tumor suppressor controls Drosha translation to prevent Ras-driven transformation. Oncogene, in press.

Task 2. Examine the mechanism behind NPM's ability to promote ribosome biogenesis and cell growth in breast epithelial cells (Months 1-36):

a. Determine the influence of NPM on ribosome biogenesis (Months 1-20). 50 mice per year.
b. Establish the role of nucleophosmin (NPM) in cell growth of *Arf*-/- MEC (Months 10-30). 50 mice per year.
c. Validate the responsiveness of a novel 5'-3'NPM-TOP luciferase reporter construct to *in vitro* mTOR signals (Months 12-36).
d. Identify the proteins that bind to the 5' and 3'-UTR of NPM mRNA to regulate its translation (Months 10-36).

We have successfully completed this entire Task. We have determined the critical role of NPM in regulating ribosome biogenesis and nuclear export (Task 2a & b). This activity is required for efficient

mRNA translation and continued cell growth. Moreover, we have identified FBP1 as a significant repressor of NPM translation. NPM was identified in our previous task as an mRNA whose translation was regulated in the absence of ARF or in the presence of hyperactive mTOR signals.

We sought to evaluate whether the NPM 5' and 3' UTRs were sufficient to modulate translation of another ORF in a manner equivalent to translational regulation of the NPM ORF. Specifically, we wanted to determine whether fusion of the NPM 5' and 3' UTRs to a firefly *luciferase* (F*luc*) ORF rendered Fluc expression sensitive to rapamycin. To test this, *Tsc1*$^{-/-}$*p53*$^{-/-}$ MEFs were transduced with plasmids encoding NPM 5' and 3' UTR-flanked F*luc*. Although NPM 5'-luc-NPM 3' protein activity increased over the duration of serum stimulation, this induction was greatly attenuated in the presence of rapamycin compared to vehicle (Fig. 7*A*). These data indicate that NPM 5'-luc-NPM 3' activity is driven by changes in translation rather than transcription. To examine whether the rapamycin-induced reduction of NPM 5'-luc-NPM 3' activity was specific for an mTOR-regulated mRNA, *Tsc1*$^{-/-}$*p53*$^{-/-}$ MEFs were transduced with plasmids encoding GAPDH 5' and 3' UTR-flanked F*luc*. Notably, rapamycin failed to affect GAPDH 5'-luc-GAPDH 3' activity at any time point evaluated (Fig. 7*B*).

To examine the independent roles of each NPM UTR as potential targets of regulation, we generated chimeric reporters by fusing the NPM 5' UTR and the GAPDH 3' UTR or the GAPDH 5' UTR and the NPM 3' UTR to the respective ends of the F*luc* ORF. Surprisingly, NPM 5'-luc-GAPDH 3' activity resembled GAPDH 5'-luc-GAPDH 3' activity, with rapamycin having no effect at any time point measured (Fig. 7*C*). GAPDH 5'-luc-NPM 3' activity, however, demonstrated rapamycin sensitivity similar to that observed with NPM 5'-luc-NPM 3' activity (Fig. 7*D*). –sensitive (Task 2c)

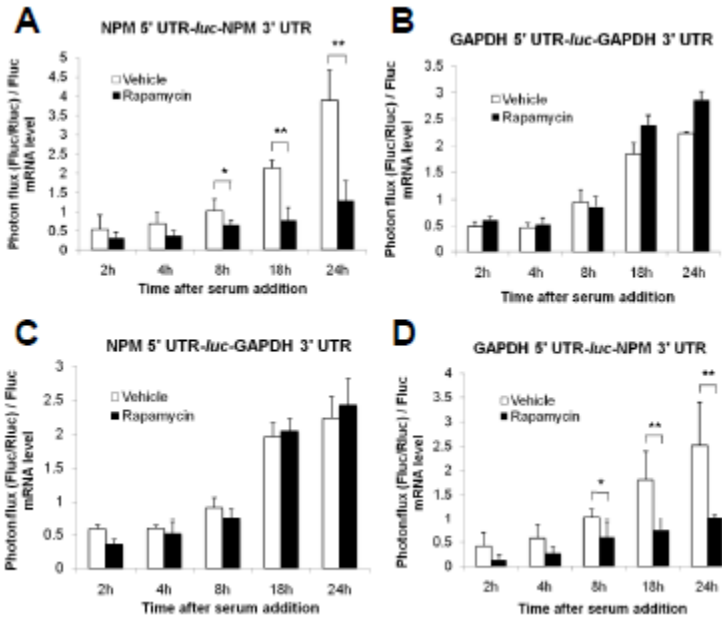

Figure 7. (*A-D*) *Tsc1*$^{-/-}$*p53*$^{-/-}$ MEFs were transfected with plasmids depicted in S2*B*. Cells were serum starved and then incubated with 10% serum in the presence or absence of rapamycin for the indicated durations. Plasmid expressing CMV-driven *Renilla* luciferase (Rluc) was used as an internal control for transfection efficiency. Photon flux was calculated by normalizing firefly *luciferase* (Fluc) activity to Rluc activity. Levels of Fluc mRNA at each time point were measured by qRT-PCR from total RNA isolated from transfected MEFs. Shown is photon flux normalized to Fluc mRNA levels. Data are mean ± s.d. of quadruplicate samples per condition from three independent experiments (* $P < 0.05$, ** $P < 0.005$, Student's *t*-test). (*A*) Rapamycin reduces NPM 5' UTR-Fluc-NPM 3' UTR activity. (*B*) Activity of GAPDH 5' UTR-Fluc-GAPDH 3' UTR is unchanged upon treatment with rapamycin. (*C*) Rapamycin has no effect on NPM 5' UTR-Fluc-GAPDH 3' UTR activity. (*D*) Activity of GAPDH 5' UTR-Fluc-NPM 3' UTR is abrogated upon rapamycin treatment. (Task 2c)

We undertook an unbiased approach to screen for putative regulatory binding proteins of the NPM 5' and 3' UTRs. We utilized an RNA pull-down assay coupled to mass spectrometry to identify proteins that bind the NPM 5' or 3' UTR. Whole cell lysates prepared from *Tsc1*$^{-/-}$*p53*$^{-/-}$ MEFs treated with vehicle or rapamycin were incubated with biotinylated NPM 5' UTR or 3' UTR RNA. Several proteins were found to preferentially interact with the NPM 3' UTR, but none appeared to bind exclusively to the NPM 5' UTR, consistent with reporter assay findings (Fig. 8, arrows) (Task 2d).

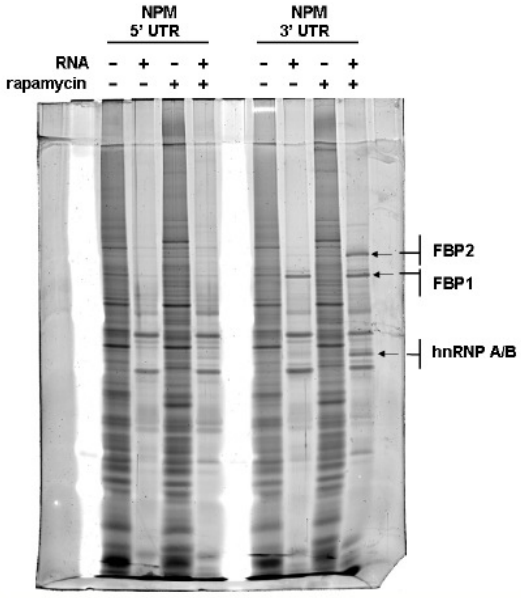

Figure 8. Identification of NPM 3' UTR binding proteins. Lanes indicated as RNA (–) represent samples pre-cleared with streptavidin sepharose. Arrows indicate proteins selected as putative regulatory binding proteins of the NPM 3' UTR, and identified proteins are shown. (Task 2d)

We next employed mass spectrometry to identify putative NPM 3' UTR binding proteins and confirmed their identities as FBP1, FBP2 (also known as KHSRP or KSRP), and heterogeneous nuclear ribonucleoprotein (hnRNP) A/B. To evaluate FBP binding specificity, we incubated biotinylated GAPDH 5' UTR, GAPDH 3' UTR, NPM 5' UTR, or NPM 3' UTR RNA with whole cell lysates from *Tsc1*$^{-/-}$*p53*$^{-/-}$ MEFs treated with vehicle or rapamycin. Consistent with analyses from mass spectrometry, however, FBP3 was undetectable. FBP1 was precipitated exclusively by the NPM 3' UTR (Fig. 9A). FBP2 was precipitated predominantly by the NPM 3' UTR, but also by the GAPDH 3' UTR and the NPM 5' UTR in vehicle-treated cells (Fig. 9A). FBP1 was immunoprecipitated from whole cell extracts prepared from *Tsc1*$^{-/-}$*p53*$^{-/-}$ MEFs treated with vehicle or rapamycin (Fig. 9B, top). Total RNA was isolated from FBP1 immunoprecipitates, and bound NPM mRNA was measured by qRT-PCR. Significantly higher numbers of NPM transcripts were associated with FBP1 in rapamycin-treated cells versus vehicle-treated cells (Fig. 9B, bottom). Moreover, FBP1 protein expression dramatically increased upon rapamycin treatment (Fig. 9C), suggesting that the enhanced number of NPM transcripts bound by FBP1 in the presence of rapamycin was a result of elevated FBP1 expression.

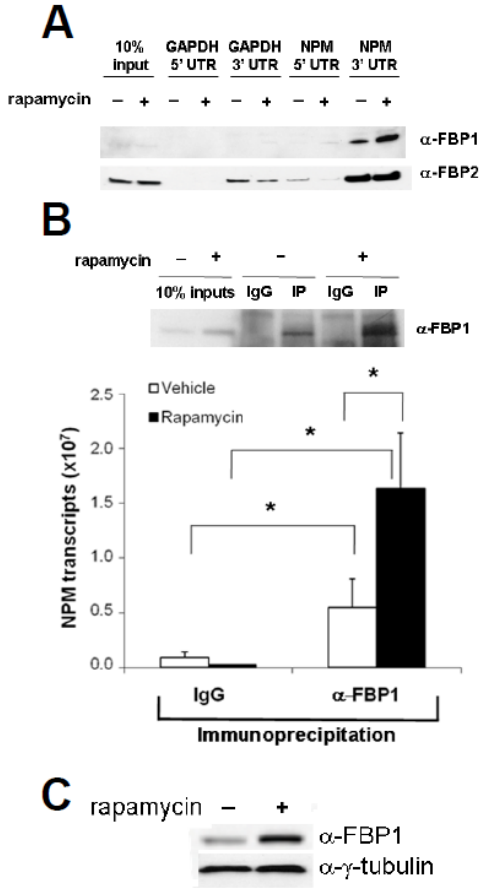

Figure 9. (*A*) FBP1 specifically interacts with the NPM 3' UTR. (*B*) Endogenous NPM mRNAs preferentially bind FBP1 in rapamycin-treated cells. FBP1 was immunoprecipitated (IP) from vehicle-treated (–) or rapamycin-treated (+) *Tsc1*$^{-/-}$*p53*$^{-/-}$ MEF lysates with anti-FBP1 antibody. Non-immune goat serum (IgG) was used as a control. NPM mRNA from immunoprecipitates was measured by qRT-PCR. Data are mean ± s.d. of triplicate samples from three independent experiments (* $P < 0.05$, Student's *t*-test). (*C*) Rapamycin results in increased FBP1 protein expression. (Task 2d)

Brady S.N., Maggi L.B., Winkeler C.L., Toso E.A., Gwinn A.S., Pelletier C.L. and **Weber J.D.** (2009). Threonine 198 phosphorylation is dispensable for nucleophosmin's essential roles in growth and proliferation. *Oncogene,* 28: 3209-3220.

Olanich M.E., Moss B.L., Townsend R.R., Piwnica-Worms D., and **Weber J.D.** (2011). Identification of FUSE-binding protein 1 as a regulatory mRNA-binding protein that represses nucleophosmin translation. *Oncogene*, 30: 77-86.

Task 3. Establish the oncogenic potential of the p68DDX5 RNA helicase (Months 24-48):

a. Determine whether p68 is required for ribosome biogenesis (Months 24-36).
b. Determine whether NPM and p68 are phenocopies of one another (Months 24-36) 50 mice per year.
c. Examine the role of p68 in breast cancer cell growth (Months 36-48) 50 mice per year.
d. Develop a high-throughput assay for p68 helicase activity (Months 36-48).

We have successfully completed this entire Task. We have shown that p68DDX5 is required for efficient transformation of cells by oncogenic RasV12. While DDX5 is not itself a potent oncogene, its activity does drive rDNA transcription. This appears to be a rate-limiting factor during ribosome biogenesis and cell growth. Additionally, DDX5 localization is altered in the absence of ARF tumor suppression, suggesting a link between its location and activity.

We next addressed whether DDX5 was necessary for breast cancer cell growth, initially focusing on cell lines exhibiting *DDX5* copy number gains. This rationale was supported by previous work studying another gene on the 17q22-24 amplicon, *PPM1D*. Depletion of DDX5 by transduction of shRNA constructs was demonstrated for ER+ breast cancer cells both with and without *DDX5* amplification (Fig 10A). The proliferation of the four ER+/*DDX5*-amplified breast cancer cells was then assessed in the presence of estradiol or fulvestrant. HCC1428 cells formed colonies in long-term growth assays conducted in estradiol, but knockdown of DDX5 prevented colony formation (Fig 10B). Many of the other breast cancer cell lines, however, poorly formed colonies when plated at low density (data not shown), so proliferation assays were conducted instead. The proliferation of MCF-7 cells cultured in estradiol was decreased by shRNA-mediated reduction of DDX5 expression (Fig 10C). In the presence of fulvestrant, the proliferation of MCF-7 cells was severely restricted. Whereas control cells survived in the presence of fulvestrant, cells expressing shRNAs against DDX5 exhibited increased cell death, resulting in fewer cells at the experimental endpoint than were originally plated (Fig 10D). Thus, DDX5 expression is required to maintain MCF-7 growth rates in the presence of estrogen and survival in the presence of fulvestrant (Task 3c).

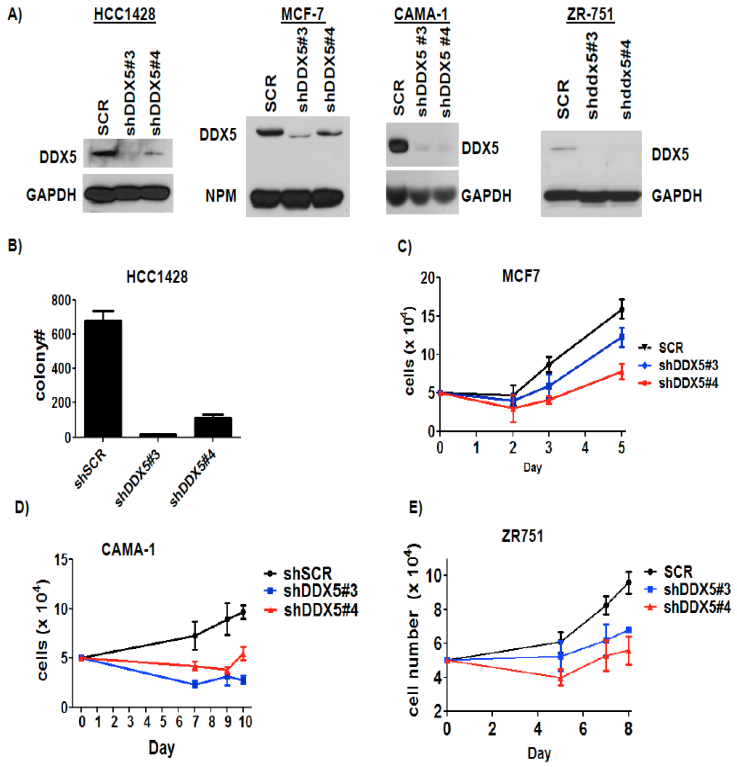

Figure 10: Effects of DDX5 knockdown on the proliferation of ER+ breast cancer cells with and without *DDX5* amplification. (A) Western blot demonstrating efficient knockdown of DDX5 in ER+ breast cancer cell lines HCC1428, MCF-7, CAMA-1, and ZR-751. (B) HCC1428 cells were transduced with shRNA and plated at a density of 5000 cells per dish to assess foci formation. After 24 days in culture in the presence of 10nM estradiol, foci were fixed, stained, and counted. MCF-7 cells were plated for a proliferation assay in the presence of (C) estradiol or (D) fulvestrant. (E) CAMA-1 and (F) ZR-751 cells were plated for a proliferation assay and cells were counted over the course of the experiment.

To analyze the requirement for DDX5 in non-transformed mammary epithelial cells, we again utilized MCF-10A cells and TLM-HMECs. Depletion of DDX5 in MCF-10A cells (Fig. 11A) reduced proliferation (Fig 11B). DDX5 interacts with NPM in TLM-HMEC s (Fig 11C). Depletion of DDX5 in TLM-HMECs (Fig. 11D) resulted in a significant reduction in colony formation (Fig 11E). These data suggest that DDX5 is required to sustain proliferation rates in both non-transformed and pre-transformed mammary epithelial cells.

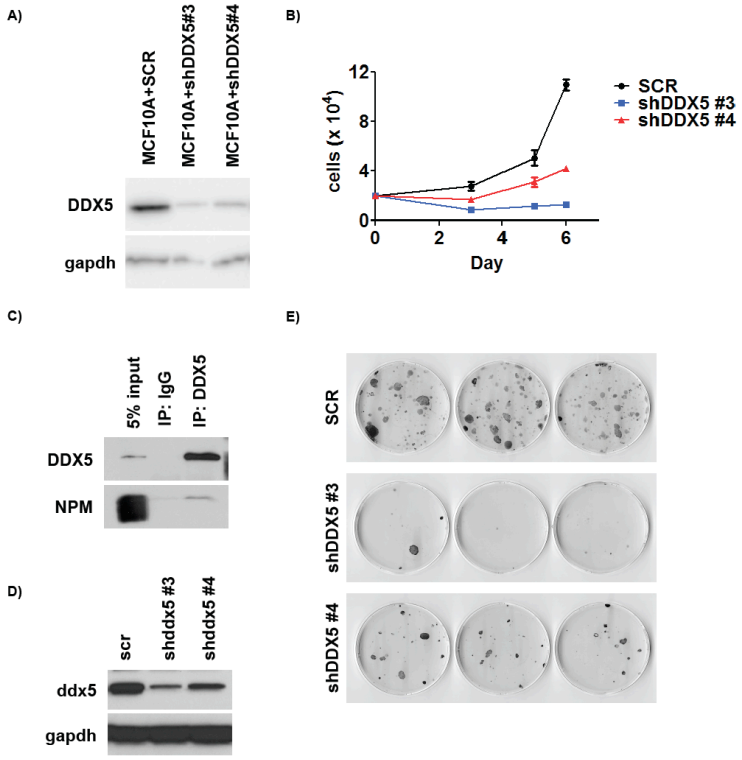

Figure 11: DDX5 is required to maintain the proliferation rates of human mammary epithelial cells. (A) Western blot demonstrating effective knockdown of DDX5 in MCF-10A cells transduced with lentiviral shRNAs. (B) Transduced MCF-10A cells were plated at a density of 2 x 10^4 cells per well of a 12-well plate for a proliferation assay. Cell counts were taken in quadruplicate over a 6 day time course. (C) Co-immunoprecipitation of DDX5 and NPM was observed in TLM-HMEC cell lysates. (D) Western blot demonstrating the efficacy of shRNA-mediated DDX5 depletion in transduced TLM-HMECs. (E) Foci formation of transduced TLM-HMECs was assessed after 17 days in culture.

Saporita A.J., Chang H-C., Winkeler C.L., Apicelli A.J., Kladney R., Wang J.C., Townsend R.R., Michel L.S., and **Weber J.D.** (2011). RNA helicase DDX5 is a p53-independent target of ARF that participates in ribosome biogenesis. *Cancer Research,* 71: 6708-17.

Task 4. Determine the contribution of ARF translation targets to breast cancer formation (Months 30-60):

a. Identify ARF translation targets (Months 30-42). 50 mice per year.
b. Clone 5' and 3' UTRs of ranked targets into luciferase reporters (Months 36-48).
c. Perform yeast three hybrid and RNA immunoprecipitation of UTRs to identify bound proteins (Months 40-50).
d. Determine whether these bound proteins regulate translation of each mRNA (Months 50-60).

We have successfully completed most of this Task. We have identified numerous mRNAs whose translation is altered in the absence of ARF. We have been able to clone most of the 3' and 5' UTRs of these mRNAs and compare them with existing sequences in the PubMed database. Our yeast three-hybrid assay did not work as planned. The overall background was far too high to gain any meaningful results from. We believe this is due to the RNA having a high affinity for the bait protein in our setting. Instead, we chose to focus on RNA immunoprecipitations like those performed in Task 2 where we were successful in identifying FBP-1 as a binding protein for NPM mRNA. We have focused on the DHX33 helicase that is negatively regulated by ARF. DHX33, like DDX5, was required for RasV12 transformation, but itself was not an oncogene. We believe that we have uncovered a novel network of RNA helicase family members that function to promote a transforming environment.

To dissect the mechanism of DHX33 reduction by ARF, we first analyzed DHX33 mRNA levels. qRT-PCR was performed on total RNAs isolated from ARF- and RasV12-infected cells at 2, 3 and 5 days post-infection. Both GAPDH mRNA and actin mRNAs were used as internal controls. We observed no significant change in DHX33 mRNA expression at each time point after ARF or Ras V12 infection of WT MEFs as compared to the empty vector control (Fig.12A). These results indicate that reduction of DHX33 by ARF does not occur by transcriptional regulation. To determine whether reduction of DHX33 by ARF induction is due to protein stability, we analyzed the half-life of DHX33 in WT MEFs following cycloheximide treatment at increasing times (Fig. 12C). We measured a half-life of 3 hours for endogenous DHX33 protein. As a control, we also determined NPM (a stable protein target of ARF) protein stability. As shown in Fig. 12C, the observed NPM half-life was 15 hours, consistent with a previous report. To determine whether DHX33 protein reduction was due to accelerated protein degradation upon ARF induction, cells were treated with MG132, a 28S proteasome inhibitor, for 6 hours. As shown in Fig. 12B, we found that DHX33 was not stabilized in the presence of MG132. As a positive control, p21CIP1 was stabilized to a significant degree with MG132 treatment, demonstrating that MG132 is functioning as expected to inhibit 26S proteasome. These results imply that reduction of DHX33 in the presence of ARF is not due to accelerated protein degradation.

To determine whether DHX33 reduction was due to translational repression of existing DHX33 mRNAs, we chose to analyze polysome-associated DHX33 mRNAs. We performed a polysome fractionation by sucrose gradient following lysis of WT MEFs that were either transduced with vector control or ARF overexpressing retroviruses (Fig. 12D). We analyzed the mRNA distribution of DHX33 in monosome and polysome fraction by qRT-PCR. As shown in Fig. 12E, we found that in ARF-infected WT MEFs, a large portion of DHX33 mRNAs (up to 60% of total mRNA) had moved into the mono-ribosome fractions (primarily associating with 40S ribosome subunit). Conversely, empty vector-infected WT MEFs exhibited a majority of their DHX33 mRNAs associated with polysomes (70%). These data clearly indicate that ARF induction causes a translational repression of DHX33 in the cytoplasm, resulting in an inhibition of translation initiation with DHX33 mRNAs being locked onto 40S ribosome subunits (Task 4a and d).

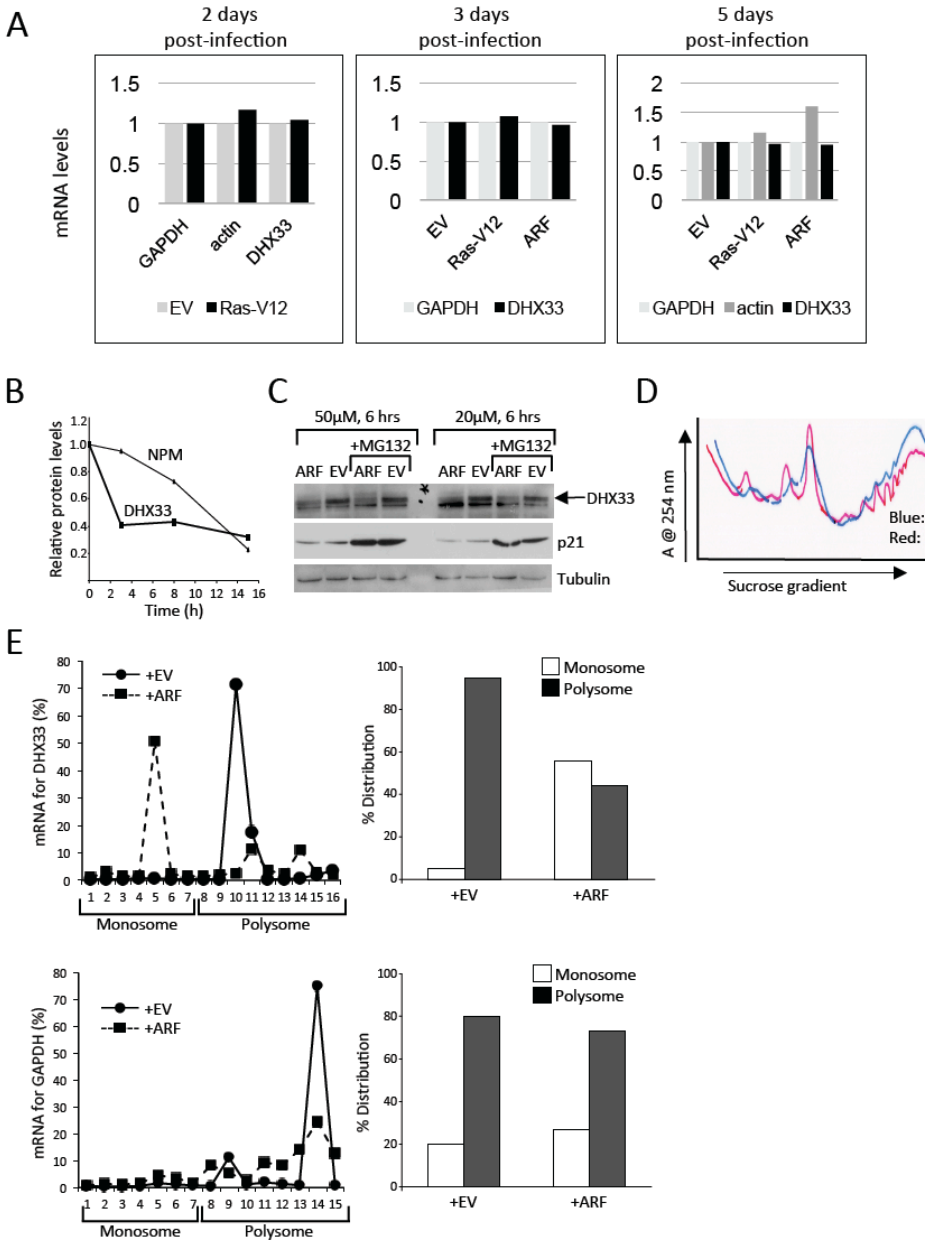

Figure 12. Induction of ARF inhibits DHX33 translation. (A) Wild type MEFs were infected with retroviruses encoding empty vector, p19ARF or RasV12 and total RNA was extracted from each sample at 2 days, 3 days or 5 days post-infection. DHX33 mRNA levels were analyzed by qPCR with GAPDH as an internal control. **(B)** Wild type MEFs were treated with cycloheximide at 60μg/ml for the indicated times. Whole cell extracts were prepared and analyzed by western blot for the DHX33 protein degradation rate, tubulin was used as a loading control, and NPM was used as a positive control for protein degradation in the presence of cycloheximide. Quantitation of the signals from the time course of DHX33 degradation and NPM degradation is depicted. **(C)** Wild type MEFs infected with retroviruses encoding empty vector (EV) or p19ARF were treated with either 20μM or 50μM of MG132 for 6 hours and total cell lysates were prepared and subjected to western blot analysis with the indicated antibodies. p21 protein stabilization was used as a positive control to monitor MG132 function. **(D)** $1.5x10^6$ wild type cells infected with retroviruses encoding empty vector or p19ARF were subjected to cytosolic polysome fractionation. Absorbance was monitored at 254nm and resultant ribosome profiles are shown for each sample. **(E)** Left: Above-mentioned fractions from mono-ribosomes or polysomes were subjected to total RNA isolation and q-PCR analysis to detect DHX33 mRNA levels. GAPDH mRNA levels were used as a control. Data presented is the percentage of mRNA from each fraction calculated from a standard curve generated by a series of diluted DHX33 plasmid. Right: Bar graph is presented as a total percentage of mRNA levels for DHX33 and GAPDH in monosome or polysome fractions under each condition.

Zhang Y., Forys J.T., Miceli A.P., Gwinn A.S., and Weber J.D. (2011). Identification of DHX33 as a mediator of rRNA synthesis and cell growth. *Molecular and Cellular Biology*, 31: 4676-4691.

Zhang Y., Saporita A.J., and **Weber J.D.** (2013). P19ARF and RasV12 offer opposing regulation of DHX33 translation to dictate tumor cell fate. *Molecular and Cellular Biology*, 33: 1594-607.

KEY RESEARCH ACCOMPLISHMENTS

- *Arf*-null mouse mammary epithelial cells (MMECs) are spontaneously immortal in culture (Task 1a)
- *Arf*-null MMECs are diploid and genomically stable (Task 1a)
- rDNA transcription is elevated in the absence of *Arf* (Task 1b)
- rRNA processing is enhanced in the absence of *Arf* (Task 1b)
- *Arf*-null mouse mammary epithelial cells (MMECs) contain unique polysome mRNA profiles (Task 1d)
- Drosha protein expression is elevated in the absence of *Arf* (Task 1e)
- *Arf*-null MECs have a distinct miRNA profile (Task 1e)
- ARF negatively regulates Drosha protein expression via a translational mechanism (Task 1e)
- ARF mRNA is not induced by mTOR pathway activation (Task 1f)
- ARF translation is altered in the absence of *Tsc1* (Task 1f)
- Drosha knockdown significantly inhibits Ras-induced transformation in the absence of ARF (Task 1e)
- mTORC1 regulates the translation of ARF (Task 1f)
- MAPK and mTOR pathways converge to regulate ARF protein expression (Task 1f)
- MAPK cross-talks with the mTOR pathway to regulate ARF (Task 1f)
- ARF mRNA is not transcribed or stabilized more in the presence of RasV12 (Task 1g)
- The 3'-UTR of NPM imparts rapamycin sensitivity (Task 2c)
- The 5' and 3' UTRs of NPM work together to regulate NPM translation in response to growth stimuli (Task 2c)
- NPM and eEF1a1 5' TOP mRNAs are translationally repressed by rapamycin (Task 2c)
- The eEF1a1 5' UTR, but not the NPM 5' UTR, is sufficient to confer rapamycin sensitivity to *luciferase* (Task 2c)
- The NPM 5' TOP motif is neither necessary nor sufficient for growth-dependent translational control of the NPM mRNA (Task 2c)

- The eEF1a1 5' TOP motif functionally dominates the NPM TOP (Task 2c)
- FBP1 interacts with the 3'-UTR of NPM to halt NPM translation (Task 2d)

- p68 increases ribosome production (Task 3a)

- ARF impairs association of DDX5 with the nuclear pre-ribosome fractions (Task 3a)
- Overexpression of DDX5 promotes ribosome output (Task 3a)
- ARF overexpression and DDX5 knockdown each reduce the cytosolic polysome profile in a p53-independent manner (Task 3a)
- *Npm1*+/- and *Ddx5*+/- genotypes partially rescue the *Arf*-/- mouse tumor phenotype (Task 3b).

- p68 is required for breast cancer cell growth and proliferation (Task 3c)

- p68 is required for RasV12-induced transformation (Task 3c)

- DDX5 is a crucial non-oncogene in human breast cancer (Task 3c)
- The ARF-regulated interaction between DDX5 and NPM is required for the growth-stimulatory effects of DDX5 (Task 3c)
- We have characterized the DDX5-NPM interaction by a split luciferase complementation assay (Task 3d)
- We have identified DHX33 as a translational target of ARF (Task 4a)
- DHX33 upregulation in the absence of ARF is important for Ras-initiated tumor formation (Task 4d)

REPORTABLE OUTCOMES

Manuscripts:

Brady S.N., Maggi L.B., Winkeler C.L., Toso E.A., Gwinn A.S., Pelletier C.L. and **Weber J.D.** (2009). Threonine 198 phosphorylation is dispensable for nucleophosmin's essential roles in growth and proliferation. *Oncogene,* 28: 3209-3220.

Dong Y., Li A., Wang J., **Weber J.D.,** and Michel L.S. (2010). Synthetic lethality through combined notch-epidermal growth factor receptor pathway inhibition in basal-like breast cancer. *Cancer Research*, 70: 5465-74.

Olanich M.E., Moss B.L., Townsend R.R., Piwnica-Worms D., and **Weber J.D.** (2011). Identification of FUSE-binding protein 1 as a regulatory mRNA-binding protein that represses nucleophosmin translation. *Oncogene*, 30: 77-86.

Wang J., Zhang K., Grabowska D., Li A., Dong Y., Day R., Humphrey P., Lewis J.S., Kladney R., Arbeit J.M., **Weber J.D.**, Chung C.H. and Michel L.S. (2011). Loss of Trop2 promotes carcinogenesis and features of epithelial to mesenchymal transition in squamous cell carcinoma. *Molecular Cancer Research*, 9: 1686-95.

Saporita A.J., Chang H-C., Winkeler C.L., Apicelli A.J., Kladney R., Wang J.C., Townsend R.R., Michel L.S., and **Weber J.D.** (2011). RNA helicase DDX5 is a p53-independent target of ARF that participates in ribosome biogenesis. *Cancer Research,* 71: 6708-17.

Zhang Y., Forys J.T., Miceli A.P., Gwinn A.S. and **Weber J.D.** (2011). Identification of DHX33 as a mediator of rRNA synthesis and cell growth. *Molecular and Cellular Biology*, 31: 4676-91.

Miceli A.P., Saporita A.J., and **Weber J.D.** (2012). Hyper-growth mTORC1 signals translationally activate the ARF tumor suppressor checkpoint. *Molecular and Cellular Biology*, 32: 348-64.

Zhang Y., Saporita A.J., and **Weber J.D.** (2013). P19ARF and RasV12 offer opposing regulation of DHX33 translation to dictate tumor cell fate. *Molecular and Cellular Biology*, 33: 1594-607.

Kuchenreuther M.J. and **Weber J.D.** (2013). The ARF tumor suppressor controls Drosha translation to prevent Ras-driven transformation. Oncogene, in press.

Abstracts/Presentations:

"Understanding and targeting cell growth networks in breast cancer" presented at the Era of Hope Conference in February 2009.

Patents/Licenses: None

Animal Models: We have generated a novel mouse model in the first year of this grant. The model is an *Arf* $^{fl/fl}$ mouse on a pure C57Bl6 background that was mated to a mixed MMTV-Cre mouse. The resulting *Arf* $^{fl/fl}$/MMTV-Cre mouse lacks ARF expression in mammary tissues. These mice will be available for free to any researcher that requests them.

In the second year, we have generated *Npm1*+/-*Arf*-/- and *Ddx5*+/-*Arf*-/- mice that will be free to any research that requests them.

In the fourth year, we have generated *Arf* $^{fl/fl}$*-Blg-Cre*, which will be free to any research that requests them.

Cell Lines:

We have developed a unique primary mouse mammary epithelial cell (MMEC) line lacking the ARF tumor suppressor. These were established directly from *Arf* knockout mice on a pure C57Bl6 background. The *Arf*-null MMECs maintain a diploid phenotype and wild-type p53. These cells are spontaneously immortal and contain no artificial genes or plasmid constructs.

We have developed a unique primary mouse mammary stem cell line lacking the ARF tumor suppressor. These were established directly from *Arf* knockout mice on a both a pure C57Bl6 background and mixed C57Bl6/129 background. The *Arf*-null stem cells maintain a diploid phenotype and wild-type p53. These cells are spontaneously immortal and contain no artificial genes or plasmid constructs.

Funding Applied for: Era of Hope Expansion Grant 2013

Employment Opportunities: Tenure granted with promotion to Associate Professor July 2008. Named Co-Director of the Breast Cancer Research Program, Siteman Cancer Center, Washington University School of Medicine, spring 2010.

CONCLUSION

Our results provide a new perspective for understanding the tumor suppressor function of ARF, which has classically been thought of as a checkpoint sensor of hyperproliferative signals. The data presented here suggest that an equally important mechanism by which ARF functions as a tumor suppressor is to limit ribosome output as a defense against oncogene activation and the attendant enhanced cellular protein requirements. Whereas loss of *Arf* results in a cellular environment permissive toward oncogenic transformation, knockdown of Drosha or DHX33 can reduce susceptibility to transformation. Therefore, in the absence of *Arf*, Drosha and DHX33 become requisite non-oncogene effectors that promote an increased translational output in accord with the higher demand for protein production required upon oncogene activation. The ability of ectopic Drosha and DHX33 expression to stimulate ribosome biogenesis and growth in wild-type MEFs further proves the central role of Drosha and DHX33 in regulating this translational output.

Our data showing the growth-stimulatory functions of Drosha in ribosome biogenesis provides a strong rationale to explain the link between Drosha and cancer. We are just beginning a new analysis of breast tumors to evaluate any gains in DHX33 expression. Although still in its infancy, most non-oncogenes are thought of as critical regulators of cellular stress responses and that their expression provides cancer cells the means to tolerate multiple stresses (9). Drosha and DHX33 may represent a class of non-oncogenes whose activities are unleashed in the absence of crucial tumor suppressors. In this setting, the role of the Drosha non-oncogene is to make a required cellular process, such as ribosome biogenesis, more efficient or prolific in preparation for the tremendous protein synthesis demands following malignant transformation. It remains to be determined whether Drosha will be an efficacious target in the treatment of cancer; however our results validate its importance in supplying the sustained ribosome output required for oncogenic transformation. Finally, DDX5 participation in ribosome biogenesis is negatively regulated by ARF, which inhibits the DDX5-NPM interaction, suggesting a dynamic interplay through which ARF and DDX5 duel for nucleolar growth control. We have established a unique split luciferase model system to begin to pre-clinically test compounds that might disrupt this interaction and prove efficacious in the treatment of cancers harboring ARF loss or DDX5 gain.

REFERENCES

1. Prives C & Hall PA (1999) The p53 pathway. *The Journal of pathology* 187(1):112-126.
2. Sherr CJ & Weber JD (2000) The ARF/p53 pathway. *Current opinion in genetics & development* 10(1):94-99.
3. Bertwistle D, Sugimoto M, & Sherr CJ (2004) Physical and functional interactions of the Arf tumor suppressor protein with nucleophosmin/B23. *Molecular and cellular biology* 24(3):985-996.

4. Brady SN, Yu Y, Maggi LB, Jr., & Weber JD (2004) ARF impedes NPM/B23 shuttling in an Mdm2-sensitive tumor suppressor pathway. *Molecular and cellular biology* 24(21):9327-9338.
5. Maggi LB, Jr*., et al.* (2008) Nucleophosmin serves as a rate-limiting nuclear export chaperone for the Mammalian ribosome. *Molecular and cellular biology* 28(23):7050-7065.
6. Yu Y*, et al.* (2006) Nucleophosmin is essential for ribosomal protein L5 nuclear export. *Molecular and cellular biology* 26(10):3798-3809.
7. Apicelli AJ*, et al.* (2008) A non-tumor suppressor role for basal p19ARF in maintaining nucleolar structure and function. *Molecular and cellular biology* 28(3):1068-1080.
8. Saporita AJ*, et al.* (2011) RNA helicase DDX5 is a p53-independent target of ARF that participates in ribosome biogenesis. *Cancer research* 71(21):6708-6717.
9. Luo J, Solimini NL, & Elledge SJ (2009) Principles of cancer therapy: oncogene and non-oncogene addiction. *Cell* 136(5):823-837.

APPENDICES

Miceli A.P., Saporita A.J., and **Weber J.D.** (2012). Hyper-growth mTORC1 signals translationally activate the ARF tumor suppressor checkpoint. *Molecular and Cellular Biology*, 32: 348-64.

Kuchenreuther M.J. and **Weber J.D.** (2013). The ARF tumor suppressor controls Drosha translation to prevent Ras-driven transformation. Oncogene, in press.

Brady S.N., Maggi L.B., Winkeler C.L., Toso E.A., Gwinn A.S., Pelletier C.L. and **Weber J.D.** (2009). Threonine 198 phosphorylation is dispensable for nucleophosmin's essential roles in growth and proliferation. *Oncogene,* 28: 3209-3220.

Olanich M.E., Moss B.L., Townsend R.R., Piwnica-Worms D., and **Weber J.D.** (2011). Identification of FUSE-binding protein 1 as a regulatory mRNA-binding protein that represses nucleophosmin translation. *Oncogene*, 30: 77-86.

Saporita A.J., Chang H-C., Winkeler C.L., Apicelli A.J., Kladney R., Wang J.C., Townsend R.R., Michel L.S., and **Weber J.D.** (2011). RNA helicase DDX5 is a p53-independent target of ARF that participates in ribosome biogenesis. *Cancer Research,* 71: 6708-17.

Zhang Y., Forys J.T., Miceli A.P., Gwinn A.S., and Weber J.D. (2011). Identification of DHX33 as a mediator of rRNA synthesis and cell growth. *Molecular and Cellular Biology*, 31: 4676-4691.

Zhang Y., Saporita A.J., and **Weber J.D.** (2013). P19ARF and RasV12 offer opposing regulation of DHX33 translation to dictate tumor cell fate. *Molecular and Cellular Biology*, 33: 1594-607.

MCB
Journals.ASM.org

Hypergrowth mTORC1 Signals Translationally Activate the ARF Tumor Suppressor Checkpoint

Alexander P. Miceli, Anthony J. Saporita, and Jason D. Weber

BRIGHT Institute, Department of Internal Medicine, Division of Molecular Oncology, and Department of Cell Biology and Physiology, Siteman Cancer Center, Washington University School of Medicine, Saint Louis, Missouri, USA

The ARF tumor suppressor is a potent sensor of hyperproliferative cues emanating from oncogenic signaling. ARF responds to these cues by eliciting a cell cycle arrest, effectively abating the tumorigenic potential of these stimuli. Prior reports have demonstrated that oncogenic Ras^{V12} signaling induces ARF through a mechanism mediated by the Dmp1 transcription factor. However, we now show that ARF protein is still induced in response to Ras^{V12} in the absence of *Dmp1* through the enhanced translation of existing *Arf* mRNAs. Here, we report that the progrowth Ras/tuberous sclerosis complex (TSC)/mTORC1 signaling pathway regulates ARF protein expression and triggers ARF-mediated tumor suppression through a novel translational mechanism. Hyperactivation of mTORC1 through *Tsc1* loss resulted in a significant increase in ARF expression, activation of the p53 pathway, and a dramatic cell cycle arrest, which were completely reversed upon *Arf* deletion. ARF protein induced from Ras^{V12} in the absence of *Dmp1* repressed anchorage-independent colony formation in soft agar and tumor burden in an allograft model. Taken together, our data demonstrate the ability of the ARF tumor suppressor to respond to hypergrowth stimuli to prevent unwarranted tumor formation.

Regulatory checkpoints are key for maintaining homeostasis in the cell. Transit through the mammalian cell cycle is tightly regulated by a series of essential checkpoints that prevent progression in the presence of hyperproliferative signals or genotoxic insults, such as DNA damage, a stalled replication fork, or improper spindle assembly (7, 9, 22). These and several other regulatory checkpoints are so critical for cellular homeostasis that their loss contributes to the deleterious events that are among the hallmarks of cancer (12).

The ARF tumor suppressor functions as an important checkpoint in the cell, acting as a key sensor of hyperproliferative signals. ARF is one of the two tumor suppressors encoded by the *CDKN2A* (*Ink4a/Arf*) locus (37). ARF functions in both p53-dependent and p53-independent manners (42). $Arf^{-/-}$ mice are highly tumor prone, predominantly developing spontaneous fibrosarcoma and lymphoma malignancies (20, 21). Deletion or silencing of the *Ink4a/Arf* locus through hypermethylation of the promoters is extremely common in a multitude of human tumors; among these are numerous examples where ARF function is specifically abrogated independently of $p16^{INK4a}$ (40). These observations underscore the significance of the antitumorigenic functions of ARF and the necessity of cancer cells to evade ARF tumor suppression.

Basal expression of ARF is nearly undetectable. However, ARF protein levels are robustly upregulated in response to excessive proliferative cues, such as those emanating from the Ras^{V12}, Myc, E1A, v-Abl, and E2F oncoproteins (3, 8, 34, 38, 56). Upon induction, ARF binds MDM2, the E3 ligase responsible for targeting p53 for proteasome-mediated degradation (52). ARF's sequestration of MDM2 in the nucleolus allows p53 to accumulate in the nucleoplasm and to activate downstream targets that trigger cell cycle arrest (53).

Cell proliferation and cell growth are intimately linked. As such, proliferative and growth stimuli often invoke cross talk at key signaling networks to properly regulate the timing of cell cycle progression and protein synthesis. A key player in this regulation is the mammalian target of rapamycin (mTOR) signal transduction pathway (36). mTOR is a conserved serine/threonine kinase that assembles into two major multiprotein-containing complexes, mTORC1 and mTORC2 (57), each of which is reported to serve a unique function in the cell (29). mTORC1 contains Raptor, LST8, Deptor, PRAS40, and mTOR and is critical for regulating protein synthesis; mTORC2 includes Rictor, LST8, Deptor, Protor, Sin1, and mTOR and plays a role in cytoskeletal organization (57). mTOR responds to several upstream stimuli, including growth factors and nutrients. Upstream signaling is propagated through Ras and phosphatidylinositol 3-kinase (PI3K) (41). In addition, the tuberous sclerosis complex (TSC) gene products are critical upstream negative regulators of mTORC1 signal transduction (15); loss of either *Tsc1* or *Tsc2* results in constitutive mTORC1 signaling and increased phosphorylation of S6K1 (ribosomal protein S6 kinase 1) and initiation factor 4E binding protein 1 (4EBP1). This has direct consequences for the protein translation machinery and the downstream gene targets that are regulated by this pathway (14). Mutations among pathway members are common in hamartoma-forming syndromes and a broad spectrum of human cancers (11, 13).

Given ARF's central role in sensing hyperproliferative signals, we hypothesized that ARF might also be sensitive to hypergrowth cues emanating from mTORC1 signaling. In this report, we investigated ARF gene expression and function in response to hyperactivation of the progrowth mTORC1 signal transduction pathway. Importantly, we also interrogated ARF function in the absence of

Received 29 July 2011 Returned for modification 30 August 2011
Accepted 30 October 2011
Published ahead of print 7 November 2011
Address correspondence to Jason D. Weber, jweber@dom.wustl.edu.
Copyright © 2012, American Society for Microbiology. All Rights Reserved.
doi:10.1128/MCB.06030-11

Downloaded from http://mcb.asm.org/ on April 16, 2013 by Washington University in St. Louis

collaborating signals from the Dmp1 transcription factor, the only known regulator of ARF induction from Ras^{V12}. Ras^{V12} expression in murine embryonic fibroblasts (MEFs) lacking *Dmp1* resulted in increased ARF protein levels, suggesting that (i) Dmp1-mediated transcription of *Arf* is not obligatory for ARF induction and (ii-another pathway downstream of Ras must modulate ARF expression. Using pharmacological and genetic manipulation, we now show that the Ras/TSC/mTORC1 pathway regulates ARF through a novel translational mechanism. Based on our findings, we propose that ARF can respond to hypergrowth signals emanating from a hyperactivated mTORC1 pathway to prevent tumor formation.

MATERIALS AND METHODS

Mice and cell culture. $Tsc1^{flox/flox}$ mice were a generous gift from Jeffrey Arbeit (Washington University, St. Louis, MO) (23), with permission from David Kwiatkowski (Harvard University, Cambridge, MA). $Tsc1^{flox/flox}$ and $Arf^{-/-}$ mice were intercrossed for several generations to generate $Tsc1^{flox/flox}$; $Arf^{-/-}$ mice. Inbred homozygous female athymic nude mice ($Foxn1^{nu}/Foxn1^{nu}$) were purchased from Jackson Laboratory (Bar Harbor, ME). Nude mice were 5 weeks old at the time of purchase and were housed in our facility until they were approximately 7 weeks of age to acclimate to the new facility before injections were performed. Low-passage (passage 3 [P3] to P5) primary murine embryonic fibroblasts for all described genotypes were established as previously described (21) and maintained in Dulbecco's modified Eagle's medium supplemented with 10% fetal bovine serum, 2 mM glutamine, 0.1 mM nonessential amino acids, 2 μg/ml gentamicin. Etoposide (Sigma, St. Louis, MO) and rapamycin (LC Laboratories, Woburn, MA) were, respectively, used at final concentrations of 50 μM and 100 nM.

Viral production and infections. pBabe-puro-H-Ras^{V12} was a generous gift from Martine Roussel (St. Jude Children's Research Hospital, Memphis, TN). pBabe-HA-ARF (where HA is hemagglutinin), pWZL-GFP-IRES-blast (where GFP is green fluorescent protein and blast is blasticidin), and pWZL-Ras^{V12}-IRES-blast have been previously described (4, 51). Retroviral production was performed as previously described (4, 39). Retroviral helper DNA was kindly provided by Charles Sawyers (University of California Los Angeles, Los Angeles, CA). Collected retrovirus was used to infect MEFs in the presence of 10 μg/ml Polybrene. Infected MEFs were selected in 2 μg/ml puromycin and were harvested for analysis at 5 days postinfection. For the production of lentiviruses encoding short hairpin RNAs, 5×10^5 293T cells were cotransfected using Lipofectamine 2000 (Invitrogen, Carlsbad, CA) with pHCMV.G, CMVΔR8.2, and pLKO.1-puro constructs. Viral supernatants were collected and pooled. Infected MEFs were selected in 2 μg/ml puromycin and were harvested for analysis at 5 days postinfection. High-titer adenoviruses encoding β-galactosidase (Ad5CMVntLacZ [Ad-LacZ]) or Cre recombinase (Ad5CMVCre [Ad-Cre]) were purchased from the Gene Transfer Vector Core, University of Iowa. For adenovirus infections, MEFs were washed with phosphate-buffered saline (PBS), trypsinized, and counted; 7.5×10^5 cells were plated in the presence of LacZ- or Cre-encoding adenovirus for 6 h. Cells were split upon reaching confluence and then harvested for analysis at 9 to 10 days postinfection.

RNAi. pLKO.1-puro constructs obtained from the Genome Center at Washington University were used for RNA interference (RNAi) against *Tsc1*. Sequences for the short hairpin RNAs are 5′-GCCTCGTATGAAG ATGGCTAT-3′ for *Tsc1* (here named siTSC1.2), 5′-GCCAGTGTTTAT GCCCTCTTT-3′ also for *Tsc1* (here named siTSC1.4), 5′-GCGGTTGCC AAGAGGTTCCAT-3′ for the luciferase control, and 5′-CCTAAGGTTA AGTCGCCCTCGCTCGAGCGAGGGCGACTTAACCTTAGG-3′ for the scrambled control. pLKO-GFP-shARF has been previously described (1); for the present studies, the GFP marker was replaced by a puromycin resistance cassette subcloned into the BamHI and KpnI sites of pLKO. Lentiviruses were packaged, and MEFs were infected as described above. For RNAi against *Raptor* and *Rictor*, short hairpin RNA oligonucleotides were purchased from Qiagen (Valencia, CA) and were transduced using the Nucleofector system (Amaxa, Walkersville, MD) according to the manufacturer's instructions. Sequences for the short hairpin RNAs recognizing *Raptor* and *Rictor*, respectively, are 5′-CCGGGTCATGACTTA CCGAGA-3′ and 5′-CAGAAAGATGATTACTGTGAA-3′.

Western blotting. Harvested cells were resuspended and sonicated in radioimmunoprecipitation assay (RIPA) lysis buffer (50 mM Tris-HCl, pH 7.4, 150 mM NaCl, 1% Triton X-100, 0.1% SDS, 0.5% deoxycholic acid) containing protease and phosphatase inhibitors (1 mM phenylmethylsulfonyl fluoride [PMSF], 0.4 U/ml aprotinin, 10 μg/ml leupeptin, 10 μg/ml pepstatin, 1 mM β-glycerophosphate, 0.1 mM NaF, 0.1 mM $NaVO_4$). Proteins (30 to 80 μg) were separated on 12.5% sodium dodecyl sulfate (SDS)-containing polyacrylamide gels. Separated proteins were transferred onto polyvinylidene difluoride (PVDF) membranes (Millipore, Boston, MA). Membranes were probed with the following antibodies: rabbit anti-Rictor (A300-459), rabbit anti-TSC1 (A300-316), and rabbit anti-glyceraldehyde-3-phosphate dehydrogenase (anti-GAPDHj A300-641) (all from Bethyl Laboratories; Montgomery, TX); rat anti-ARF (ab26696; Abcam, Cambridge, MA); mouse anti-MDM2 (op115; Calbiochem/EMD Chemicals, Gibbstown, NJ); mouse antiactin (sc8432), mouse anti-p21 (sc6246), rabbit antinucleophosmin (anti-NPM; sc6013), mouse anti-γ-tubulin (sc17787), and rabbit anti-Ras (sc520) (all from Santa Cruz Biotechnology, Santa Cruz, CA); rabbit anti-p53 (2524), rabbit anti-phospho-extracellular signal-regulated kinase 1 and 2 (anti-phospho-ERK1/2), Thr 202/Tyr 204 (4377), rabbit anti-ERK1/2 (9102), rabbit anti-phospho-S6, Ser 240/244 (2215), mouse anti-S6 (2317), rabbit anti-Raptor (4978), rabbit anti-phospho-4EBP1, Thr37/46 (2855), rabbit anti-YEBP1 (9452), and rabbit anti-p70 S6K1 (9202) (all from Cell Signaling Technologies, Danvers, MA). Secondary horseradish peroxidase-conjugated anti-rabbit, anti-rat, or anti-mouse antibodies (Jackson ImmunoResearch, West Grove, PA) were added, and Amersham ECL Plus (GE Healthcare, Piscataway, NJ) was used to visualize the bands.

Quantitative RT-PCR and endpoint PCR. Total RNA was extracted from cells with a Nucleospin RNAII system (Clontech, Mountain View, CA) according to the manufacturer's instructions. Reverse transcription (RT) reactions were performed using a SuperScript III first-strand synthesis system (Invitrogen, Carlsbad, CA) with an oligo(dT) primer. Real-time PCR was performed on an iCycler apparatus (Bio-Rad, Hercules, CA) using iQ Sybr Green Supermix (Bio-Rad, Hercules, CA). Fold change was calculated using the $\Delta\Delta C_T$ (where C_T is threshold cycle) method (28). To measure *Arf* mRNA, the following primers were used: forward, 5′-GA GTACAGCAGCGGGAGCAT-3′; reverse, 5′-ATCATCATCACCTGGTC CAGGATTCC-3′. To measure *Gapdh* mRNA, the following primers were used: forward, 5′-GCTGGGGCTCACCTGAAGGG-3′; reverse: 5′-GGA TGACCTTGCCCACAGCC-3′.

To assess the presence of *Dmp1* mRNA in MEF samples, total RNA was isolated, first-strand synthesis was used to generate cDNA with an oligo(dT) primer, and endpoint PCR analysis was performed. Primers used for detecting *Dmp1* were the following: forward, 5′-CTGTAGCTGAAAG AGTGGGTA-3′; reverse, 5′-TGTATTATCTTCCAAGCGGGC-3′ (19). PCRs were separated on an agarose gel and stained with ethidium bromide.

RNA and protein stability. Infected MEFs were treated with either 4 μg/ml actinomycin D (Sigma, St. Louis, MO) to assess mRNA stability or 25 μg/ml cycloheximide (Sigma, St. Louis, MO) to assess protein stability. Cells were harvested over a time course of 0, 2, 4, 6, or 8 h posttreatment and subjected, respectively, to RNA isolation, cDNA synthesis reaction, and quantitative reverse transcription-PCR (qRT-PCR) analysis or to Western blot analysis.

Immunoprecipitation. Infected MEFs were freshly harvested, and cells were resuspended and sonicated in EBC lysis buffer (50 mM Tris-HCl, pH 7.4, 120 mM NaCl, 0.5% NP-40, 1 mM EDTA). Then, 300 μg of protein lysate was immunoprecipitated overnight with a rabbit anti-ARF polyclonal antibody or normal rabbit IgG (sc2027; Santa Cruz Biotech-

Downloaded from http://mcb.asm.org/ on April 16, 2013 by Washington University in St. Louis

nology, Santa Cruz, CA). Immune complexes recovered by protein A-Sepharose (GE Healthcare, Piscataway, NJ) were washed three times with EBC buffer and were denatured. Proteins were separated on 12.5% sodium dodecyl sulfate (SDS)-containing polyacrylamide gels and were transferred onto PVDF membranes (Millipore, Boston, MA) and subjected to direct immunoblotting as indicated.

Indirect IF and BrdU incorporation. Infected MEFs were plated onto coverslips. Cells were washed with PBS and fixed at room temperature using 10% formalin–10% methanol, followed by incubation with 1% NP-40 at room temperature for 5 min. Cells were stained with antibodies recognizing ARF (ab26696; Abcam, Cambridge, MA) or MDM2 (op115; Calbiochem/EMD Chemicals, Gibbstown, NJ, followed by the corresponding secondary antibodies conjugated with Alexa Fluor 488 or Alexa Fluor 594 (Invitrogen, Carlsbad, CA), respectively. Cells were then counterstained for nuclei with SlowFade Gold Antifade mounting reagent with 4′,6-diamidino-2-phenylindole (DAPI; Invitrogen, Carlsbad, CA). Fluorescence signals were detected using a Nikon epifluorescent compound microscope fitted with a Nikon FDX-35 charge-coupled-device camera. For measurement of DNA replication, 5-bromodeoxyuridine (BrdU) (Sigma, St. Louis, MO) was added to the culturing medium for 2, 18 or 24 h, as indicated in the figure legends, at a final concentration of 10 μM. Cells were then treated for immunofluorescence (IF) analysis as noted above and additionally incubated with 1.5 N HCl at room temperature for 10 min. A mouse monoclonal antibody recognizing BrdU (Amersham/GE Healthcare, Piscataway, NJ) was used.

Cell proliferation assay, focus formation, and soft-agar formation. For cell proliferation assays, equal numbers of cells (5×10^4 *Dmp1*$^{-/-}$ MEFs; 1×10^5 *Tsc1*$^{flox/flox}$ or *Tsc1*$^{flox/flox}$; *Arf*$^{-/-}$ MEFs) were replated in triplicate. Every 24 h thereafter, cells were harvested and counted using a hemacytometer. For focus formation, 5×10^3 infected cells were plated in triplicate onto 10-cm^2 dishes. Cells were grown for 14 days in complete medium and then were fixed with 100% methanol and stained for 30 min with 50% Giemsa. For soft-agar colony formation, 1×10^3 infected cells were seeded in triplicate on 60-mm dishes and allowed to grow for 21 days in complete medium supplemented with fetal bovine serum and Noble agar.

Apoptosis analysis. Infected MEFs were stained with fluorescein isothiocyanate (FITC)-annexin V and propidium iodide using a Dead Cell Apoptosis Kit (V13242; Molecular Probes/Invitrogen, Carlsbad, CA) according to the manufacturer's specifications. Cells were analyzed by flow cytometry using a Becton Dickinson FACSCalibur cell sorter with CELLQuest Pro (version 5.2) analytical software.

Ribosome fractionation, RNA isolation, and qRT-PCR. Cells were treated with cycloheximide (10 μg/ml) for 5 min before being harvested. Equal numbers of cells (3×10^6) were lysed, and cytosolic extracts were subjected to ribosome fractionation as previously described (33, 46) using a density gradient system (Teledyne ISCO, Lincoln, NE). RNA was isolated from monosome, disome, and polysome fractions using RNAsolv (Omega Bio-Tek, Norcross, GA) according to the manufacturer's specifications. Reverse transcription reactions were performed using a SuperScript III first-strand synthesis system (Invitrogen, Carlsbad, CA) with an oligo(dT) primer. Real-time PCR was performed on an iCycler apparatus (Bio-Rad, Hercules, CA) using SsoFast EvaGreen Supermix (Bio-Rad, Hercules, CA) to amplify *Arf* or *Gapdh* from monosome/disome and polysome fractions. Numbers of *Arf* or *Gapdh* transcripts per fraction were calculated from a standard curve generated from serial dilutions of a known quantity of subcloned *Arf* or *Gapdh* cDNA. *Arf* or *Gapdh* mRNA distribution per fraction was calculated as a percentage of the total number of transcripts in all collected fractions. For the ribosome profiling analysis shown in Fig. 6, cells were treated with puromycin (Sigma, St. Louis, MO) at a final concentration of 1 mM for 3 h.

Tumorigenic assay. Infected MEFs were trypsinized and counted. A total of 2×10^6 cells were resuspended in PBS and injected subcutaneously into the left flank of athymic nude *Foxn1*^{nu}/*Foxn1*^{nu} mice. A sample size of five mice per condition was used. Tumor growth was monitored every day by palpation at the injection site, and the diameter of the tumors was measured in two different planes using a digital caliper. Tumor volume was calculated with the following formula: (height^2 $\times$ length)/2, where height represents the smaller of the two measurements.

Densitometry, image, and statistical analysis. Autofluorograms and immunoblot films were scanned using an ImageScannerIII apparatus (GE Healthcare, Piscataway, NJ), and densities were determined using ImageQuant, version 2005 (GE Healthcare, Piscataway, NJ). Statistical analyses were performed using a Student's *t* test.

RESULTS

ARF is responsive to Ras^{V12} and is functional in the absence of *Dmp1*. Previous reports have demonstrated that ARF responds to the Ras^{V12} oncoprotein through a mechanism mediated by the Dmp1 transcription factor (17, 18, 44). However, it was also noted that ARF's induction from Ras^{V12} is compromised, but not completely lost, in the absence of *Dmp1* (16, 18). We sought to further understand the putative regulation and function of ARF in the absence of cooperating transcriptional signals. *Dmp1*$^{-/-}$ MEFs were infected with a retrovirus encoding Ras^{V12} and harvested at 5 days postinfection for gene expression analysis; confirmation of *Dmp1*-null status of the MEFs was performed by PCR analysis of reverse transcribed cDNA (Fig. 1A). Consistent with prior findings (16, 18), we observed that ARF protein is still increased in response to Ras^{V12} overexpression in the absence of *Dmp1* (Fig. 1B). Strikingly, *Arf* mRNA levels were not significantly altered from Ras^{V12} overexpression in *Dmp1*-deficient cells (Fig. 1C). Collectively, these data indicate that transcriptional activation of *Arf* gene expression is not obligatory for inducing ARF protein levels in response to Ras^{V12}. These observations also indicate that the Ras/Dmp1 pathway is not the only mechanism by which ARF can sense the oncogenic cues of Ras^{V12} signaling.

Since ARF is sensitive to the oncogenic stimulus of Ras^{V12} in *Dmp1*-null cells, we hypothesized that basal ARF could still exert its important antiproliferative functions in these cells. To test this, we infected *Dmp1*$^{-/-}$ MEFs with a lentivirus encoding a short hairpin targeting a scrambled control or *Arf* exon 1β (siScramble and siARF, respectively) (1), the ARF-specific exon of the *CDKN2A* locus. As shown by Western blot analysis, ARF protein levels were dramatically reduced (~90%) compared to those of the scrambled control (Fig. 2A). To determine the effect of acute knockdown of ARF on cellular proliferation, equal numbers of *Dmp1*$^{-/-}$ MEFs expressing the short hairpin against *Arf* or scrambled control were seeded in triplicate, and total numbers of cells were counted over 5 days. Acute knockdown of ARF significantly increased the rate of proliferation of *Dmp1*$^{-/-}$ MEFs (Fig. 2B). Additionally, 5-bromodeoxyuridine (BrdU) incorporation was also monitored to measure the extent of cells entering S phase (Fig. 2C and D). Acute knockdown of ARF caused a significant increase in the percentage of cells undergoing DNA replication; this was observed with both a short (2 h) and a longer (18 h) pulse of BrdU (Fig. 2D and C, respectively). Acute knockdown of ARF did not dramatically alter the amount of cells undergoing apoptosis (4.6% for *Dmp1*$^{-/-}$ MEFs infected with siScramble-encoding virus and 3% for siARF-encoding virus) (Fig. 2E).

Ras/TSC/mTORC1 pathway can regulate ARF. Our data indicate that ARF is induced in response to oncogenic Ras^{V12} independently of Dmp1 transcriptional activity. We hypothesized that the mTORC1 signal transduction pathway could potentially regulate ARF expression. This critical cell growth regulatory pathway coordinates ribosome biogenesis and mRNA translation. Regula-

Downloaded from http://mcb.asm.org/ on April 16, 2013 by Washington University in St. Louis

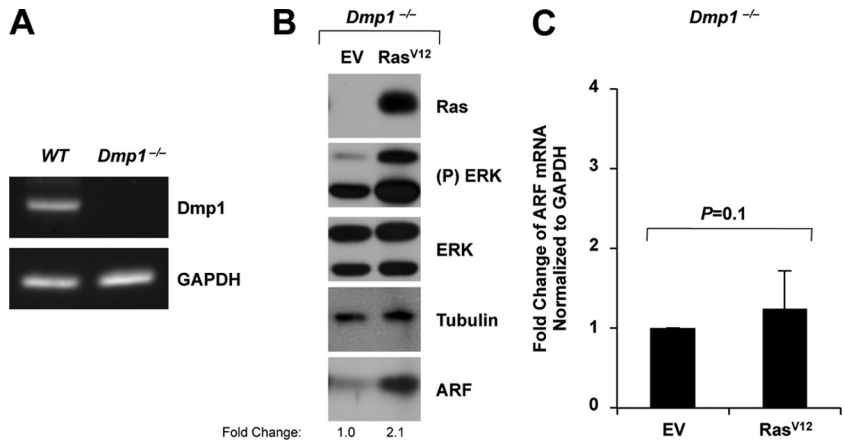

FIG 1 In the absence of *Dmp1*, Ras^{V12} induces ARF protein, but not ARF mRNA. (A) First-strand cDNA was synthesized from total RNA isolated from wild-type (WT) or $Dmp1^{-/-}$ MEFs, and endpoint PCR analysis was performed using primers specific for *Dmp1* or *Gapdh*. PCRs were separated on an agarose gel and stained with ethidium bromide. (B and C) $Dmp1^{-/-}$ MEFs were transduced with retroviruses encoding an empty vector control (EV) or Ras^{V12} and were harvested at 5 days postinfection for gene expression analysis. (B) Infected cells were lysed, and separated proteins were immunoblotted for the indicated proteins. Expression fold change over empty vector is indicated (B). First-strand cDNA was synthesized from isolated total RNA, and quantitative RT-PCR analysis was performed. *Arf* mRNA levels were normalized to *Gadph* mRNA levels. Fold change was calculated using the $\Delta\Delta C_T$ method. Data are the mean ± standard deviation of five independent experiments, and *P* values were calculated using the Student *t* test (C). (P), phosphorylated.

tion by this pathway is often associated with translational control of target genes whose protein levels, but not mRNA levels, are modulated in particular cellular contexts (10, 24, 43). To begin evaluating this pathway, wild-type and $Dmp1^{-/-}$ MEFs were transduced with a retrovirus encoding Ras^{V12} and subsequently treated with rapamycin, the pharmacological inhibitor of mTORC1 signaling, for 24 h prior to harvesting (Fig. 3A and B). Repressed levels of phospho-S6K1 (Thr 389) and phospho-S6 (Ser 240/244) revealed that mTORC1 signaling was disrupted by rapamycin exposure (Fig. 3A and B). For strains of both genotypes, the induced levels of ARF protein expression were sensitive to rapamycin treatment (Fig. 3A and B), suggesting that mTORC1 signaling is essential for ARF's induction from Ras.

We next wanted to interrogate the involvement of the Ras/mTORC1 pathway in regulating ARF protein levels using genetic manipulations. Tuberous sclerosis complex 1 (TSC1) is an upstream member of the mTORC1 pathway. TSC1 forms a complex with TSC2 that negatively regulates mTORC1 signal transduction (48). We hypothesized that activation of the mTORC1 pathway by acute knockdown of TSC1 would induce ARF protein levels. To test this, wild-type MEFs were infected with lentiviruses encoding small interfering RNAs (siRNAs) recognizing *Tsc1*. Two hairpins were used to reduce TSC1 expression (Fig. 3C). ARF protein levels were upregulated from transient knockdown of TSC1 in a dose-dependent manner (Fig. 3C). Additionally, $Tsc1^{flox/flox}$ MEFs were infected with adenoviruses encoding Cre recombinase or a β-galactosidase (LacZ) control. Enhanced levels of phospho-S6K1 (Thr 389) and phospho-S6 (Ser 240/244) demonstrated that hyperactivation of mTORC1 signaling occurred from loss of *Tsc1* (Fig. 3D). Genetic ablation of *Tsc1* also caused an increase in ARF protein levels (Fig. 3D), corroborating the results observed from using RNAi against *Tsc1*. Moreover, we infected wild-type MEFs with Ad-LacZ or Ad-Cre to ensure that this finding was not a nonspecific effect of Cre recombinase or the adenoviral infection protocol (Fig. 3E). Additionally, $Tsc1^{+/flox}$ and $Tsc1^{flox/flox}$ MEFs were infected with Ad-Cre or Ad-LacZ to evaluate a dose-dependent loss of *Tsc1* on ARF protein levels (Fig. 3F). Loss of one copy of *Tsc1* was sufficient to induce ARF protein expression, while loss of both copies of *Tsc1* induced ARF protein expression to a greater extent (Fig. 3F).

To investigate whether the ARF induction observed from the loss of *Tsc1* is dependent on TSC/mTORC1 signaling, we infected $Tsc1^{flox/flox}$ MEFs with Ad-Cre or the Ad-LacZ control and then treated them with rapamycin for 24 h prior to harvesting. Diminished levels of phospho-S6K1 (Thr 389) and phospho-S6 (Ser 240/244) demonstrated that rapamycin successfully blocked mTORC1 signaling (Fig. 3G). As seen before with infection with a retrovirus encoding Ras^{V12} (Fig. 3A and B), ARF protein levels induced from the loss of *Tsc1* were sensitive to rapamycin treatment (Fig. 3G).

To confirm the contributions of mTORC1 signaling following *Tsc1* deletion to regulation of ARF, RNA interference was used to acutely knockdown *Raptor* or *Rictor* (Fig. 3H and I). Acute knockdown of *Raptor*, but not *Rictor*, abrogated the induction of ARF expression from the ablation of *Tsc1* (Fig. 3H and I). These data provide further support that mTORC1, but not mTORC2, is necessary for mediating the induction of ARF from the loss of *Tsc1*. Taken together, these data demonstrate that hyperactivation of Ras/TSC/mTORC1 pathway can regulate ARF protein levels.

ARF induction from mTORC1 hyperactivation uses a novel translational mechanism. Given that mTORC1 signal transduction plays a crucial role in the translational regulation of specific mRNA transcripts, we hypothesized that this might be an underlying mechanism responsible for inducing ARF protein levels. To test this, we assessed different aspects of *Arf* gene expression in the face of mTORC1 hyperactivation. For each of these experiments, $Tsc1^{flox/flox}$ MEFs were infected with Ad-Cre or Ad-LacZ as before. Despite the increases in ARF protein expression, no significant changes were observed in *Arf* mRNA levels following *Tsc1* loss (Fig. 4A). Next, we evaluated *Arf* mRNA stability and observed a rate of *Arf* mRNA decay that was nearly identical in Ad-LacZ- and Ad-Cre-infected $Tsc1^{flox/flox}$ cells (Fig. 4B). Moreover, the rate of ARF protein decay was faster in Ad-Cre-infected $Tsc1^{flox/flox}$ MEFs than in Ad-LacZ-infected cells (Fig. 4C and D), suggesting that a higher rate of ARF protein must be synthesized in order to in-

Downloaded from http://mcb.asm.org/ on April 16, 2013 by Washington University in St. Louis

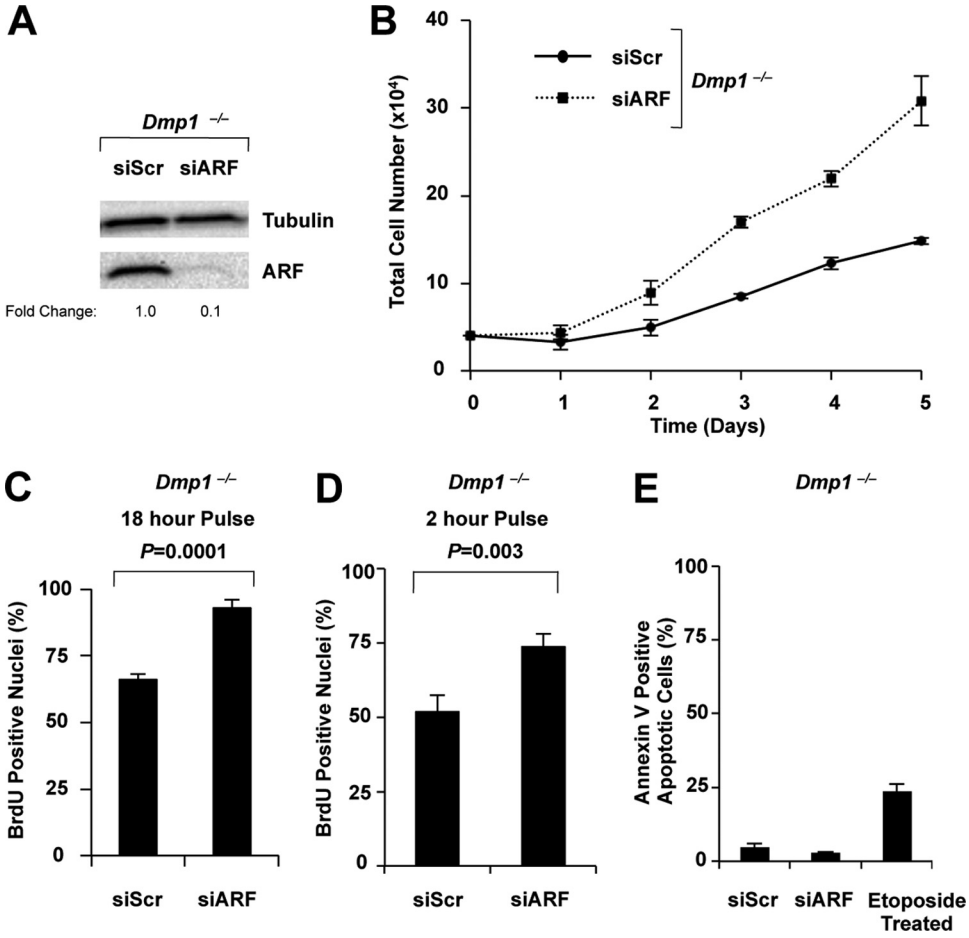

FIG 2 ARF remains functional in the absence of *Dmp1*. *Dmp1*$^{-/-}$ MEFs were infected with lentiviruses encoding a short hairpin against *Arf* (siARF) or the siScramble control (siScr). (A) Infected cells were lysed, and separated proteins were immunoblotted for the indicated proteins. Expression fold change over the siScramble control is indicated. (B) A total of 5×10^4 cells were seeded in triplicate for each indicated time point. Cells were trypsinized and counted with a hemacytometer each day for 5 days thereafter. (C and D) Infected cells were seeded on coverslips and were pulsed with BrdU for 18 or 2 h, as indicated. Indirect immunofluorescence analysis was used to score BrdU incorporation. Representative data are depicted as the mean ± standard deviation of 50 nuclei counted in triplicate, and *P* values were calculated using the Student *t* test. (E) Infected cells were harvested and stained with FITC-annexin V and propidium iodide and subjected to flow cytometry analysis. Representative data are expressed as the mean ± standard deviation of 10,000 events performed in triplicate, and *P* values were calculated using the Student *t* test.

crease steady-state levels in the cell. We also assessed the rate of protein decay of ectopic HA-ARF expressed in Ad-Cre-infected *Tsc1*$^{flox/flox}$; *Arf*$^{-/-}$ MEFs (Fig. 4E and F) and noted a similarly accelerated half-life for HA-ARF (~4 h). This observation supports the notion that ARF protein is being degraded at a high rate in the absence of *Tsc1* compared to ARF's normally observed half-life of ~6 h (25).

To further test the hypothesis that translational regulation could be the molecular mechanism responsible for eliciting ARF's induction from mTORC1 hyperactivation, we assessed the association of *Arf* mRNA with actively translating polyribosomes. To accomplish this task, cytosolic ribosomes were isolated by sucrose gradient centrifugation from equal numbers of *Dmp1*$^{-/-}$ MEFs infected with a retrovirus encoding either Ras^{V12} or an empty vector control (Fig. 5A and B). Ribosomal subunits were detected by measuring RNA absorbance at 254 nm by continuous UV monitoring (Fig. 5B). To assess the distribution of *Arf* mRNA transcripts in individual fractions comprising isolated monosomes, disomes, or polysomes, total RNA was isolated from each sucrose gradient fraction, and *Arf* mRNA levels were determined with qRT-PCR. Strikingly, *Arf* mRNA transcripts associated with different polyribosome fractions in *Dmp1*-null cells infected with retroviruses encoding Ras^{V12} and empty vector (Fig. 5C). In *Dmp1*$^{-/-}$ MEFs infected with a Ras^{V12}-encoding retrovirus, *Arf* mRNA was pooled to a heavier polyribosome fraction, indicating that there is a greater extent of *Arf* mRNAs being actively translated by multiple ribosomes (more ribosomes associated per mRNA) in these cells (Fig. 5C). These data support the hypothesis that ARF is translationally regulated in the presence of oncogenic Ras^{V12} signals.

To address the possibility that general gains in global protein translation could account for the increased translation of *Arf* mRNA transcripts, we evaluated the distribution of *Gapdh* mRNA in sucrose gradient fractions in *Dmp1*$^{-/-}$ MEFs infected with a retrovirus encoding either Ras^{V12} or an empty vector control (Fig. 5D). No dramatic differences in the distribution of *Gapdh* mRNA transcripts were observed across isolated monosomes or polyribosomes, in contrast to the distribution observed for *Arf* mRNA (Fig.

Downloaded from http://mcb.asm.org/ on April 16, 2013 by Washington University in St. Louis

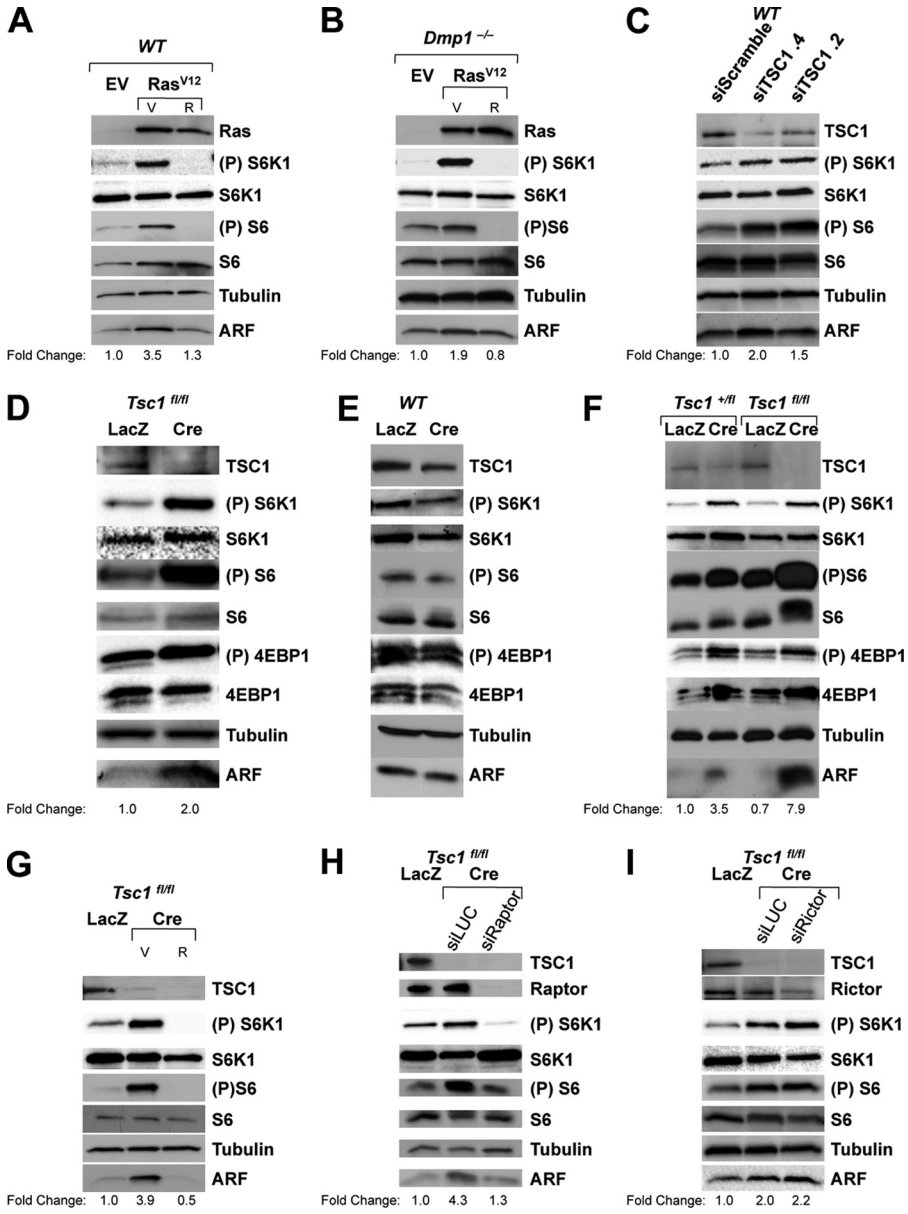

FIG 3 Ras/TSC/mTORC1 pathway can regulate ARF. Infected cells were lysed, and separated proteins were immunoblotted for the indicated proteins. Expression fold change over empty vector (EV), siScramble, or LacZ control is indicated. (A and B) WT or *Dmp1*$^{-/-}$ MEFs were infected with retroviruses encoding an empty vector control or Ras^{V12} and were harvested at 5 days postinfection. Ras^{V12}-infected cells were treated with 100 nM rapamycin (R) or vehicle (V) for 24 h prior to harvesting. (C) Wild-type MEFs were infected with lentiviruses encoding short hairpins against *Tsc1* or the siScramble control and were harvested at 7 days postinfection. (D to F) *Tsc1*$^{flox/flox}$, WT, or *Tsc1*$^{+/flox}$ MEFs (as indicated) were infected with adenoviruses encoding β-galactosidase (LacZ) or Cre recombinase and were harvested at 9 days postinfection. (G to I) *Tsc1*$^{flox/flox}$ MEFs were infected with adenoviruses encoding β-galactosidase (LacZ) or Cre recombinase and harvested at 9 days postinfection. (G) Ad-Cre-infected cells were treated with 100 nM rapamycin (R) or vehicle (V) control for 24 h prior to harvesting. (H and I) Ad-Cre-infected cells were then transduced with viruses encoding short hairpins recognizing *Raptor* (siRaptor) or *Rictor* (siRictor) or a luciferase control (siLUC) at 5 days postinfection and then harvested at 9 days postinfection for Western blot analysis. P, phosphorylated.

5C). This suggests that the gain in *Arf* mRNA association with actively translating polyribosomes is a selective phenotype caused by Ras^{V12} oncogenic signaling in the absence of *Dmp1*.

To confirm that *Arf* mRNA transcripts are actually associating with actively translating polyribosomes, we assessed whether puromycin could release *Arf* mRNA transcripts from the polyribosome fractions. Puromycin treatment causes a block in translation elongation and a premature release of the nascent polypeptide chain from actively translating polyribosomes (2, 45). To accomplish this, *Dmp1*$^{-/-}$ MEFs were infected with blasticidin-resistant retroviral constructs encoding either GFP or Ras^{V12}. Consistent with earlier findings, ARF protein is increased in response to Ras^{V12} overexpression in the absence of *Dmp1* (Fig. 6A). *Dmp1*$^{-/-}$ MEFs infected with a retrovirus encoding GFP or Ras^{V12} were treated with 1 mM puromycin for 3 h (45, 49). Cytosolic ribosomes were isolated by sucrose gradient centrifugation from equal numbers of cells, and ribosomal subunits were monitored as before (Fig. 6B). *Dmp1*$^{-/-}$ MEFs treated with puromycin

Downloaded from http://mcb.asm.org/ on April 16, 2013 by Washington University in St. Louis

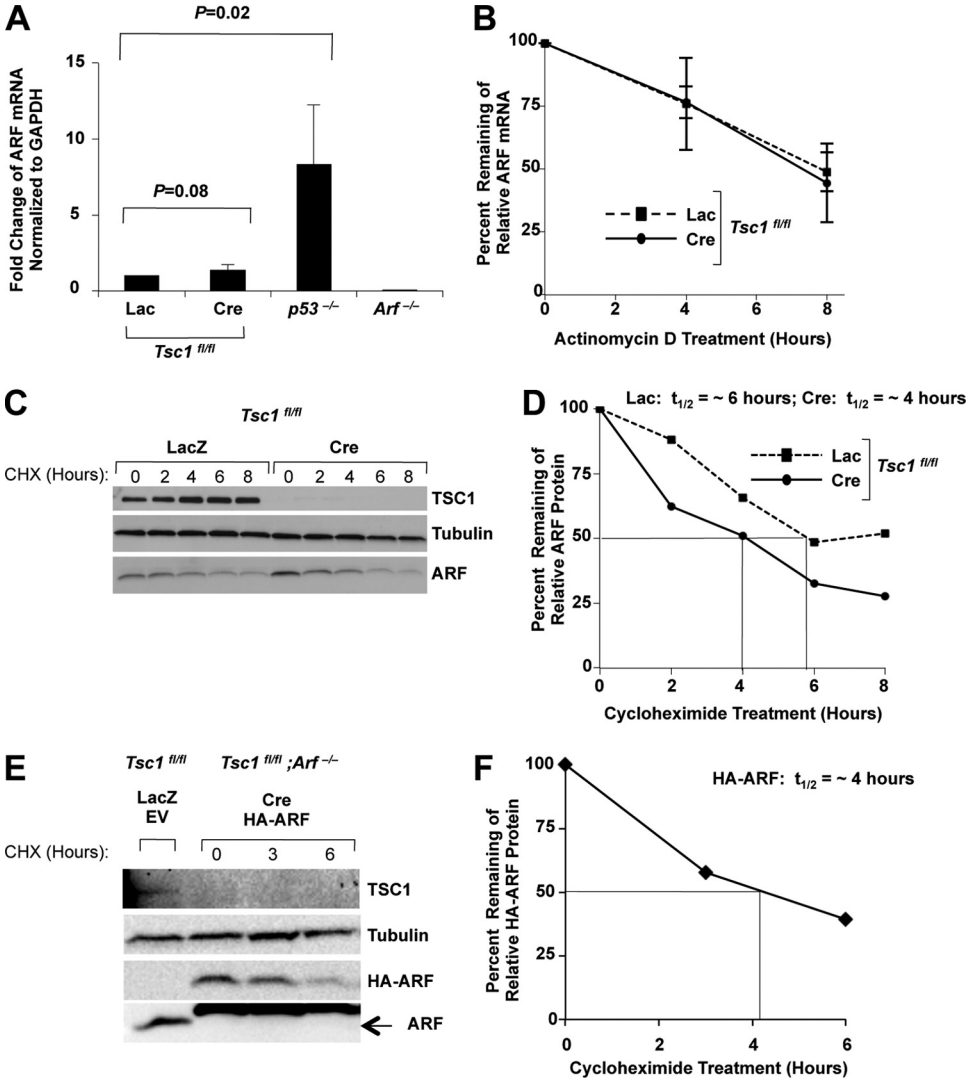

FIG 4 Loss of *Tsc1* does not induce ARF through transcription, mRNA stability, or protein stability. (A to D) *Tsc1*$^{flox/flox}$ MEFs were infected with adenoviruses encoding β-galactosidase (LacZ) or Cre recombinase and were harvested at 9 days postinfection for gene expression analysis. First-strand cDNA was synthesized from isolated total RNA, and quantitative RT-PCR analysis was performed. *Arf* mRNA levels were normalized to *Gadph* mRNA levels (A). Fold change was calculated using the $\Delta\Delta C_T$ method. Data are the mean ± standard deviation of three independent experiments, and *P* values were calculated using the Student *t* test. (B) Cells were treated with 4 μg/ml actinomycin D for the indicated time points. First-strand cDNA was synthesized from isolated total RNA, and quantitative RT-PCR analysis was performed as described for panel A. Data are represented as percent remaining of *Arf* mRNA normalized to *Gadph* levels relative to the respective zero hour treatment. (C) Cells were treated with 25 μg/ml cycloheximide (CHX) and were harvested at the indicated time points for Western blot analysis. Representative immunoblots are depicted. Densitometry quantification of immunoblots from panel C is depicted in panel D. Data are represented as percent remaining of ARF protein levels normalized to tubulin protein levels relative to the respective 0-h treatment. (E and F) *Tsc1*$^{flox/flox}$ or *Tsc1*$^{flox/flox}$; *Arf*$^{-/-}$ MEFs were infected with adenoviruses encoding β-galactosidase (LacZ) or Cre recombinase and retroviruses encoding an empty vector control or HA-ARF, as indicated. Cells were treated with 25 μg/ml cycloheximide and were harvested at the indicated time points for Western blot analysis. Representative immunoblots are depicted. In panel F, densitometry quantification of the immunoblots shown in panel E is depicted for cells infected with a retrovirus encoding HA-ARF. Data are represented as percent remaining of HA-ARF protein normalized to tubulin protein levels relative to the 0-h treatment. $t_{1/2}$, half-life.

and infected with GFP- and Ras^{V12}-encoding retroviruses showed dramatic increases in the amplitude of the 80S peak, along with the complete disappearance of the polysome peaks (Fig. 6B). *Arf* mRNA distribution in fractions was then determined (Fig. 6C and D). *Arf* mRNA distribution in puromycin-treated, GFP-expressing cells mimicked the distribution of *Arf* mRNA in untreated GFP-expressing cells (Fig. 6C). This surprising finding suggests that *Arf* mRNA found on the polysome peaks in these GFP-expressing cells could in fact be "pseudo-polysomes" as opposed to actual polyribosomes (49). In contrast, puromycin treatment released *Arf* mRNA from the polysome peaks in *Dmp1*$^{-/-}$ MEFs infected with Ras^{V12}-encoding retrovirus(Fig. 6D), indicating that *Arf* mRNA transcripts are indeed associating with actively translating polyribosomes in response to oncogenic Ras^{V12} signaling.

To determine whether inhibition of mTORC1 signaling could similarly displace *Arf* mRNA distribution from polysome peaks, *Dmp1*$^{-/-}$ MEFs were transduced with a retrovirus encoding

Downloaded from http://mcb.asm.org/ on April 16, 2013 by Washington University in St. Louis

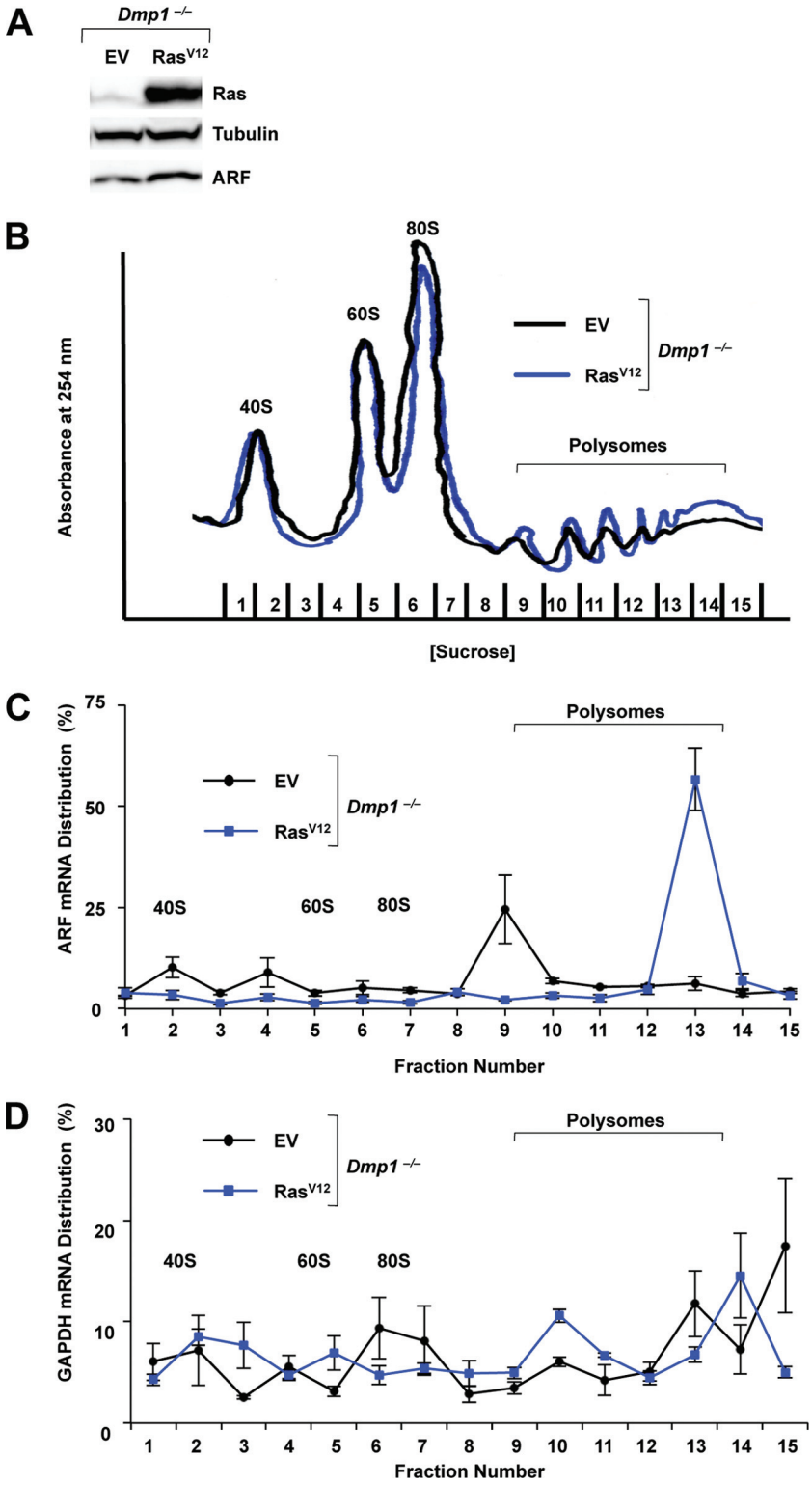

FIG 5 *Arf* mRNA association with actively translating polyribosomes increases from Ras^{V12} signaling in the absence of *Dmp1*. $Dmp1^{-/-}$ MEFs were transduced with retroviruses encoding an empty vector control (EV) or Ras^{V12} and were harvested at 5 days postinfection. Cytosolic extracts from equal number of cells (3×10^6) treated for 5 min with cycloheximide (10 μg/ml) were separated on 7 to 47% sucrose gradients with constant UV monitoring (254 nm). (A) Excess cells were lysed, and separated proteins were immunoblotted for the indicated proteins. (B) A representative graph depicts the A_{254} absorbance of ribosome subunits over increasing sucrose density. (C) Total RNA was isolated from each sucrose gradient fraction, and first-strand cDNA was synthesized for each fraction. Monosome-, disome-, and polysome-associated *Arf* mRNA levels were measured with qRT-PCR and were calculated as a percentage of total *Arf* mRNA collected in all fractions. Data are the mean ± standard error of the mean of three independent experiments. (D) Monosome-, disome-, and polysome-associated *Gapdh* mRNA levels were measured as described for panel C.

Downloaded from http://mcb.asm.org/ on April 16, 2013 by Washington University in St. Louis

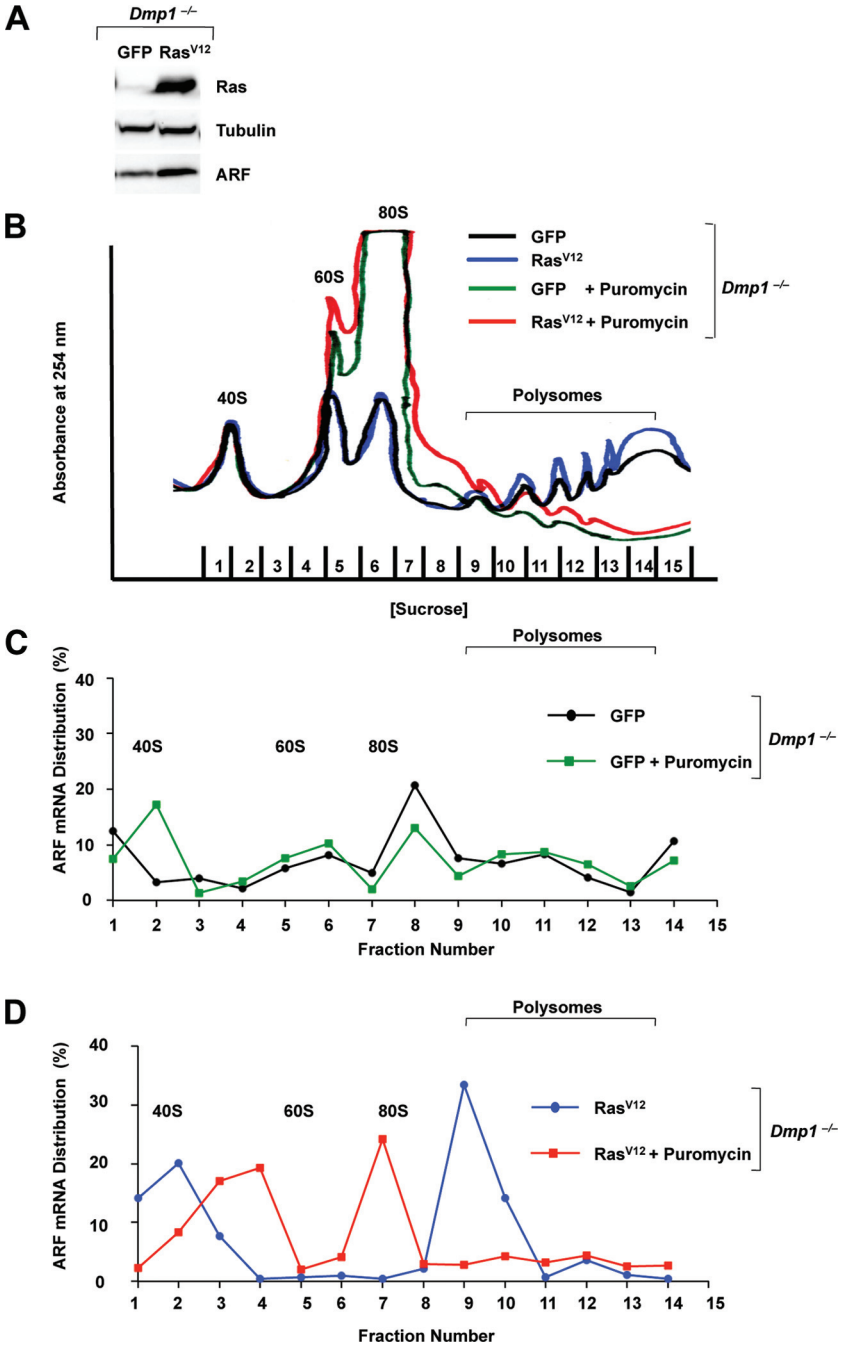

FIG 6 *Arf* mRNA association with actively translating polyribosomes caused by hypergrowth stimuli can be disrupted with puromycin exposure. Retroviruses were generated with pWZL-GFP-IRES-blast or pWZL-Ras^{V12}-IRES-blast. *Dmp1*$^{-/-}$ MEFs were transduced with these retroviruses, and infected cells were analyzed at 5 days postinfection. Cells were treated with 1 mM puromycin for 3 h, and then cytosolic extracts from equal numbers of cells (3×10^6) treated for 5 min with cycloheximide (10 μg/ml) were separated on 7 to 47% sucrose gradients with constant UV monitoring (254 nm). (A) Excess untreated cells were lysed, and separated proteins were immunoblotted for the indicated proteins. (B) A representative graph depicts the A_{254} absorbance of ribosome subunits over increasing sucrose density. (C) Total RNA was isolated from each sucrose gradient fraction, and first-strand cDNA was synthesized for each fraction. Monosome-, disome-, and polysome-associated *Arf* mRNA levels were measured with qRT-PCR and were calculated as a percentage of total *Arf* mRNA collected in all fractions. (D) Monosome-, disome-, and polysome-associated *Arf* mRNA levels were measured as described for panel C.

Ras^{V12} and subsequently treated with rapamycin for 24 h prior to harvesting. Ribosomal subunits were monitored as before (Fig. 7A and B). Although rapamycin did not completely displace *Arf* mRNA from translating polyribosomes, rapamycin treatment did shift *Arf* mRNA away from the heavy polyribosome fractions, where it accumulates in response to Ras^{V12} (Fig. 7C). This finding demonstrates the sensitivity of *Arf* mRNA association with translating polyribosomes to rapamycin exposure. To further interrogate the effects of mTORC1 signaling on the association of *Arf* mRNA with actively translating polyribosomes, *Tsc1*$^{flox/flox}$ MEFs

Downloaded from http://mcb.asm.org/ on April 16, 2013 by Washington University in St. Louis

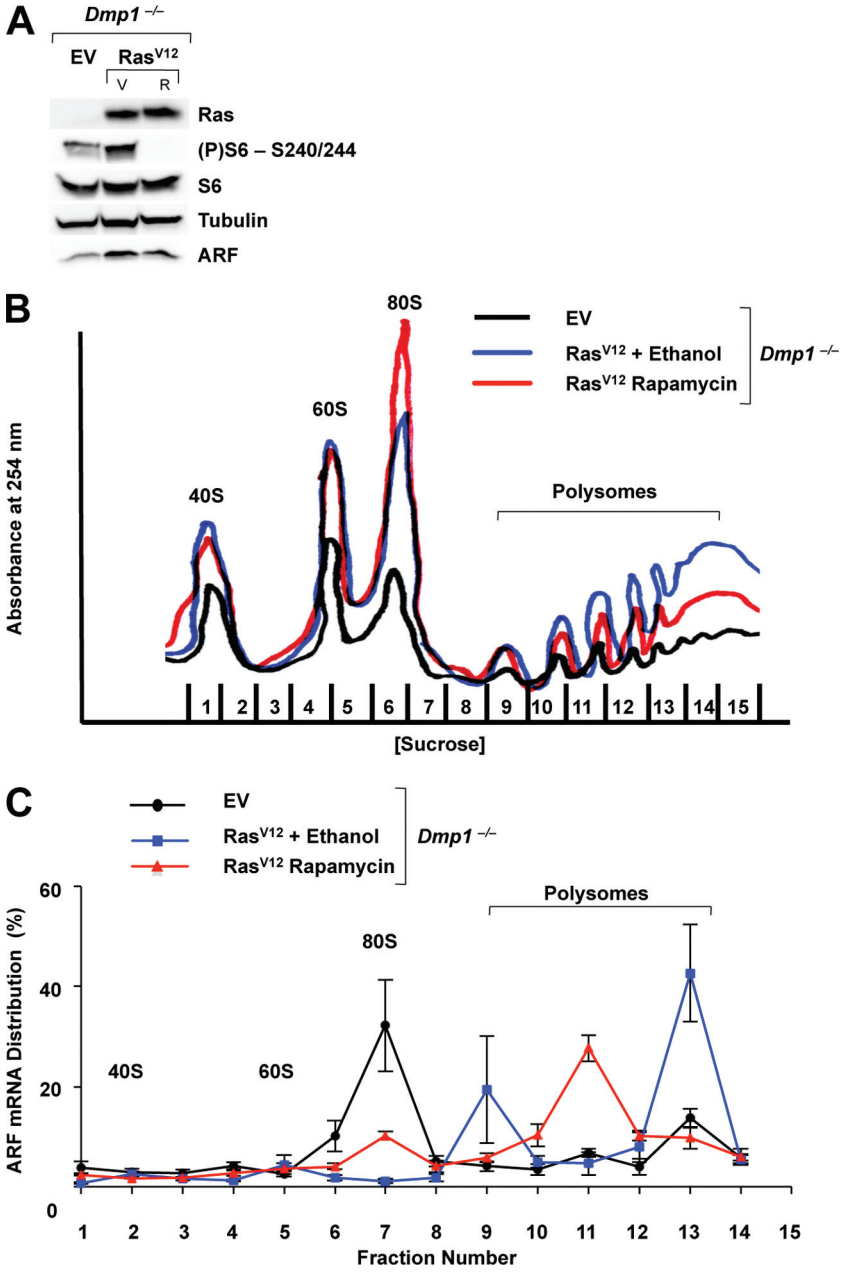

FIG 7 *Arf* mRNA is partially displaced from actively translating polyribosomes by rapamycin exposure. *Dmp1*$^{-/-}$ MEFs were transduced with retroviruses encoding an empty vector control (EV) or Ras^{V12} and were harvested at 5 days postinfection. Cells infected with Ras^{V12}-encoding virus were treated with 100 nM rapamycin (R) or vehicle (V) for 24 h prior to harvesting. Cytosolic extracts from equal numbers of cells (3×10^6) treated for 5 min with cycloheximide (10 μg/ml) were separated on 7 to 47% sucrose gradients with constant UV monitoring (254 nm). (A) Excess cells were lysed, and separated proteins were immunoblotted for the indicated proteins. (B) A representative graph depicts the A_{254} absorbance of ribosome subunits over increasing sucrose density. (C) Total RNA was isolated from each sucrose gradient fraction, and first-strand cDNA was synthesized for each fraction. Monosome-, disome-, and polysome-associated *Arf* mRNA levels were measured with qRT-PCR and were calculated as a percentage of total *Arf* mRNA collected in all fractions. Data are the mean ± standard error of the mean of three independent experiments. (P), phosphorylated.

were infected with Ad-Cre or the Ad-LacZ control and were subjected to ribosome profiling (Fig. 8A and B). We found that more *Arf* mRNA pooled to heavier polyribosome fractions upon the loss of *Tsc1* (Fig. 8C). Taken together, these findings support the hypothesis that ARF is translationally regulated in the presence of hyperactivated Ras/TSC/mTORC1 signaling.

ARF induction activates a p53 response. To determine whether the ARF protein translationally induced from *Tsc1* loss is functional, we assessed several aspects of ARF biology. ARF binds to and sequesters MDM2 in the nucleolus, allowing p53 protein levels to accumulate and become active in the nucleoplasm (53). *Tsc1*$^{flox/flox}$ MEFs infected with Ad-Cre or the Ad-LacZ control were analyzed for MDM2 and ARF colocalization (Fig. 9A and B). In both Ad-Cre- and Ad-LacZ-infected cells, ARF exhibited nu-

Downloaded from http://mcb.asm.org/ on April 16, 2013 by Washington University in St. Louis

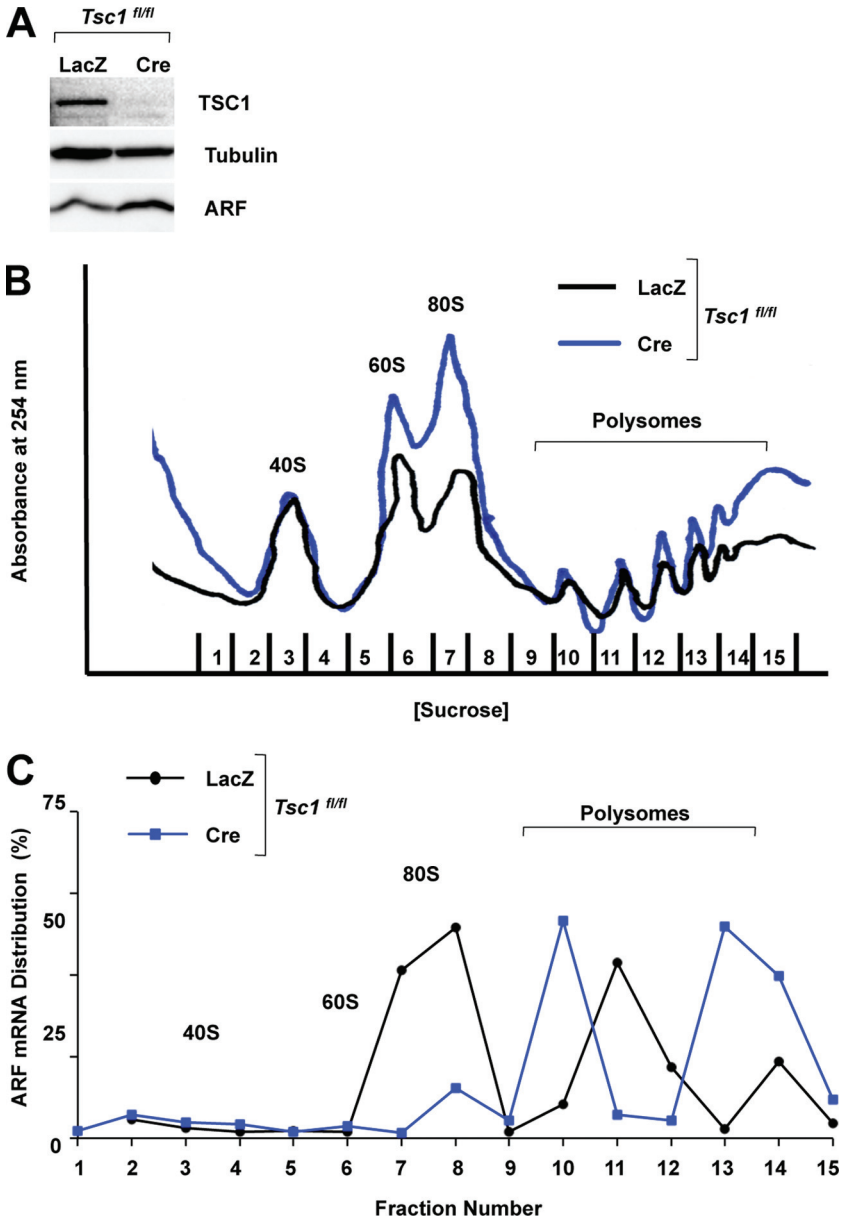

FIG 8 *Arf* mRNA association with actively translating polyribosomes increases from the loss of *Tsc1*. $Tsc1^{flox/flox}$ MEFs were infected with adenoviruses encoding β-galactosidase (LacZ) or Cre recombinase and harvested at 9 days postinfection. Cytosolic extracts from equal numbers of cells (3×10^6) treated for 5 min with cycloheximide (10 μg/ml) were separated on 7 to 47% sucrose gradients with constant UV monitoring (254 nm). (A) Excess cells were lysed, and separated proteins were immunoblotted for the indicated proteins. (B) A representative graph depicts the A_{254} of ribosome subunits over increasing sucrose density. (C) Total RNA was isolated from each sucrose gradient fraction, and first-strand cDNA was synthesized for each fraction. Monosome-, disome-, and polysome-associated *Arf* mRNA levels were measured with qRT-PCR and were calculated as a percentage of total *Arf* mRNA collected in all fractions.

cleolar subcellular localization (Fig. 9A and B). Furthermore, we found that ARF and MDM2 had increased colocalization in nucleoli in Ad-Cre-infected $Tsc1^{flox/flox}$ MEFs compared to levels in Ad-LacZ-infected cells (Fig. 9A and B). Next, ARF-MDM2 complexes were immunoprecipitated from infected $Tsc1^{flox/flox}$ lysates with a polyclonal antibody recognizing ARF and immunoblotted for MDM2 (Fig. 9C). Induced ARF protein displayed strong binding to MDM2 in Ad-Cre-infected $Tsc1^{flox/flox}$ MEFs (Fig. 9C). Collectively, these data suggest that the loss of *Tsc1* increases ARF protein expression and its ability to bind to and relocalize MDM2 into the nucleolus.

To examine whether this increase in ARF-MDM2 binding resulted in p53 activation, infected $Tsc1^{flox/flox}$ lysates were probed for p53 and two of its downstream target genes, p21 and MDM2. p53, MDM2, and p21 displayed 2-fold increases in protein levels following *Tsc1* loss (Fig. 9D). Similarly, the induction of p53, p21, and MDM2 was completely abrogated in Ad-Cre-infected $Tsc1^{flox/flox}$; $Arf^{-/-}$ MEFs (Fig. 9D), implying that ARF is necessary for facilitating the induction of p53 and its target genes in response to *Tsc1* loss. Alternatively, infected $Tsc1^{flox/flox}$ MEFs were treated with rapamycin 24 h prior to harvesting. The induction of ARF caused by the loss of *Tsc1* was disrupted due to rapamycin expo-

Downloaded from http://mcb.asm.org/ on April 16, 2013 by Washington University in St. Louis

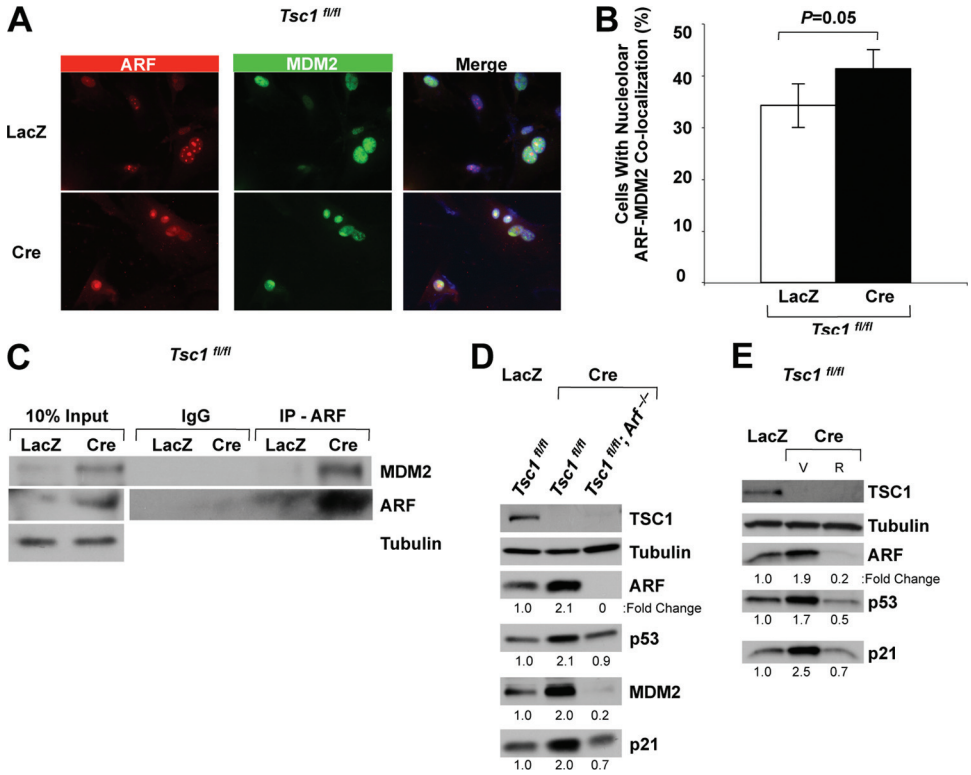

FIG 9 ARF induced from hypergrowth stimuli activates a p53 response. *Tsc1*$^{flox/flox}$ MEFs were infected with adenoviruses encoding β-galactosidase (LacZ) or Cre recombinase and were harvested at 9 days postinfection for analysis. (A) Infected cells were seeded onto coverslips, fixed, and stained for indirect immunofluorescence analysis with specific primary antibodies for ARF and MDM2 and for Alexa Fluor 594 and Alexa Fluor 488, respectively. Cells were counterstained for nuclei with SlowFade Gold Antifade mounting reagent with DAPI. (B) Quantification of nucleolar ARF-MDM2 colocalization is depicted from indirect immunofluorescence analysis as described for panel A. Representative data are expressed as the mean ± standard deviation of 50 nuclei counted in triplicate, and *P* values were calculated using the Student *t* test. (C) Lysates from infected cells were immunoprecipitated with a rabbit polyclonal antibody directed against ARF or normal rabbit IgG. Proteins immune complexes were separated, transferred to PVDF membranes, and immunoblotted with the indicated antibodies. (D and E) Infected cells were lysed, and separated proteins were immunoblotted for indicated proteins. Expression fold change over the LacZ control is indicated (D). Ad-Cre-infected cells were treated with 100 nM rapamycin (R) or vehicle (V) control for 24 h prior to harvesting (E).

sure (Fig. 9E), and, consequently, the induction of p53, p21, and MDM2 was similarly abrogated in the absence of ARF induction (Fig. 9E).

ARF/p53 response causes cell cycle arrest. Given that hyperactivation of mTORC1 signaling increases ARF protein expression and that ARF induces p53 and its downstream targets, we hypothesized that ARF was responsible for eliciting a cell cycle arrest in response to mTORC1 hyperactivation. To test this, cell proliferation was monitored each day for 6 days. The rate of proliferation of Ad-Cre-infected *Tsc1*$^{flox/flox}$ MEFs was markedly reduced compared to that of Ad-LacZ-infected cells (Fig. 10A and B), consistent with the ARF-dependent activation of p53 (Fig. 9). However, this proliferation defect was absent upon *Tsc1* loss in cells also lacking *Arf* (Fig. 10B). Of note, changes in cell death (Fig. 10C) do not account for the decrease in total cell number observed in Ad-Cre-infected *Tsc1*$^{flox/flox}$ cells. Additionally, BrdU incorporation was measured (Fig. 10D). As seen before, Ad-Cre-infected *Tsc1*$^{flox/flox}$ MEFs exhibited a significant decrease in BrdU incorporation compared to Ad-LacZ-infected cells (Fig. 10D). Notably, this decrease was completely rescued in the absence of *Arf* (Fig. 10D). Furthermore, acute knockdown of TSC1 reduced BrdU incorporation in wild-type MEFs (Fig. 10E), corresponding with their dose-dependent induction of ARF protein (Fig. 3C).

Since ARF serves to prevent proliferation in response to loss of *Tsc1*, we hypothesized that removal of ARF would permit cells with hyperactivated mTOR to proliferate long-term without being properly checked. To test this, *Tsc1*$^{flox/flox}$; *Arf*$^{-/-}$ MEFs were infected with Ad-Cre or the Ad-LacZ control and subjected to long-term focus formation analysis (Fig. 10F and G). Significantly more foci formed by hyperactivating mTOR signaling in *Arf*$^{-/-}$ cells, and there was an increase in total focus area (Fig. 10H and I). Taken together, this indicates that ARF keeps cell proliferation in check by responding to heightened levels of mTORC1 signaling to induce cell cycle arrest.

Translationally regulated ARF represses transformation and tumorigenesis. The observation that ARF induces a p53-mediated cell cycle arrest in response to hypergrowth cues emanating from hyperactivation of mTORC1 signal transduction led us to test the hypothesis that ARF could inhibit transformation and tumorigenesis in response to these hypergrowth cues. We infected *Dmp1*$^{-/-}$ MEFs or *Arf*$^{-/-}$ MEFs with a retrovirus encoding Ras^{V12} or an empty vector control and assessed anchorage-independent growth in soft agar (Fig. 11A). In MEFs infected with Ras^{V12}-encoding virus, *Dmp1*$^{-/-}$ cells formed significantly fewer colonies in soft agar than *Arf*$^{-/-}$ cells (Fig. 11B). To determine if the induced levels of ARF in *Dmp1*$^{-/-}$ MEFs infected with Ras^{V12}-encoding virus were responsible for the inhibition of colony formation, infected *Dmp1*$^{-/-}$ MEFs were also transduced with virus encoding an siRNA recognizing ARF or a scrambled

Downloaded from http://mcb.asm.org/ on April 16, 2013 by Washington University in St. Louis

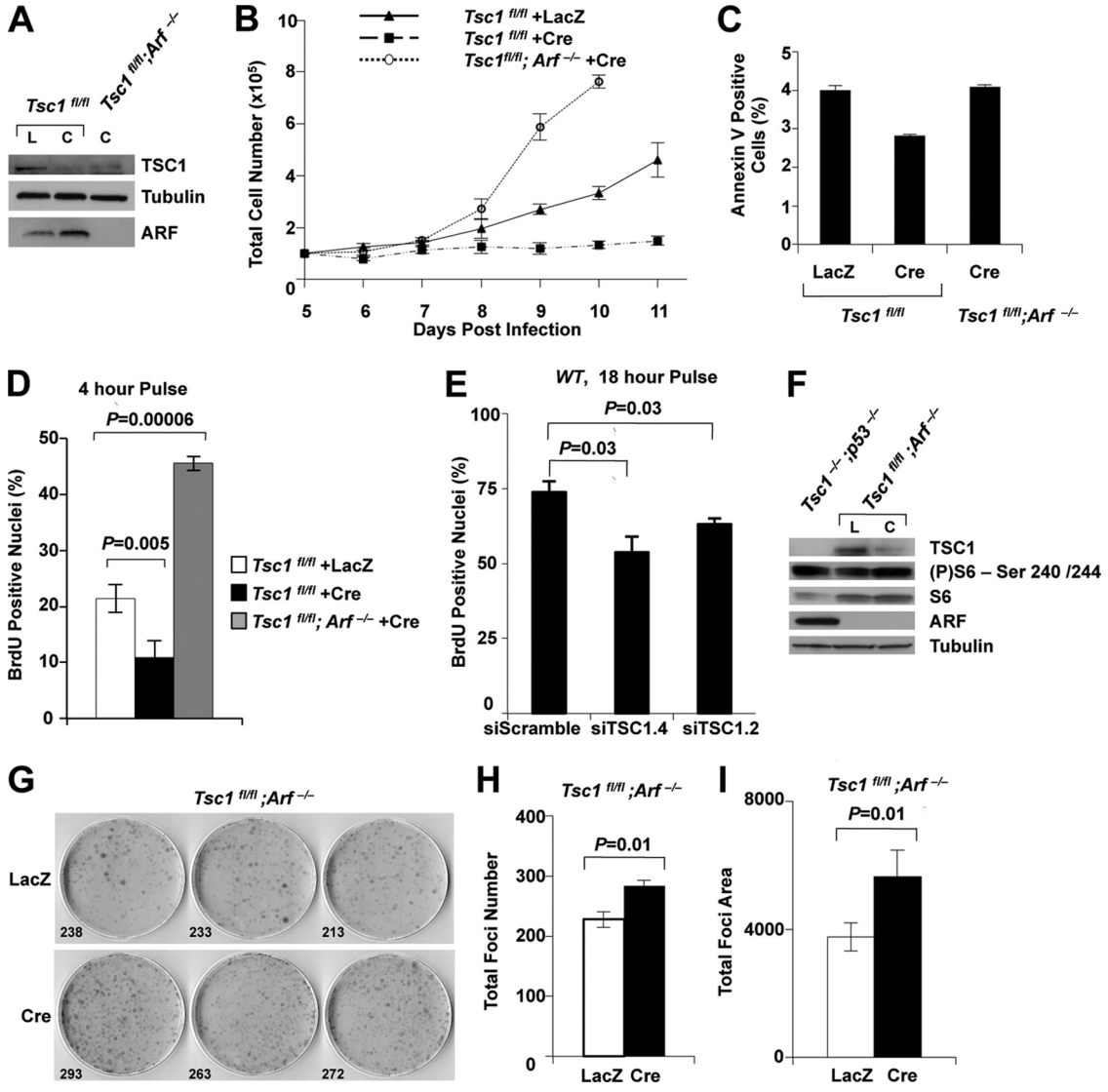

FIG 10 ARF/p53 response induces a cell cycle arrest. (A to D) *Tsc1*$^{flox/flox}$ or *Tsc1*$^{flox/flox}$; *Arf*$^{-/-}$ MEFs were infected with adenoviruses encoding β-galactosidase (LacZ) or Cre recombinase as indicated. Infected cells were lysed, and separated proteins were immunoblotted for indicated proteins (A). A total of 1×10^5 cells were seeded in triplicate for each indicated time point at 5 days postinfection. Cells were then trypsinized and counted with a hemacytometer each day for 6 days thereafter (B). Infected cells were harvested and stained with FITC-annexin V and propidium iodide and subjected to flow cytometry analysis (C). Representative data are depicted as the mean ± standard deviation of 10,000 events performed in triplicate. (D) Infected cells were seeded on coverslips at 9 days postinfection. On day 10 postinfection, cells were pulsed with BrdU for 4 h. Indirect immunofluorescence analysis was used to score BrdU incorporation. Representative data are expressed as the mean ± standard deviation of 50 nuclei counted in triplicate, and *P* values were calculated using the Student *t* test. (E) Wild-type MEFs were infected with lentiviruses encoding short hairpins against *Tsc1* or the siScramble control and were seeded on coverslips at 7 days postinfection for BrdU incorporation. Cells were pulsed with BrdU for 18 h, and analysis was performed as described for panel D. (F to I) *Tsc1*$^{flox/flox}$; *Arf*$^{-/-}$ MEFs were infected with adenoviruses encoding β-galactosidase (LacZ [L]) or Cre recombinase (C) as indicated. A total of 5×10^3 cells were seeded in triplicate onto 10-cm^2 dishes for focus formation analysis. Infected cells were lysed, and separated proteins were immunoblotted for the indicated proteins (F). Cells were grown for 14 days in complete medium and were fixed and stained with Giemsa (G). Panels H and I show, respectively, the quantification of the total number of foci and total focus area of representative images from panel G. (P), phosphorylatd.

control. Knockdown of ARF restored the ability of *Dmp1*$^{-/-}$ MEFs infected with Ras^{V12}-encoding virus to form colonies in soft agar, thereby phenocopying the colony-forming potential of infected *Arf*$^{-/-}$ MEFs (Fig. 11B). No dramatic changes in apoptotic cell death were observed, suggesting that changes in cell death do not account for the differences observed in colony formation (Fig. 11C).

To determine whether translationally regulated ARF could repress tumorigenesis in an allograft model, we assessed tumor formation and burden of *Dmp1*$^{-/-}$ or *Arf*$^{-/-}$ MEFs infected with Ras^{V12}-encoding virus by subcutaneously injecting MEFs into the flanks of nude mice (Fig. 11D and E); as before, *Dmp1*$^{-/-}$ MEFs were also infected with a virus encoding an siRNA recognizing ARF or a scrambled control (siScramble) in order to determine the specificity of ARF's involvement in preventing tumorigenesis (Fig. 11E, inset). Strikingly, tumor onset and growth were markedly reduced in mice injected with *Dmp1*$^{-/-}$ MEFs infected with siScramble-encoding virus compared to *Arf*$^{-/-}$ MEFs (Fig. 11D and E). Furthermore, acute

Downloaded from http://mcb.asm.org/ on April 16, 2013 by Washington University in St. Louis

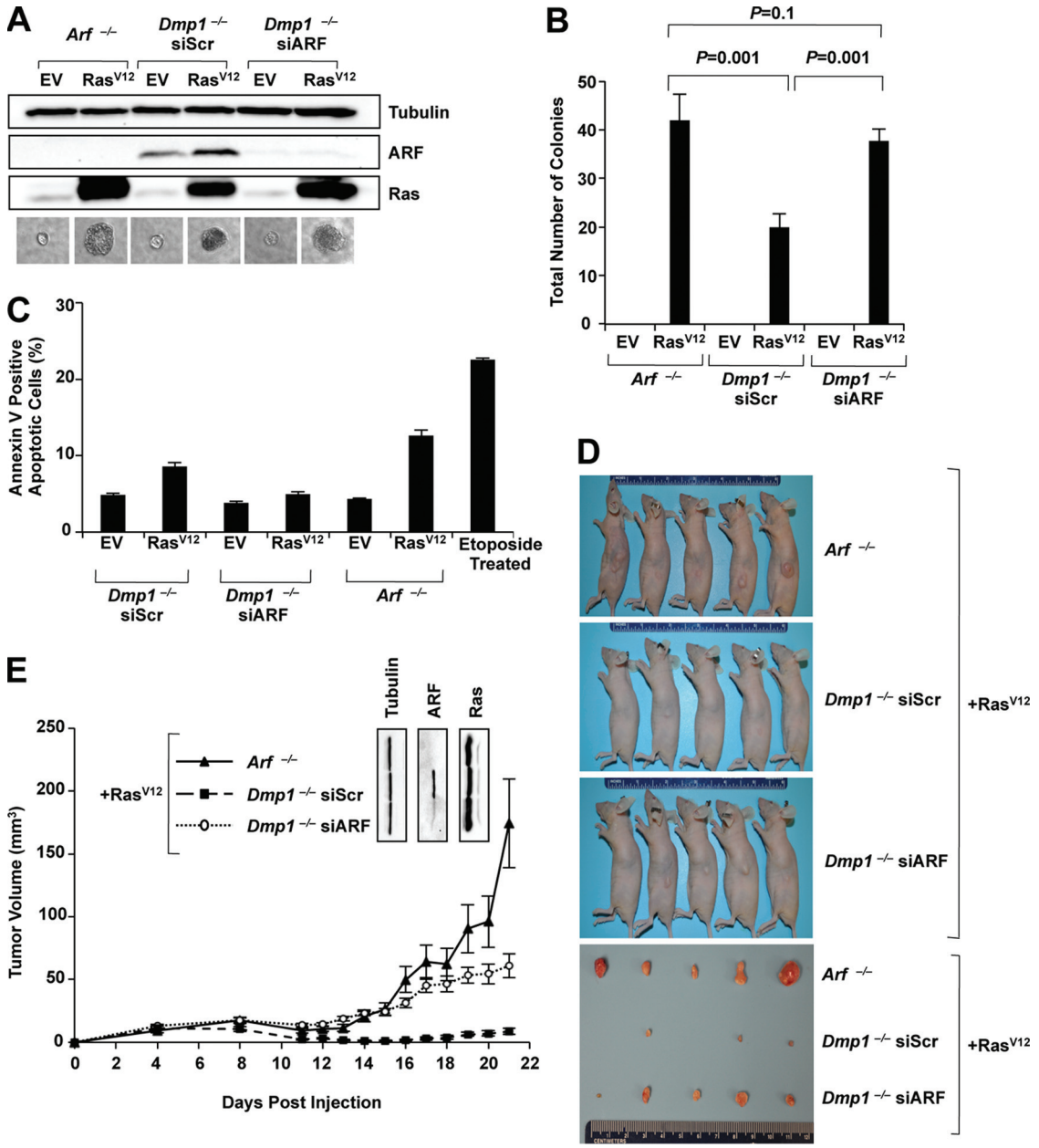

FIG 11 ARF induced from hypergrowth cues can repress oncogenic transformation. $Arf^{-/-}$ or $Dmp1^{-/-}$ MEFs were infected with lentivirus encoding an empty vector control or Ras^{V12}. $Dmp1^{-/-}$ MEFs were also infected with lentiviruses encoding short hairpin against *Arf* or the siScramble control, as indicated. (A and B) A total of 1×10^3 cells were seeded in triplicate in medium containing soft agar and were assessed for colony formation 21 days later. (A) Infected cells were lysed, and separated proteins were immunoblotted for indicated proteins. Representative images of colonies are also depicted. (B) Quantification of the number of colonies. Representative data are expressed as the mean ± standard deviation, and *P* values were calculated using the Student *t* test. (C) Infected cells were harvested and stained with FITC-annexin V and propidium iodide and subjected to flow cytometry analysis. Representative data are expressed as the mean ± standard deviation of 10,000 events performed in triplicate. (D and E) A total of 2×10^6 cells infected with lentivirus encoding Ras^{V12} were subcutaneously injected into the left flank of athymic nude mice. Five mice were injected per condition, such that each mouse received one injection site. (D) Images of mice and excised tumors are depicted. (E) Tumor diameter was measured in two planes with a digital caliper on successive days postinjection. Tumor volume is expressed as the mean ± standard error of the mean. Excess infected cells from the day of injection were lysed, and separated proteins were immunoblotted for indicated proteins (inset).

knockdown of ARF in $Dmp1^{-/-}$ MEFs restored the tumorigenic potential of these cells, partially phenocopying the tumor burden observed in $Arf^{-/-}$ MEFs infected with Ras^{V12}-encoding virus (Fig. 11D and E). Collectively, these data support the model that ARF acts as a critical checkpoint against hypergrowth stimuli and that in response to these stimuli, ARF can repress cellular transformation (Fig. 12).

DISCUSSION

ARF is a key tumor suppressor responsible for safeguarding the cell against oncogenic stimuli. While it has long been appreciated that ARF can inhibit cell cycle progression, both through p53-dependent and p53-independent mechanisms, the context of stimuli to which ARF responds has predominantly been categorized as hyperproliferative cues. Our results now demonstrate that

Downloaded from http://mcb.asm.org/ on April 16, 2013 by Washington University in St. Louis

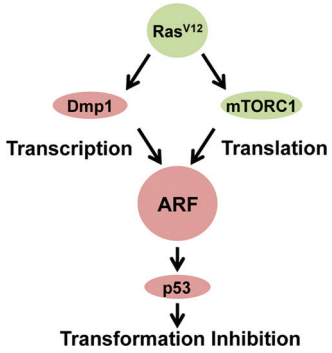

FIG 12 Model. Hypergrowth stimuli emanating from hyperactivation of the mTORC1 pathway induce an ARF checkpoint through a novel translational mechanism. In response to these oncogenic cues, ARF can activate a p53-mediated cell cycle arrest that represses cellular transformation.

ARF has a novel and important role sensing unwarranted hypergrowth stimuli, such as those emanating from robust activation of the mTORC1 signaling pathway. Given that cellular growth and proliferation are in fact two distinct biological processes, albeit highly integrated, we envision a broader range of oncogenic stimuli to which ARF can respond in its antitumorigenic efforts. Since oncogenic stimuli provide the selective pressure for the outgrowth of cancer cells that evade ARF tumor suppression (50), it is important to better understand the array of oncogenic stimuli that are susceptible to ARF tumor surveillance.

In agreement with other groups, we observed that ARF is still capable of responding to Ras^{V12} without transcriptional induction of *Arf* mRNAs by Dmp1. We found that the mTORC1 pathway regulates ARF protein levels through a novel translational mechanism; *Arf* mRNA showed enhanced association with actively translating polyribosomes in response to Ras^{V12} and *Tsc1* loss. ARF induced from *Tsc1* loss facilitated p53 pathway activation and cell cycle arrest. Furthermore, translationally regulated ARF protein repressed anchorage-independent colony formation in soft agar and tumor burden in an allograft model. Therefore, we propose that the cell utilizes this ARF checkpoint as a means to keep excessive progrowth cues under scrutiny.

Of note, *Tsc1*$^{-/-}$ MEFs have been reported to display a lower proliferative rate than *Tsc1*$^{+/-}$ or *Tsc1*$^{+/+}$ MEFs (26). Also, Zhang et al. have shown that primary *Tsc2*$^{-/-}$ MEFs display early senescence in conjunction with a higher expression of p21 (55). Our data suggest that this increase in p21 and the resultant decrease in proliferation could be facilitated in part by the translational ARF induction that ensues from the activation of mTORC1; we observed that p21 induction was abrogated upon the removal of *Arf* in *Tsc1*$^{-/-}$ cells and that loss of *Arf* rescued the proliferation defect observed in cells lacking *Tsc1*.

We envisage collaboration between the Ras/TSC/mTORC1 and the Ras/Dmp1 pathways which together coordinate ARF induction from oncogenic Ras^{V12} overexpression. The involvement of the mTORC1 pathway could explain why Ras^{V12}-mediated ARF induction is compromised, but not completely lost, in a *Dmp1*$^{-/-}$ setting. Given the absolute necessity for cancer cells to bypass ARF's checkpoint against oncogenic stimuli, it is not surprising that multiple regulatory mechanisms would allow ARF to sense as many oncogenic cues as possible.

Deregulation of the members of the mTOR pathway is implicated in the mechanism driving hamartoma-forming diseases. Tuberous sclerosis complex is characterized by the potential for hamartoma formation in a wide spectrum of organs (14). Loss or reduction in function of the TSC1-TSC2 protein complex and the resulting constitutive mTOR signaling are the contributing factors for this disease (6). Our finding that loss of *Tsc1* induces an ARF response could give some insight as to why benign hamartomas, as opposed to more aggressive neoplastic tumors, arise in this disease. It is possible that the ARF growth checkpoint could play a putative role in repressing the proliferation of hamartoma-forming cells, thereby inhibiting their progression to a more aggressive neoplastic tumor; these hypotheses would need to be formally tested. It is of note that analysis of pleomorphic xanthoastrocytoma (PXA), a rare astrocytic tumor in the cerebral hemispheres of children and young adults, was reported to have homozygous deletion of the *CDKN2A/p14*^{Arf} and *CDKN2B* loci as well as reduced *Tsc1* mRNA expression as defining molecular alterations (54). This finding suggests that concomitant loss of *Tsc1* and *Arf* can contribute to the mechanisms driving tumorigenesis.

In the current study, we have described the involvement of the mTORC1 pathway in the regulation of the ARF tumor suppressor via a translational mechanism. It has been readily shown that mTORC1 signaling can induce the selective translation of specific mRNA targets. One such example is the stimulation of p53 translation that occurs upon the loss of *Tsc1* in response to stress conditions (27). It was shown that mTOR can regulate p53 protein synthesis and that hyperactivation of the mTOR pathway can increase sensitivity to DNA damage and energy starvation. In fact, other reports have further elucidated potential mechanisms by which p53 can be translationally regulated (5, 47). Additionally, mTORC1 signaling has been reported to specifically modulate the translation of myeloid cell leukemia sequence 1 (Mcl-1) (32). Loss of *Tsc2* in Eμ-Myc cells increases the translation of Mcl-1, and this modulation of Mcl-1 by mTORC1 is relevant to the chemosensitivity of these tumors. Also, mTORC1 signal transduction modulates the translation of nucleophosmin through a mechanism mediated by FBP1 acting as a regulatory RNA binding protein (33, 35). Here, we show that ARF is another translationally regulated gene product as *Arf* mRNA has enhanced association with actively translating polyribosomes in response to enhanced mTORC1 signal transduction. Translational control of ARF, as well as of these other translationally regulated mRNAs, can serve as a versatile and robust mode of regulation for essential cellular functions.

Further elucidation of the molecular mechanism driving ARF's responsiveness to mTORC1 signaling is of great significance. The implications include the potential identification of novel downstream players not otherwise thought of in the context of the ARF/p53 regulatory network whose interrogation could potentially open avenues to new cancer therapeutics.

ACKNOWLEDGMENTS

We thank all the members of the Weber lab for their comments and technical assistance. We also thank David Kwiatkowski and Jeffrey Arbeit for the *Tsc1*$^{flox/flox}$ mice, Robert Weinberg for the pWZL-GFP-IRES-blast and pWZL-Ras^{V12}-IRES-blast constructs, and Martine Roussel for the pBabe-puro-Ras^{V12} construct. We are very grateful to David Beebe, Jeffrey Arbeit, Ron Bose, and Fanxin Long for insightful discussions.

A.P.M. was supported by Department of Defense Breast Cancer Research Program award X81XWH-08-BCRP-PREDOC. A.J.S. was sup-

Downloaded from http://mcb.asm.org/ on April 16, 2013 by Washington University in St. Louis

ported by Komen for the Cure grant KG091234. This work was supported by NIH grant CA120436 and an Era of Hope Scholar Award in Breast Cancer Research (BC007304) to J.D.W.

Views and opinions of, and endorsements by, the authors do not reflect those of the U.S. Army or the Department of Defense.

REFERENCES

1. **Apicelli AJ, et al.** 2008. A non-tumor suppressor role for basal p19ARF in maintaining nucleolar structure and function. Mol. Cell. Biol. **28**: 1068–1080.
2. **Azzam ME, Algranati ID.** 1973. Mechanism of puromycin action: fate of ribosomes after release of nascent protein chains from polysomes. Proc. Natl. Acad. Sci. U. S. A. **70**:3866–3869.
3. **Bates S, et al.** 1998. p14ARF links the tumour suppressors RB and p53. Nature **395**:124–125.
4. **Brady SN, Yu Y, Maggi LB, Jr, Weber JD.** 2004. ARF impedes NPM/B23 shuttling in an Mdm2-sensitive tumor suppressor pathway. Mol. Cell. Biol. **24**:9327–9338.
5. **Chen J, Kastan MB.** 2010. 5′-3′-UTR interactions regulate p53 mRNA translation and provide a target for modulating p53 induction after DNA damage. Genes Dev. **24**:2146–2156.
6. **Crino PB, Nathanson KL, Henske EP.** 2006. The tuberous sclerosis complex. New Engl. J. Med. **355**:1345–1356.
7. **Dai Y, Grant S.** 2010. New insights into checkpoint kinase 1 in the DNA damage response signaling network. Clin. Cancer Res. **16**:376–383.
8. **de Stanchina E, et al.** 1998. E1A signaling to p53 involves the p19(ARF) tumor suppressor. Genes Dev. **12**:2434–2442.
9. **Elledge SJ.** 1996. Cell cycle checkpoints: preventing an identity crisis. Science **274**:1664–1672.
10. **Grech G, et al.** 2008. Igbp1 is part of a positive feedback loop in stem cell factor-dependent, selective mRNA translation initiation inhibiting erythroid differentiation. Blood **112**:2750–2760.
11. **Guertin DA, Sabatini DM.** 2007. Defining the role of mTOR in cancer. Cancer Cell **12**:9–22.
12. **Hanahan D, Weinberg RA.** 2011. Hallmarks of cancer: the next generation. Cell **144**:646–674.
13. **Hay N, Sonenberg N.** 2004. Upstream and downstream of mTOR. Genes Dev. **18**:1926–1945.
14. **Inoki K, Corradetti MN, Guan KL.** 2005. Dysregulation of the TSC-mTOR pathway in human disease. Nat. Genet. **37**:19–24.
15. **Inoki K, Guan KL.** 2009. Tuberous sclerosis complex, implication from a rare genetic disease to common cancer treatment. Hum. Mol. Genet. **18**: R94–100.
16. **Inoue K, Mallakin A, Frazier DP.** 2007. Dmp1 and tumor suppression. Oncogene **26**:4329–4335.
17. **Inoue K, Roussel MF, Sherr CJ.** 1999. Induction of ARF tumor suppressor gene expression and cell cycle arrest by transcription factor DMP1. Proc. Natl. Acad. Sci. U. S. A. **96**:3993–3998.
18. **Inoue K, et al.** 2000. Disruption of the ARF transcriptional activator DMP1 facilitates cell immortalization, Ras transformation, and tumorigenesis. Genes Dev. **14**:1797–1809.
19. **Inoue K, Zindy F, Randle DH, Rehg JE, Sherr CJ.** 2001. Dmp1 is haplo-insufficient for tumor suppression and modifies the frequencies of Arf and p53 mutations in Myc-induced lymphomas. Genes Dev. **15**: 2934–2939.
20. **Kamijo T, Bodner S, van de Kamp E, Randle DH, Sherr CJ.** 1999. Tumor spectrum in ARF-deficient mice. Cancer Res. **59**:2217–2222.
21. **Kamijo T, et al.** 1997. Tumor suppression at the mouse INK4a locus mediated by the alternative reading frame product p19ARF. Cell **91**: 649–659.
22. **Kastan MB, Bartek J.** 2004. Cell-cycle checkpoints and cancer. Nature **432**:316–323.
23. **Kladney RD, et al.** 2010. Tuberous sclerosis complex 1: an epithelial tumor suppressor essential to prevent spontaneous prostate cancer in aged mice. Cancer Res. **70**:8937–8947.
24. **Knaup KX, et al.** 2009. Mutual regulation of hypoxia-inducible factor and mammalian target of rapamycin as a function of oxygen availability. Mol. Cancer Res. **7**:88–98.
25. **Kuo ML, den Besten W, Bertwistle D, Roussel MF, Sherr CJ.** 2004. N-terminal polyubiquitination and degradation of the Arf tumor suppressor. Genes Dev. **18**:1862–1874.
26. **Kwiatkowski DJ, et al.** 2002. A mouse model of TSC1 reveals sex-dependent lethality from liver hemangiomas, and up-regulation of p70S6 kinase activity in Tsc1 null cells. Hum. Mol. Genet. **11**:525–534.
27. **Lee CH, et al.** 2007. Constitutive mTOR activation in TSC mutants sensitizes cells to energy starvation and genomic damage via p53. EMBO J. **26**:4812–4823.
28. **Livak KJ, Schmittgen TD.** 2001. Analysis of relative gene expression data using real-time quantitative PCR and the $2^{-\Delta\Delta CT}$ method. Methods **25**: 402–408.
29. **Ma XM, Blenis J.** 2009. Molecular mechanisms of mTOR-mediated translational control. Nat. Rev. Mol. Cell Biol. **10**:307–318.
30. Reference deleted.
31. Reference deleted.
32. **Mills JR, et al.** 2008. mTORC1 promotes survival through translational control of Mcl-1. Proc. Natl. Acad. Sci. U. S. A. **105**:10853–10858.
33. **Olanich ME, Moss BL, Piwnica-Worms D, Townsend RR, Weber JD.** 2011. Identification of FUSE-binding protein 1 as a regulatory mRNA-binding protein that represses nucleophosmin translation. Oncogene **30**: 77–86.
34. **Palmero I, Pantoja C, Serrano M.** 1998. p19ARF links the tumour suppressor p53 to Ras. Nature **395**:125–126.
35. **Pelletier CL, et al.** 2007. TSC1 sets the rate of ribosome export and protein synthesis through nucleophosmin translation. Cancer Res. **67**:1609–1617.
36. **Proud CG.** 2007. Signalling to translation: how signal transduction pathways control the protein synthetic machinery. Biochem. J. **403**:217–234.
37. **Quelle DE, Zindy F, Ashmun RA, Sherr CJ.** 1995. Alternative reading frames of the INK4a tumor suppressor gene encode two unrelated proteins capable of inducing cell cycle arrest. Cell **83**:993–1000.
38. **Radfar A, Unnikrishnan I, Lee HW, DePinho RA, Rosenberg N.** 1998. p19(Arf) induces p53-dependent apoptosis during abelson virus-mediated pre-B cell transformation. Proc. Natl. Acad. Sci. U. S. A. **95**: 13194–13199.
39. **Roussel MF, Theodoras AM, Pagano M, Sherr CJ.** 1995. Rescue of defective mitogenic signaling by D-type cyclins. Proc. Natl. Acad. Sci. U. S. A. **92**:6837–6841.
40. **Saporita AJ, Maggi LB Jr, Apicelli AJ, Weber JD.** 2007. Therapeutic targets in the ARF tumor suppressor pathway. Curr. Med. Chem. **14**: 1815–1827.
41. **Shaw RJ, Cantley LC.** 2006. Ras, PI(3)K and mTOR signalling controls tumour cell growth. Nature **441**:424–430.
42. **Sherr CJ.** 2006. Divorcing ARF and p53: an unsettled case. Nat. Rev. Cancer **6**:663–673.
43. **Spriggs KA, Bushell M, Willis AE.** 2010. Translational regulation of gene expression during conditions of cell stress. Mol. Cell **40**:228–237.
44. **Sreeramaneni R, Chaudhry A, McMahon M, Sherr CJ, Inoue K.** 2005. Ras-Raf-Arf signaling critically depends on the Dmp1 transcription factor. Mol. Cell. Biol. **25**:220–232.
45. **Stefani G, Fraser CE, Darnell JC, Darnell RB.** 2004. Fragile X mental retardation protein is associated with translating polyribosomes in neuronal cells. J. Neurosci. **24**:7272–7276.
46. **Strezoska Z, Pestov DG, Lau LF.** 2000. Bop1 is a mouse WD40 repeat nucleolar protein involved in 28S and 5.8S RRNA processing and 60S ribosome biogenesis. Mol. Cell. Biol. **20**:5516–5528.
47. **Takagi M, Absalon MJ, McLure KG, Kastan MB.** 2005. Regulation of p53 translation and induction after DNA damage by ribosomal protein L26 and nucleolin. Cell **123**:49–63.
48. **Tee AR, et al.** 2002. Tuberous sclerosis complex-1 and -2 gene products function together to inhibit mammalian target of rapamycin (mTOR)-mediated downstream signaling. Proc. Natl. Acad. Sci. U. S. A. **99**: 13571–13576.
49. **Thermann R, Hentze MW.** 2007. Drosophila miR2 induces pseudo-polysomes and inhibits translation initiation. Nature **447**:875–878.
50. **Volanakis EJ, Sherr CJ.** 2010. Developmental strategies for evasion of Arf tumor suppression. Cell Cycle **9**:14–15.
51. **Watnick RS, Cheng YN, Rangarajan A, Ince TA, Weinberg RA.** 2003. Ras modulates Myc activity to repress thrombospondin-1 expression and increase tumor angiogenesis. Cancer Cell **3**:219–231.
52. **Weber JD, et al.** 2000. Cooperative signals governing ARF-mdm2 interaction and nucleolar localization of the complex. Mol. Cell. Biol. **20**: 2517–2528.

Downloaded from http://mcb.asm.org/ on April 16, 2013 by Washington University in St. Louis

53. **Weber JD, Taylor LJ, Roussel MF, Sherr CJ, Bar-Sagi D.** 1999. Nucleolar Arf sequesters Mdm2 and activates p53. Nat. Cell Biol. **1**:20–26.
54. **Weber RG, et al.** 2007. Frequent loss of chromosome 9, homozygous CDKN2A/p14(ARF)/CDKN2B deletion and low TSC1 mRNA expression in pleomorphic xanthoastrocytomas. Oncogene **26**:1088–1097.
55. **Zhang H, et al.** 2003. Loss of Tsc1/Tsc2 activates mTOR and disrupts PI3K-Akt signaling through downregulation of PDGFR. J. Clin. Invest. **112**:1223–1233.
56. **Zindy F, et al.** 1998. Myc signaling via the ARF tumor suppressor regulates p53-dependent apoptosis and immortalization. Genes Dev. **12**:2424–2433.
57. **Zoncu R, Efeyan A, Sabatini DM.** 2011. mTOR: from growth signal integration to cancer, diabetes and ageing. Nat. Rev. Mol. Cell Biol. **12**:21–35.

Downloaded from http://mcb.asm.org/ on April 16, 2013 by Washington University in St. Louis

Oncogene (2013), 1–8
© 2013 Macmillan Publishers Limited All rights reserved 0950-9232/13
www.nature.com/onc

ORIGINAL ARTICLE

The ARF tumor-suppressor controls Drosha translation to prevent Ras-driven transformation

MJ Kuchenreuther[1,2] and JD Weber[1,2,3]

ARF is a multifunctional tumor suppressor that acts as both a sensor of oncogenic stimuli and as a key regulator of ribosome biogenesis. Recently, our group established the DEAD-box RNA helicase and microRNA (miRNA) microprocessor accessory subunit, DDX5, as a critical target of basal ARF function. To identify other molecular targets of ARF, we focused on known interacting proteins of DDX5 in the microprocessor complex. Drosha, the catalytic core of the microprocessor complex, has a critical role in the maturation of specific non-coding RNAs, including miRNAs and ribosomal RNAs (rRNAs). Here, we report that chronic or acute loss of *Arf* enhanced Drosha protein expression. This induction did not involve Drosha mRNA transcription or protein stability but rather relied on the increased translation of existing Drosha mRNAs. Enhanced Drosha expression did not alter global miRNA production but rather modified expression of a subset of miRNAs in the absence of *Arf*. Elevated Drosha protein levels were required to maintain the increased rRNA synthesis and cellular proliferation observed in the absence of *Arf*. *Arf*-deficient cells transformed by oncogenic Ras^{V12} were dependent on increased Drosha expression as Drosha knockdown was sufficient to inhibit Ras-dependent cellular transformation. Thus, we propose that ARF regulates Drosha mRNA translation to prevent aberrant cell proliferation and Ras-dependent transformation.

Oncogene advance online publication, 14 January 2013; doi:10.1038/onc.2012.601

Keywords: ARF; Drosha; translation; tumor suppression; rRNA

INTRODUCTION

Cancer initiation and progression are hallmarked by the loss of regulatory mechanisms that control cellular growth and proliferation. The *CDKN2A* (*Ink4a/Arf*) locus encodes two distinct tumor suppressors, p16INK4a and p19ARF (p14ARF in humans).[1] ARF has classically been regarded as an activator of p53 through its ability to bind and sequester Mdm2, the E3 ubiquitin ligase for p53, in the nucleolus.[2–5] Recently, numerous p53-independent functions have been attributed to ARF,[6] including its regulation of ribosomal RNA (rRNA) synthesis and ribosome biogenesis.[7] ARF accomplishes this, at least in part, through its repressive interaction with the ribosome chaperone nucleophosmin (NPM) thereby limiting steady-state ribosome biogenesis and growth.[1,8–10]

Recently, a nucleolar proteomic screen expanded on the mechanism through which ARF controls rRNA synthesis by identifying a novel relationship between ARF and the DEAD-box RNA helicase, DDX5.[11] Basal ARF proteins restrict DDX5 access to the nucleolus and antagonize the DDX5–NPM interaction. This interference is sufficient to disrupt DDX5's role in rRNA transcription and rRNA processing. An assessment of other proteins that are involved in ribosome biogenesis, especially those that associate with NPM and/or DDX5 could reveal additional modes through which ARF acts as a potent tumor suppressor.

Drosha is a RNase III endonuclease that was originally linked with the processing of rRNAs and is now widely studied in the context of microRNA (miRNA) biogenesis.[12,13] miRNAs represent a class of short, endogenous, non-coding RNAs that control gene expression by inhibiting translation and/or inducing degradation of specific target mRNAs.[14] Similar to rRNAs, most miRNAs initially exist as long primary transcripts (pri-miRNAs) that are processed through a series of enzymatic cleavage steps to generate mature miRNAs.[15–17] Drosha forms two different complexes, a small microprocessor complex that contains only Drosha and DGCR8 and a larger complex that contains accessory proteins, including DDX5.[18,19] Although both complexes are capable of processing pri-miRNAs, only the latter has demonstrated the ability to process pre-rRNAs.[20]

Abnormalities in mature miRNA levels as well as in the expression of miRNA processing enzymes have been linked with various types of disease.[21] Although some studies suggest that there are correlations between decreased Drosha expression and tumor incidence and prognosis, other studies have shown that reducing Drosha expression impairs rRNA processing and cellular proliferation.[22–26] Despite Drosha's apparent link to human diseases, little is known about its regulation. Previous studies have shown that Drosha is stabilized through its protein–protein interaction with DGCR8, but outside of this, no other forms of transcriptional or post-transcriptional regulation are known.[27]

Given ARF's multifaceted involvement in mediating ribosome biogenesis and its newly characterized relationship with DDX5, a component of the Drosha processing complex, we sought to determine whether ARF impacted Drosha. In this report, we show that Drosha is post-transcriptionally regulated in an ARF-dependent manner. We identify Drosha as a unique translational target of the ARF tumor suppressor. Moreover, we show that the

[1]BRIGHT Institute, Washington University School of Medicine, St Louis, MO, USA; [2]Department of Internal Medicine, Division of Molecular Oncology, Washington University School of Medicine, St Louis, MO, USA and [3]Department of Cell Biology, Siteman Cancer Center, Washington University School of Medicine, St Louis, MO, USA. Correspondence: Dr JD Weber, BRIGHT Institute, Department of Internal Medicine, Division of Molecular Oncology, Washington University School of Medicine, 660 South Euclid Avenue, Campus 8069, St Louis, MO 63110, USA.
E-mail: jweber@dom.wustl.edu
Received 15 June 2012; revised 7 September 2012; accepted 7 November 2012

increased Drosha expression in the absence of *Arf* is required for efficient Ras-mediated cell transformation through Drosha's ability to regulate rRNA synthesis and cell proliferation.

RESULTS

Loss of Arf induces Drosha expression

Previous reports have demonstrated that ARF serves as a major regulator of ribosome biogenesis[7] and that this is due, at least in part, to its modulation of DDX5 localization and function.[7,11] Moreover, other studies have established a clear link between DDX5 and Drosha in the processing of double-stranded RNAs, including rRNAs.[18,20] To test whether a relationship exists between Drosha and ARF, we first compared Drosha protein levels using wild-type (WT) and $Arf^{-/-}$ mouse embryonic fibroblasts (MEFs). Higher levels of Drosha protein were observed in cells with genetic ablation of *Arf* exon 1β (Figure 1a, left). We explored this result further by acutely manipulating the expression of ARF using either a lentivirus encoding a short hairpin RNA (shRNA) targeting *Arf* exon 1β, the ARF-specific exon of the *CDKN2A* locus, or an ARF overexpressing retrovirus. Consistent with the previous finding, acute knockdown of basal ARF expression resulted in heightened Drosha expression (Figure 1b). Conversely, ectopic overexpression of ARF lowered Drosha expression (Figure 1c). ARF-mediated regulation of Drosha protein expression was not MEF-specific as similar trends were observed using $Arf^{flox/flox}$ mouse astrocytes infected with adenoviruses encoding Cre recombinase (Figure 1d). The array of genetic techniques used to disrupt ARF activity demonstrates a novel link between these two proteins and warranted a closer examination into the mechanism through which ARF suppresses Drosha.

ARF suppresses the translation of Drosha mRNA

To determine how basal ARF modulates Drosha expression, we assessed different aspects of *Drosha* gene expression in response to ARF manipulation. Despite the increases in Drosha protein expression, no significant changes were observed in Drosha mRNA levels following *Arf* loss, acute ARF knockdown, or ectopic overexpression of ARF as determined by quantitative reverse transcription–PCR (RT-PCR; Figures 1a–d, right; Supplementary Figure S1). Next, we treated WT and $Arf^{-/-}$ MEFs with Actinomycin D to evaluate Drosha mRNA stability and observed similar rates of Drosha mRNA decay in the presence or absence of *Arf* (Figure 2a). Taken together, these data indicate that ARF may post-transcriptionally regulate Drosha expression.

Previous reports identified a positive relationship between Drosha and its microprocessor partner, DGCR8, such that Drosha protein is stabilized when bound to DGCR8.[27] To address potential changes in Drosha protein stability in response to *Arf* loss, Drosha protein expression was measured in WT and $Arf^{-/-}$ MEFs following cycloheximide treatment. The rate of Drosha turnover remained unchanged in the presence or absence of *Arf* despite the fact that we observed significantly more Drosha at the original time of treatment in cells lacking *Arf* (Figures 2b and c). Furthermore, treatment of WT MEFs with the proteosomal inhibitor MG-132 failed to induce Drosha protein levels to those observed in $Arf^{-/-}$ MEFs (Figure 2d). These data suggest that the differences in Drosha protein expression were not caused by altered protein stability that led us to hypothesize that Drosha might be translationally regulated by ARF.

Basal ARF negatively regulates multiple aspects of ribosome biogenesis, including rDNA transcription, rRNA processing, and ribosome nuclear export.[7,9,28–30] Although it is possible that ARF's antagonizing role in these processes may disrupt the global translation of all mRNAs, existing data suggest that select genes may be translationally regulated by ARF.[31] Having ruled out ARF regulation of Drosha transcription, mRNA, and protein stability, we sought to determine the effects of *Arf* loss on the translation of existing Drosha mRNAs. We compared the percentage of Drosha mRNA transcripts associated with actively translating polyribosomes (polysomes) in WT and $Arf^{-/-}$ MEFs. Ribosomes were detected in lysates separated in sucrose gradients by continuous measurement of RNA absorbance (A_{254nm}). Loss of *Arf* enhanced the overall formation of polysomes actively engaged in mRNA translation as previously described (Figure 3b).[9]

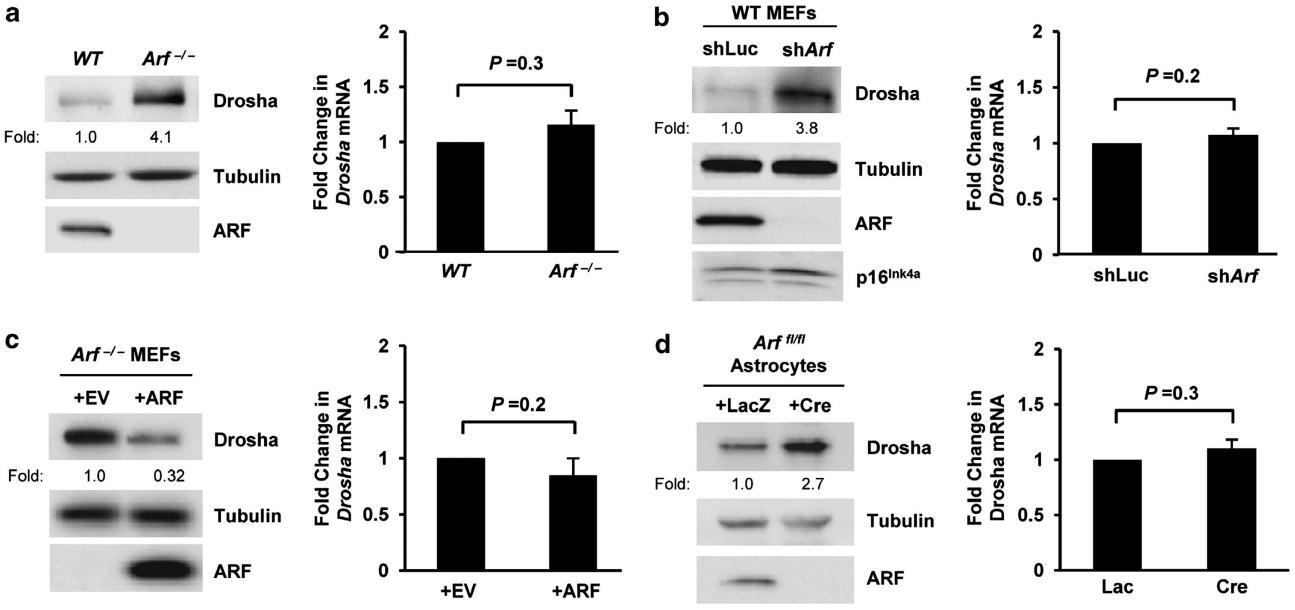

Figure 1. *Arf* negatively regulates Drosha protein expression in a transcriptionally independent manner. (**a**–**d**, left columns) Cells of the indicated genotype were lysed, and separated proteins were immunoblotted for the indicated proteins. $Arf^{flox/flox}$ astrocytes were infected with adenoviruses encoding β-galactosidase (LacZ) or Cre recombinase and were harvested at 5 days post-infection for gene expression analysis. Drosha expression fold change relative to WT or control infected cells is indicated. (**a**–**d**, right columns) Quantitative RT-PCR analysis was performed. Drosha mRNA levels were normalized to *Gapdh* mRNA levels. Fold change was calculated using the $\Delta\Delta C_T$ method. Data are the mean ± s.e.m. ($N = 3$). EV, empty vector.

© 2013 Macmillan Publishers Limited

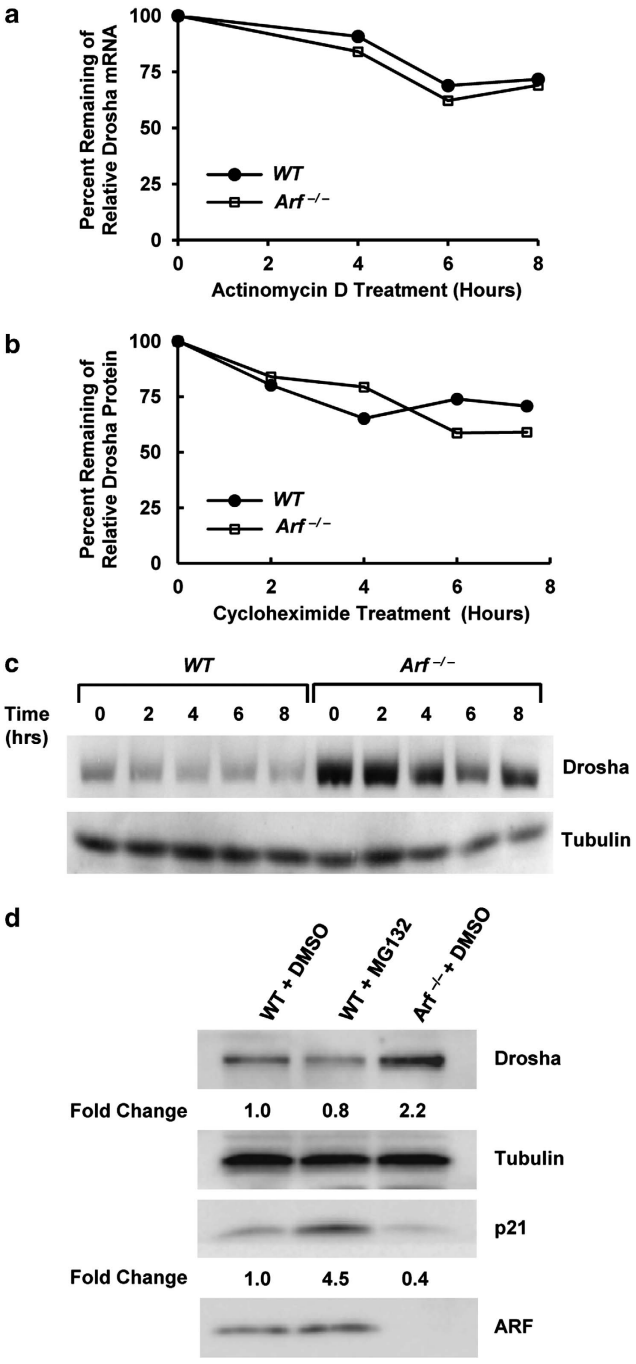

Figure 2. Loss of *Arf* has no effect on Drosha mRNA or protein stability. (**a**) WT and $Arf^{-/-}$ MEFs were treated with 4 μg/ml actinomycin D for the indicated times. Quantitative RT-PCR analysis was performed. Data are represented as the percentage of Drosha mRNA remaining after normalization to *Gapdh* levels at $t = 0$. (**b**, **c**) Cells were treated with 25 μg/ml cycloheximide and were harvested at the indicated times for immunoblot analysis. Densitometry quantification is depicted in panel **b** and data are represented as percentage of remaining Drosha protein levels normalized to γ-tubulin. (**d**) WT MEFs were treated with 40 μM MG-132 or dimethyl sulfoxide (DMSO) for 8 h, and changes in Drosha and p21 (positive control) protein levels were measured.

Quantitative RT-PCR was performed to evaluate the distribution of Drosha mRNA transcripts in monosome-, disome-, and polysome-containing fractions. Drosha mRNAs were abundant in the heavier polysome fractions 11–13 in the absence of *Arf*, shifting away from lighter polysomes in fraction 9 from WT cells (Figure 3c). Importantly, GAPDH (glyceraldehyde 3-phosphate dehydrogenase) mRNA transcript distribution remained unchanged across polysomes (Figure 3d), suggesting that *Arf* loss does not globally affect the translation of every cellular transcript but rather leads to selective mRNA translation.

ARF knockdown alters the expression of only a subset of mature miRNAs despite higher levels of Drosha

To begin to understand the downstream effects of heightened Drosha translation, we sought to compare global miRNA expression patterns upon ARF knockdown. It was previously reported that alterations in known miRNA processing factors failed to alter specific mature miRNA expression, suggesting that the microprocessor itself does not act at a rate-limiting stage of this process in some instances.[32] Nevertheless, in order to measure the impact of ARF knockdown on the miRNA signature of these cells, a Taqman array platform was used to quantify the changes in expression of over 300 mouse-specific miRNAs. The goal was to identify miRNA expression that was significantly altered (>1.4-fold change). Although approximately 50% of all miRNAs examined on the array were either undetectable or present at very low levels ($C_T > 31$) in MEFs, there were 34 miRNAs that underwent significant changes in expression (11 upregulated and 23 downregulated) upon ARF knockdown and subsequent Drosha elevation (Figures 4a and b; Supplementary Figure S2). These findings imply that gains in Drosha expression, at least via loss of ARF, can significantly modify the miRNA landscape within the cell.

Reduced Drosha expression impairs rRNA processing and cellular proliferation in the absence of *Arf*

Similar to its accessory protein partner, DDX5, Drosha has been implicated in rRNA processing.[8,33] As it has been shown that cells lacking *Arf* process rRNA precursors more efficiently than their WT counterparts,[7,9] we hypothesized that reducing Drosha expression in $Arf^{-/-}$ MEFs would impair rRNA processing. Two independent lentiviral shRNA constructs encoding different Drosha-specific shRNAs were used to obtain sufficient knockdown relative to the luciferase control hairpin (Figure 5a). We monitored the processing of the initial 47S pre-rRNA transcript via [methyl-^{3}H]-methionine pulse-chase analysis[7] revealing a delayed accumulation of mature 28S and 18S rRNAs in cells following Drosha knockdown (Figure 5b). In a separate experiment, WT MEFs were infected with a retrovirus encoding Drosha to determine whether elevated Drosha levels could accelerate ribosome biogenesis. Here, we discovered a more rapid accumulation of mature 28S and 18S rRNAs in cells expressing Drosha versus vector-transduced cells (Supplementary Figure S3). Together, these data imply that Drosha is not only required to enhance the processing of nascent rRNA transcripts in the absence of *Arf* but also that the upregulation of Drosha associated with *Arf* loss is sufficient for increased rRNA maturation.

Drosha's role in facilitating rRNA synthesis suggested that it might also be critical for cell proliferation. In cells depleted of Drosha by shRNA knockdown, we observed a dramatic decrease in proliferation rates relative to control-infected cells (Figure 5c). Furthermore, $Arf^{-/-}$ MEFs were dependent on elevated Drosha expression for long-term proliferation; $Arf^{-/-}$ MEFs plated at low density formed fewer colonies following Drosha knockdown after 12 days in culture (Figure 5d). Taken together, our results show that cells lacking *Arf* rely on augmented Drosha expression to maintain aberrant and rapid cellular proliferation rates.

Drosha knockdown promotes apoptosis

To investigate whether the decrease in proliferation was linked to a change in cell viability, we analyzed the cell-cycle distribution of

© 2013 Macmillan Publishers Limited

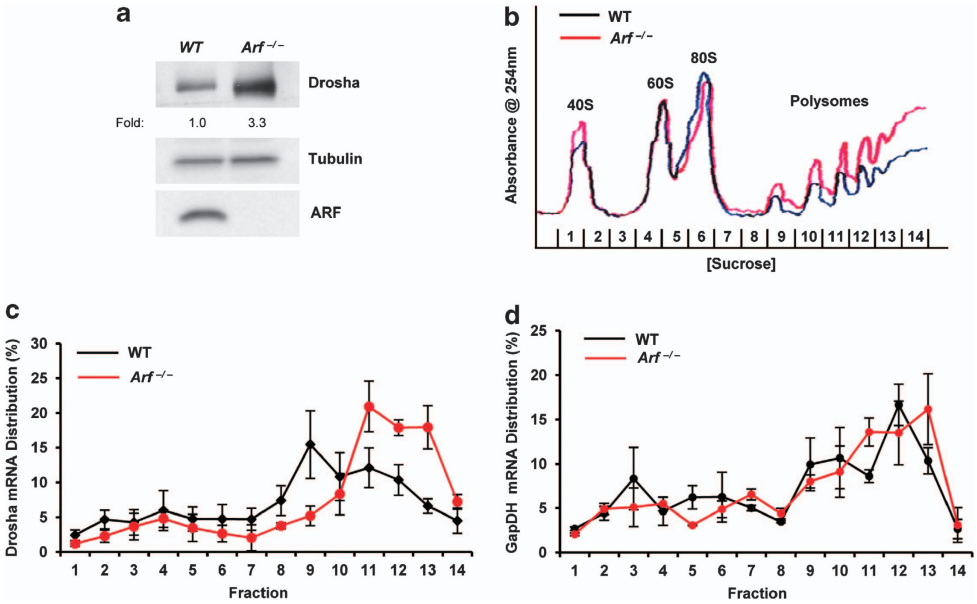

Figure 3. Translation of Drosha mRNAs is augmented upon loss of *Arf*. (**a**) Endogenous Drosha protein levels are elevated in MEFs that lack *Arf* compared with WT MEFs. (**b**) Cytosolic extracts were prepared from equal number of WT and $Arf^{-/-}$ MEFs that had been treated for 5 min with cycloheximide (10 μg/ml). Extracts were then subjected to differential density centrifugation and analyzed via constant ultraviolet monitoring (254 nm). (**c**, **d**) Monosome-, disome-, and polysome-associated Drosha mRNA levels were measured with quantitative RT-PCR and were calculated as a percentage of total Drosha mRNA present in all the fractions. Data are the mean ± s.e.m. ($N = 3$).

both knockdown and control cells using flow cytometry (Supplementary Figure S4a). In accordance with the aforementioned proliferation data, the G1 and G2/M distribution of Drosha-depleted cells was significantly reduced compared with control knockdown cells. In addition, the population of sub-G1 cells was significantly larger upon Drosha knockdown (5.19% shLuc versus 49.53% shDrosha 1 or 37.78% shDrosha 2), which represented cells with a hypodiploid genome because of DNA degradation, a commonly associated feature of cells undergoing apoptosis (Figure 6a).

In order to determine whether apoptosis accounted for the differences in $Arf^{-/-}$ cell proliferation upon Drosha knockdown, we sought to quantify the population of cells undergoing apoptosis by flow cytometric analyses with FITC (fluorescein isothiocyanate)-Annexin-V and propidium iodide double staining. $Arf^{-/-}$ cells maintain an active p53 response to DNA damaging agents, and transient etoposide treatment properly induced apoptosis in these cells (Supplementary Figure S4b). Approximately 60–70% of Drosha-depleted $Arf^{-/-}$ MEFs stained positive for Annexin V compared with only 10% of control cells (Figure 6c), indicating that Drosha knockdown decreases cell proliferation, at least in part, by greatly increasing apoptosis. Caspase-mediated cleavage of the PARP (poly ADP-ribose polymerase) protein is an indicator of cells undergoing apoptosis. In agreement with our observed Annexin-V staining, enhanced cleavage of PARP was observed in Drosha-knockdown cells relative to control knockdown (Figure 6b).

Ras^{V12}-induced transformation of $Arf^{-/-}$ MEFs requires Drosha

ARF protects normal cells from oncogenic Ras^{V12} transformation by activating a p53-dependent growth arrest or apoptotic response.[34] However, in the absence of *Arf*, MEFs transduced with Ras^{V12} undergo cellular transformation, an event that can be both observed and quantified by anchorage-independent growth in soft agar.[35] To determine whether elevated Drosha levels phenocopied *Arf* loss, WT MEFs ectopically expressing Drosha and oncogenic Ras^{V12} were plated in soft agar. Unlike Ras^{V12}-transduced $Arf^{-/-}$ MEFs, Drosha did not cooperate with Ras^{V12} to transform WT cells. Furthermore, unlike Ras^{V12}, Drosha alone was unable to transform $Arf^{-/-}$ MEFs, suggesting that Drosha does not act as a *bona fide* oncogene to drive cellular transformation (Supplementary Figure S5).

Although overexpression of Drosha alone was not sufficient to transform immortal $Arf^{-/-}$ cells, we hypothesized that Drosha might be necessary for Ras^{V12} transformation in the absence of *Arf*. To test this hypothesis, $Arf^{-/-}$ MEFs were first infected with retroviruses encoding oncogenic Ras^{V12} followed by transduction of Drosha-specific shRNAs (Figure 7a). Reduction of Drosha protein expression was sufficient to impair Ras^{V12}-driven colony formation and anchorage-independent growth as indicated by a reduction in both the number of colonies and their overall size (Figures 7b and c), implying that *Arf*-deficient cells transformed by oncogenic Ras^{V12} require elevated Drosha expression to maintain the transformed phenotype.

DISCUSSION

The tumor-suppressor nature of ARF was originally ascribed to its ability to stabilize and activate p53 in the presence of oncogenic stress. Over the past decade, numerous groups have established ARF as a potent multifaceted tumor suppressor that is not only crucial for the cellular response to oncogene activation but also capable of monitoring steady-state ribosome synthesis and growth in a p53-independent manner.[2–5,8,9,28,29] Aside from the p53-MDM2 network, NPM was one of the first proteins to be associated with ARF;[8,30] this novel interaction suppresses ribosome nuclear export, a rate-limiting step of ribosome biogenesis.[10,36] More recently, a dynamic relationship between ARF and the DDX5 RNA helicase was revealed, further illustrating how ARF is able to control ribosome output through the coordinated regulation of rRNA transcription and rRNA processing.[7,11] Given that loss of *Arf*, a common event in cancer, enhances several important steps of ribosome maturation, one

© 2013 Macmillan Publishers Limited

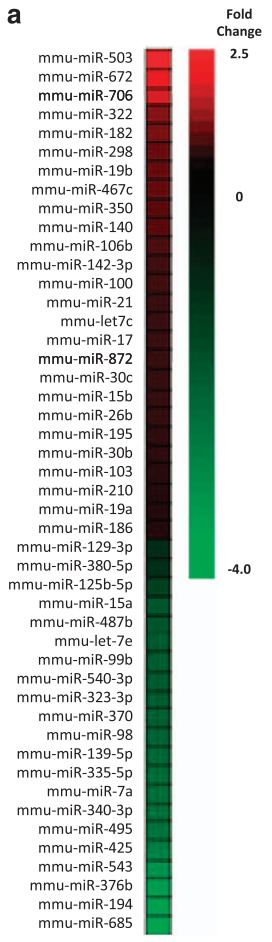

b

miRNA	Fold Change
mmu-miR-503	2.42
mmu-miR-672	2.17
mmu-miR-708	2.02
mmu-miR-322	1.62
mmu-miR-182	1.59
mmu-miR-298	1.51
mmu-miR-19b	1.50
mmu-miR-467c	1.50
mmu-miR-350	1.45
mmu-miR-140	1.45
mmu-miR-139-5p	1.77
mmu-miR-335-5p	1.82
mmu-miR-7a	1.84
mmu-miR-340-3p	1.87
mmu-miR-495	1.93
mmu-miR-425	2.12
mmu-miR-543	2.60
mmu-miR-376b	2.89
mmu-miR-194	2.94
mmu-miR-685	3.94

Figure 4. The expression of only a subset of miRNAs is altered upon ARF knockdown. (**a**) Global miRNA expression profiles of WT MEFs infected with shLuc or sh*Arf*-encoded lentivirus were determined by TaqMan MicroRNA quantitative RT-PCR in three separate experiments. Only miRNAs ($N = 147$) that were present at appreciable quantities in at least one condition (C_T value <31) were used for analysis. miRNA expression fold changes were calculated for each replicate and then averaged. The heat map shows the fold changes in expression for a subset of miRNAs in WT sh*Arf* MEFs relative to WT shLuc MEFs. Each colored block represents the expression of 1 miRNA (labeled on the left). Expression signals are converted into color (red, high signal; green, low signal). Color intensities are proportional to the variation of expression as indicated in the scale bar. (**b**) Table depicting the 10 most up- and downregulated miRNAs in WT sh*Arf* cells relative to WT shLuc cells.

might predict that a global increase in protein translation would ensue under these conditions. Although future work pertaining to this hypothesis is required, a previous study as well as the data presented here, present a scenario that disruption of *Arf* expression likely initiates a selective translational program that accounts for an overall pro-growth phenotype.[31] The initiation of this selective translational program could provide a more permissive cellular environment for secondary oncogenic driver mutations, resulting in a more robust transformative phenotype.

The RNase III endonuclease, Drosha, participates in several essential cellular processes, most notably, the processing of pre-rRNA and pri-miRNA intermediate species. Given the role of these small non-coding RNAs in development and disease, it is conceivable that the machinery responsible for their maturation must be tightly monitored. To date, very little is known about the mechanisms through which Drosha is regulated. Here, we presented evidence that Drosha expression is controlled at the level of translation in an ARF-dependent manner. Although we have demonstrated that existing Drosha mRNAs are excluded from polysomes in the presence of ARF, further studies will be needed to provide insight into the precise mechanism through which ARF antagonizes Drosha transcript association with polyribosomes. Given Drosha's ability to promote rRNA processing and increase cytosolic ribosome availability, this could represent a feed-forward loop. Heightened Drosha levels would stimulate ribosome production that, in turn, would enhance Drosha mRNA translation. However, this over-simplified loop does not take into account any selective translation. Rather, translational selectivity could occur through miRNA-directed translation. Here, we show that loss of *Arf* and the concomitant increase in Drosha levels impact the miRNA profile of these cells, albeit not globally. This is in agreement with previous findings that the Drosha-containing microprocessor does not serve as a rate-limiting factor in miRNA processing.[32] It is possible that one or more of the 23 miRNAs that were repressed upon ARF knockdown might target the Drosha transcript. This could account for the lack of Drosha translational repression under these conditions.

Preceding studies have yielded conflicting results regarding Drosha's role in cell growth, proliferation, and transformation.[22–26] Alterations in *RNASEN* (gene encoding mouse and human Drosha) copy number have been correlated with specific types of cancer, but there is no clear trend that exclusively establishes this RNA-processing enzyme as a tumor suppressor or oncogene. Our findings indicate that in *Arf*-deficient primary mouse fibroblasts, Drosha has an important role in mediating enhanced cell growth and proliferation. Drosha knockdown impaired rRNA processing, ribosome biogenesis, and reduced the proliferation rate of cells while activating an apoptotic cell death response. Furthermore, we uncovered a critical role for elevated Drosha expression in maintaining Ras^{V12}-induced cellular transformation. Given the well-established association between increased translation rates, proliferation, and neoplastic transformation, perhaps Drosha makes a required cellular process, such as ribosome biogenesis, more efficient to accommodate the overwhelming protein synthesis demands following exposure to oncogenic stimuli. In this setting, oncogenic Ras requires the elevated ribosome biogenesis that heightened Drosha provides. In the absence of *Arf* and presence of activated Ras^{V12}, loss of Drosha expression acts as a synthetic lethal event-triggering apoptosis. Thus, we have established a novel regulatory link between Drosha and ARF that not only defines the growth properties of these two proteins but also highlights new mechanisms through which they function to establish a pro- or anti-tumor regimen.

MATERIALS AND METHODS

Cell culture and reagents

Low passage (P3–P5) primary B6/129 WT and $Arf^{-/-}$ MEFs were isolated and cultured as previously described.[10] For western blot analysis, membranes were probed with the following antibodies: rabbit anti-Drosha (ab12286; Abcam, Cambridge, MA, USA); rat anti-p19ARF (sc-32748), rabbit anti-p16INK4a (sc1207), mouse anti-p21 (sc6246), rabbit anti-Ras (sc520), and mouse anti-γ-tubulin (sc17787; all from Santa Cruz Biotechnology, Santa Cruz, CA, USA); rabbit anti-cleaved PARP (#9544; Cell Signaling, Danvers, MA, USA). For apoptosis assay, etoposide (Sigma, St Louis, MO, USA) was used at a final concentration of 50 μM.

Plasmids and viral production

For Drosha overexpression, the *Drosha* ORF was first PCR amplified using cDNA derived from MEF total RNA. The following primers were used: forward 5′-GACGATATCGGACGCATCGAGATGCAAGG-3′, reverse 5′-GACG ATATCCCACTCCTGCCCTCGTTTAC-3′. The *Drosha* ORF was then cloned into the pBabe-puro retroviral backbone. The EcoRV sites flanking the ORF allowed for blunt-end ligation into the SnaBI site of pBabe-puro.

© 2013 Macmillan Publishers Limited

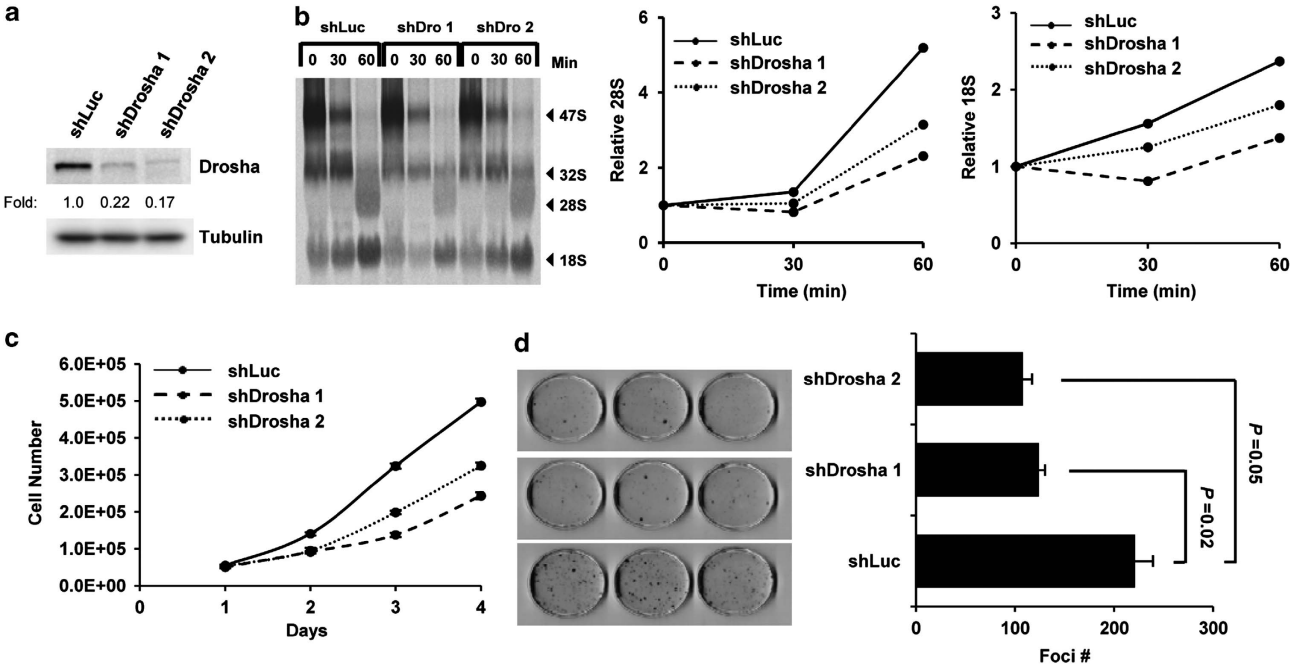

Figure 5. Drosha knockdown reduces proliferation and impairs ribosomal RNA maturation. (**a**) Infected $Arf^{-/-}$ MEFs were lysed, and separated proteins were immunoblotted to confirm Drosha knockdown. (**b**) shLuc and shDrosha $Arf^{-/-}$ MEFs were labeled with [methyl-^{3}H]-methionine and chased for the indicated times. Radiolabeled RNA was separated on an agarose gel, transferred to a membrane, and visualized by autoradiography (left panel). Relative band intensities were determined for rRNA in the processing assay and plotted over time (right panels). The band intensities for all conditions were first individually normalized to their respective 47S levels at $T=0$ and then fold change was calculated. (**c**, **d**) Following Drosha knockdown, cells were plated in triplicate at a density of 5×10^4 per well in a 6-well plate for a proliferation assay and counted over a 4-day time period (**c**). These cells were also seeded in triplicate at 5×10^3 cells per dish in parallel and grown for 12 days. Foci were fixed in methanol, stained with Giemsa, and counted (**d**).

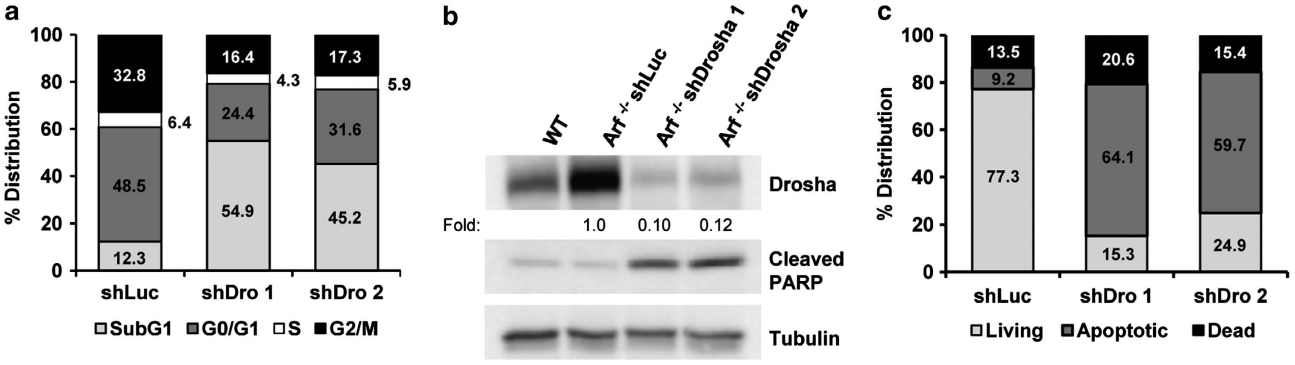

Figure 6. shRNA-mediated knockdown of Drosha in MEFs promotes cell death via apoptosis. (**a**) Quantification of the cell-cycle distribution of shLuc and shDrosha $Arf^{-/-}$ MEFs as determined by flow cytometry. (**b**) Immunoblot analysis examining PARP cleavage in response to Drosha knockdown. (**c**) Percentage of living, apoptotic (Annexin V-positive), and dead (propidium idiode-positive and double-positive) shLuc and shDrosha cells determined by flow cytometry. Data are expressed as the mean ± s.d. of 10 000 events performed in triplicate.

pBabe-puro-H-Ras^{V12} was a generous gift from Martine Roussel (St, Jude Children's Research Hospital, Memphis, TN, USA) and pBabe-HA-ARF has been previously described.[10] Retroviral production was performed as previously described,[37] and collected retrovirus was used to infect MEFs in the presence of 10 μg/ml polybrene.

pLKO.1-puro constructs obtained from the Genome Institute at Washington University were used for RNA interference (RNAi) against *Drosha* and *Arf*. Sequences for the shRNAs are 5′-CCTGGACAAGTTGATAGG ATA-3′ for *Drosha* (here named shDrosha 1), 5′-CTTCGAGAAGTCTGGCTC AAT-3′ also for *Drosha* (here named shDrosha 2), and 5′-TCTACT GGTCTGCCTAAAGGT-3′ for the luciferase control. pLKO-puro-shARF has been previously described.[38] For lentiviral production, 5×10^6 293T cells were cotransfected with pCMV-VSV-G, pCMVΔR8.2, and pLKO.1-puro constructs using Lipofectamine 2000 (Invitrogen, Carlsbad, CA, USA). Forty-eight hours post-transfection, viral supernatants were collected and pooled.

Quantitative RT-PCR

Total RNA and RNA from monosome, disome, and polysome fractions were extracted using RNA-*Solv* (Omega Bio-tek, Norcross, GA, USA). For polysome profiling experiments, first-strand cDNA synthesis and real-time PCR were done as previously described.[39] To amplify Drosha and GAPDH mRNAs, the following primers were used: Drosha forward, 5′-CGATGGCCAATTGTTTTGAAGCC-3′; Drosha reverse, 5′-CGGACGTGAGT GAAGATCACTC-3′; GAPDH forward, 5′-GCTGGGGCTCACCTGAAGG-3′; and GAPDH reverse, 5′-GGATGACCTTGCCCACAGC-3′. Real-time PCR was performed on an iCycler apparatus (Bio-Rad, Hercules, CA, USA) using iQ

© 2013 Macmillan Publishers Limited

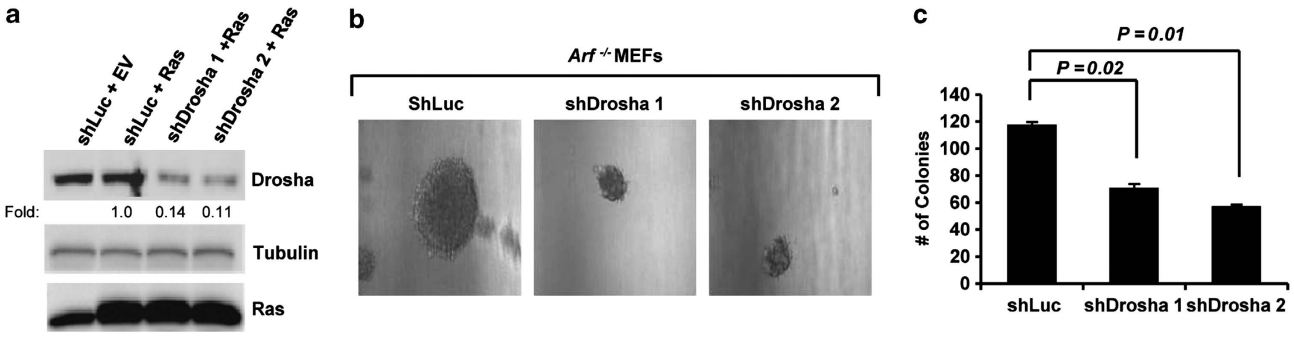

Figure 7. Drosha knockdown significantly inhibits Ras-induced colony formation of $Arf^{-/-}$ MEFs. (**a**) Immunoblot analysis to confirm Ras overexpression and Drosha knockdown in $Arf^{-/-}$ MEFs. (**b**, **c**) A total of 5×10^4 infected cells per condition were seeded in triplicate onto soft agar plates and were grown for 3 weeks. Colonies were examined under a microscope and counted. Colony number is expressed as the mean ± s.e.m.

Sybr Green Supermix (Bio-Rad). Fold change was calculated using the $\Delta\Delta C_T$ method.[40] *Drosha* and *Gapdh* transcripts per cell were calculated by extrapolation from a standard curve generated from serial dilutions of a known quantity of subcloned cDNA.

RNA and protein stability

To assess mRNA stability, MEFs were treated with 4 μg/ml actinomycin D (Sigma), harvested at 0, 2, 4, and 8 h post-treatment, and subjected to RNA isolation, cDNA synthesis reaction, and quantitative RT-PCR analysis using the real-time primers for Drosha and GAPDH listed above. A second pair of Drosha primers was also used to ensure specificity; Drosha forward 5′-GATTGCCAACATGCTCCAGTGG-3′; Drosha reverse, 5′-GCTAGGAGGTGGC-GAAGTTTCAC-3′. To examine protein stability, cells were treated with 25 μg/ml cycloheximide (Sigma), harvested at 0, 2, 4, 6, and 8 h post-treatment and subjected to western blot analysis. For proteosomal inhibition experiment, MEFs were treated with dimethyl sulfoxide (mock) or 40 μM MG-132 (Sigma) for 8 h and then subjected to western blot analysis.

Ribosome fractionation

WT and $Arf^{-/-}$ MEFs were treated with cycloheximide (10 μg/ml) for 5 min before harvesting to stall ribosomes on mRNAs. Cells were counted, and cytosolic extracts prepared from 3×10^6 cells were subjected to ribosome fractionation as previously described[38,41] using a density gradient system (Teledyne ISCO, Lincoln, NE, USA). *Drosha* and *Gapdh* mRNA distribution per fraction was calculated as a percentage of the total number of transcripts in all collected fractions.

Ribosomal RNA processing

Equal numbers of infected WT or $Arf^{-/-}$ MEFs were grown in methionine-free starvation media containing 10% dialyzed fetal bovine serum for 15 min. Cells were treated with 50 μCi/ml [methyl-^{3}H]-methionine for 30 min and chased in complete media spiked with cold methionine (10 μmol/l) for the indicated times. Extracted RNA was separated on agarose-formaldehyde gels and transferred to a Hybond XL membrane (GE Healthcare, Piscataway, NJ, USA). The membrane was cross-linked and sprayed with En^{3}Hance (Perkin-Elmer, Waltham, MA, USA) before autoradiography. Band intensities were quantitated using ImageQuant TL (GE Healthcare).

Screening of miRNA expression

WT MEFs were infected with a control- or ARF-specific shRNA for 72 h before extraction of total RNA using the miRNeasy kit (Qiagen, Courtaboeuf, France). TaqMan Megaplex RT was performed using 750 ng of input RNA according to the manufacturer's protocol, and real-time PCR was run on the 384-well micro-fluidic TaqMan miRNA Array Card A using the Applied Biosystems 7900HT Real-Time PCR System (Applied Biosystems, now Life Technologies; Carlsbad, CA, USA). Data were processed and exported with Applied Biosystems SDSv2.2.1 software. Once again, relative quantification was performed using the ΔΔCt method, using U6 as a reference.

Foci formation and proliferation assays

For cell proliferation assays, infected $Arf^{-/-}$ MEFs were plated in triplicate at 5×10^4 cells per well. Every 24 h thereafter, cells were harvested and counted using a hemacytometer (Hausser Scientific, Horsham, PA, USA). Cells were grown for 14 days in complete medium and then were fixed with 100% methanol and stained for 30 min with 50% Giemsa. Colonies were quantified using ImageQuant TL (GE Healthcare).

Cell-cycle distribution analysis

Infected $Arf^{-/-}$ MEFs (1×10^6) were washed once in phosphate-buffered saline (1% fetal bovine serum) and then fixed in ice cold 100% ethanol. DNA was stained with propidium iodide (20 μg/ml; Sigma) in the presence of 1 mg/ml RNase A (Sigma). Cells were analyzed for DNA content by flow cytometry using a FACSCalibur instrument (Becton Dickinson Instruments, Franklin Lakes, NJ, USA). The data were analyzed using CELLQUEST analysis software (Becton Dickinson).

Apoptosis analysis

Equal numbers of infected $Arf^{-/-}$ MEFs were stained with FITC-Annexin V and propidium iodide using the Vybrant Apoptosis Assay Kit #3 (V13242; Molecular Probes/Invitrogen, Carlsbad, CA, USA) according to the manufacturer's protocol. For a positive control, cells were treated with etoposide (50 μM) for 16 h. Cells were analyzed by flow cytometry as described above.

Soft agar

$Arf^{-/-}$ MEFs were first infected with Ras^{V12} or pBabe empty vector and then selected in puromycin (2 μg/ml). Following drug selection, the cells were infected with pLKO1.1 luciferase or pLKO1.1 shDrosha. For soft-agar colony formation, 1×10^4 infected cells were seeded in triplicate on 60-mm dishes, and the cells were relayered with soft agar on a weekly basis. After 3 weeks, plates were examined under a microscope, and the colonies were counted.

CONFLICT OF INTEREST

The authors declare no conflict of interest

ACKNOWLEDGEMENTS

We thank the members of the Weber lab for their technical input and suggestions. The Children's Discovery Institute and the Genome Institute at Washington University provided lentiviral knockdown constructs. MJK was supported by the Siteman Cancer Center, Cancer Biology Pathway Training Grant (T32 CA113275). Grants from the National Institutes of Health (R01 CA120436) and Department of Defense Era of Hope Scholar Award (BC075004) to JDW supported this work.

© 2013 Macmillan Publishers Limited

REFERENCES

1 Quelle DE, Zindy F, Ashmun RA, Sherr CJ. Alternative reading frames of the INK4a tumor suppressor gene encode two unrelated proteins capable of inducing cell cycle arrest. *Cell* 1995; **83**: 993–1000.
2 Kamijo T, Weber JD, Zambetti G, Zindy F, Roussel MF, Sherr CJ. Functional and physical interactions of the ARF tumor suppressor with p53 and Mdm2. *Proc Natl Acad Sci USA* 1998; **95**: 8292–8297.
3 Weber JD, Taylor LJ, Roussel MF, Sherr CJ, Bar-Sagi D. Nucleolar Arf sequesters Mdm2 and activates p53. *Nat Cell Biol* 1999; **1**: 20–26.
4 Pomerantz J, Schreiber-Agus N, Liegeois NJ, Silverman A, Alland L, Chin L *et al.* The Ink4a tumor suppressor gene product, p19Arf, interacts with MDM2 and neutralizes MDM2's inhibition of p53. *Cell* 1998; **92**: 713–723.
5 Zhang Y, Xiong Y, Yarbrough WG. ARF promotes MDM2 degradation and stabilizes p53: ARF-INK4a locus deletion impairs both the Rb and p53 tumor suppression pathways. *Cell* 1998; **92**: 725–734.
6 Sherr CJ. Divorcing ARF and p53: an unsettled case. *Nat Rev Cancer* 2006; **6**: 663–673.
7 Sugimoto M, Kuo ML, Roussel MF, Sherr CJ. Nucleolar Arf tumor suppressor inhibits ribosomal RNA processing. *Mol Cell* 2003; **11**: 415–424.
8 Bertwistle D, Sugimoto M, Sherr CJ. Physical and functional interactions of the Arf tumor suppressor protein with nucleophosmin/B23. *Mol Cell Biol* 2004; **24**: 985–996.
9 Apicelli AJ, Maggi Jr. LB, Hirbe AC, Miceli AP, Olanich ME, Schulte-Winkeler CL *et al.* A non-tumor suppressor role for basal p19ARF in maintaining nucleolar structure and function. *Mol Cell Biol* 2008; **28**: 1068–1080.
10 Brady SN, Yu Y, Maggi Jr. LB, Weber JD. ARF impedes NPM/B23 shuttling in an Mdm2-sensitive tumor suppressor pathway. *Mol Cell Biol* 2004; **24**: 9327–9338.
11 Saporita AJ, Chang HC, Winkeler CL, Apicelli AJ, Kladney RD, Wang J *et al.* RNA helicase DDX5 is a p53-independent target of ARF that participates in ribosome biogenesis. *Cancer Res* 2011; **71**: 6708–6717.
12 Wu H, Xu H, Miraglia LJ, Crooke ST. Human RNase III is a 160-kDa protein involved in preribosomal RNA processing. *J Biol Chem* 2000; **275**: 36957–36965.
13 Denli AM, Tops BB, Plasterk RH, Ketting RF, Hannon GJ. Processing of primary microRNAs by the Microprocessor complex. *Nature* 2004; **432**: 231–235.
14 Calin GA, Croce CM. MicroRNA signatures in human cancers. *Nat Rev Cancer* 2006; **6**: 857–866.
15 Lee Y, Ahn C, Han J, Choi H, Kim J, Yim J *et al.* The nuclear RNase III Drosha initiates microRNA processing. *Nature* 2003; **425**: 415–419.
16 Lee Y, Kim M, Han J, Yeom KH, Lee S, Baek SH *et al.* MicroRNA genes are transcribed by RNA polymerase II. *Embo J* 2004; **23**: 4051–4060.
17 Gregory RI, Yan KP, Amuthan G, Chendrimada T, Doratotaj B, Cooch N *et al.* The Microprocessor complex mediates the genesis of microRNAs. *Nature* 2004; **432**: 235–240.
18 Shiohama A, Sasaki T, Noda S, Minoshima S, Shimizu N. Nucleolar localization of DGCR8 and identification of eleven DGCR8-associated proteins. *Exp Cell Res* 2007; **313**: 4196–4207.
19 Han J, Lee Y, Yeom KH, Kim YK, Jin H, Kim VN. The Drosha-DGCR8 complex in primary microRNA processing. *Genes Dev* 2004; **18**: 3016–3027.
20 Fukuda T, Yamagata K, Fujiyama S, Matsumoto T, Koshida I, Yoshimura K *et al.* DEAD-box RNA helicase subunits of the Drosha complex are required for processing of rRNA and a subset of microRNAs. *Nat Cell Biol* 2007; **9**: 604–611.
21 Kloosterman WP, Plasterk RH. The diverse functions of microRNAs in animal development and disease. *Dev Cell* 2006; **11**: 441–450.
22 Merritt WM, Lin YG, Han LY, Kamat AA, Spannuth WA, Schmandt R *et al.* Dicer, Drosha, and outcomes in patients with ovarian cancer. *N Engl J Med* 2008; **359**: 2641–2650.
23 Lin RJ, Lin YC, Chen J, Kuo HH, Chen YY, Diccianni MB *et al.* microRNA signature and expression of Dicer and Drosha can predict prognosis and delineate risk groups in neuroblastoma. *Cancer Res* 2010; **70**: 7841–7850.
24 Sand M, Gambichler T, Skrygan M, Sand D, Scola N, Altmeyer P *et al.* Expression levels of the microRNA processing enzymes Drosha and dicer in epithelial skin cancer. *Cancer Invest* 2010; **28**: 649–653.
25 Sugito N, Ishiguro H, Kuwabara Y, Kimura M, Mitsui A, Kurehara H *et al.* RNASEN regulates cell proliferation and affects survival in esophageal cancer patients. *Clin Cancer Res* 2006; **12**: 7322–7328.
26 Muralidhar B, Winder D, Murray M, Palmer R, Barbosa-Morais N, Saini H *et al.* Functional evidence that Drosha overexpression in cervical squamous cell carcinoma affects cell phenotype and microRNA profiles. *J Pathol* 2011; **224**: 496–507.
27 Han J, Pedersen JS, Kwon SC, Belair CD, Kim YK, Yeom KH *et al.* Posttranscriptional crossregulation between Drosha and DGCR8. *Cell* 2009; **136**: 75–84.
28 Lessard F, Morin F, Ivanchuk S, Langlois F, Stefanovsky V, Rutka J *et al.* The ARF tumor suppressor controls ribosome biogenesis by regulating the RNA polymerase I transcription factor TTF-I. *Mol Cell* 2010; **38**: 539–550.
29 Ayrault O, Andrique L, Larsen CJ, Seite P. Human Arf tumor suppressor specifically interacts with chromatin containing the promoter of rRNA genes. *Oncogene* 2004; **23**: 8097–8104.
30 Itahana K, Bhat KP, Jin A, Itahana Y, Hawke D, Kobayashi R *et al.* Tumor suppressor ARF degrades B23, a nucleolar protein involved in ribosome biogenesis and cell proliferation. *Mol Cell* 2003; **12**: 1151–1164.
31 Kawagishi H, Nakamura H, Maruyama M, Mizutani S, Sugimoto K, Takagi M *et al.* ARF suppresses tumor angiogenesis through translational control of VEGFA mRNA. *Cancer Res* 2010; **70**: 4749–4758.
32 Diederichs S, Haber DA. Dual role for argonautes in microRNA processing and posttranscriptional regulation of microRNA expression. *Cell* 2007; **131**: 1097–1108.
33 Oskowitz AZ, Penfornis P, Tucker A, Prockop DJ, Pochampally R. Drosha regulates hMSCs cell cycle progression through a miRNA independent mechanism. *Int J Biochem Cell Biol* 2011; **43**: 1563–1572.
34 Palmero I, Pantoja C, Serrano M. p19ARF links the tumour suppressor p53 to Ras. *Nature* 1998; **395**: 125–126.
35 Kamijo T, Zindy F, Roussel MF, Quelle DE, Downing JR, Ashmun RA *et al.* Tumor suppression at the mouse INK4a locus mediated by the alternative reading frame product p19ARF. *Cell* 1997; **91**: 649–659.
36 Maggi Jr. LB, Kuchenruether M, Dadey DY, Schwope RM, Grisendi S, Townsend RR *et al.* Nucleophosmin serves as a rate-limiting nuclear export chaperone for the Mammalian ribosome. *Mol Cell Biol* 2008; **28**: 7050–7065.
37 Roussel MF, Theodoras AM, Pagano M, Sherr CJ. Rescue of defective mitogenic signaling by D-type cyclins. *Proc Natl Acad Sci USA* 1995; **92**: 6837–6841.
38 Miceli AP, Saporita AJ, Weber JD. Hypergrowth mTORC1 signals translationally activate the ARF tumor suppressor checkpoint. *Mol Cell Biol* 2012; **32**: 348–364.
39 Olanich ME, Moss BL, Piwnica-Worms D, Townsend RR, Weber JD. Identification of FUSE-binding protein 1 as a regulatory mRNA-binding protein that represses nucleophosmin translation. *Oncogene* 2010; **30**: 77–86.
40 Livak KJ, Schmittgen TD. Analysis of relative gene expression data using real-time quantitative PCR and the 2(-Delta Delta C(T)) Method. *Methods* 2001; **25**: 402–408.
41 Strezoska Z, Pestov DG, Lau LF. Bop1 is a mouse WD40 repeat nucleolar protein involved in 28S and 5. 8S RRNA processing and 60S ribosome biogenesis. *Mol Cell Biol* 2000; **20**: 5516–5528.

Supplementary Information accompanies the paper on the Oncogene website (http://www.nature.com/onc)

© 2013 Macmillan Publishers Limited

Oncogene (2009) 28, 3209–3220
© 2009 Macmillan Publishers Limited All rights reserved 0950-9232/09 $32.00
www.nature.com/onc

ORIGINAL ARTICLE

Nucleophosmin protein expression level, but not threonine 198 phosphorylation, is essential in growth and proliferation

SN Brady[1,3], LB Maggi Jr[1,3], CL Winkeler[1], EA Toso[1], AS Gwinn[1], CL Pelletier[1] and JD Weber[1,2]

[1]*Department of Internal Medicine, Division of Molecular Oncology, Siteman Cancer Center, St Louis, MO, USA and* [2]*Department of Cell Biology and Physiology, Washington University School of Medicine, St Louis, MO, USA*

Nucleophosmin (NPM), an oligomeric phosphoprotein and nucleolar target of the ARF tumor suppressor, contributes to several critical cellular processes. Previous studies have shown that the human NPM's phosphorylation by cyclin E–cyclin-dependent kinase 2 (cdk2) on threonine (Thr) 199 regulates its translocation from the centrosome during cell cycle progression. Given our previous finding that ARF directly binds NPM, impeding its transit to the cytoplasm and arresting cells before S-phase entry, we hypothesized that ARF might also inhibit NPM phosphorylation. However, ARF induction did not impair phosphorylation of the cdk2 target residue in murine NPM, Thr[198]. Furthermore, phosphorylation of Thr[198] occurred throughout the cell cycle and was concomitant with increases in overall NPM expression. To investigate the cell's presumed requirement for NPM-Thr[198] phosphorylation in promoting the processes of growth and proliferation, we examined the effects of a non-phosphorylatable NPM mutant, T198A, in a clean cell system in which endogenous NPM had been removed by RNA interference. Here, we show that the T198A mutant is fully capable of executing NPM's described roles in nucleocytoplasmic shuttling, ribosome export and cell cycle progression. Moreover, the proliferative defects observed with stable NPM knockdown were restored by mutant NPM-T198A expression. Thus, we demonstrate that the reduction in NPM protein expression blocks cellular growth and proliferation, whereas phosphorylation of NPM-Thr[198] is not essential for NPM's capacity to drive cell cycle progression and proliferation.
Oncogene (2009) **28,** 3209–3220; doi:10.1038/onc.2009.178; published online 29 June 2009

Keywords: NPM; ribosome; p19ARF; centrosome

Introduction

A highly abundant and evolutionarily conserved nucleolar phosphoprotein, nucleophosmin/B23 (NPM), exhibits a dynamic subcellular localization throughout the cell cycle and has been reported to interact with RNA and a diverse suite of proteins, including p19/p14^{ARF}, p53, nucleolin, ribosomal protein L5, GADD45a and a host of viral proteins (Li, 1997; Liu and Yung, 1999; Colombo *et al*., 2002; Brady *et al*., 2004; Gao *et al*., 2005; Yu *et al*., 2006). Consequently, NPM has been described as a key player in a number of cellular processes, such as the genotoxic stress response, ribosome biogenesis and centrosome duplication (Spector *et al*., 1984; Okuda, 2002; Yang *et al*., 2002; Maggi *et al*., 2008). Although a proteomic analysis of isolated centrosomes failed to corroborate previous reports of NPM's direct association with the centrosome, several studies in cell culture systems and mouse models have indicated that NPM is a critical regulator of genomic stability and centrosome duplication, be it through a direct or indirect mechanism (Tokuyama *et al*., 2001; Grisendi *et al*., 2005).

To ensure the transmission of an intact, diploid genome from one generation to the next, mitotic cells must temporally coordinate the processes of centrosome duplication, DNA replication and cell cycle progression (Winey, 1999). Fibroblasts derived from *Npm1*$^{-/-}$ embryos rapidly display centrosomal amplification and chromosomal instability in the culture, leading to activation of p53, induction of p21-mediated growth arrest and premature expression of senescence markers (Grisendi *et al*., 2005). Previous studies have shown that human NPM was bound to single, unreplicated centrosomes in late G_1 and underwent phosphorylation by cyclin E–cyclin-dependent kinase 2 (cdk2) at threonine 199 (Thr[199]; Thr[198] in murine NPM), prompting NPM's dissociation from the centrosome and its subsequent duplication (Okuda *et al*., 2000; Tokuyama *et al*., 2001). Other groups have observed NPM's interaction with duplicated centrosomes in mitotic cells (Zatsepina *et al*., 1999), yet independent groups failed to detect NPM in preparations of purified centrosomes (Andersen *et al*., 2003; Cha *et al*., 2004). Consequently, NPM's physical association with the centrosome and its purported role as a direct catalyst of centrosome duplication continue to be subjects of discussion and debate in the field.

In addition to NPM's phosphorylation by cyclin E–cdk2, its nuclear export by the Ran–Crm1 complex has also been implicated in NPM's induction of centrosome duplication. Overexpression of NPM nuclear export signal mutants or treatment with leptomycin

Correspondence: Dr JD Weber, Department of Internal Medicine, Division of Molecular Oncology, Washington University School of Medicine, 660 South Euclid Avenue, Campus Box 8069, St Louis, MO 63110, USA.
E-mail: jweber@im.wustl.edu
[3]These authors contributed equally to this work.
Received 4 December 2008; revised 3 May 2009; accepted 27 May 2009; published online 29 June 2009

B, an inhibitor of Crm1-mediated nuclear export, effectively impedes NPM export, resulting in NPM's accumulation in the nucleus and its dissociation from the centrosome (Shinmura *et al*., 2005; Wang *et al*., 2005). In addition, human cells treated with leptomycin B or small interfering RNAs (siRNAs) targeting NPM display centrosome amplification, indicating that Crm1-mediated NPM nuclear export suppresses repeated centrosome duplication cycles, presumably through NPM's observed localization to the centrosome (Shinmura *et al*., 2005; Wang *et al*., 2005). Using similar methods in primary mouse embryonic fibroblasts (MEFs), we have previously demonstrated that NPM expression and nucleocytoplasmic shuttling are required for cell cycle progression (Brady *et al*., 2004; Yu *et al*., 2006). The integration of our findings with previously published reports (Tokuyama *et al*., 2001; Shinmura *et al*., 2005; Wang *et al*., 2005) suggests that NPM may use its robust expression, nuclear export and phosphorylation at Thr^{198} to temporally coordinate the processes of centrosome duplication and cellular proliferation.

To date, phosphorylation of NPM-Thr^{198} has not definitively been shown to be essential for cell growth and proliferation. Nonetheless, centrosomes and their duplication are believed to play a crucial role in cell cycle progression, although recent studies have challenged this view (Hinchcliffe *et al*., 2001; Khodjakov and Rieder, 2001; Uetake *et al*., 2007). Recalling that an alanine substitution mutant (T199A) of human NPM failed to dissociate from the centrosome and initiate duplication (Tokuyama *et al*., 2001), we reasoned that parallel mutation of Thr^{198} in the murine NPM ortholog would severely compromise the proliferation of primary MEFs. Also, given our previous finding that the ARF tumor suppressor effectively blocked NPM nuclear export (Brady *et al*., 2004), a critical factor in NPM's promotion of centrosome duplication and cellular proliferation, we hypothesized that ARF might also inhibit NPM-Thr^{198} phosphorylation. Here, we report that ARF cannot attenuate the phosphorylation of NPM. Moreover, we demonstrate that NPM expression levels, and not Thr^{198} phosphorylation, define the cell's capacity to synthesize and export ribosomes, progress through the cell cycle and proliferate.

Results

NPM is pro-growth in the absence of Arf and a potent transforming oncogene in the absence of p53

To further investigate NPM's contribution to cell proliferation and transformation, the impact of NPM overexpression in immortal $Arf^{-/-}$ or $p53^{-/-}$ MEFs was tested. Similar to transduction with oncogenic Ras^{V12}, exogenous expression of NPM induced a significant increase in $Arf^{-/-}$ cell size, as evidenced by flow cytometric measurements of forward and side scatter (Figure 1a). In agreement with previous findings in immortalized rodent cells (Kondo *et al*., 1997), overexpression of NPM significantly increased the size of $p53^{-/-}$-transformed cell colonies that grew in soft agar, although not to the extent of Ras^{V12} (Figure 1b).

To further address the putative role of NPM in promoting cell proliferation and transformation, 60 tissue samples from breast, prostate and colon carcinomas, were analyzed using NPM immunohistochemistry. Approximately 10–18% of Ki-67-positive tumor samples exhibited negative staining for NPM (Figure 1c, top panels), indicating that a subset of highly proliferative tumors does not upregulate NPM expression to drive proliferation. However, the remaining 82–90% of Ki-67-positive tumors did show positive staining for NPM, and nearly 50% of these samples displayed a strong nuclear/nucleolar NPM expression pattern, regardless of tumor type (Figure 1c, bottom panels).

$Arf^{-/-}$ MEFs, although immortal, remain diploid (Kamijo *et al*., 1997) and retain normal numbers of centrosomes when passaged in culture (Figure 1d, right panels). Genetic ablation of *Npm1* results in centrosome amplification and genomic instability in MEFs (Grisendi *et al*., 2005), suggesting that NPM plays a critical regulatory role maintaining proper centrosome duplication. Given this and other corroborating reports (Okuda *et al*., 2000; Tokuyama *et al*., 2001; Wang *et al*., 2005), the influence of exogenous NPM expression on the ploidy and centrosome amplification in $Arf^{-/-}$ MEFs was examined. As shown in Figure 1d, NPM overexpression did not impact the overall chromosome number in $Arf^{-/-}$ MEFs, nor did it alter the number of centrosomes in these cells. Taken together, these findings demonstrate that the pro-growth and transforming properties of NPM are not coupled to the regulation of DNA ploidy changes or centrosome number.

Cell cycle position or ARF induction does not alter phosphorylation of NPM-Thr^{198}

In response to hyper-proliferative cues, such as oncogenic signals emanating from Myc, E1A and Ras, ARF is induced, and antagonizes Mdm2, to promote p53-dependent pathways of growth arrest (Sherr and Weber, 2000). We have previously shown that ARF uses a common domain at its N terminus to bind both Mdm2 and NPM, resulting in the nucleolar sequestration of each protein independent of the other (Brady *et al*., 2004). ARF not only delocalizes Mdm2 to the nucleolus, away from active pools of nucleoplasmic p53, but also impairs Mdm2's E3 ubiquitin ligase activity, thereby negatively regulating Mdm2 through two distinct mechanisms (Honda and Yasuda, 1999; Tao and Levine, 1999; Weber *et al*., 1999). Thus, ARF might employ a similar two-pronged approach attenuating NPM's growth-promoting functions. As phosphorylation of human NPM by cyclin E–cdk2 was reported to be essential for the initiation of centrosome duplication in late G_1 (Tokuyama *et al*., 2001), we considered that ARF might inhibit NPM phosphorylation in addition to retaining it in the nucleolus to arrest cell growth before S-phase entry (Weber *et al*., 2000).

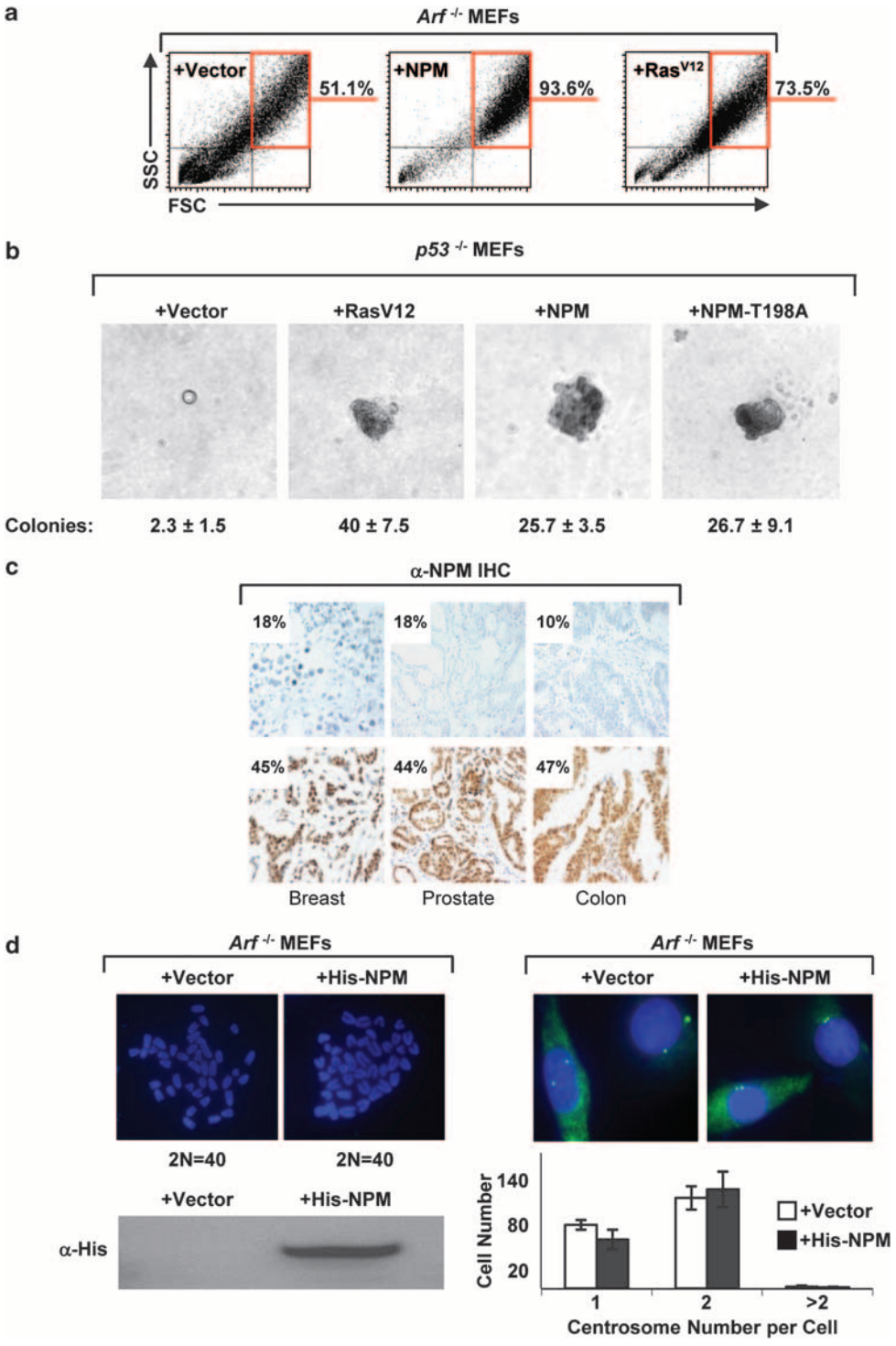

Figure 1 Nucleophosmin (NPM) drives oncogenic growth and proliferation. (**a**) *Arf*$^{-/-}$ mouse embryonic fibroblasts (MEFs) infected with retroviruses encoding the control vector, His-tagged NPM or H-Ras^{V12}, were fixed and subjected to forward and side scatter analysis by flow cytometry. The upper right quadrant represents the cell population showing increased size. (**b**) *p53*$^{-/-}$ MEFs infected with retroviruses encoding the control vectors, H-Ras^{V12}, His-NPM and His-NPM T198A, were seeded (3×10^3) in quadruplicate wells of a 24-well plate in media containing soft agar and were assessed for colony formation 14 days later. (**c**) Primary human breast, prostate and colon carcinoma tissue microarrays were obtained and immunohistochemically stained for NPM protein expression. Representative samples displaying negative staining for NPM are shown in the top panels and those exhibiting strong positive staining for NPM are shown in the bottom panels. The percentage of analyzed tumors showing positive NPM protein expression for each carcinoma type is indicated in the insets. (**d**) *Arf*$^{-/-}$ MEFs were infected with retroviruses encoding the control vector or His-tagged NPM for 72 h, and were treated with colcemid, harvested and fixed for preparation and visualization of chromosomes with DAPI (4',6-diamidino-2-phenylindole) (representative of 75 metaphase spreads counted, upper left). Cells infected in parallel were fixed and immunofluorescently stained with antibodies recognizing γ-tubulin to label centrosomes, and nuclei were demarcated with DAPI (upper right). For each condition, centrosomes from over 200 cells were counted in three separate experiments ($n = 3$) and results graphed (plot, lower right). Exogenous His-tagged NPM protein expression was confirmed by western blot analysis (lower left).

Alignment of human and mouse NPM amino acid sequences revealed 94% identity and 97% similarity. As shown in Figure 2a (lower panel), Thr[199] in human NPM corresponds to Thr[198] in murine NPM. A polyclonal antibody raised against a phosphopeptide surrounding Thr[198] in murine NPM was generated to specifically detect phospohoThr[198] in NPM (Figure 2a, underlined sequence). The phosphospecific NPM-Thr[198] antibody (NPM-pT198) reacted with a protein band migrating at approximately 38 kDa in whole cell lysates from asynchronously growing triple knockout (TKO) MEFs (*Arf*$^{-/-}$*p53*$^{-/-}$*Mdm2*$^{-/-}$) (Figure 2a, lane 1), but failed to detect the corresponding band in lysates from contact-inhibited TKO MEFs (Figure 2a, lane 2) or in purified recombinant NPM proteins expressed in *Escherichia coli* (Figure 2a, lane 3). Re-probing of this membrane with a monoclonal antibody recognizing NPM showed that a 38 kDa protein band was present in all three lanes, indicating that the polyclonal antibody reacts specifically with NPM phospho-Thr[198] proteins, but does not cross-react with non-phosphorylated NPM. In addition, TKO MEFs infected with siRNAs targeting the 3′-UTR of endogenous NPM were used to show specificity of the antibody to Thr[198]. Phosphorylation of Thr[198] was reduced at a level consistent with reduction in total NPM protein after siNPM infection (Figure 2a, right panel). Rescue of NPM knockdown with an ectopic RNA interference-resistant NPM-GFP (green fluorescent protein) protein resulted in a restoration of NPM phosphorylation at Thr[198] (Figure 2a, right panel, lane 3 arrow), whereas rescue with an NPM T198A-GFP mutant resulted in a non-observable phosphorylation with the phospho-T198 antibody (Figure 2a, right panel, lane 4). This demonstrates that our NPM phospho-T198 antibody is specific for Thr[198].

To determine whether or not phosphorylation of murine NPM-Thr[198] is a cyclin E–cdk2-specific event within the context of cell cycle progression, TKO MEFs were serum-starved and synchronized in G_0, evidenced by the cells' low expression levels of cyclin D1 protein (Figure 2b, lane 2). After release into serum, phospho-Thr[198] NPM expression increased, achieving maximal levels at 24-h post-serum addition (Figure 2b). Notably, the observed increase in phospho-Thr[198] NPM levels coincided with the increased expression of total NPM protein (Figure 2b). Quantitative comparison of protein band intensities confirmed that phospho-Thr[198] NPM protein levels increased in parallel with total NPM protein expression. Given that cyclin D1 protein expression levels were maximal at approximately 8 h after the cells' release into serum, yet abundant levels of phospho-T198 NPM were already evident by 4-h post-stimulation, this result suggests that cyclin E–cdk2 is not the sole kinase which phosphorylates NPM-Thr[198] within the cell (Figure 2b). These data instead indicate that NPM-Thr[198] seems to be constitutively phosphorylated throughout the cell cycle rising only when overall protein levels of NPM increase, and likely undergoes phosphorylation at Thr[198] by one or more kinases, with overall NPM abundance being the limiting substrate. To further explore this possibility, cells were growth arrested at various points of the cell cycle. Aphidicolin-induced G1/S-phase arrest did not alter phospho-T198 compared with dimethyl sulfoxide controls (Figure 2c, lane 2). We did observe a modest increase in Thr[198] phosphorylation (1.4-fold) with nocodazole treatment, consistent with an overall increase in NPM abundance (Figure 2b). Inhibition of cdk2 with roscovitine resulted in no change in Thr[198] phosphorylation (Figure 2c, lane 4), suggesting that kinases other than cdk2 are quite capable of phosphorylating this residue throughout the cell cycle.

Given that ARF's interaction with NPM represents one of its p53-independent functions, ARF's impact on NPM-Thr[198] phosphorylation in TKO MEFs was examined. Retroviral-mediated transduction of p19^{ARF} into TKO MEFs failed to produce an appreciable change in phospho-Thr[198] NPM protein levels (Figure 2d, lanes 1 and 3). TKO MEFs that were transduced to express p19$^{ARF\Delta1-14}$, a mutant lacking the

Figure 2 Characterization of murine nucleophosmin-threonine 198 (NPM-Thr[198]) phosphorylation. (**a**) Whole cell lysates from actively cycling (lane 1) and contact-inhibited (lane 2) triple knockout mouse embryonic fibroblasts (TKO MEFs), and purified recombinant murine NPM proteins (lane 3) were equally loaded and separated on denaturing polyacrylamide gels, followed by western blot analysis with antibodies recognizing total NPM or phospho-Thr[198] NPM (NPM-pT198). Shown is the amino acid alignment for the cyclin-dependent kinase (cdk) target region of human (upper sequence) and murine (lower sequence) NPM, with a line denoting the phosphopeptide that was used to generate the custom phosphospecific NPM-Thr[198] antibody. TKO MEFs were infected with lentiviruses encoding siLuc, siNPM or siNPM + NPM-GFP (green fluorescent protein), or siNPM + NPM T198A-GFP and harvested 48-h post-infection for western blot analysis using antibodies recognizing phospho-NPM T198, NPM or GFP. The arrow points to the shifted form of NPM-pT198-GFP. (**b**) Low-passage (p4) TKO MEFs were synchronized into quiescence by culturing in medium containing 0.1% serum for 48 h. Cells were released into medium containing 10% serum and harvested at the indicated time points. Whole cell lysates were separated by sodium dodecyl sulfate polyacrylamide gel electrophoresis (SDS–PAGE), and protein expression levels for cyclin D1, cyclin B1, NPM and NPM-pT198 were determined by immunoblotting with the appropriate antibodies; γ-tubulin was included as a control for equal protein loading. Levels of NPM and NPM-pT198 were quantified by densitometry and graphed as percent of asynchronous levels. Data are representative of three independent experiments ($n = 3$). (**c**) TKO MEFs were treated for 24 h with aphidicolin (1 μg/ml), nocodazole (1 μg/mol/l) or roscovitine (10 μg/mol/l), and harvested for western blot analysis using antibodies recognizing NPM, cyclin B1, γ-tubulin and phospho-NPM T198. Fold change indicates levels of phospho-NPM to total NPM after normalization to γ-tubulin. (**d**) TKO MEFs were infected with retroviruses encoding the SRα-MSV-tkneo vector, full-length p19^{ARF} or a p19$^{ARF\Delta1-14}$ mutant, which lacks the NPM-binding domain. Cells were harvested and lysed at 4 days post-viral transduction, and protein lysates were separated by SDS-PAGE. Expression levels of ectopic ARF and endogenous NPM proteins were assessed by western blot analysis with the indicated antibodies, and equal protein loading was confirmed by immunoblotting for γ-tubulin.

NPM-binding domain (Brady *et al*., 2004), showed a very subtle increase in phospho-Thr[198] NPM levels (Figure 2d, lane 2). In combination with the earlier result showing that NPM-Thr[198] is constitutively phosphorylated, these data indicate that this particular NPM phosphorylation site is not subject to either positive (that is, cdk-mediated) or negative (that is, ARF-directed) regulation throughout the cell cycle, but is

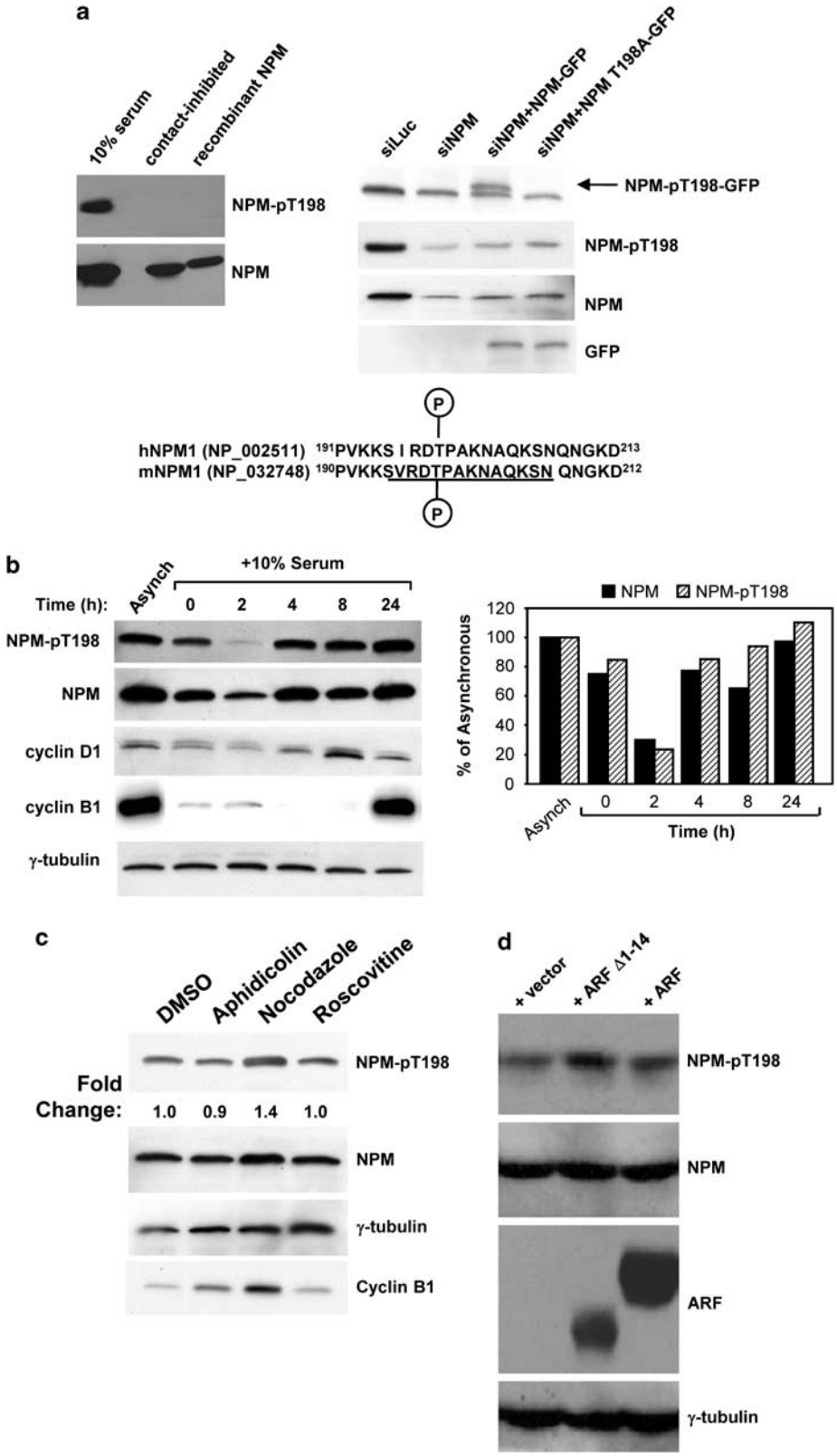

instead constantly being phosphorylated as total levels of NPM rise in the cell.

Mutation of NPM-Thr^{198} does not impair its oligomerization or nucleocytoplasmic shuttling

Although this current study demonstrates that ARF induction does not influence NPM-Thr^{198} phosphorylation (Figure 2c), our previously published findings have shown that ARF effectively blocks NPM nucleocytoplasmic shuttling, a critical function of NPM that is essential for cellular growth and proliferation (Brady *et al*., 2004; Yu *et al*., 2006). Thus, the requirement of phosphorylation of Thr^{198} for NPM's nucleocytoplasmic shuttling was examined using a non-phosphorylatable alanine substitution mutant, T198A.

Given NPM's well-documented capacity to form homo-oligomers (Liu and Chan, 1991; Yung and Chan, 1987; Namboodiri *et al*., 2004), the ability of ectopically-expressed T198A to hetero-oligomerize with endogenous NPM was examined. We have previously shown that NPM functional mutants often form hetero-oligomers with wild-type NPM and act as dominant-negative NPM molecules, inhibiting the function of wild-type NPM (Yu *et al*., 2006). Immunoprecipitation of retrovirally transduced His-tagged wild-type NPM or mutant T198A proteins from TKO MEFs, followed by NPM western blot analysis revealed that T198A formed complexes with endogenous NPM proteins, similar to ectopic wild-type NPM (Figure 3a). If NPM-T198A mutants were non-functional, we expected that they would act as dominant-negative mutants, preventing the

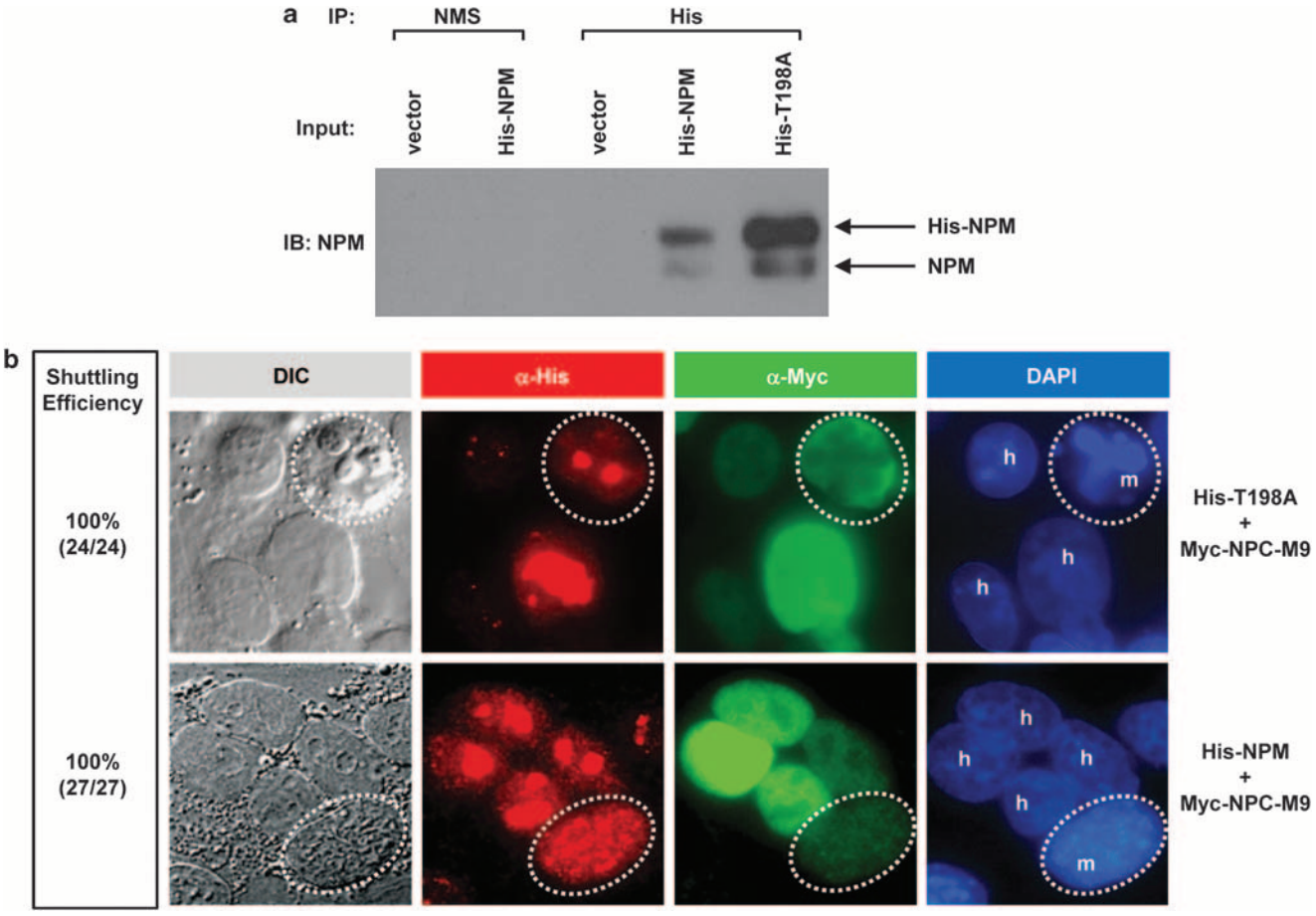

Figure 3 A non-phosphorylatable T198A nucleophosmin (NPM) mutant is not a dominant-negative mutant and displays normal nucleocytoplasmic shuttling. (**a**) Triple knockout mouse embryonic fibroblasts (TKO MEFs) were transduced with SRα-MSV-tkneo retroviruses encoding the control vector or His-tagged NPM proteins (wild type or T198A mutant, as indicated). Cells were harvested at 4 days post-infection, and protein complexes were immunoprecipitated on agarose beads using non-immune mouse serum (NMS) or an antibody recognizing the His tag. Washed beads were boiled in sample buffer, and proteins were separated by sodium dodecyl sulfate polyacrylamide gel electrophoresis (SDS–PAGE) and transferred to polyvinylidene fluoride membranes. Expression of endogenous NPM (lower band), and ectopic His-tagged wild type or T198A-mutant NPM (upper band) proteins was visualized using an antibody against NPM. (**b**) NIH 3T3 cells were seeded onto HeLa cells that had been cotransfected with a plasmid encoding a Myc-tagged NPC-M9-positive shuttling control and a His-tagged plasmid encoding either wild type or T198A-mutant NPM. Heterokaryon assays were carried out as described in the Materials and methods, and expression of NPC-M9, and either wild type or T198A-mutant NPM was visualized using antibodies recognizing the Myc epitope (green) and His tag (red), respectively; nuclei were demarcated with DAPI (4',6-diamidino-2-phenylindole). Human and mouse nuclei are labeled h and m, respectively, and mouse cells are circled in white. Shuttling efficiency numbers are provided for a total of three independent experiments.

function of endogenous wild-type NPM. Heterokaryon shuttling assays using constructs encoding either wild-type NPM or mutant T198A were then performed to answer this biological question. This experimental system assesses NPM's capacity to shuttle between the nucleus and cytoplasm, a property that defines NPM's role in promoting cell growth and proliferation (Yu *et al*., 2006; Maggi *et al*., 2008), demonstrated by the transit of the visibly-tagged protein of interest from a transfected human donor cell into an untransfected murine recipient cell (Tao and Levine, 1999; Yu *et al*., 2006). Similar to wild-type NPM (24/24, 100% shuttling), mutant NPM-T198A shuttled from the nuclei/nucleoli of transiently transfected human HeLa cells into the nuclei/nucleoli of fused, untransfected mouse NIH3T3 cells, demonstrating that NPM's nucleocytoplasmic shuttling is not dependent on its phosphorylation at Thr[198] and is not inhibited by mutant NPM-T198A molecules (Figure 3b).

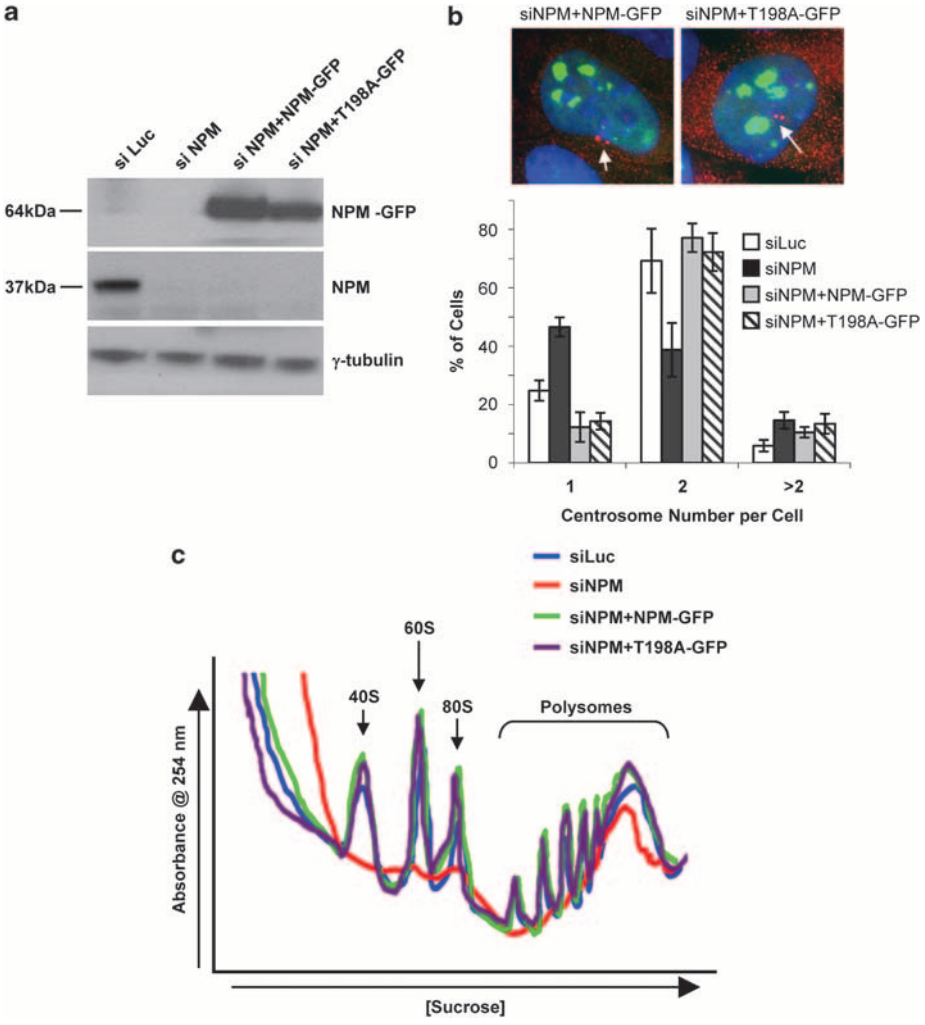

Figure 4 Nucleophosmin-threonine 198 (NPM-Thr[198]) phosphorylation is dispensable for centrosome duplication, rRNA synthesis and ribosome export. (**a**) Triple knockout mouse embryonic fibroblasts (TKO MEFs) were infected with green fluorescent protein (GFP)-tagged lentiviruses encoding short hairpin RNAs directed against luciferase (siLuc) or NPM (siNPM), as well siNPM lentiviruses encoding siRNA-resistant NPM wild type or T198A-mutant cDNAs (siNPM + 6NPM and siNPM + T198A, respectively). Cells were selected in puromycin for 2 days, and at 48-h post-selection, whole cell lysates were harvested, separated on sodium dodecyl sulfate polyacrylamide gel electrophoresis (SDS-PAGE) and immunoblotted with an antibody recognizing NPM to verify protein knockdown and ectopic expression of wild type and T198A-mutant NPM-GFP fusion proteins (38 kDa endogenous protein and ~64 kDa NPM-GFP fusion protein); equal protein loading was confirmed by western blot analysis for γ-tubulin. (**b**) TKO MEFs infected with the indicated lentiviruses were re-plated onto glass coverslips, and at 96-h post-selection, were fixed and stained with an antibody recognizing γ-tubulin to permit visualization and quantitation of centrosome number per cell. Shown is the overlay of pFLRu-siNPM-NPM-GFP or pFLRu-siNPM-T198A-GFP expression (green), γ-tubulin-marked centrosomes (red) and nuclei marked with DAPI (4',6-diamidino-2-phenylindole) (blue). For each condition, 200 cells were counted in three separate experiments, and the results from a representative experiment are shown in the bar graph. (**c**) At 48-h post-selection for expression of the indicated lentiviruses, cytosolic extracts from 3×10^6 TKO MEFs per condition were isolated and separated over a 7–47% sucrose gradient. Gradients were fractionated and ribosomal subunits were detected by measuring RNA absorbance at 254 nm.

NPM knockdown impairs ribosome biogenesis and centrosome duplication, but is rescued by mutant NPM-T198A

The T198A mutant's ability to hetero-oligomerize with endogenous NPM and shuttle to the cytoplasm could potentially mask this mutant's true phenotype. More specifically, the T198A mutant does not display dominant-negative behavior within the cell, unlike our previously described NPMdL mutant, which blocks NPMdL-NPM hetero-oligomers from shuttling (Yu *et al*., 2006). To address this possibility, an NPM knockdown-rescue lentiviral construct was engineered encoding both a short hairpin RNA targeting the 3′-UTR of murine NPM (siNPM) and an siRNA-resistant cDNA corresponding to either wild type (siNPM + NPM-GFP) or mutant (siNPM + T198A-GFP) murine NPM. This strategy allowed the simultaneous reduction of endogenous NPM protein levels and ectopic expression of GFP-tagged NPM rescue proteins with high efficiency in TKO MEFs, as confirmed by NPM western blot analysis (Figure 4a).

Knockdown of endogenous NPM in TKO MEFs resulted in an increase in the number of cells containing a single centrosome and a concomitant decrease in the number of cells exhibiting two centrosomes (Figure 4b, black bars). A slight, but reproducible, increase in the number of cells displaying more than two centrosomes was observed, which is consistent with another group's findings in *Npm1*$^{-/-}$ MEFs (Figure 4b, black bars) (Grisendi *et al*., 2005). Ectopic expression of wild-type NPM and T198A reversed some of the centrosome defects observed upon NPM loss (cells with two centrosomes), but neither was capable of limiting cells with centrosome numbers greater than two (Figure 4b, gray and hatched bars). In addition, colocalization of ectopic wild type or T198A NPM with centrosomes was not observed, although cells displaying NPM-GFP-positive nucleoli adjacent to tubulin-positive centrosomes were observed (Figure 4b, arrows).

We have previously shown that NPM nucleocytoplasmic shuttling is essential for nuclear export and for the formation of cytosolic ribosomes (Yu *et al*., 2006; Maggi *et al*., 2008). Having confirmed that the T198A mutant efficiently shuttles from the nucleolus/nucleus to the cytoplasm (Figure 3b), we next aimed to determine whether NPM-Thr^{198} phosphorylation is necessary for NPM's established role in the assembly and transport of translationally competent ribosomes. We observed that knockdown of NPM in TKO MEFs produced a striking reduction in the populations of 40S, 60S and 80S cytosolic ribosomal subunits, as well as a significant attenuation in the levels of actively translating polysomes (Figure 4c). Importantly, expression of either wild-type NPM or the T198A mutant was sufficient to rescue the siNPM-induced ribosomal defect, restoring all cytosolic ribosomal populations to levels present in control siLuc-infected cells (Figure 4c). Consistent with our findings from nuclear export assays, this result demonstrates that NPM plays a critical role in ribosome biogenesis that is not dependent on its phosphorylation at Thr^{198}.

Cell proliferation is dependent on NPM expression levels, but not its phosphorylation at Thr^{198}

A previous study has suggested that phosphorylation of human NPM at Thr^{199} is necessary for proper S-phase entry and cellular proliferation (Tokuyama *et al*., 2001). Given that the T198A mutant was fully competent in executing NPM's described roles in shuttling, centrosome duplication and ribosome biogenesis (Figures 3 and 4), the influence of the T198A mutant on cellular proliferation was examined. Stable knockdown of endogenous NPM in TKO MEFs severely compromised the cells' ability to enter S-phase, as evidenced by decreased cyclin A expression (Figure 5a) and bromodeoxyuridine (BrdU) incorporation into replicating DNA (Figure 5c). Ectopic expression of either wild-type NPM or T198A-mutant siRNA-resistant proteins was sufficient to fully rescue incorporation of BrdU into the DNA of NPM knockdown cells (Figure 5c). In addition, knockdown of NPM in diploid Arf$^{-/-}$ MEFs resulted in a substantial increase in G1 cells (Figure 5b), suggesting that loss of NPM imposes a block before S-phase entry. To further investigate the potential long-term effects of NPM loss on cell proliferation, foci formation assays were conducted in parallel. Stable knockdown of NPM significantly inhibited foci formation by TKO MEFs, a proliferative defect that was fully reversed upon rescue with either wild-type NPM or T198A-mutant siRNA-resistant proteins (Figure 5d). Thus, these data demonstrate that phosphorylation of NPM on Thr^{198} is dispensable for cell cycle progression

Figure 5 Nucleophosmin (NPM) expression, but not threonine 198 (Thr^{198}) phosphorylation, is essential for cell cycle progression and cell proliferation. (**a**) Triple knockout mouse embryonic fibroblasts (TKO MEFs) infected with lentiviruses encoding siLuc or siNPM expression constructs were harvested 48-h post-infection for western blot analysis using antibodies recognizing NPM, cyclin D1, cyclin E, cyclin A, cyclin B1 and γ-tubulin. (**b**) *Arf*$^{-/-}$ MEFs infected with lentiviruses encoding siLuc or siNPM expression constructs were harvested 48-h post-infection, fixed, stained with propidium iodide and analyzed by flow cytometry. Cell cycle analysis was performed using FACSCalibur software and plotted (lower right panel). Cell lysates were harvested from duplicate plates for western blot analysis using antibodies recognizing NPM, phospho-NPM T198 and γ-tubulin. (**c**) TKO MEFs were infected with siNPM lentiviruses encoding siRNA-resistant NPM wild type or T198A-mutant cDNAs and at 96-h post-selection, were re-plated onto glass coverslips, allowed to adhere and pulsed with 10 μmol/l bromodeoxyuridine (BrdU). At 20 h after BrdU addition, cells were fixed, stained and quantitated for incorporation of BrdU. For each condition, 200 cells were counted in three separate experiments, and results from a representative experiment were plotted (left panel). Shown are the relative patterns for BrdU uptake (red) and NPM-GFP or T198A-GFP rescue expression (green) for a given field of cells for each condition; cell nuclei are demarcated by DAPI (4',6-diamidino-2-phenylindole) (right panel). (**d**) TKO MEFs infected and selected as in (**a**) were re-plated in duplicates at a density of 3×10^2 per 100 mm dish. Fresh media was replenished every fourth day for a period of 12 days, at which time cells were fixed in methanol, stained with Giemsa and counted.

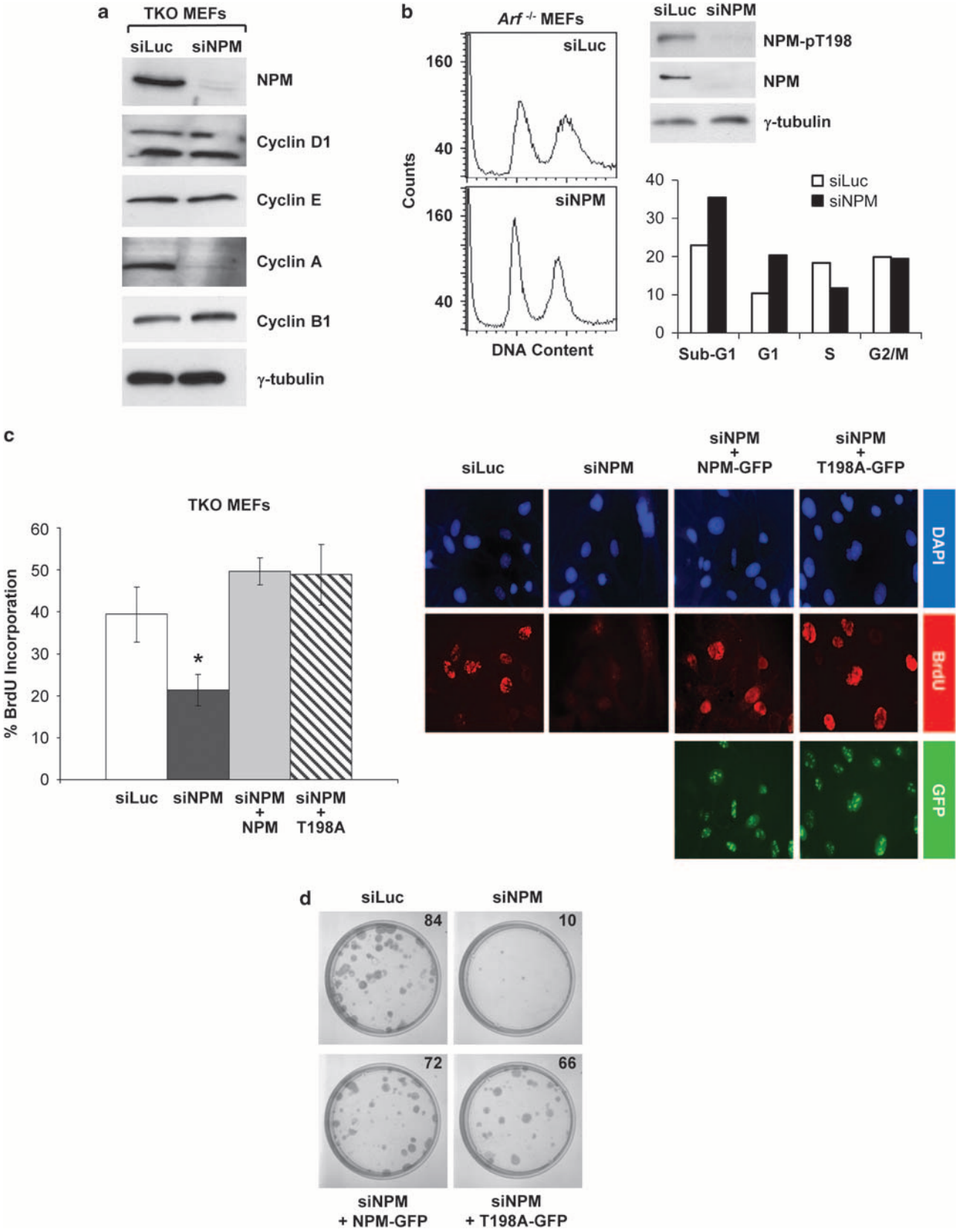
a
TKO MEFs
siLuc
siNPM
NPM
Cyclin D1
Cyclin E
Cyclin A
Cyclin B1
γ-tubulin
b
Arf -/- MEFs
siLuc
siNPM
160
40
Counts
DNA Content
siLuc siNPM
NPM-pT198
NPM
γ-tubulin
40
30
20
10
0
siLuc
siNPM
Sub-G1
G1
S
G2/M
c
TKO MEFs
% BrdU Incorporation
60
50
40
30
20
10
0
*
siLuc
siNPM
siNPM + NPM
siNPM + T198A
siLuc
siNPM
siNPM + NPM-GFP
siNPM + T198A-GFP
DAPI
BrdU
GFP
d
siLuc
siNPM
84
10
72
66
siNPM + NPM-GFP
siNPM + T198A-GFP

and cellular proliferation, whereas adequate NPM protein expression is essential.

Discussion

A multifunctional and dynamic nucleolar phosphoprotein, NPM, has been described as a critical mediator and regulator of numerous processes within the cell, including protein chaperoning, ribosome biogenesis, centrosome duplication and genomic stability (Okuwaki *et al*., 2001; Okuda, 2002; Okuwaki *et al*., 2002; Colombo *et al*., 2005; Maggi *et al*., 2008). Given this list of disparate, but basic, cellular functions that require NPM, it is not surprising that NPM also plays essential roles in embryonic development (Grisendi *et al*., 2005) and cell cycle progression (Brady *et al*., 2004).

In support of this hypothesis, ectopic expression of NPM in immortalized fibroblasts not only increased cell size but also supplied the cell with signals that are necessary for enhanced proliferation and anchorage-independent growth. On the basis of our data and that of other groups, we propose that upregulation of NPM can promote transformation. In agreement with this idea, a subset of adult leukemias carries an NPM mutation, which encodes a second nuclear export signal at NPM's extreme carboxy terminus (Falini *et al*., 2005). Further study of this mutant revealed that it dictates increased nucleocytoplasmic shuttling of NPM (Colombo *et al*., 2006), and our laboratory has previously shown that proper cell cycle progression requires NPM nuclear export (Brady *et al*., 2004). In addition, numerous laboratories (Itahana *et al*., 2003; Bertwistle *et al*., 2004; Brady *et al*., 2004) have demonstrated that NPM is a functional target of the nucleolar ARF tumor suppressor, implying that the transformation properties of NPM can be antagonized by the ARF tumor suppressor. The fact that we have shown NPM to be oncogenic in the absence of *p53* and *Arf* suggests that NPM's role in promoting transformation is not to simply antagonize these two tumor suppressors.

Previous studies have demonstrated that human NPM undergoes phosphorylation at Thr^{199} (Thr^{198} in mouse), and that cyclin E–cdk2 targets this Thr residue to relieve NPM-mediated repression of centrosome duplication and cell cycle progression (Okuda *et al*., 2000; Tokuyama *et al*., 2001). In considering this argument, one would predict that centrosome duplication would be repressed under conditions of increased NPM expression or nuclear export. However, this has not been observed in acute myelogenous leukemia patients who carry $NPMc^+$ mutants (Falini *et al*., 2005) or in our current study of the cellular effects of NPM overexpression. Although intriguing, the existing model concerning the role of NPM and its phosphorylation at Thr^{199} in the process of centrosome duplication does not account for the mounting evidence which links NPM overexpression and nuclear export to increased cell growth and proliferation. We have provided evidence that induction of NPM protein expression is the critical limiting factor in NPM's ability to promote cell growth and proliferation.

Our studies have revealed that ARF's binding to NPM cannot block phosphorylation of NPM at Thr^{198}. In addition, a non-phosphorylatable mutant of NPM, T198A, does not block cell cycle progression, centrosome duplication, nuclear export or cytosolic ribosome accumulation in the absence of endogenous wild-type NPM. Moreover, we observed that NPM-Thr^{198} is constitutively phosphorylated throughout the cell cycle, and any increase in Thr^{198} phosphorylation parallels the increase in total NPM protein expression. Although our data indicates that phosphorylation of NPM-Thr^{198} does not influence NPM function, we do not discount the importance of NPM in centrosome duplication. In agreement with others' published findings from NPM knockout mice (Grisendi *et al*., 2005) and cell lines (Okuda *et al*., 2000; Tokuyama *et al*., 2001), we have shown that loss of NPM deregulates centrosome duplication. However, we propose that this might be a downstream effect, which may not be directly mediated by NPM. In cells undergoing acute NPM loss, we observed a decrease in the number of actively translating ribosomes at time points (48 h) preceding the observed defects in centrosome duplication and S-phase entry (96–120 h). Therefore, our data supports a model in which NPM's direct command over ribosome biogenesis and protein translation could result in indirect changes in a downstream target that plays a critical role in the process of centrosome duplication. Thus, translational targets of the ribosome might in turn also promote cellular proliferation and transformation.

Materials and methods

Cell culture

The $Arf^{-/-}$ MEFs, $Arf^{-/-}/p53^{-/-}/Mdm2^{-/-}$ MEFs (TKO MEFs, provided by Gerard Zambetti, St Jude Children's Research Hospital), NIH3T3 and HeLa cells were maintained in Dulbecco's modified Eagle's medium supplemented with 10% fetal bovine serum, 2 mM L-glutamine, 0.1 mM non-essential amino acids and 100 U each of penicillin and streptomycin. TKO MEFs were synchronized into quiescence by culturing at sub-confluency in medium supplemented with 0.1% fetal bovine serum for 48 h.

Plasmid constructs

The pSRα-MSV-tkneo retroviral expression vectors encoding $p19^{ARF}$, $p19^{ARF\Delta 1\text{-}14}$ and full-length murine NPM were used as described previously (Brady *et al*., 2004). The His-T198A NPM mutant was amplified from pET28a-NPM using the following mutagenic primers: 5′-ATCTGTACGAGATGCA CCAGCCAAAAATGC-3′ (sense) and 5′-GTGCATTTTTGG CTGGTGCATCTCGTACAG-3′ (antisense). The resultant His-T198A cDNA was sub-cloned into pcDNA3.1 using *Eco*RI and *Bam*HI, and into pSRα-MSV-tkneo using *Eco*RI; pcDNA3.1-Myc-NPC-M9 was gift from J Alan Diehl (University of Pennsylvania, USA). The pFLRu-GFP-siLuc and pFLRu-GFP-siNPM vectors were provided by Gregory Longmore (Washington University, USA) (Pelletier *et al*., 2007). To generate the pFLRu-siNPM-NPM-GFP and pFLRu-siNPM-T198A-GFP rescue constructs, murine cDNAs encoding wild type or T198A-mutant NPM were sub-cloned into the *Eco*RI and *Bam*HI sites of the pFLRu-GFP-siNPM vector. The

lentiviral envelope and packaging vectors, pHCMV.G and CMVΔR8.2, were gifts from Sheila Stewart (Washington University).

Virus production and infection
Retroviral production and infection using pBabe-H-Ras^{V12} and SRα-MSV-tkneo vectors were carried out according to methods described previously (Brady *et al*., 2004; Roussel *et al*., 1995). Lentiviruses encoded by the pFLRu-GFP vectors were packaged in 293T cells after cotransfection of the pHCMV.G, CMVΔR8.2 and pFLRu-GFP lentiviral vectors using Fugene 6 (Roche, Indianapolis, IN, USA). Primary MEFs were infected for 4 h with freshly harvested lentiviral supernatants in the presence of 8 μg/ml protamine sulfate, and at 24-h post-infection, puromycin (2 μg/ml) was added to the cells for a selection period of 48 h where appropriate.

Flow cytometry
The *Arf*$^{-/-}$ MEFs were infected with retroviruses encoding the control vector, His-NPM or Ras^{V12}, and were harvested at 72 h. Cells were fixed and resuspended in 1X phosphate-buffered saline/1% fetal bovine serum with or without propidium iodide before analysis using a FACSCalibur (Becton Dickson, Rockville, MD, USA).

Foci formation
Mouse embryonic fibroblasts were infected with lentiviral expression supernatants and were seeded (2×10^3) onto 100 mm dishes. Cells were grown for 14 days in complete medium, fixed in 100% methanol and stained for 30 min with 50% Giemsa.

Soft agar colony formation
The *p53*$^{-/-}$ MEFs were infected with control vector, His-NPM, His-NPM-T198A or Ras^{V12} retroviruses, and were seeded (1×10^3) in triplicates onto 60 mm dishes. Colonies were allowed to grow for 14 days in complete medium supplemented with fetal bovine serum and Noble Agar.

Immunohistochemistry using the common cancer tissue array
The TARP4 tissue array was purchased from NCI Tissue Array Research Project. The tissues used to construct arrays were obtained from the Cooperative Human Tissue Network (CHTN). Each tissue array slide contained 600 samples. De-paraffinized tissue sections were first treated with 3% H_2O_2 for 30 min followed by antigen retrieval by heating in citra plus solution (BioGenex, San Ramon, CA, USA). After subjecting to avidin block, biotin block and power block for 15 min, the sections were incubated with mouse anti-NPM antibody (Zymed, San Francisco, CA, USA) for 1 h. After further incubation with biotinylated multi-link antibody for 45 min and peroxidase-labeled streptavidin for 30 min, the staining was developed by reaction with 3,3′-diaminobenzidine tetrahydrochloride substrate–chromogen solution.

Karyotyping analysis
The *Arf*$^{-/-}$ MEFs were infected with control vector or His-NPM retroviruses, and at 72-h post-infection were treated with colcemid (10 μg/ml) for 16 h. Cells were harvested in 75 mM KCl for 6 min at 37 °C. Cells were fixed in methanol:acetic acid (3:1) and washed. The cells were resuspended in 2 ml fixative and one drop was allowed to fall onto frosted glass slide. DNA was stained with DAPI (4′,6-diamidino-2-phenylindole) and fluorescent signals were detected.

Immunoprecipitation and western blot analysis
Immunoprecipitation of cell lysates was performed as previously described (Brady *et al*., 2004). Antibodies recognizing γ-tubulin, cyclin D1, His (Santa Cruz, Santa Cruz, CA, USA), p19^{ARF} (Abcam, Cambridge, MA, USA), NPM (Zymed) and NPM (custom rabbit polyclonal, Sigma, St Louis, MO, USA) were used in western blot analyses. The custom phosphospecific polyclonal antibody recognizing phospho-NPM (Thr^{198}) was generated commercially (Zymed) and raised against the following phosphopeptide: CSVRDpTPAKN (Tufts University Peptide Core).

Heterokaryon assay
The HeLa cells (2×10^5) were seeded onto glass cover slips in six-well dishes and transfected with constructs encoding either His-tagged wild type or T198A-mutant NPM in combination with a Myc-tagged NPC-M9 plasmid (a gift from J Alan Diehl, University of Pennsylvania). Heterokaryon assays were performed as previously described (Yu *et al*., 2006).

Indirect immunoflourescence
The *Arf*$^{-/-}$ or TKO MEFs were infected with SRα-MSV-tkneo retroviruses or pFLRu-GFP lentiviruses as indicated, and seeded onto glass cover slips. Cells were washed with phosphate-buffered saline, fixed at room temperature using 10% formalin/10% methanol, followed by 1% NP-40 in phosphate-buffered saline for 5 min at room temperature. Cells were stained with an antibody recognizing γ-tubulin (Sigma), followed by FITC or rhodamine X-conjugated immunoglobulins. Nuclei were counterstained with DAPI.

BrdU incorporation
The *Arf*$^{-/-}$ or TKO MEFs were infected with SRα-MSV-tkneo retroviruses or pFLRu-GFP lentiviruses as indicated. Cells were seeded onto glass cover slips and subjected to BrdU incorporation analysis (Brady *et al*., 2004).

Ribosome fractionation
At 4 days post-infection with pFLRu-GFP lentiviruses, TKO MEFs were subjected to ribosome fractionation analysis (Maggi *et al*., 2008).

Conflict of interest

The authors declare no conflict of interest.

Acknowledgements

We are indebted to Sheila Stewart, Gregory Longmore, J Alan Diehl, Martine Roussel, Charles Sherr and Gerard Zambetti for gifts of plasmid constructs, antibodies and primary TKO MEFs. In addition, we would like to thank Sheila Stewart, Helen Piwnica-Worms, Michael Tomasson and John Majors for insightful discussions throughout the course of this study. SNB was supported by the Cancer Biology Pathway. CLP was a trainee in the Lucille P Markey Special Emphasis Pathway in Human Pathobiology. JDW was funded through the National Institutes of Health and Department of Defense Era of Hope Scholar Award in Breast Cancer Research.

References

Andersen JS, Wilkinson CJ, Mayor T, Mortensen P, Nigg EA, Mann M. (2003). Proteomic characterization of the human centrosome by protein correlation profiling. *Nature* **426**: 570–574.

Bertwistle D, Sugimoto M, Sherr CJ. (2004). Physical and functional interactions of the Arf tumor suppressor protein with nucleophosmin/B23. *Mol Cell Biol* **24**: 985–996.

Brady SN, Yu Y, Maggi Jr LB, Weber JD. (2004). ARF impedes NPM/B23 shuttling in an Mdm2-sensitive tumor suppressor pathway. *Mol Cell Biol* **24**: 9327–9338.

Cha H, Hancock C, Dangi S, Maiguel D, Carrier F, Shapiro P. (2004). Phosphorylation regulates nucleophosmin targeting to the centrosome during mitosis as detected by cross-reactive phosphorylation-specific MKK1/MKK2 antibodies. *Biochem J* **378**: 857–865.

Colombo E, Bonetti P, Lazzerini Denchi E, Martinelli P, Zamponi R, Marine JC *et al*. (2005). Nucleophosmin is required for DNA integrity and p19Arf protein stability. *Mol Cell Biol* **25**: 8874–8886.

Colombo E, Marine JC, Danovi D, Falini B, Pelicci PG. (2002). Nucleophosmin regulates the stability and transcriptional activity of p53. *Nat Cell Biol* **4**: 529–533.

Colombo E, Martinelli P, Zamponi R, Shing DC, Bonetti P, Luzi L *et al*. (2006). Delocalization and destabilization of the Arf tumor suppressor by the leukemia-associated NPM mutant. *Cancer Res* **66**: 3044–3050.

Falini B, Mecucci C, Tiacci E, Alcalay M, Rosati R, Pasqualucci L *et al*. (2005). Cytoplasmic nucleophosmin in acute myelogenous leukemia with a normal karyotype. *N Engl J Med* **352**: 254–266.

Gao H, Jin S, Song Y, Fu M, Wang M, Liu Z *et al*. (2005). B23 regulates GADD45a nuclear translocation and contributes to GADD45a-induced cell cycle G2-M arrest. *J Biol Chem* **280**: 10988–10996.

Grisendi S, Bernardi R, Rossi M, Cheng K, Khandker L, Manova K *et al*. (2005). Role of nucleophosmin in embryonic development and tumorigenesis. *Nature* **437**: 147–153.

Hinchcliffe EH, Miller FJ, Cham M, Khodjakov A, Sluder G. (2001). Requirement of a centrosomal activity for cell cycle progression through G1 into S phase. *Science* **291**: 1547–1550.

Honda R, Yasuda H. (1999). Association of p19(ARF) with Mdm2 inhibits ubiquitin ligase activity of Mdm2 for tumor suppressor p53. *EMBO J* **18**: 22–27.

Itahana K, Bhat KP, Jin A, Itahana Y, Hawke D, Kobayashi R *et al*. (2003). Tumor suppressor ARF degrades B23, a nucleolar protein involved in ribosome biogenesis and cell proliferation. *Mol Cell* **12**: 1151–1164.

Kamijo T, Zindy F, Roussel MF, Quelle DE, Downing JR, Ashmun RA *et al*. (1997). Tumor suppression at the mouse INK4a locus mediated by the alternative reading frame product p19ARF. *Cell* **91**: 649–659.

Khodjakov A, Rieder CL. (2001). Centrosomes enhance the fidelity of cytokinesis in vertebrates and are required for cell cycle progression. *J Cell Biol* **153**: 237–242.

Kondo T, Minamino N, Nagamura-Inoue T, Matsumoto M, Taniguchi T, Tanaka N. (1997). Identification and characterization of nucleophosmin/B23/numatrin which binds the anti-oncogenic transcription factor IRF-1 and manifests oncogenic activity. *Oncogene* **15**: 1275–1281.

Li YP. (1997). Protein B23 is an important human factor for the nucleolar localization of the human immunodeficiency virus protein Tat. *J Virol* **71**: 4098–4102.

Liu HT, Yung BY. (1999). *in vivo* interaction of nucleophosmin/B23 and protein C23 during cell cycle progression in HeLa cells. *Cancer Lett* **144**: 45–54.

Liu QR, Chan PK. (1991). Formation of nucleophosmin/B23 oligomers requires both the amino- and the carboxyl-terminal domains of the protein. *Eur J Biochem* **200**: 715–721.

Maggi Jr LB, Kuchenruether M, Dadey DY, Schwope RM, Grisendi S, Townsend RR *et al*. (2008). Nucleophosmin serves as a rate-limiting nuclear export chaperone for the mammalian ribosome. *Mol Cell Biol* **28**: 7050–7065.

Namboodiri VM, Schmidt-Zachmann MS, Head JF, Akey CW. (2004). Purification, crystallization and preliminary X-ray analysis of the N-terminal domain of NO38, a nucleolar protein from Xenopus laevis. *Acta Crystallogr D Biol Crystallogr* **60**: 2325–2327.

Okuda M. (2002). The role of nucleophosmin in centrosome duplication. *Oncogene* **21**: 6170–6174.

Okuda M, Horn HF, Tarapore P, Tokuyama Y, Smulian AG, Chan PK *et al* (2000). Nucleophosmin/B23 is a target of CDK2/cyclin E in centrosome duplication. *Cell* **103**: 127–140.

Okuwaki M, Matsumoto K, Tsujimoto M, Nagata K. (2001). Function of nucleophosmin/B23, a nucleolar acidic protein, as a histone chaperone. *FEBS Lett* **506**: 272–276.

Okuwaki M, Tsujimoto M, Nagata K. (2002). The RNA binding activity of a ribosome biogenesis factor, nucleophosmin/B23, is modulated by phosphorylation with a cell cycle-dependent kinase and by association with its subtype. *Mol Biol Cell* **13**: 2016–2030.

Pelletier CL, Maggi Jr LB, Brady SN, Scheidenhelm DK, Gutmann DH, Weber JD. (2007). TSC1 Sets the rate of ribosome export and protein synthesis through nucleophosmin translation. *Cancer Res* **67**: 1609–1617.

Roussel MF, Theodoras AM, Pagano M, Sherr CJ. (1995). Rescue of defective mitogenic signaling by D-type cyclins. *Proc Natl Acad Sci USA* **92**: 6837–6841.

Sherr CJ, Weber JD. (2000). The ARF/p53 pathway. *Curr Opin Genet Dev* **10**: 94–99.

Shinmura K, Tarapore P, Tokuyama Y, George KR, Fukasawa K. (2005). Characterization of centrosomal association of nucleophosmin/B23 linked to Crm1 activity. *FEBS Lett* **579**: 6621–6634.

Spector DL, Ochs RL, Busch H. (1984). Silver staining, immunofluorescence, and immunoelectron microscopic localization of nucleolar phosphoproteins B23 and C23. *Chromosoma* **90**: 139–148.

Tao W, Levine AJ. (1999). P19(ARF) stabilizes p53 by blocking nucleo-cytoplasmic shuttling of Mdm2. *Proc Natl Acad Sci USA* **96**: 6937–6941.

Tokuyama Y, Horn HF, Kawamura K, Tarapore P, Fukasawa K. (2001). Specific phosphorylation of nucleophosmin on Thr(199) by cyclin-dependent kinase 2-cyclin E and its role in centrosome duplication. *J Biol Chem* **276**: 21529–21537.

Uetake Y, Loncarek J, Nordberg JJ, English CN, La Terra S, Khodjakov A *et al*. (2007). Cell cycle progression and *de novo* centriole assembly after centrosomal removal in untransformed human cells. *J Cell Biol* **176**: 173–182.

Wang W, Budhu A, Forgues M, Wang XW. (2005). Temporal and spatial control of nucleophosmin by the Ran-Crm1 complex in centrosome duplication. *Nat Cell Biol* **7**: 823–830.

Weber JD, Jeffers JR, Rehg JE, Randle DH, Lozano G, Roussel MF *et al*. (2000). p53-independent functions of the p19 (ARF) tumor suppressor. *Genes Dev* **14**: 2358–2365.

Weber JD, Taylor LJ, Roussel MF, Sherr CJ, Bar-Sagi D. (1999). Nucleolar Arf sequesters Mdm2 and activates p53. *Nat Cell Biol* **1**: 20–26.

Winey M. (1999). Cell cycle: driving the centrosome cycle. *Curr Biol* **9**: R449–R452.

Yang C, Maiguel DA, Carrier F. (2002). Identification of nucleolin and nucleophosmin as genotoxic stress-responsive RNA-binding proteins. *Nucleic Acids Res* **30**: 2251–2260.

Yu Y, Maggi Jr LB., Brady SN, Apicelli AJ, Dai MS, Lu H *et al*. (2006). Nucleophosmin is essential for ribosomal protein L5 nuclear export. *Mol Cell Biol* **26**: 3798–3809.

Yung BY, Chan PK. (1987). Identification and characterization of a hexameric form of nucleolar phosphoprotein B23. *Biochim Biophys Acta* **925**: 74–82.

Zatsepina OV, Rousselet A, Chan PK, Olson MO, Jordan EG, Bornens M. (1999). The nucleolar phosphoprotein B23 redistributes in part to the spindle poles during mitosis. *J Cell Sci* **112**: 455–466.

Oncogene (2011) 30, 77–86
© 2011 Macmillan Publishers Limited All rights reserved 0950-9232/11
www.nature.com/onc

ORIGINAL ARTICLE

Identification of FUSE-binding protein 1 as a regulatory mRNA-binding protein that represses nucleophosmin translation

ME Olanich[1,2,3], BL Moss[1,4,5], D Piwnica-Worms[1,4,5], RR Townsend[6] and JD Weber[1,2,3]

[1]*BRIGHT Institute, Washington University School of Medicine, St Louis, MO, USA;* [2]*Departments of Internal Medicine, Division of Molecular Oncology, Washington University School of Medicine, St Louis, MO, USA;* [3]*Cell Biology, Washington University School of Medicine, St Louis, MO, USA;* [4]*Developmental Biology, Washington University School of Medicine, St Louis, MO, USA;* [5]*Molecular Imaging Center, Mallinckrodt Institute of Radiology, Washington University School of Medicine, St Louis, MO, USA and* [6]*Division of Metabolism and Proteomics Center, Siteman Cancer Center, Washington University School of Medicine, St Louis, MO, USA*

Nucleophosmin (NPM/B23) is a multifunctional oncoprotein whose protein expression levels dictate cellular growth and proliferation rates. NPM is translationally responsive to hyperactive mammalian target of rapamycin (mTOR) signals, but the mechanism of this regulation is not understood. Using chimeric translational reporters, we found that the 3′ untranslated region (UTR) of the NPM messenger (m)RNA is sufficient to mediate its translational modulation by mTOR signalling. We show that far upstream element (FUSE)-binding protein 1 (FBP1) interacts specifically with the 3′ UTR of NPM to repress translation. Overexpression of FBP1 resulted in translational repression of NPM mRNAs, whereas depletion of FBP1 caused a dramatic increase in NPM translation and resulted in enhanced overall cell proliferation. Thus, we propose that FBP1 is a key regulator of cell growth and proliferation through its ability to selectively bind the NPM 3′ UTR and repress NPM translation.
Oncogene (2011) **30,** 77–86; doi:10.1038/onc.2010.404; published online 30 August 2010

Keywords: FBP1; Nucleophosmin; ribosome biogenesis; translation

Introduction

Translational regulation functions as a critical mode by which cells direct protein expression. Translational control of select messenger (m)RNAs is often mediated by regulatory proteins that interact with sequence elements within the 5′ and/or 3′ untranslated regions (UTRs) of transcripts (Gebauer and Hentze, 2004). Compared with regulatory protein–RNA interactions in the 3′ UTR, however, those in the 5′ UTR are relatively rare (Jackson *et al*., 2010). Consistent with this notion, numerous studies have demonstrated important regulatory protein–mRNA interactions in the 3′ UTRs of various transcripts (Irwin *et al*., 1997; Brennan and Steitz, 2001; Wickens *et al*., 2002; Zhang *et al*., 2002; Mazan-Mamczarz *et al*., 2003; de Moor *et al*., 2005; Galban *et al*., 2008; Hamilton *et al*., 2008). Thus, it is clear that UTRs, and particularly the 3′ UTR, are essential regulators of the protein expression machinery.

Nucleophosmin (NPM/B23) is a nucleolar oncoprotein involved in a myriad of central cellular processes, including ribosome biogenesis (Okuwaki *et al*., 2002), protein chaperoning (Okuwaki *et al*., 2001), centrosome duplication (Okuda *et al*., 2000), transcriptional regulation (Colombo *et al*., 2002) and cellular growth and proliferation (Brady *et al*., 2004; Grisendi *et al*., 2005, 2006). NPM has a crucial role in modulating the rate of 40S and 60S ribosomal subunit export from the nucleolus/nucleus to the cytoplasm, thereby functioning as a chaperone for the ribosome (Yu *et al*., 2006; Maggi *et al*., 2008). Through this mechanism, NPM is able to enhance protein synthesis and promote cellular growth (Maggi *et al*., 2008). NPM is overexpressed in several neoplasms, such as ovarian, colon, prostate, bladder and gastric cancers (Sandsmark *et al*., 2007; Qi *et al*., 2008). As a potent oncoprotein, it is important to understand the regulation of NPM expression.

Previous data demonstrated that NPM protein expression is induced by hyperactive mammalian target of rapamycin (mTOR) signalling caused by either overexpression of constitutively active H-Ras or loss of *Tsc1* (Pelletier *et al*., 2007). Induction of NPM protein expression is clearly mTOR-dependent, as NPM induction was abrogated upon treatment with rapamycin, a selective inhibitor of mTOR (Wullschleger *et al*., 2006), or overexpression of TSC1 (Pelletier *et al*., 2007). Interestingly, NPM mRNA expression is insensitive to rapamycin, suggesting that NPM is regulated primarily at the level of translation.

Here, we establish that NPM expression is controlled translationally and that the NPM 3′ UTR alone is sufficient to impart endogenous NPM-like translational modulation onto a *luciferase* reporter open reading frame (ORF). Additionally, we identified far upstream element (FUSE)-binding protein 1 (FBP1) as a novel

Correspondence: Dr JD Weber, Department of Internal Medicine, Division of Molecular Oncology, Washington University School of Medicine, 660 South Euclid Avenue, Campus Box 8069, St Louis, MO 63110, USA.
E-mail: jweber@dom.wustl.edu
Received 27 April 2010; revised 21 July 2010; accepted 22 July 2010; published online 30 August 2010

NPM 3′ UTR mRNA-binding protein that represses translation of the NPM transcript. Through modulation of NPM, FBP1 has an important role in the regulation of cell growth and proliferation.

Results

Inhibition of mTOR induces NPM mRNA exclusion from actively translating ribosomes

Signals emanating from hyperactivated mTOR signalling stimulate the translation of NPM, resulting in increased NPM protein expression in the absence of significant changes in NPM mRNA levels (Pelletier *et al*., 2007). To further examine the apparent translational control of NPM, *Tsc1*$^{-/-}$*p53*$^{-/-}$ mouse embryonic fibroblasts (MEFs), which display activated mTOR (Tee *et al*., 2002), were treated with rapamycin. NPM protein induction was attenuated upon rapamycin treatment (Figure 1a), even in the presence of slightly elevated levels of NPM transcripts (Supplementary Figure 1a), indicating that the rapamycin-induced reduction in NPM protein expression is not due to reduced cellular NPM mRNAs.

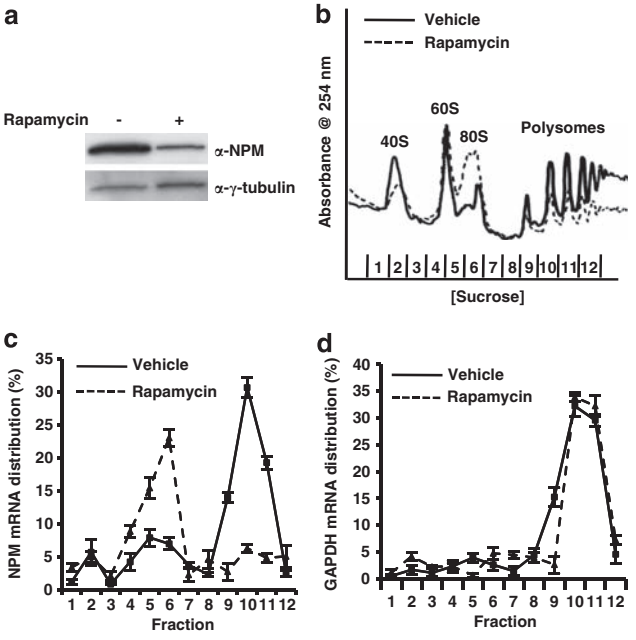

Figure 1 Translation of NPM mRNAs is abrogated upon inhibition of mTOR. *Tsc1*$^{-/-}$*p53*$^{-/-}$ MEFs were treated with vehicle (−) or rapamycin (+). (**a**) Rapamycin treatment results in reduced NPM protein levels. (**b**) Polysome formation is decreased in cells treated with rapamycin. (**c**) NPM mRNAs are excluded from actively translating polysomes upon treatment with rapamycin. Monosome/disome- and polysome-associated NPM mRNAs were measured by qRT–PCR and were calculated as percentage of total NPM mRNAs. Data are mean ± s.d. of three independent experiments. (**d**) Monosomal/disomal and polysomal distributions of GAPDH mRNAs are unaffected by rapamycin. GAPDH mRNAs measured by qRT–PCR from RNA extracted from sucrose gradient fractions are shown as percentage of total GAPDH mRNAs. Values are mean ± s.d. of three independent experiments.

We hypothesized that rapamycin treatment might result in the exclusion of NPM mRNAs from actively translating polyribosomes or polysomes. To test this, cytosolic ribosomes were isolated by sucrose gradient centrifugation from equal numbers of *Tsc1*$^{-/-}$*p53*$^{-/-}$ MEFs treated with vehicle or rapamycin. Ribosomal subunits were detected by continuous measurement of RNA absorbance (A_{254nm}). Treatment with rapamycin dramatically reduced the overall formation of polysomes actively engaged in mRNA translation (Figure 1b). To evaluate the distribution of NPM transcripts in monosomes/disomes and polysomes, NPM mRNA levels in sucrose gradient fractions were measured by quantitative real-time PCR. Strikingly, despite a modest increase in the total cellular pool of NPM mRNAs in rapamycin-treated cells compared with vehicle-treated cells (Supplementary Figure 1a), the percentage of NPM transcripts associated with actively translating polysomes was dramatically diminished upon rapamycin treatment (Figure 1c). Accumulation of NPM mRNAs was apparent in monosomes/disomes, particularly 80S fractions, in cells treated with rapamycin (Figure 1c), which is consistent with previous studies (Jefferies *et al*., 1997). To test that our findings for NPM were specific for an mRNA that is translationally responsive to mTOR signals, we treated cells with rapamycin and analyzed GAPDH mRNAs. Rapamycin had no effect on the distribution of GAPDH mRNAs in monosome/disome or polysome fractions (Figure 1d), consistent with previous findings (Terada *et al*., 1994). Importantly, unchanged GAPDH transcript distribution upon rapamycin treatment suggests that inhibition of mTOR did not globally affect all cellular mRNA translation, which is in accordance with previous reports (Mendez *et al*., 1996). Taken together, these data indicate that NPM expression is responsive to hyperactive mTOR signalling at the level of translation.

The NPM 3′ UTR is sufficient to confer NPM-like translational regulation properties to a luciferase ORF

Recognition and binding of elements within the 5′ and 3′ UTRs of mRNAs by regulatory proteins is a common mechanism underlying selective mRNA translational control (Gebauer and Hentze 2004). Indeed, previous reports have indicated that various mRNAs are subject to such regulation (Irwin *et al*., 1997; Pontrelli *et al*., 2004; Takagi *et al*., 2005; Jiang *et al*., 2006; Sidiropoulos *et al*., 2007; Zhang *et al*., 2008). To determine whether a comparable mechanism may be responsible for the translational regulation of NPM, we first identified the 5′ UTR sequence of the NPM transcript by rapid amplification of complementary DNA ends (RACE) (Supplementary Figure 2a; GenBank accession number GU214027). Like the human NPM 5′ UTR (Meyuhas 2000), RACE revealed that the murine NPM 5′ UTR contains a canonical terminal oligopyrimidine tract also contained in the 5′ UTRs of transcripts encoding ribosomal proteins, elongation factors and other components of the translational machinery (Proud 2007, 2009). For use as a control, we utilized RACE to

determine the sequence of the GAPDH 5′ UTR (GenBank accession number GU214026). We attained the complete NPM and GAPDH 3′ UTR sequences from GenBank (accession numbers BC054755.1 and NM_008084.2, respectively) (Supplementary Figure 2a).

To investigate whether the NPM 5′ and 3′ UTRs may be important for regulation of the NPM mRNA, we sought to evaluate whether the NPM 5′ and 3′ UTRs were sufficient to modulate translation of another ORF in a manner equivalent to translational regulation of the NPM ORF. Specifically, we wanted to determine whether fusion of the NPM 5′ and 3′ UTRs to a firefly *luciferase* (F*luc*) ORF rendered Fluc expression sensitive to rapamycin. To test this, *Tsc1*$^{-/-}$*p53*$^{-/-}$ MEFs were transduced with plasmids encoding NPM 5′ and 3′ UTR-flanked F*luc* (NPM 5′-*luc*-NPM 3′; Supplementary Figure 2b). Although NPM 5′-luc-NPM 3′ protein activity increased over the duration of serum stimulation, this induction was greatly attenuated in the presence of rapamycin compared with vehicle (Figure 2a). As demonstrated with endogenous NPM (Pelletier *et al*., 2007) (Figure 1a; Supplementary Figure 1a), these data indicate that NPM 5′-luc-NPM 3′ activity is driven by changes in translation rather than transcription. To examine whether the rapamycin-induced reduction of NPM 5′-luc-NPM 3′ activity was specific for an mTOR-regulated mRNA, *Tsc1*$^{-/-}$*p53*$^{-/-}$ MEFs were transduced with plasmids encoding GAPDH 5′ and 3′ UTR-flanked F*luc* (GAPDH 5′-*luc*-GAPDH 3′; Supplementary Figure 2b). Notably, rapamycin failed to affect GAPDH 5′-luc-GAPDH 3′ activity at any time point evaluated (Figure 2b).

To examine the independent roles of each NPM UTR as potential targets of regulation, we generated chimeric reporters by fusing the NPM 5′ UTR and the GAPDH 3′ UTR or the GAPDH 5′ UTR and the NPM 3′ UTR to the respective ends of the F*luc* ORF (Supplementary Figure 2b). Surprisingly, NPM 5′-luc-GAPDH 3′ activity resembled GAPDH 5′-luc-GAPDH 3′ activity, with rapamycin having no effect at any time point measured (Figure 2c). GAPDH 5′-luc-NPM 3′ activity, however, demonstrated rapamycin sensitivity similar to that observed with NPM 5′-luc-NPM 3′ activity (Figure 2d). Collectively, these data suggest that sequences within the NPM 3′ UTR, but not in the NPM 5′ UTR, mediate regulation of NPM mRNA

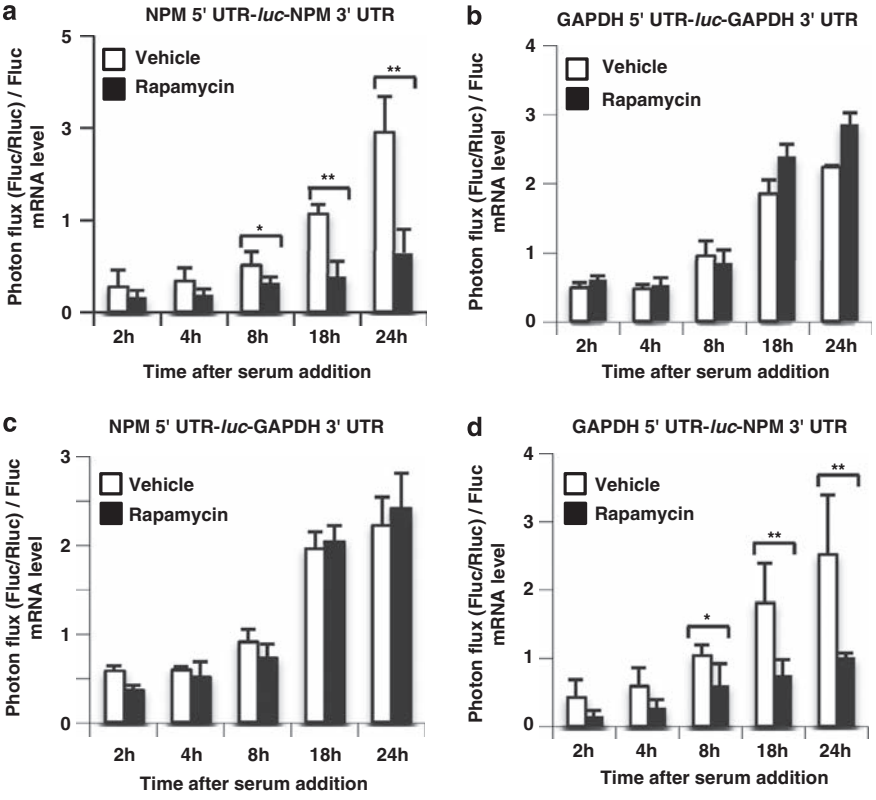

Figure 2 The NPM 3′ UTR is sufficient to confer NPM-like translational control to a *luciferase* ORF. (**a**–**d**) *Tsc1*$^{-/-}$*p53*$^{-/-}$ MEFs were transfected with plasmids depicted in Supplementary Figure 2b. Cells were serum starved and then incubated with 10% serum in the presence or absence of rapamycin for the indicated durations. Plasmid expressing CMV-driven *Renilla* luciferase (Rluc) was used as an internal control for transfection efficiency. Photon flux was calculated by normalizing firefly *luciferase* (Fluc) activity to Rluc activity. Levels of Fluc mRNA at each time point were measured by qRT–PCR from total RNA isolated from transfected MEFs. Shown is photon flux normalized to Fluc mRNA levels. Data are mean ± s.d. of quadruplicate samples per condition from three independent experiments (*$P<0.05$, **$P<0.005$, Student's *t*-test). (**a**) Rapamycin reduces NPM 5′ UTR-Fluc-NPM 3′ UTR activity. (**b**) Activity of GAPDH 5′ UTR-Fluc-GAPDH 3′ UTR is unchanged upon treatment with rapamycin. (**c**) Rapamycin has no effect on NPM 5′ UTR-Fluc-GAPDH 3′ UTR activity. (**d**) Activity of GAPDH 5′ UTR-Fluc-NPM 3′ UTR is abrogated upon rapamycin treatment.

translation, as the NPM 3′ UTR alone was sufficient to render the F*luc* ORF rapamycin-sensitive. Given that rapamycin sensitivity of 5′ terminal oligopyrimidine tract mRNAs ranges from resistance to marked repression (Patursky-Polischuk *et al*., 2009), these data are in accordance with the poorly understood role of the 5′ terminal oligopyrimidine tract. Our findings are consistent with reports highlighting the paucity of regulatory protein–RNA interactions in the 5′ UTR, but the abundance of examples for 3′ UTR–protein regulation (Jackson *et al*., 2010).

FBP1 interacts specifically with the NPM 3′ UTR

Although reporter assay data (Figures 2a–d) indicated that only the NPM 3′ UTR is important for modulation of the NPM mRNA, we undertook an unbiased approach to screen for putative regulatory binding proteins of the NPM 5′ and 3′ UTRs. We utilized an RNA pull-down assay coupled to mass spectrometry to identify proteins that bind the NPM 5′ or 3′ UTR. Whole cell lysates prepared from *Tsc1*$^{-/-}$*p53*$^{-/-}$ MEFs treated with vehicle or rapamycin were incubated with biotinylated NPM 5′ UTR or 3′ UTR RNA. Several proteins were found to preferentially interact with the NPM 3′ UTR, but none appeared to bind exclusively to the NPM 5′ UTR, consistent with reporter assay findings (Figure 3a, arrows). We next employed mass spectrometry to identify putative NPM 3′ UTR binding proteins and confirmed their identities as FBP1, FBP2 (also known as KHSRP or KSRP) and heterogeneous nuclear ribonucleoprotein A/B (Figure 3a; Supplementary Figure 3). It should be noted that mass spectrometry also identified non-FBP1 and 2 peptides from the stained bands depicted, suggesting that proteins other than FBP1 and 2 co-exist at this molecular weight on the gel. As the A/B subfamily of heterogeneous nuclear ribonucleoproteins refer to several promiscuous, multifunctional RNA binding proteins (He and Smith, 2009), subsequent experiments focused on evaluating the roles of FBPs in NPM translational regulation.

The FBP family is most noted for its transcriptional activation of c-*myc* (Duncan *et al*., 1994; He *et al*., 2000); however, the FBPs have also been reported to bind several RNAs, though *in vitro* studies only (Chung *et al*., 2006). To evaluate FBP binding specificity, we incubated biotinylated GAPDH 5′ UTR, GAPDH 3′ UTR, NPM 5′ UTR or NPM 3′ UTR RNA with whole cell lysates from *Tsc1*$^{-/-}$*p53*$^{-/-}$ MEFs treated with vehicle or rapamycin. FBP1 and FBP2 were visualized by western blot analysis of UTR-precipitated samples (Figure 3b). Although FBP3 was not identified by mass spectrometry (Figure 3a; Supplementary Figure 3), we also analyzed it by immunoblot assay, as it is a member of the highly related FBP protein family. Consistent with analyses from mass spectrometry, however, FBP3 was undetectable. FBP1 was precipitated exclusively by the NPM 3′ UTR (Figure 3b). FBP2 was precipitated predominantly by the NPM 3′ UTR, but also by the GAPDH 3′ UTR and the NPM 5′ UTR in vehicle-treated cells (Figure 3b). The more promiscuous RNA

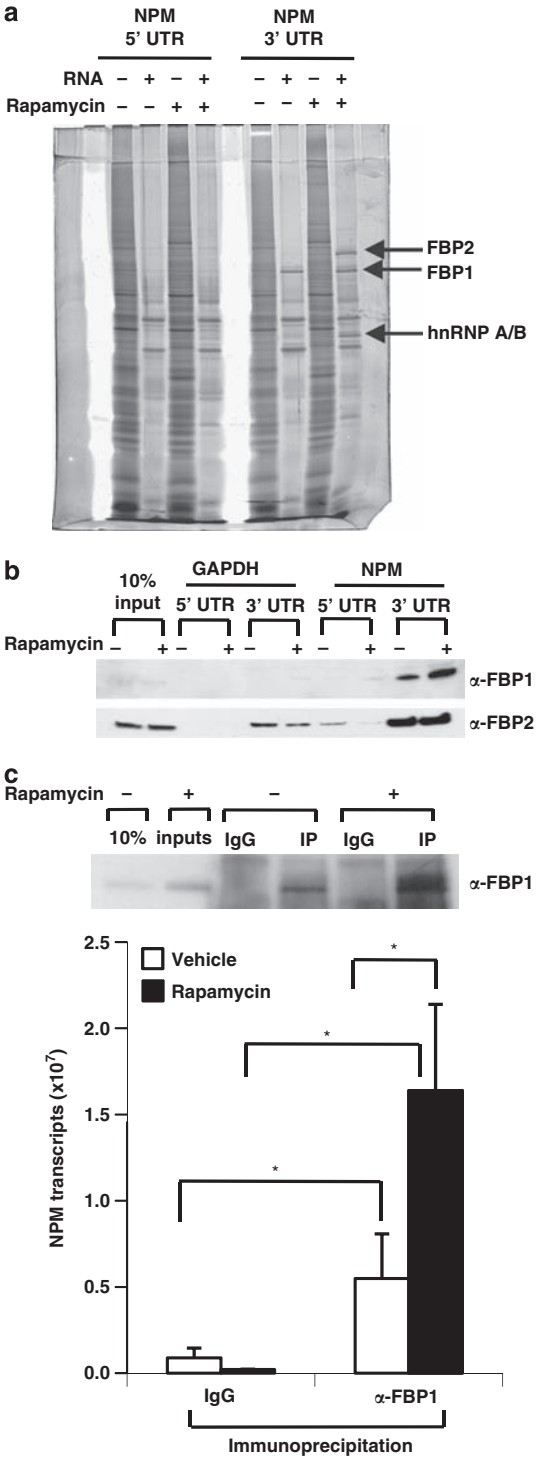

Figure 3 FBP1 interacts specifically with the NPM 3′ UTR. (**a**) Identification of NPM 3′ UTR binding proteins. Lanes indicated as RNA (−) represent samples pre-cleared with streptavidin sepharose. Arrows indicate proteins selected as putative regulatory binding proteins of the NPM 3′ UTR, and identified proteins are shown. (**b**) FBP1 specifically interacts with the NPM 3′ UTR. (**c**) Endogenous NPM mRNAs preferentially bind FBP1 in rapamycin-treated cells. FBP1 was immunoprecipitated from vehicle-treated (−) or rapamycin-treated (+) *Tsc1*$^{-/-}$*p53*$^{-/-}$ MEF lysates with anti-FBP1 antibody. Non-immune goat serum (IgG) was used as a control. NPM mRNA from immunoprecipitates was measured by qRT–PCR. Data are mean ± s.d. of triplicate samples from three independent experiments (*$P<0.05$, Student's *t*-test).

binding by FBP2 is in agreement with previous reports implicating FBP2 in RNA editing, RNA trafficking, RNA stabilization and RNA decay (Min *et al*., 1997; Kroll *et al*., 2002; Snee *et al*., 2002; Briata *et al*., 2003, 2005; Gherzi *et al*., 2004; Li *et al*., 2009). However, given that the interaction of FBP1 with the NPM 3′ UTR appeared to be specific, especially in the presence of rapamycin, we focused on the role of FBP1 in modulating NPM translation.

We next sought to verify the interaction of FBP1 with endogenous NPM mRNAs. FBP1 was immunoprecipitated from whole cell extracts prepared from *Tsc1*$^{-/-}$*p53*$^{-/-}$ MEFs treated with vehicle or rapamycin (Figure 3c, top). Total RNA was isolated from FBP1 immunoprecipitates, and bound NPM mRNA was measured by quantitative real-time PCR. Significantly higher numbers of NPM transcripts were associated with FBP1 in rapamycin-treated cells versus vehicle-treated cells (Figure 3c, bottom). Interestingly, FBP1 protein expression dramatically increased upon inhibition of mTOR (Supplementary Figure 4), suggesting that the enhanced affinity of FBP1 for the NPM 3′ UTR in the presence of rapamycin was a result of induced FBP1 expression. Additionally, we did not observe any post-translational modification in identified FBP1 peptides by mass spectrometry (Supplementary Figure 3), again suggesting that a change in FBP1 expression may be sufficient to drive its interaction with the NPM 3′ UTR.

FBP1 overexpression represses NPM translation

To explore the functional role of FBP1 in NPM translational regulation, we evaluated the effects of FBP1 overexpression. Ectopic expression of Flag epitope-FBP1 in *Tsc1*$^{-/-}$*p53*$^{-/-}$ MEFs drastically reduced NPM protein levels (Figure 4a). Consistent with FBP1 functioning as a translational regulator of NPM expression, NPM mRNA levels remained unchanged upon FBP1 overexpression (Supplementary Figure 1b). We questioned whether FBP1 overexpression could mimic inhibition of mTOR by reducing polysome-associated NPM transcripts. To test this, cytosolic ribosomes were isolated by sucrose gradient centrifugation from equal numbers of *Tsc1*$^{-/-}$*p53*$^{-/-}$ MEFs transduced with vector or Flag-tagged FBP1. Unlike rapamycin treatment, FBP1 overexpression failed to dramatically diminish the overall formation of polysomes (Figure 4b). Distribution of NPM transcripts in monosome/disome and polysome fractions, however, was analogous to the NPM mRNA distribution observed upon inhibition of mTOR (Figure 4c and Figure 1c). In cells overexpressing FBP1, exclusion of NPM mRNAs from polysomes and accumulation in 80S fractions was visible although less pronounced compared with the shift of NPM transcripts from polysomes to monosomes/disomes measured in rapamycin-treated cells (Figure 4c and Figure 1c).

Mechanistically, we questioned whether FBP1 overexpression induces the formation of processing bodies or stress granules. To test this, we transduced *Tsc1*$^{-/-}$*p53*$^{-/-}$ MEFs with vector or Flag-tagged FBP1. We treated cells with arsenite as a positive control to stimulate processing body and stress granule assembly (Kedersha *et al*., 2005; Wilczynska *et al*., 2005; Yu *et al*., 2005).

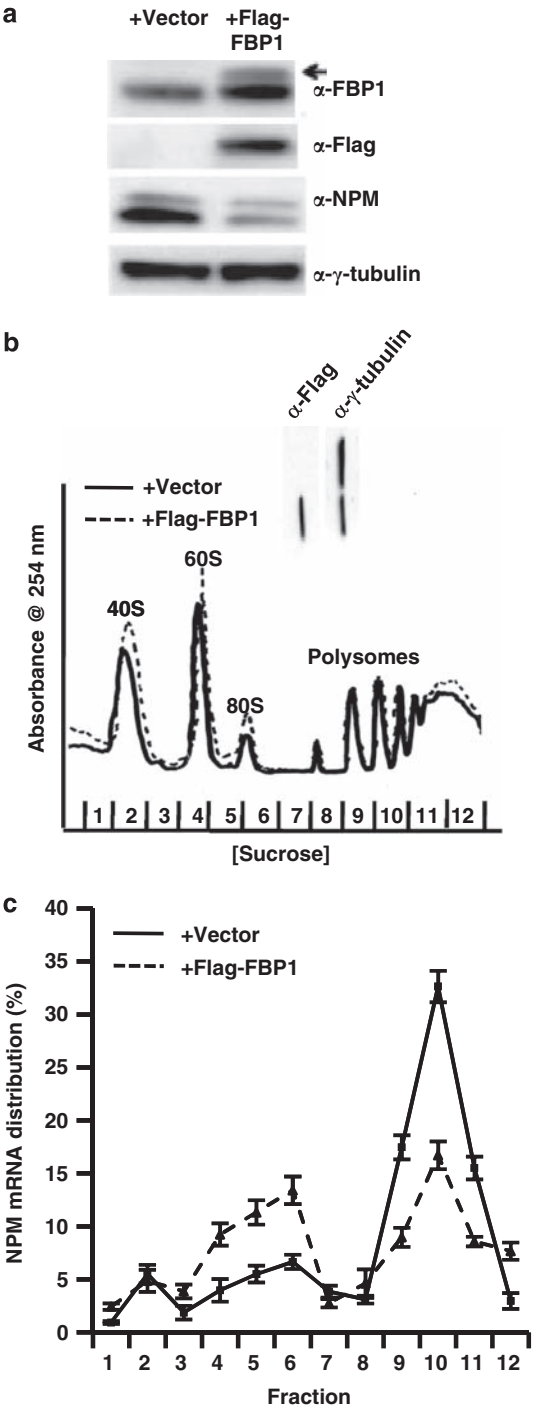

Figure 4 FBP1 overexpression represses NPM translation. (**a**) Overexpression of FBP1 results in reduced NPM protein levels. (**b**) Overexpression of FBP1 fails to affect polysome formation. (**c**) NPM mRNAs are excluded from actively translating polysomes upon FBP1 overexpression. Monosome/disome- and polysome-associated NPM mRNAs were measured by qRT–PCR and were calculated as percentage of total NPM mRNAs. Data are mean ± s.d. of triplicate samples from three independent experiments.

As demonstrated by immunofluorescent detection of TIA-1, a marker of stress granules (Yang *et al*., 2006), arsenite treatment but not ectopic expression of Flag-FBP1 induced stress granule accumulation (Supplementary Figure 5). Thus, FBP1 overexpression is not sufficiently stressful to stimulate aggregation of stalled translation pre-initiation complexes (Kedersha *et al*., 2005). Nonetheless, these findings demonstrate that FBP1 represses NPM translation.

Depletion of FBP1 enhances NPM translation and cell proliferation

To further investigate the functional role of FBP1 as a translational regulator of NPM expression, we transduced *Tsc1*$^{-/-}$*p53*$^{-/-}$ MEFs with control small interfering (si)RNA or two different siRNAs targeting murine FBP1. The presence of FBP1-siRNA #2 caused a marked reduction in FBP1 protein, whereas FBP1-siRNA #3 yielded a more modest decrease (Figure 5a). Increase in NPM protein expression correlated with the amount of FBP1 reduction, as siRNA #2 resulted in higher NPM induction than that observed with siRNA #3 (Figure 5a). Again, consistent with NPM protein expression being regulated independent of transcription, NPM mRNA levels remained constant in the presence of either siRNA targeting FBP1 (Supplementary Figure 1c).

We next wanted to determine whether depletion of FBP1 leads to enhanced polysome-associated NPM transcripts. We isolated cytosolic ribosomes by sucrose gradient centrifugation from equal numbers of *Tsc1*$^{-/-}$*p53*$^{-/-}$ MEFs transduced with control siRNA or two siRNAs targeting FBP1. Depletion of FBP1 resulted in elevated formation of polysomes actively engaged in mRNA translation (Figure 5b). As observed with NPM protein induction (Figure 5a), polysome enhancement corresponded with the degree of FBP1 reduction (Figure 5b). Furthermore, also relative to the amount of FBP1 depletion, NPM transcripts associated with actively translating polysomes were dramatically elevated in the presence of siRNAs targeting FBP1 compared with control siRNA (Figure 5c).

Based on the striking enhancement of ribosome recruitment to NPM mRNAs observed upon FBP1 depletion and previous reports demonstrating the ability of NPM to potently promote proliferation (Maggi *et al*., 2008; Brady *et al*., 2009), we sought to explore the effects of FBP1-mediated NPM induction on cellular proliferation. In cells depleted of FBP1, we observed increased proliferation rates relative to control siRNA-transfected cells (Figure 5d). Again, enhancement of proliferation correlated with the amount of FBP1 reduction. Importantly, enhanced proliferation was abrogated in cells depleted of FBP1 and NPM (Figure 5e), indicating that elevated NPM protein expression indeed underlies the increased proliferation rates observed upon FBP1 depletion. Taken together, these findings indicate that FBP1 is necessary to restrain NPM translation and, thereby, cell proliferation.

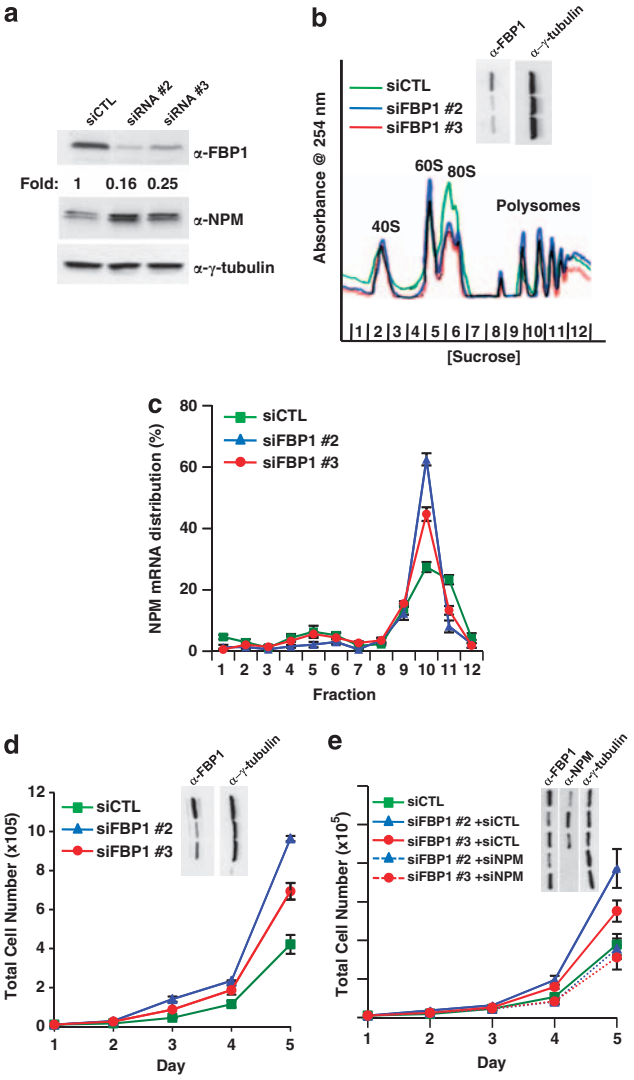

Figure 5 FBP1 depletion enhances NPM translation. (**a**) FBP1 knockdown increases levels of NPM protein. *Tsc1*$^{-/-}$*p53*$^{-/-}$ MEFs were transfected with control siRNA (siCTL) or two different siRNAs targeting FB1. (**b**) Knockdown of FBP1 results in increased polysome formation. (**c**) NPM mRNAs are recruited to actively translating polysomes upon FBP1 depletion. Monosomal/disomal and polysomal NPM mRNAs were measured by qRT–PCR and were calculated as percentage of total NPM mRNAs. Data are mean ± s.d. of triplicate samples from three independent experiments. (**d**) Knockdown of FBP1 leads to enhanced cell proliferation. (**e**) Co-depletion of FBP1 and NPM abrogates elevated cell proliferation.

Discussion

Here, we have demonstrated that NPM expression is regulated at the level of translation and that the 3′ UTR of the NPM mRNA is sufficient to confer rapamycin sensitivity to a reporter ORF. Further analyses identified FBP1 as a protein that selectively interacts with the NPM 3′ UTR. FBP1 overexpression and knockdown data are consistent with FBP1 functioning to negatively regulate translation of NPM mRNAs.

Though we have demonstrated that NPM mRNAs are largely excluded from polysomes by FBP1, further

studies will be needed to provide insight into the precise mechanism by which FBP1 binding to the NPM 3′ UTR negatively regulates NPM translation. It appears that FBP1 represses NPM translation by interfering with translation initiation, as the shift in NPM mRNA distribution from polysomes to monosomes/disomes is indicative of a reduced translation initiation rate (Meyuhas, 2000).

Collectively, our data suggest that FBP1 acts as a suppressor of proliferation through its direct repression of NPM translation. This is consistent with the requirement of NPM expression for continued cellular proliferation and growth both *in vitro* and *in vivo* (Grisendi *et al*., 2005; Maggi *et al*., 2008; Brady *et al*., 2009). By targeting NPM, FBP1 appears to at least mimic the functional activity of the ARF tumor suppressor. Numerous studies have shown that ARF binds directly to NPM to inhibit its activity and prevent cell growth (Itahana *et al*., 2003; Bertwistle *et al*., 2004; Brady *et al*., 2004). Through its ability to repress NPM translation, FBP1 also antagonizes NPM to suppress cell growth and proliferation. Of particular interest is the question of whether FBP1, like ARF, utilizes its anti-NPM function to serve as a tumor suppressor.

Materials and methods

Cell culture and transfection

Tsc1$^{-/-}$*p53*$^{-/-}$ MEFs were maintained in DMEM supplemented as described previously (Pelletier *et al*., 2007). For bioluminescence assays, transfections were performed using Lipofectamine 2000 transfection reagent (Invitrogen, Carlsbad, CA, USA). All other transfections were carried out using the Nucleofector system (Amaxa, Walkersville, MD, USA) according to the manufacturer's instructions.

5′ RACE and 3′ UTR sequences

Sequences of the GAPDH and NPM 5′ UTRs were obtained by 5′ RACE using GeneRacer (Invitrogen) according to the manufacturer's instructions. For the GAPDH 5′ UTR and the NPM 5′ UTR, the forward GeneRacer 5′ nested primer (5′-GGACACTGACATGGACTGAAGGAGTA-3′) was used. For the GAPDH 5′ UTR, we used the following gene-specific reverse primer: 5′-GCATTGCTGACAATCTTGAGTGAG TTG-3′. The following gene-specific reverse primer was used for the NPM 5′ UTR: 5′-CATGTCCATATCCATCGAGT CTTCCAT-3′. Sequences of the GAPDH and NPM 3′ UTRs were obtained from GenBank (accession numbers NM_008084.2 and BC054755.1, respectively).

Plasmids

The GAPDH 5′ UTR, GAPDH 3′ UTR, NPM 5′ UTR and NPM 3′ UTR were PCR-amplified from genomic DNA of wild type C57BL/6 mice. The following primers were used: GAPDH 5′ UTR: forward, 5′-CTCTCTGCTCCTCCCTGTT CCAG-3′; reverse, 5′-TTTGTCTACGGGACGAGGCTG-3′; GAPDH 3′ UTR: forward, 5′-GAAACCCTGGACCACC CACCCC-3′; reverse, 5′-TTTTTTTTTTTTTTTTTTT-3′; NPM 5′ UTR: forward, 5′-CTTTCCTTGGCGTGATTCCG-3′; reverse, 5′-GAGGTGGAGGCGCGCACTT-3′; NPM 3′ UTR: forward, 5′-GAAAAGGGTTTAAACAG-3′; reverse, 5′-TTTTTTTTTTTTTTTTTT-3′. The GAPDH 5′ UTR, GAPDH 3′ UTR, NPM 5′ UTR and NPM 3′ UTR PCR products were cloned into the pCR 2.1-TOPO vector (Invitrogen) for use in *in vitro* transcription. For bioluminescence assays, the GAPDH 5′ UTR and the NPM 5′ UTR were sub-cloned into the HindIII and NcoI sites of the pGL3-Control vector (Promega, Madison, WI, USA). The GAPDH 3′ UTR and the NPM 3′ UTR were sub-cloned into the XbaI and HpaI sites of pGL3-Control. pRluc-N3(h) (BioSignal Packard, Waltham, MA, USA) was used as a control for transfection efficiency.

Western blot analyses

Tsc1$^{-/-}$*p53*$^{-/-}$ MEFs were lysed by sonication in EBC buffer as previously described (Maggi *et al*., 2008). The following antibodies were used at the dilutions indicated: anti-NPM (Santa Cruz, Santa Cruz, CA, USA, sc6013; 1:1000), anti-γ-tubulin (Santa Cruz, sc17787; 1:500), anti-FBP1 (Abcam, Cambridge, MA, USA, ab28732; 1:1600; western blot only), anti-FBP1 (Santa Cruz, sc11101; 1:500; immunoprecipitation only), anti-FBP2 (Abnova, Taipei City, Taiwan, H00008570-A01; 1:2000), anti-FBP3 (Santa Cruz, sc11103; 1:500), and anti-Flag M2 (Sigma, St Louis, MO, USA, F1804; 1:1000). ImageScanner III (GE Healthcare, Piscataway, NJ, USA) was used to scan autoradiograms, and densities were measured with ImageQuant V. 2005 (GE Healthcare).

Immunoprecipitations

Tsc1$^{-/-}$*p53*$^{-/-}$ MEFs were treated with vehicle or rapamycin for 48 h and lysed by sonication in EBC buffer as described above. Whole cell lysates (500 μg) were pre-cleared with 50 μl of protein A/G PLUS-agarose (Santa Cruz, sc2003) for 1 h at 4 °C with rotation. Pre-cleared lysates were then subjected to immunoprecipitation using anti-FBP1 antibody (Santa Cruz, sc11101) or non-immune goat serum (Santa Cruz, 2028).

Quantitative RT–PCR

Total RNA was extracted from *Tsc1*$^{-/-}$*p53*$^{-/-}$ MEFs with RNA-*Solv* (Omega Bio-tek, Norcross, GA, USA). Reverse transcription reactions were performed using the SuperScript III first-strand synthesis system (Invitrogen) with oligo d(T) primer according to the manufacturer's instructions. Real-time PCR was performed on an iCycler apparatus (Bio-Rad, Hercules, CA, USA). To amplify NPM and GAPDH mRNAs from monosome/disome and polysome fractions, we used SsoFast EvaGreen supermix (Bio-Rad) and the following primers: NPM: forward, 5′-GGAAGACTCGATGGATA TGG-3′; reverse, 5′-CTTCAACCGTAAGACCACAGG-3′; GAPDH: forward, 5′-GCTGGGGCTCACCTGAAGGG-3′; reverse, 5′-GGATGACCTTGCCCACAGCC-3′. To measure NPM mRNA in immunoprecipitates, the primers used are described above. Numbers of NPM transcripts per cell were calculated by extrapolation from a standard curve generated from serial dilutions of a known quantity of subcloned NPM complementary DNA. To amplify NPM mRNA or firefly luciferase mRNA not isolated from ribosome fractions or immunoprecipitates, iQ Sybr green supermix (Bio-Rad) was used. Histone 3.3 mRNA was amplified as an expression control. For NPM, the primers used are described above. The following other primers were used: firefly luciferase: forward, 5′-CCCTGGTTCCTGGAACAATT-3′; reverse, 5′-GCAACC CCTTTTTGGAAACG-3′; histone 3.3: forward, 5′-CGTG AAATCAGACGCTATCAGAA-3′; reverse, 5′-TCGCACCA GACGCTGAAAG-3′.

Bioluminescence imaging

Phenol red-free DMEM was supplemented with 10% fetal bovine serum and with D-luciferin (150 μg/ml; Biosynth, Itasca,

IL, USA) or coelenterazine (1 μg/ml; Biotium, Hayward, CA, USA). Assay plates were imaged using an IVIS100 imaging system (Xenogen Caliper, Hopkinton, MA, USA). Acquisition parameters were as follows: acquisition time, 60 s (firefly luciferase) or 300 s (*Renilla* luciferase); binning, 4; field of view, 10 cm; f/stop, 1; filter, open. Photon flux data were analyzed with Living Image (Xenogen Caliper) and Igor (Wavemetrics, Portland, OR, USA) image analysis software platforms, and expressed as the ratio of Fluc to Rluc as described (Gross and Piwnica-Worms, 2005).

Ribosome fractionation
Cells were treated with cycloheximide (10 μg/ml) before harvesting and counting. Equal numbers of cells (3×10^6) were lysed, and cytosolic extracts were subjected to ribosome fractionation as previously described (Strezoska *et al*., 2000) using a density gradient system (Teledyne ISCO, Lincoln, NE, USA).

In vitro *transcription*
DNA templates for *in vitro* transcription were GAPDH 5′ UTR, GAPDH 3′ UTR, NPM 5′ UTR and NPM 3′ UTR PCR products cloned into the pCR 2.1-TOPO vector (Invitrogen). To increase proximity of the UTR sequence to the T7 promoter, we excised the EcoRV-ApaI fragment between the PCR product and T7 promoter. DNA was linearized by digestion with BstXI. We used the Megashortscript kit (Ambion, Austin, TX, USA) for transcription with 0.5 mM biotinylated UTP (Enzo Life Sciences, Plymouth Meeting, PA, USA) and 7.5 mM ATP, CTP, GTP and UTP.

RNA pull-down assay
For analysis by mass spectrometry, whole cell lysates (500 μg) prepared from *Tsc1*$^{-/-}$*p53*$^{-/-}$ MEFs treated with vehicle or rapamycin were pre-cleared with 50 μl streptavidin sepharose (GE Healthcare). Pre-cleared lysates were then incubated with biotinylated GAPDH 5′ or 3′ UTR RNA or NPM 5′ or 3′ UTR RNA (20 μg) in binding buffer (10 mM HEPES (pH 7.5), 90 mM potassium acetate, 1.5 mM magnesium acetate, 40 mM KCl, 2.5 mM DTT, 0.05% NP40, protease inhibitor cocktail and 0.5 mM PMSF). Protein and biotinylated RNA mixtures were recovered by incubation with 50 μl streptavidin sepharose. Eluted proteins were separated on 10% polyacrylamide SDS gels and stained with SYPRO-Ruby dye. To validate results from mass spectrometry, RNA pull-down assays were performed as described, but amounts of whole cell lysate and biotinylated UTR RNA were halved.

Nano-LC FT-mass spectrometry (MS) analysis
MS was performed using the system previously described (King *et al*., 2006). The survey scans ($m/z = 350$–2000) were acquired using FTICR-MS with a resolution of 100 000 at $m/z = 421.75$ with a target value of 500 000. The ten most intense ions from survey scans were isolated in the ion trap and analyzed after reaching a target value of 10 000. The MS/MS isolation width was 2.5 Da and the normalized collision energy was 35% using wide band activation. The electrospray ionization was accomplished with a spray voltage of 2.2 kV without sheath gas. The ion transfer tube temperature was 200 °C.

RNA interference
The following HP GenomeWide (Qiagen, Valencia, CA, USA) siRNA oligonucleotides were used: FBP1-2 (5′-CAGG AACGGGCTGGTGTTAAA-3′), FBP1-3 (5′-ATGCTTTGT GATATAAATGTA-3′) and NPM1-3 (5′-CAAGTTCATT AATTATGTGAA -3′). As a control, si*CONTROL* RISC-free siRNA (Dharmacon, Lafayette, CO, USA, D- 001220-01-05) was used. *Tsc1*$^{-/-}$*p53*$^{-/-}$ MEFs (2×10^6) were transfected with 0.2 nM of oligonucleotide using the Nucleofector system (Amaxa) according to the manufacturer's instructions. Cells were assayed 48 h after transfection.

FBP1 overexpression
Tsc1$^{-/-}$*p53*$^{-/-}$ MEFs (2×10^6) were transfected with pGL3 Control (Promega; 2 μg) or Flag-FBP1 (Origene, Rockville, MD, USA; 2 μg) using the Nucleofector system (Amaxa) according to the manufacturer's instructions. Cells were assayed 24 h post-transfection.

Immunofluorescence
Tsc1$^{-/-}$*p53*$^{-/-}$ MEFs were transduced with pGL3 Control (Promega; 2 μg) or Flag-FBP1 (Origene; 2 μg) using the Nucleofector system (Amaxa). To induce formation of stress granules, cells were treated with 0.5 mM sodium arsenite (Sigma, S7400) for 1 h. Cells were fixed with 4% paraformaldehyde and were permeabilized with methanol. The following antibodies were used at the dilutions indicated: anti-Flag M2 (Sigma, F1804; 1:100) and anti-TIA-1 (Santa Cruz, sc1751; 1:100).

Conflict of interest

The authors declare no conflict of interest.

Acknowledgements

We thank the members of the Weber, Townsend and Piwnica-Worms laboratories for their advice and technical assistance. The *luciferase* reporter work was initiated through a Pilot Grant from the Washington University Imaging Center. MEO was supported by NIH 5T32 GM007067. This research was supported with Grants from the National Institutes of Health, P30 CA91842 to the Siteman Comprehensive Cancer Center and P41RR000954 and UL1 RR024992 from the National Center for Research Resources to the Proteomics Center. DPW and BLM were supported by NIH P50 CA94056. This work was supported by NIH Grant CA128007 and an Era of Hope Scholar Award in Breast Cancer Research (BC007304) to JDW.

References

Bertwistle D, Sugimoto M, Sherr CJ. (2004). Physical and functional interactions of the Arf tumor suppressor protein with nucleophosmin/B23. *Mol Cell Biol* **24**: 985–996.

Brady SN, Maggi Jr LB, Winkeler CL, Toso EA, Gwinn AS, Pelletier CL *et al*. (2009). Nucleophosmin protein expression level, but not threonine 198 phosphorylation, is essential in growth and proliferation. *Oncogene* **28**: 3209–3220.

Brady SN, Yu Y, Maggi Jr LB, Weber JD. (2004). ARF impedes NPM/B23 shuttling in an Mdm2-sensitive tumor suppressor pathway. *Mol Cell Biol* **24**: 9327–9338.

Brennan CM, Steitz JA. (2001). HuR and mRNA stability. *Cell Mol Life Sci* **58**: 266–277.

Briata P, Forcales SV, Ponassi M, Corte G, Chen CY, Karin M *et al*. (2005). p38-dependent phosphorylation of the mRNA decay-promoting factor KSRP controls the stability of select myogenic transcripts. *Molecular Cell* **20**: 891–903.

Briata P, Ilengo C, Corte G, Moroni C, Rosenfeld MG, Chen CY *et al*. (2003). The Wnt/beta-catenin—>Pitx2 pathway controls the turnover of Pitx2 and other unstable mRNAs. *Molecular Cell* **12**: 1201–1211.

Chung HJ, Liu J, Dundr M, Nie Z, Sanford S, Levens D. (2006). FBPs are calibrated molecular tools to adjust gene expression. *Mol Cell Biol* **26**: 6584–6597.

Colombo E, Marine JC, Danovi D, Falini B, Pelicci PG. (2002). Nucleophosmin regulates the stability and transcriptional activity of p53. *Nat Cell Biol* **4**: 529–533.

de Moor CH, Meijer H, Lissenden S. (2005). Mechanisms of translational control by the 3′ UTR in development and differentiation. *Semin Cell Dev Biol* **16**: 49–58.

Duncan R, Bazar L, Michelotti G, Tomonaga T, Krutzsch H, Avigan M *et al*. (1994). A sequence-specific, single-strand binding protein activates the far upstream element of c-myc and defines a new DNA-binding motif. *Genes Dev* **8**: 465–480.

Galban S, Kuwano Y, Pullmann Jr R, Martindale JL, Kim HH, Lal A *et al*. (2008). RNA-binding proteins HuR and PTB promote the translation of hypoxia-inducible factor 1alpha. *Mol Cell Biol* **28**: 93–107.

Gebauer F, Hentze MW. (2004). Molecular mechanisms of translational control. *Nat Rev Mol Cell Biol* **5**: 827–835.

Gherzi R, Lee KY, Briata P, Wegmuller D, Moroni C, Karin M *et al*. (2004). A KH domain RNA binding protein, KSRP, promotes ARE-directed mRNA turnover by recruiting the degradation machinery. *Molecular Cell* **14**: 571–583.

Grisendi S, Bernardi R, Rossi M, Cheng K, Khandker L, Manova K *et al*. (2005). Role of nucleophosmin in embryonic development and tumorigenesis. *Nature* **437**: 147–153.

Grisendi S, Mecucci C, Falini B, Pandolfi PP. (2006). Nucleophosmin and cancer. *Nat Rev Cancer* **6**: 493–505.

Gross S, Piwnica-Worms D. (2005). Real-time imaging of ligand-induced IKK activation in intact cells and in living mice. *Nat Methods* **2**: 607–614.

Hamilton BJ, Wang XW, Collins J, Bloch D, Bergeron A, Henry B *et al*. (2008). Separate cis-trans pathways post-transcriptionally regulate murine CD154 (CD40 ligand) expression: a novel function for CA repeats in the 3′-untranslated region. *J Biol Chem* **283**: 25606–25616.

He L, Liu J, Collins I, Sanford S, O'Connell B, Benham CJ *et al*. (2000). Loss of FBP function arrests cellular proliferation and extinguishes c-myc expression. *EMBO J* **19**: 1034–1044.

He Y, Smith R. (2009). Nuclear functions of heterogeneous nuclear ribonucleoproteins A/B. *Cell Mol Life Sci* **66**: 1239–1256.

Irwin N, Baekelandt V, Goritchenko L, Benowitz LI. (1997). Identification of two proteins that bind to a pyrimidine-rich sequence in the 3′-untranslated region of GAP-43 mRNA. *Nucleic Acids Res* **25**: 1281–1288.

Itahana K, Bhat KP, Jin A, Itahana Y, Hawke D, Kobayashi R *et al*. (2003). Tumor suppressor ARF degrades B23, a nucleolar protein involved in ribosome biogenesis and cell proliferation. *Mol Cell* **12**: 1151–1164.

Jackson RJ, Hellen CU, Pestova TV. (2010). The mechanism of eukaryotic translation initiation and principles of its regulation. *Nat Rev Mol Cell Biol* **11**: 113–127.

Jefferies HB, Fumagalli S, Dennis PB, Reinhard C, Pearson RB, Thomas G. (1997). Rapamycin suppresses 5′TOP mRNA translation through inhibition of p70s6k. *EMBO J* **16**: 3693–3704.

Jiang Y, Xu XS, Russell JE. (2006). A nucleolin-binding 3′ untranslated region element stabilizes beta-globin mRNA *in vivo*. *Mol Cell Biol* **26**: 2419–2429.

Kedersha N, Stoecklin G, Ayodele M, Yacono P, Lykke-Andersen J, Fritzler MJ *et al*. (2005). Stress granules and processing bodies are dynamically linked sites of mRNP remodeling. *J Cell Biol* **169**: 871–884.

King JB, Gross J, Lovly CM, Rohrs H, Piwnica-Worms H, Townsend RR. (2006). Accurate mass-driven analysis for the characterization of protein phosphorylation. Study of the human Chk2 protein kinase. *Anal Chem* **78**: 2171–2181.

Kroll TT, Zhao WM, Jiang C, Huber PW. (2002). A homolog of FBP2/KSRP binds to localized mRNAs in Xenopus oocytes. *Development* **129**: 5609–5619.

Li H, Chen W, Zhou Y, Abidi P, Sharpe O, Robinson WH *et al*. (2009). Identification of mRNA binding proteins that regulate the stability of LDL receptor mRNA through AU-rich elements. *J Lipid Res* **50**: 820–831.

Maggi LB, Kuchenruether M, Dadey DYA, Schwope RM, Grisendi S, Townsend RR *et al*. (2008). Nucleophosmin serves as a rate-limiting nuclear export chaperone for the mammalian ribosome. *Mol Cell Biol* **28**: 7050–7065.

Mazan-Mamczarz K, Galban S, Lopez de Silanes I, Martindale JL, Atasoy U, Keene JD *et al*. (2003). RNA-binding protein HuR enhances p53 translation in response to ultraviolet light irradiation. *Proc Natl Acad Sci USA* **100**: 8354–8359.

Mendez R, Myers Jr MG, White MF, Rhoads RE. (1996). Stimulation of protein synthesis, eukaryotic translation initiation factor 4E phosphorylation, and PHAS-I phosphorylation by insulin requires insulin receptor substrate 1 and phosphatidylinositol 3-kinase. *Mol Cell Biol* **16**: 2857–2864.

Meyuhas O. (2000). Synthesis of the translational apparatus is regulated at the translational level. *Eur J Biochem* **267**: 6321–6330.

Min H, Turck CW, Nikolic JM, Black DL. (1997). A new regulatory protein, KSRP, mediates exon inclusion through an intronic splicing enhancer. *Genes Dev* **11**: 1023–1036.

Okuda M, Horn HF, Tarapore P, Tokuyama Y, Smulian AG, Chan PK *et al*. (2000). Nucleophosmin/B23 is a target of CDK2/cyclin E in centrosome duplication. *Cell* **103**: 127–140.

Okuwaki M, Matsumoto K, Tsujimoto M, Nagata K. (2001). Function of nucleophosmin/B23, a nucleolar acidic protein, as a histone chaperone. *FEBS Lett* **506**: 272–276.

Okuwaki M, Tsujimoto M, Nagata K. (2002). The RNA binding activity of a ribosome biogenesis factor, nucleophosmin/B23, is modulated by phosphorylation with a cell cycle-dependent kinase and by association with its subtype. *Mol Biol Cell* **13**: 2016–2030.

Patursky-Polischuk I, Stolovich-Rain M, Hausner-Hanochi M, Kasir J, Cybulski N, Avruch J *et al*. (2009). The TSC-mTOR pathway mediates translational activation of TOP mRNAs by insulin largely in a raptor- or rictor-independent manner. *Mol Cell Biol* **29**: 640–649.

Pelletier CL, Maggi LB, Brady SN, Scheidenhelm DK, Gutmann DH, Weber JD. (2007). TSC1 sets the rate of ribosome export and protein synthesis through nucleophosmin translation. *Cancer Research* **67**: 1609–1617.

Pontrelli L, Sidiropoulos KG, Adeli K. (2004). Translational control of apolipoprotein B mRNA: regulation via cis elements in the 5′ and 3′ untranslated regions. *Biochemistry* **43**: 6734–6744.

Proud CG. (2007). Signalling to translation: how signal transduction pathways control the protein synthetic machinery. *Biochemical Journal* **403**: 217–234.

Proud CG. (2009). mTORC1 signalling and mRNA translation. *Biochemical Society Transactions* **37**: 227–231.

Qi W, Shakalya K, Stejskal A, Goldman A, Beeck S, Cooke L *et al*. (2008). NSC348884, a nucleophosmin inhibitor disrupts oligomer formation and induces apoptosis in human cancer cells. *Oncogene* **27**: 4210–4220.

Sandsmark DK, Pelletier C, Weber JD, Gutmann DH. (2007). Mammalian target of rapamycin: master regulator of cell growth in the nervous system. *Histol Histopathol* **22**: 895–903.

Sidiropoulos KG, Zastepa A, Adeli K. (2007). Translational control of apolipoprotein B mRNA via insulin and the protein kinase C signaling cascades: evidence for modulation of RNA-protein interactions at the 5′UTR. *Arch Biochem Biophys* **459**: 10–19.

Snee M, Kidd GJ, Munro TP, Smith R. (2002). RNA trafficking and stabilization elements associate with multiple brain proteins. *J Cell Sci* **115**: 4661–4669.

Strezoska Z, Pestov DG, Lau LF. (2000). Bop1 is a mouse WD40 repeat nucleolar protein involved in 28S and 5. 8S RRNA processing and 60S ribosome biogenesis. *Mol Cell Biol* **20**: 5516–5528.

Takagi M, Absalon MJ, McLure KG, Kastan MB. (2005). Regulation of p53 translation and induction after DNA damage by ribosomal protein L26 and nucleolin. *Cell* **123**: 49–63.

Tee AR, Fingar DC, Manning BD, Kwiatkowski DJ, Cantley LC, Blenis J. (2002). Tuberous sclerosis complex-1 and -2 gene products function together to inhibit mammalian target of rapamycin (mTOR)-mediated downstream signaling. *Proc Natl Acad Sci USA* **99**: 13571–13576.

Terada N, Patel HR, Takase K, Kohno K, Nairn AC, Gelfand EW. (1994). Rapamycin selectively inhibits translation of mRNAs encoding elongation factors and ribosomal proteins. *Proc Natl Acad Sci USA* **91**: 11477–11481.

Wickens M, Bernstein DS, Kimble J, Parker R. (2002). A PUF family portrait: 3′UTR regulation as a way of life. *Trends Genet* **18**: 150–157.

Wilczynska A, Aigueperse C, Kress M, Dautry F, Weil D. (2005). The translational regulator CPEB1 provides a link between dcp1 bodies and stress granules. *J Cell Sci* **118**: 981–992.

Wullschleger S, Loewith R, Hall MN. (2006). TOR signaling in growth and metabolism. *Cell* **124**: 471–484.

Yang WH, Yu JH, Gulick T, Bloch KD, Bloch DB. (2006). RNA-associated protein 55 (RAP55) localizes to mRNA processing bodies and stress granules. *RNA* **12**: 547–554.

Yu JH, Yang WH, Gulick T, Bloch KD, Bloch DB. (2005). Ge-1 is a central component of the mammalian cytoplasmic mRNA processing body. *RNA* **11**: 1795–1802.

Yu Y, Maggi LB, Brady SN, Apicelli AJ, Dai MS, Lu H *et al*. (2006). Nucleophosmin is essential for ribosomal protein L5 nuclear export. *Mol Cell Biol* **26**: 3798–3809.

Zhang J, Tsaprailis G, Bowden GT. (2008). Nucleolin stabilizes Bcl-X L messenger RNA in response to UVA irradiation. *Cancer Res* **68**: 1046–1054.

Zhang T, Kruys V, Huez G, Gueydan C. (2002). AU-rich element-mediated translational control: complexity and multiple activities of trans-activating factors. *Biochem Soc Trans* **30**: 952–958.

Supplementary Information accompanies the paper on the Oncogene website (http://www.nature.com/onc)

Published OnlineFirst September 21, 2011; DOI: 10.1158/0008-5472.CAN-11-1472

Molecular and Cellular Pathobiology

Cancer Research

RNA Helicase DDX5 Is a p53-Independent Target of ARF That Participates in Ribosome Biogenesis

Anthony J. Saporita[1,2], Hsiang-Chun Chang[1,2], Crystal L. Winkeler[1,2], Anthony J. Apicelli[1,2], Raleigh D. Kladney[1,2], Jianbo Wang[3], R. Reid Townsend[4], Loren S. Michel[3], and Jason D. Weber[1,2]

Abstract

The p19ARF tumor suppressor limits ribosome biogenesis and responds to hyperproliferative signals to activate the p53 checkpoint response. Although its activation of p53 has been well characterized, the role of ARF in restraining nucleolar ribosome production is poorly understood. Here we report the use of a mass spectroscopic analysis to identify protein changes within the nucleoli of *Arf*-deficient mouse cells. Through this approach, we discovered that ARF limited the nucleolar localization of the RNA helicase DDX5, which promotes the synthesis and maturation of rRNA, ultimately increasing ribosome output and proliferation. ARF inhibited the interaction between DDX5 and nucleophosmin (NPM), preventing association of DDX5 with the rDNA promoter and nuclear pre-ribosomes. In addition, *Arf*-deficient cells transformed by oncogenic RasV12 were addicted to DDX5, because reduction of DDX5 was sufficient to impair RasV12-driven colony formation in soft agar and tumor growth in mice. Taken together, our findings indicate that DDX5 is a key p53-independent target of the ARF tumor suppressor and is a novel non-oncogene participant in ribosome biogenesis. *Cancer Res; 71(21); 6708–17. ©2011 AACR.*

Introduction

The role of ARF in regulating p53 is well established, but the mechanisms by which it exerts its p53-independent tumor suppressor function are yet to be fully characterized. A common theme in p53-independent activity of ARF is its ability to regulate nucleolar ribosome biogenesis (1, 2), but mechanistic details of its involvement have remained elusive. Understanding the p53-independent functions of ARF in the nucleolus is an increasingly important focus in cancer biology.

The nucleolus is a dynamic organelle that assembles around ribosomal DNA (rDNA) repeats and is the cellular center for ribosome biogenesis. Characterization of the nucleolar proteome has revealed the broad spectrum of resident proteins (3). As nucleoli lack membranes, proteins freely diffuse into and out of nucleoli in response to varying conditions (4). Some of the most important residents of nucleoli are proteins that regulate ribosome production, including p19ARF (p14ARF in humans).

The canonical function of ARF is to activate p53 by binding and sequestering the p53 inhibitor Mdm2 (5–8). *Arf* null mice develop spontaneous tumors consisting of predominantly fibrosarcomas and lymphomas (9, 10). However, ARF also possesses p53-independent roles that contribute to its growth-inhibitory function and suppression of tumorigenesis (11). For example, basal ARF maintains nucleolar structure and function (12), at least in part, through its ability to interact with nucleophosmin (NPM; refs. 1, 13–16). The ability of ARF to regulate the nucleolar localization of Mdm2 (6) and the nuclear export of NPM (15) suggests that ARF may monitor nucleolar function by regulating the composition of the nucleolar proteome. To determine how the presence or absence of basal ARF affects nucleolar protein composition, we conducted a proteomic screen using isolated nucleoli from wild-type and $Arf^{-/-}$ mouse embryonic fibroblasts (MEF). Among the proteins enriched in nucleoli in the absence of *Arf* was DDX5, a DEAD-box protein also known as p68 RNA helicase.

The DEAD-box family of RNA helicases is defined by a conserved Asp-Glu-Ala-Asp motif that interacts with Mg^{2+} and is involved in ATP hydrolysis (17). DEAD-box proteins also contain several conserved motifs that have been shown to function in ATP binding, ATPase activity, and helicase activity (18). Many cellular functions of DEAD-box RNA helicases have been attributed to RNA duplex unwinding and ribonucleoprotein (RNP) complex remodeling (19). In yeast, several RNA helicases have been shown to facilitate ribosome biogenesis (20), which involves both the processing of rRNA as well as its assembly into functional RNP complexes. Given that the cellular center for ribosome synthesis is the nucleolus, it is

Authors' Affiliations: [1]BRIGHT Institute and Department of Internal Medicine, [2]Division of Molecular Oncology, Divisions of [3]Medical Oncology and [4]Metabolism and Proteomics Center, Siteman Cancer Center, Washington University School of Medicine, St. Louis, Missouri

Note: Supplementary data for this article are available at Cancer Research Online (http://cancerres.aacrjournals.org/).

Corresponding Author: Jason D. Weber, BRIGHT Institute, Department of Internal Medicine, Division of Molecular Oncology, Washington University School of Medicine, 660 South Euclid Avenue, Campus 8069, St. Louis, MO 63110. Phone: 314-747-3896; Fax: 314-747-2797; E-mail: jweber@dom.wustl.edu

doi: 10.1158/0008-5472.CAN-11-1472

©2011 American Association for Cancer Research.

Downloaded from cancerres.aacrjournals.org on April 16, 2013. © 2011 American Association for Cancer Research.

Published OnlineFirst September 21, 2011; DOI: 10.1158/0008-5472.CAN-11-1472

not surprising that many RNA helicases have been identified as components of the nucleolar proteome (1, 4).

The involvement of several known oncogenes and tumor suppressors in the regulation of protein synthesis underscores the importance of ribosomes and mRNA translational control in cancer (21). Thus, the ability of ARF to direct balanced RNA metabolism in the nucleolus could provide insights into how this major cellular axis might impact tumorigenesis. Apart from its classical function as a sensor of hyperproliferative signals (22–24), we now show that ARF limits non-oncogene-driven ribosome biogenesis to inhibit cellular transformation.

Materials and Methods

Cell culture and reagents

Primary MEFs were isolated and cultured as described (15). Rabbit anti-DDX5 (A300-523A) was purchased from Bethyl Laboratories. Mouse anti-NPM (catalog no. 32-5200) was purchased from Zymed. Rat anti-p19ARF (ab26696) was purchased from Abcam. H-Ras, p21, and γ-tubulin antibodies were purchased from Santa Cruz Biotechnology.

Nucleolar isolation

Nucleoli were isolated from 2×10^8 cells, essentially as described by Andersen and colleagues (3). Additional details for the nucleolar isolation protocol are included with the Supplementary Material.

Proteomic analysis

Gel preparation, analysis, and mass spectrometry were done as previously described (25). Wild-type nucleolar isolates were labeled with Cy3 and *Arf*$^{-/-}$ nucleolar isolates were labeled with Cy5. Samples were mixed and subjected to 2-dimensional (2D) SDS-PAGE. First-dimension isoelectric focusing was done on immobilized pH gradient strips in an Ettan IPGphor system (GE Healthcare). Second-dimension separation was done on 10% isocratic SDS-PAGE gels (20 × 24 cm). Imaging was done using a Typhoon 9400 scanner (GE Healthcare) and Decyder DIA and BVA software (GE Healthcare) was used to quantify matched gel spots. Spots showing more than 2-fold differences in intensity were isolated and identified by matrix-assisted laser desorption/ionization–time-of-flight/time-of-flight mass spectrometry.

Immunofluorescence

Cells were fixed with 4% paraformaldeyde in PBS for 10 minutes. Cells were permeabilized with 1% NP-40, blocked in 5% FBS, and stained with rabbit anti-DDX5 and mouse anti-NPM, followed by fluorescein isothiocyanate (FITC)-conjugated anti-mouse and Rhodamine-X–conjugated anti-rabbit (both from Jackson ImmunoResearch). Samples were counterstained with 4′, 6-diamidino-2-phenylindole and mounted with Vectashield (Vector Labs). Four independent MEF isolates were used to assess localization of DDX5. Images were acquired using a ×100 oil immersion lens on a Zeiss LSM5 Pascal Vario Two UGB coupled to Axiovert 200 confocal microscope.

Quantitative real-time PCR

Total RNA was isolated from wild-type and *Arf*$^{-/-}$ MEFs using Illustra RNAspin columns (GE Healthcare) according to manufacturer's protocol. First-strand cDNA synthesis and real-time PCR were done as previously described (26).

[methyl-^{3}H]-methionine labeling of rRNA

Equal numbers of MEFs were subjected to starvation in methionine-free media containing 10% dialyzed FBS for 15 minutes. Cells were treated with 50 μCi/mL [methyl-^{3}H]-methionine and chased in complete media containing an excess of unlabeled methionine (10 μmol/L) for the indicated times. Samples were lysed in RNASolv reagent (Omega Biotek) and extracted RNA was separated on agarose-formaldehyde gels and transferred to a Hybond XL membrane (GE Healthcare). The membrane was cross-linked and sprayed with En^{3}Hance (Perkin-Elmer) prior to autoradiography. Band intensities were quantitated using ImageQuant TL (Amersham Biosciences).

Chromatin immunoprecipitation

Wild-type and *Arf*$^{-/-}$ MEFs were cross-linked with formaldehyde and cell lysates were immunoprecipitated with the indicated antibodies at 4°C overnight. Samples were then washed with low salt, high salt, LiCl, and TE buffers, prior to elution. Cross-links were reversed by addition of NaCl and samples were subjected to RNase A and proteinase K treatments. DNA was purified from samples using QIAquick PCR purification kits (QIAGEN). Quantitative real-time PCR (qRT-PCR) was done as detailed above with primer sets specific to rDNA loci. Additional details for the chromatin immunoprecipitation (ChIP) protocol are provided in Supplementary Material.

rRNA immunoprecipitation

Arf$^{-/-}$ MEFs were starved as described above and labeled with [methyl-^{3}H]-methionine for 4 hours. Cells were harvested, lysed, and subjected to immunoprecipitation and RNA extraction as previously described (26).

Ribosome fractionation

Cells were treated with cycloheximide, collected, and fractionated by sucrose gradient centrifugation as previously described (26). Total protein was precipitated from individual fractions with trichloroacetic acid and analyzed by Western blot.

Foci formation and proliferation assays

MEFs were plated in triplicate at the indicated concentrations and foci formation and proliferation assays were conducted as previously described (27).

Soft agar

Arf$^{-/-}$ MEFs were infected with short hairpin RNAs (shRNA) against luciferase or DDX5, prior to infection with either Ras^{V12} or empty vector (pBabe). Cells were seeded onto soft agar at 10^4 cells per 6-cm^2 dish and grown for 3 weeks. Cells

Downloaded from cancerres.aacrjournals.org on April 16, 2013. © 2011 American Association for Cancer Research.

Published OnlineFirst September 21, 2011; DOI: 10.1158/0008-5472.CAN-11-1472

were relayered with soft agar on a weekly basis and visible colonies were counted after 3 weeks.

Tumorigenesis assay

Arf$^{-/-}$ MEFs were infected with RasV12 and either shDDX5 or shSCR. Fibroblasts were trypsinized and resuspended in PBS at a concentration of 2×10^7 cells/mL. Athymic nude mice were injected s.c. with 2×10^6 cells along their left flank, with sample sizes of 5 mice per condition. Tumor size was monitored over an 18-day time course using calipers to measure the tumors in 2 dimensions. Tumor volume was calculated using the formula:

Volume = $[(\text{height})^2 \times \text{length}]/2$, in which height equals the smallest of the 2 measurements.

Results

p19ARF interferes with the nucleolar localization of DDX5 RNA helicase

A proteomic screen was conducted to identify targets that displayed differential nucleolar localization in the presence or absence of basal ARF. Adapting a protocol from Andersen and colleagues (3), we isolated nucleoli from wild-type and *Arf*$^{-/-}$ MEFs. Isolated nucleoli maintained *in vivo* morphology (Fig. 1A) were positive for nucleolar proteins by immunofluorescence (Fig. 1B) and were free of nucleoplasmic contaminants (Fig. 1C). Nucleolar isolates were subjected to comparative 2D differential gel electrophoresis (2D-DIGE) proteomic analysis. Twenty-six spots which showed differences greater than 2.5 SDs from the mean change were excised, and 19 were positively identified by mass spectroscopy (Supplementary Table S1). Among the differences between wild-type and *Arf*$^{-/-}$ MEFs, enhanced nucleolar expression (10-fold) of DDX5 RNA helicase was observed in the absence of *Arf* (Fig. 1D). Immunofluorescence revealed enhanced nucleolar colocalization of DDX5 with NPM in *Arf*$^{-/-}$ MEFs (Fig. 1E). Biochemical fractionation confirmed the increased presence of DDX5 in *Arf*$^{-/-}$ nucleoli relative to wild-type nucleoli (Fig. 1F).

To investigate whether nucleolar exclusion of DDX5 is mediated by ARF through its activation of p53, we treated *Arf*$^{-/-}$ MEFs with nutlin-3, a pharmacologic inhibitor of Mdm2. Instead of stimulating DDX5 nucleolar exclusion, nucleolar localization of DDX5 persisted in the presence of nutlin-3 (Supplementary Fig. S1). This shows that p53 activation is not responsible for the ARF-dependent nucleolar exclusion of DDX5 observed in wild-type MEFs, consistent with a p53-independent role for ARF in regulating DDX5 localization.

ARF regulates the association of DDX5 with rDNA, rRNA, and nuclear preribosomes

The nucleolar localization of DDX5, along with its function as an RNA helicase, suggested that DDX5 might be involved in the biogenesis of rRNA. The regulation of DDX5 localization by basal ARF led us to investigate whether ARF could control ribosome biogenesis through regulation of DDX5 function. Both p19ARF (mouse) and p14ARF (human) inhibit rRNA transcription (12, 28, 29), and DDX5 has been ascribed roles as a transcriptional regulator (18). However, it is unknown whether DDX5 regulates transcription at nucleolar *rDNA* loci. We conducted ChIP experiments to determine whether DDX5 associated with the *rDNA* promoter at 2 previously identified binding sites of the RNA polymerase I transcription factor UBF (30). ARF regulated DDX5 association with these sites, such that DDX5 occupancy at the *rDNA* promoter was over 2-fold greater in *Arf*$^{-/-}$ MEFs compared with wild-type MEFs (Fig. 2A).

In addition, DDX5 has been shown to be involved in processing of the 5.8S rRNA (31) and the 28S rRNA from their respective rRNA precursors (32). By immunoprecipitation, we observed an interaction between DDX5 and the 28S and 18S rRNA species (Fig. 2B). This association with mature rRNA suggests that DDX5 could be involved at multiple stages in the production and assembly of ribosomes. In wild-type MEFs the interaction of DDX5 with rRNA was decreased relative to *Arf*$^{-/-}$ cells, suggesting that ARF can inhibit this association as well.

We hypothesized that ARF may interfere with the ability of DDX5 to stimulate ribosome biogenesis by impeding access of DDX5 to maturing pre-ribosomes. Nuclear lysates obtained from wild-type and *Arf*$^{-/-}$ MEFs were separated by sucrose gradient centrifugation. Enhanced association of DDX5 with the 40S and 60S pre-ribosomal fractions was observed in the *Arf*$^{-/-}$ nuclear lysates relative to the corresponding wild-type fractions (Fig. 2D). These changes were not due to altered expression because wild-type and *Arf*$^{-/-}$ MEFs expressed similar levels of DDX5 protein in both whole-cell lysate (Fig. 1F) and nuclear extract (Fig. 2C).

DDX5 enhances the synthesis and processing of ribosomal RNA

To determine whether DDX5 could accelerate ribosome biogenesis, wild-type MEFs were transduced with a Flag-epitope-tagged DDX5 or a mutant (K144N) deficient in ATP binding (Fig. 3A). The *K144N* mutation in the Walker A motif abrogates not only ATP binding but also the ATPase and helicase activities of DDX5 (32). The earliest observed effect of DDX5 on ribosome biogenesis was at the level of 47S pre-rRNA transcription, in which both Flag-DDX5 and Flag-DDX5-K144N increased the amount of 47S transcript per cell (Fig. 3B). The ability of DDX5 to regulate transcription of 47S pre-RNA concurred with its aforementioned association at the *rDNA* promoter. Monitoring the processing of the 47S pre-rRNA transcript by pulse-chase analysis, we discovered a more rapid accumulation of mature 28S and 18S rRNAs in cells expressing Flag-DDX5 or Flag-K144N versus vector-transduced cells (Fig. 3C and D). To determine whether the accelerated production of rRNA equated with increased protein synthesis, cytosolic fractions were collected for ribosome profile analysis. Both Flag-DDX5 and Flag-DDX5-K144N enhanced the amplitude of the actively translating polyribosome fraction (Fig. 3E), indicating that ectopic expression of Flag-DDX5 ultimately increases ribosome availability for translation, and that helicase activity is not required for this induction. These results indicate that DDX5 stimulates the production of functional ribosomes by increasing the total amount of mature rRNA.

Downloaded from cancerres.aacrjournals.org on April 16, 2013. © 2011 American Association for Cancer Research.

Published OnlineFirst September 21, 2011; DOI: 10.1158/0008-5472.CAN-11-1472

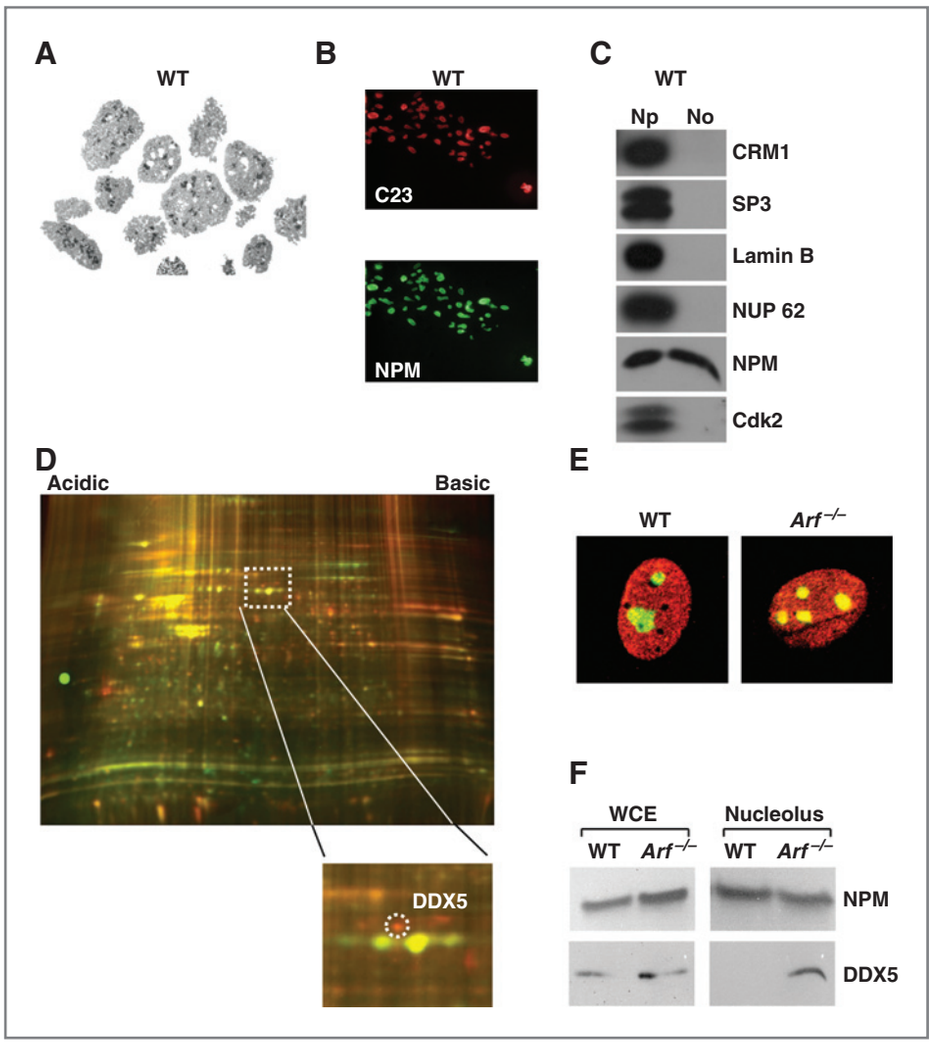

Figure 1. ARF maintains the nucleolar exclusion of DDX5. A, nucleoli were isolated from wild-type (WT) and *Arf* $^{-/-}$ MEFs. Nucleolar morphology (shown for WT) was assessed by electron microscopy. B, nucleoli (shown for WT) were analyzed by immunofluorescence microscopy for the nucleolar markers C23/nucleolin (red, Texas Red) and NPM (green, FITC). C, immunoblotting of nucleolar and nucleoplasmic fractions was done to determine purity (shown for WT). D, proteins from isolated nucleoli were differentially labeled with Cy3 and Cy5 fluorophores and were subjected to 2D DIGE. E, localization of NPM and DDX5 in wild-type and *Arf* $^{-/-}$ MEFs was determined by immunofluorescence. F, Western blotting of nucleolar lysates for NPM and DDX5 revealed a change in nucleolar DDX5 expression between genotypes.

DDX5 stimulates proliferation in MEFs

The ability of DDX5 to stimulate rRNA synthesis suggested that it might also be critical for growth and proliferation. The enhanced ribosome biogenesis caused by DDX5 overexpression corresponds to an increased proliferative capacity, as evidenced by the ability of Flag-DDX5 and Flag-DDX5-K144N to stimulate foci formation in wild-type MEFs (Fig. 4A). Furthermore, using 2 different shRNA constructs, we showed that knockdown of DDX5 reduced proliferation of *Arf* $^{-/-}$ MEFs in a dose-dependent manner (Fig. 4B and C). The dependency on DDX5 for unrestricted growth was not exclusive to *Arf* $^{-/-}$ MEFs, as foci formation in *p53* $^{-/-}$ MEFs was impaired by shRNAs targeting DDX5 (Supplementary Fig. S2A and B). DDX5 has been linked to p53 function in several reports, either as a transcriptional coactivator (33) or as a partner of p53 in microRNA processing (34). Whereas these relationships suggest that DDX5 could inhibit growth through its interactions with p53, our data point to the opposite conclusion, specifically that the dominant role of DDX5 is not growth inhibition, as would be inferred from the aforementioned studies, but rather growth stimulation.

Knockdown of DDX5 phenocopies the p53-independent functions of ARF on ribosome output

DDX5 stimulates ribosome production, whereas ARF inhibits ribosome biogenesis at several stages: 47S transcription, rRNA processing, and rRNA export (12, 29, 35). Ultimately, the effects of *Arf* loss are exhibited by the enhanced ribosome profiles of *Arf* $^{-/-}$ MEFs relative to wild-type MEFs (12). It was unclear, however, whether these effects of ARF on the cellular ribosome profile were truly p53-independent. To characterize the p53-independent functions of ARF on ribosome biogenesis, we utilized TKO (*p53* $^{-/-}$, *Mdm2* $^{-/-}$, and *Arf* $^{-/-}$) MEFs, in which the entire ARF–Mdm2–p53 axis has been removed (11). By adding ARF back into TKO MEFs, we investigated growth-inhibitory effects of ARF that are completely independent of p53. HA-ARF expression reduced cytosolic ribosomes in the actively translating polyribosome fraction (Fig. 5A), showing a p53-independent role for ARF in the regulation of

Downloaded from cancerres.aacrjournals.org on April 16, 2013. © 2011 American Association for Cancer Research.

Published OnlineFirst September 21, 2011; DOI: 10.1158/0008-5472.CAN-11-1472

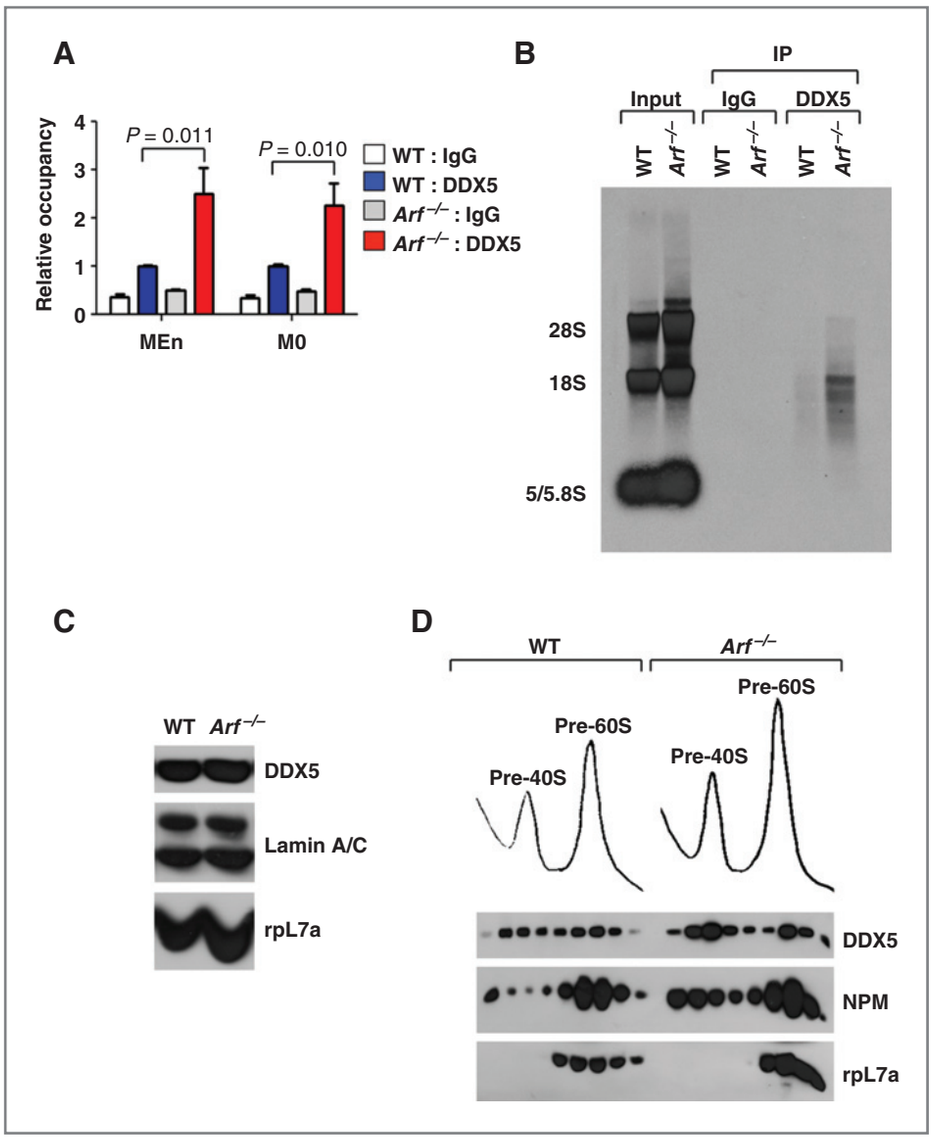

Figure 2. ARF impairs association of DDX5 with nuclear pre-ribosomes. A, wild-type (WT) and *Arf* $^{-/-}$ MEFs were collected for ChIP using DDX5 or IgG control antibodies. qRT-PCR with primers flanking 2 regions, MEn and M0, on the rDNA promoter was used to amplify DNA isolated from the immunoprecipitates. B, WT and *Arf* $^{-/-}$ MEFs were labeled with [methyl-^{3}H]-methionine and DDX5 was immunoprecipitated from cell lysates. Radiolabeled RNA isolated from the DDX5 immunoprecipitate was visualized by autoradiography. C, nuclear extract from WT and *Arf* $^{-/-}$ MEFs was analyzed by Western blot. D, nuclear extracts from WT and *Arf* $^{-/-}$ MEFs were subjected to sucrose density centrifugation. RNA absorbance was monitored at 254 nm as samples were fractionated and isolated proteins were analyzed by Western blot. IP, immunoprecipitation.

ribosome output. Knockdown of DDX5 in TKO MEFs mimicked the effects of ARF overexpression on cytosolic ribosome content (Fig. 5B), causing a decrease in polyribosome peak amplitude. Thus, a DDX5 loss-of-function is equivalent to a p53-independent ARF gain-of-function on ribosome output.

ARF inhibits the interaction between DDX5 and NPM

We previously identified an interaction between NPM and DDX5 while probing for NPM binding partners (26). Like DDX5, NPM is a multifunctional protein, with key roles at multiple stages of ribosome biogenesis. NPM associates with the *rDNA* locus (36), regulating transcription and processing of the rRNA (1). Furthermore, NPM functions as a nuclear export chaperone for ribosomes (26), a function that is antagonized by ARF (15). Interestingly, early embryonic lethality is a phenotype of both *Npm1*$^{-/-}$ and *Ddx5*$^{-/-}$ mice (13, 31, 37). We hypothesized that ARF impaired DDX5 function through regulation of its interaction with NPM.

Given the ability of ARF to regulate both proteins individually, we tested whether ARF effected the interaction between DDX5 and NPM. Comparison of wild-type and *Arf*$^{-/-}$ MEF lysates by coimmunoprecipitation revealed that ARF significantly reduced the interaction of DDX5 with NPM (Fig. 6A). We then sought to determine the NPM-binding domain on DDX5 to assess whether this interaction was critical for the growth-stimulatory abilities of DDX5. Little has been reported on the proteins that interact with DDX5 through its C-terminal domain. Given the possibility that core domain mutations might directly impair conserved features that are critical in the DEAD-box helicase family and complicate any interpretations of its overall importance, we instead focused on mutations in the C-terminus. A panel of overlapping C-terminal deletion mutations was introduced to DDX5 in a GST-fusion

Downloaded from cancerres.aacrjournals.org on April 16, 2013. © 2011 American Association for Cancer Research.

Published OnlineFirst September 21, 2011; DOI: 10.1158/0008-5472.CAN-11-1472

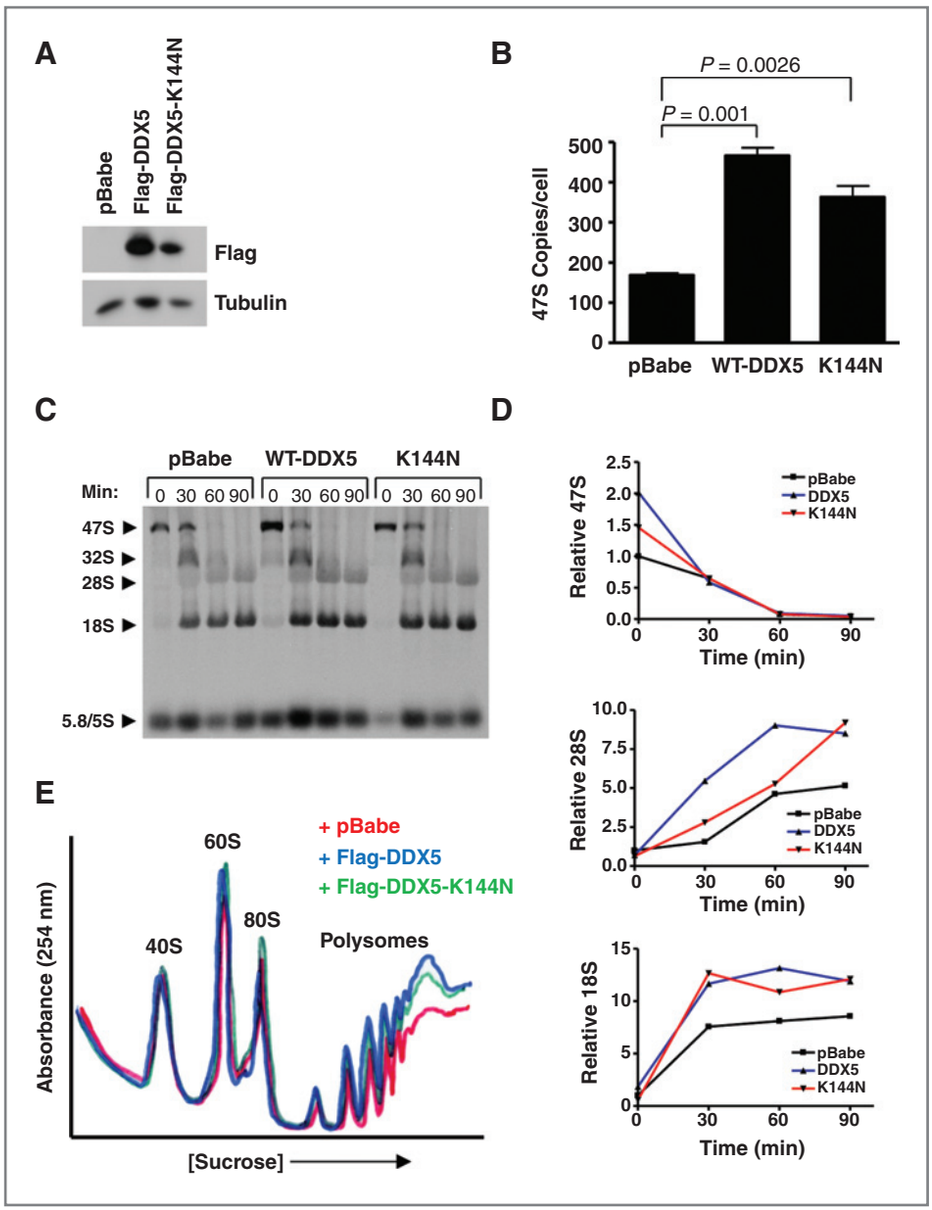

Figure 3. Overexpression of DDX5 promotes ribosome output. Wild-type (WT) MEFs were transduced with empty vector or Flag-DDX5 retroviruses. A, flag immunoblot shows expression of the retroviral fusion protein. B, total RNA was analyzed by qRT-PCR to determine copy number of the 47S pre-rRNA transcript. C, cells were labeled with [methyl-^{3}H]-methionine and chased for the indicated times. Total RNA was extracted, separated on an agarose gel, and transferred to membranes. Radiolabeled RNA was visualized by autoradiography. D, relative band intensities were determined for rRNA in the processing assay. 47S, 28S, and 18S rRNAs were individually normalized to the pBabe sample at $t = 0$ and tracked throughout the time course. E, cytosolic extracts from 2.5×10^6 cells were separated by sucrose density gradient centrifugation. Ribosome profiles were obtained by measuring the absorbance of RNA at 254 nm.

protein expression vector. *In vitro* immunoprecipitation reactions using His-tagged NPM and GST-DDX5 or its mutants mapped an NPM interaction motif to residues 500 to 610 at the C-terminus of DDX5 (Fig. 6B). For further experiments, we chose a smaller mutant within this domain, DDX5Δ520–550. Whereas ectopically expressed Flag-DDX5 interacted with endogenous NPM in $Arf^{-/-}$ MEFs, the Δ520–550 mutant displayed no visible interaction (Fig. 6C). Flag-DDX5-Δ520–550 also had reduced occupancy of the *rDNA* promoter compared with wild-type Flag-DDX5 (Fig. 6D) and did not stimulate 47S pre-rRNA transcription (Fig. 6E). Furthermore, whereas Flag-DDX5 associated with nuclear pre-ribosomal fractions containing the 40S and 60S ribosomal subunits, Flag-DDX5-Δ520–550 was almost completely absent from the 60S fractions containing the large ribosomal protein rpL7a (Fig. 6F). Finally, in transduced $Arf^{-/-}$ MEFs, Flag-DDX5-Δ520–550 expression did not affect proliferation compared with the empty vector control, whereas Flag-DDX5 expression enhanced proliferation (Fig. 6G). Thus, it seems that DDX5 cooperates with NPM, through a direct interaction that is antagonized by ARF, to stimulate rRNA synthesis and proliferation.

RasV12-induced transformation of $Arf^{-/-}$ MEFs requires DDX5

Transduction of wild-type MEFs with oncogenic RasV12 results in ARF induction and growth arrest (22). Conversely, transduction of RasV12 transforms $Arf^{-/-}$ MEFs, as determined by colony formation in soft agar. To determine whether DDX5 meets the criteria of a classic oncogene, wild-type MEFs expressing Flag-DDX5, alone or in combination with RasV12,

Downloaded from cancerres.aacrjournals.org on April 16, 2013. © 2011 American Association for Cancer Research.

Published OnlineFirst September 21, 2011; DOI: 10.1158/0008-5472.CAN-11-1472

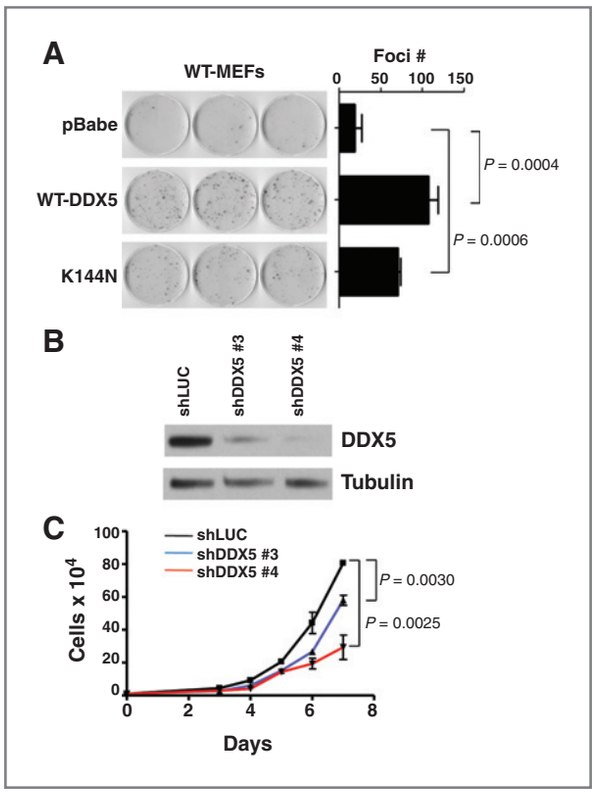

Figure 4. DDX5 stimulates growth and proliferation. A, wild-type (WT) MEFs expressing empty vector, Flag-DDX5, or Flag K144N were plated at 10^3 cells per dish and grown for 12 days. Foci were fixed in methanol and stained with Giemsa. B, *Arf* $^{-/-}$ MEFs were infected with lentiviral shRNAs targeting luciferase (control) or DDX5. Western blot shows the efficacy of DDX5 knockdown. C, cells were plated in triplicate at a density of 10^4 per well in a 6-well plate for a proliferation assay and counted over a 7-day time course.

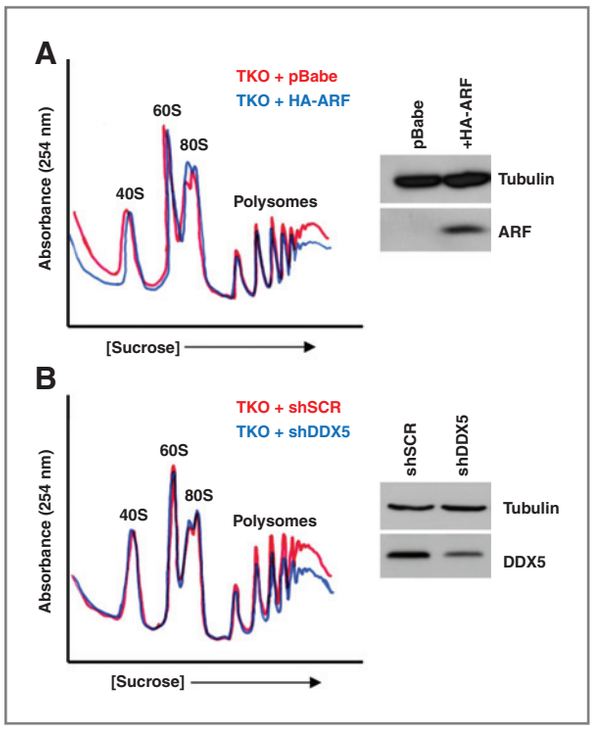

Figure 5. ARF overexpression and DDX5 knockdown each reduce cytosolic polyribosomes in a p53-independent manner. Cytosolic extracts from TKO (*Arf/p53/Mdm2* $^{-/-}$) MEFs expressing HA-ARF (A) or shDDX5 (B) were loaded onto a sucrose density gradient and samples were monitored for the absorbance of RNA at 254 nm. Expression of ARF and DDX5 was assessed by Western blot (side panels).

were plated in soft agar to evaluate anchorage-independent growth. Whereas RasV12-transduced *Arf* $^{-/-}$ MEFs plated in parallel formed robust colonies, wild-type MEFs expressing Flag-DDX5 and RasV12 did not form colonies (Supplementary Fig. S3A). Furthermore, unlike RasV12, Flag-DDX5 was unable to stimulate transformation of TKO MEFs (Supplementary Fig. S3B). This suggests that DDX5 is not an oncogene as it cannot, in combination with *Arf* loss, *p53* loss, or RasV12 overexpression, drive transformation.

Despite not being sufficient to transform cells, it remained possible that DDX5 was necessary for transformation. To determine whether DDX5 is required for oncogenic transformation in the absence of *Arf*, we transduced *Arf* $^{-/-}$ MEFs with shRNA against DDX5 followed by ectopic expression of RasV12 (Fig. 7A). Knockdown of DDX5 impaired the ability of RasV12 to stimulate colony formation and anchorage-independent growth (Fig. 7B), suggesting that transformation of MEFs by RasV12 requires the cooperation of DDX5.

To determine whether Ras-transformed fibroblasts could form tumors *in vivo*, *Arf* $^{-/-}$ MEFs transduced with RasV12 and shDDX5 or a scrambled shRNA were s.c. inoculated into the flanks of nude mice. RasV12-induced tumor growth in nude mice was reduced by knockdown of DDX5 (Fig. 7C and D). The dependence on DDX5 for the growth of these *Arf* null tumors suggests that DDX5 may function as a non-oncogene by sustaining the levels of ribosome production required by transformed cells to maintain their accelerated proliferation rates.

Discussion

The role of ARF in regulating p53 is well established, but the mechanisms by which it exerts its p53-independent tumor suppressor function are yet to be fully characterized. Our group and others have recently shown the regulation of translation by ARF, but mechanistic details of its involvement are limited. Both mouse and human ARF interact with nucleolar proteins involved in ribosome biogenesis as well as ribosomal components themselves (1, 38). Furthermore, ectopic expression of human p14ARF decreases polyribosomes in a p53-independent manner (38). ARF has recently been linked to ribosome biogenesis through its regulation of TTF-1 (29) and its ability to inhibit ribosome export via its nucleolar interaction with NPM (15, 38). Here we have shown that ARF can control the protein composition of the nucleolus, the central organelle in ribosome biogenesis. Our observation that ARF can regulate DDX5 RNA helicase provides a mechanistic explanation for the inhibitory effects of ARF on 47S rRNA transcription and processing (35).

Downloaded from cancerres.aacrjournals.org on April 16, 2013. © 2011 American Association for Cancer Research.

Published OnlineFirst September 21, 2011; DOI: 10.1158/0008-5472.CAN-11-1472

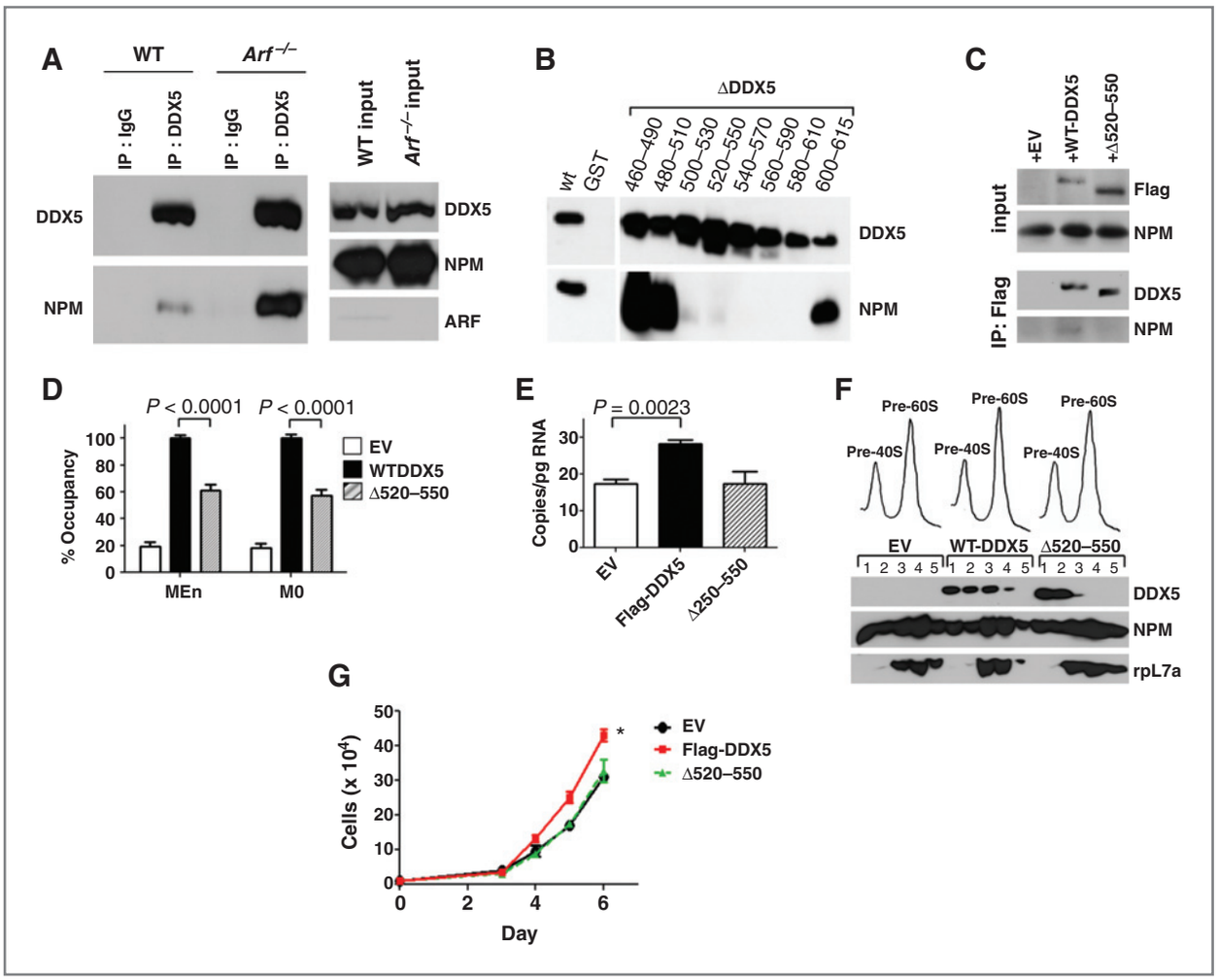

Figure 6. The ARF-regulated interaction between DDX5 and NPM is required for the growth-stimulatory effects of DDX5. A, the interaction between DDX5 and NPM was compared in lysates from wild-type (WT) and *Arf* $^{-/-}$ MEFs by coimmunoprecipitation with antibodies against DDX5. B, a panel of GST-Flag-DDX5 mutants was subjected to GST-pull-down following incubation with His-NPM proteins, and immunoblotting was done with antibodies recognizing DDX5 and NPM. C, *Arf* $^{-/-}$ MEFs expressing Flag-DDX5 or Flag-DDX5-Δ520–550 were subjected to immunoprecipitation with an antibody against the Flag epitope. D, *Arf* $^{-/-}$ MEFs were subjected to ChIP reactions with an antibody against the Flag epitope. DNA recovered from the reactions was subjected to qRT-PCR using primers to 2 different areas, MEn and M0, within the rDNA promoter. E, qRT-PCR for the 47S pre-rRNA from total RNA isolated from WT MEFs. F, nuclei from *Arf* $^{-/-}$ MEFs expressing Flag-DDX5 or Flag-DDX5-Δ520–550 were subjected to sucrose gradient centrifugation. Expression of rpL7a or Flag-tagged proteins in the isolated fractions was determined by Western blot. G, *Arf* $^{-/-}$ MEFs were plated in triplicate at 20,000 cells per well for a proliferation assay and counted daily over a time course. IP, immunoprecipitation. *, $P = 0.0058$.

Our data suggest that most of the endogenous pool of DDX5 may be excluded from nucleoli and inactive in ribosome biogenesis, until a cellular perturbation stimulates this activity. Consistent with this model, upon loss of *Arf* a substantial increase in nucleolar DDX5 was observed, accompanied by tremendous gains in ribosome production. Surprisingly, both DDX5 and the helicase-dead DDX5 mutant (K144N) were able to stimulate 47S transcription and cellular ribosome output. The ability of DDX5-K144N to increase 47S pre-rRNA transcription is consistent with reports that helicase activity may be dispensable for the activities of DDX5 as a transcriptional coregulator (33, 39). NPM was important for DDX5 to associate with the *rDNA* promoter and to facilitate 47S pre-rRNA transcription. The DDX5 NPM-binding mutant was also unable to associate with the nuclear 60S pre-ribosomal fraction or enhance proliferation, further underscoring the link between the effects of DDX5 on ribosome biogenesis with those on growth and proliferation. Clearly, the formation of DDX5–NPM complexes, enhanced in the absence of *Arf*, is necessary for the nucleolar gain-of-function activity reported here for DDX5.

Our results provide a new perspective for understanding the tumor suppressor function of ARF, which has classically been thought of as a checkpoint sensor of hyperproliferative signals. The data presented here suggest that an equally important mechanism by which ARF functions as a tumor suppressor is to limit ribosome output as a defense against oncogene activation and the attendant enhanced cellular protein synthesis requirements. Therefore, in the absence of *Arf*, DDX5 becomes a

Downloaded from cancerres.aacrjournals.org on April 16, 2013. © 2011 American Association for Cancer Research.

Published OnlineFirst September 21, 2011; DOI: 10.1158/0008-5472.CAN-11-1472

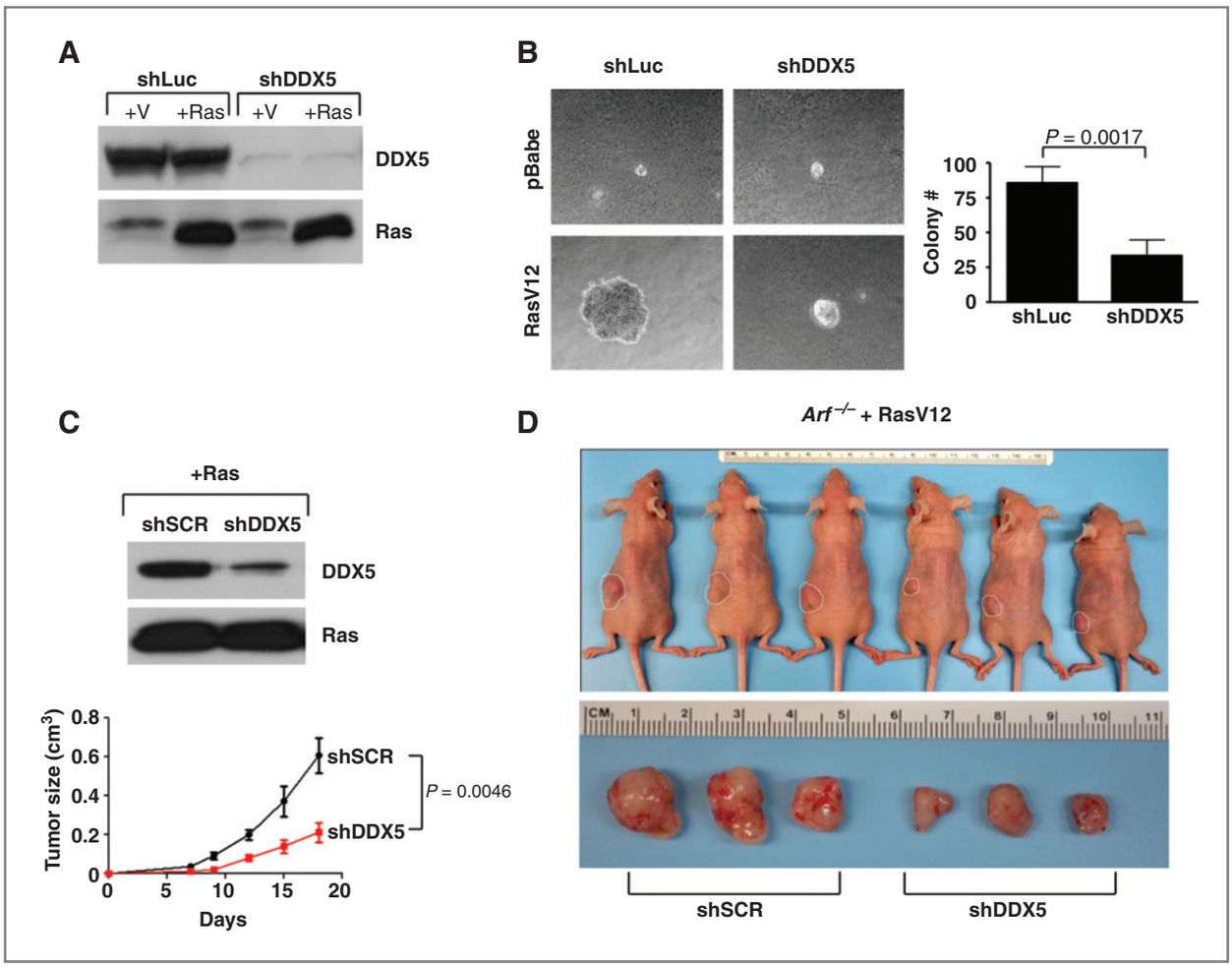

Figure 7. Non-oncogene addiction to DDX5 in transformed *Arf* $^{-/-}$ *MEFs*. A, *Arf* $^{-/-}$ MEFs were infected with shRNAs against luciferase or DDX5. Cells were then infected with either oncogenic Ras^{V12} or empty vector (pBabe), and expression was confirmed by Western blot. B, cells were seeded onto soft agar and grown for 3 weeks. C, *Arf* $^{-/-}$ MEFs were infected with RasV12, then subsequently infected with shDDX5 or scrambled shRNA. A total of 2×10^6 cells were used for s.c. injection into nude mice. Tumor burden was monitored over an 18-day time course. At the endpoint, mice were sacrificed and tumors were excised and photographed. Images of 3 representative mice and their tumors (the 3 mice with tumor volumes closest to the median) are shown in D.

requisite non-oncogene effector that promotes an increased translational output, in accord with the higher demand for protein production required upon oncogene activation. The ability of ectopic DDX5 expression to stimulate ribosome biogenesis and growth further proves the central role of DDX5 in regulating this translational output.

Our data showing the growth-stimulatory functions of DDX5 in ribosome biogenesis provides a strong rationale to explain the link between DDX5 and cancer. Although this concept is still in its infancy, most non-oncogenes are thought of as critical regulators of cellular stress responses and that their expression provides cancer cells the means to tolerate multiple stresses (40). It is unclear how DDX5 and ribosome biogenesis fit into this stress tolerance model. Rather, DDX5 may represent a class of nononcogenes whose activities are unleashed in the absence of crucial tumor suppressors. In this setting, the role of the DDX5 non-oncogene is to make a required cellular process, such as ribosome biogenesis, more efficient or prolific in preparation for the tremendous protein synthesis demands following malignant transformation. It remains to be determined whether DDX5 will be an efficacious target in the treatment of cancer; however, our results validate its importance in supplying the sustained ribosome output required for oncogenic transformation. In summary, DDX5 participation in ribosome biogenesis is negatively regulated by ARF, which inhibits the DDX5–NPM interaction, suggesting a dynamic interplay through which ARF and DDX5 duel for nucleolar growth control.

Disclosure of Potential Conflicts of Interest

No potential conflicts of interest were disclosed.

Acknowledgments

The authors thank the members of the Weber laboratory for their advice and technical assistance and Greg Longmore, Alan Diehl, Charles Sherr, and Martine Roussel for insightful comments and reagents.

Downloaded from cancerres.aacrjournals.org on April 16, 2013. © 2011 American Association for Cancer Research.

Published OnlineFirst September 21, 2011; DOI: 10.1158/0008-5472.CAN-11-1472

Grant Support

A.J. Saporita was supported by Komen for the Cure KG091234. This work was supported by NIH grant CA120436, American Cancer Society grant RSG-08-286-01-GMC, and an Era of Hope Scholar Award in Breast Cancer Research (BC007304) to J.D. Weber.

The costs of publication of this article were defrayed in part by the payment of page charges. This article must therefore be hereby marked *advertisement* in accordance with 18 U.S.C. Section 1734 solely to indicate this fact.

Received May 3, 2011; revised July 18, 2011; accepted August 23, 2011; published OnlineFirst September 21, 2011.

References

1. Bertwistle D, Sugimoto M, Sherr CJ. Physical and functional interactions of the Arf tumor suppressor protein with nucleophosmin/B23. Mol Cell Biol 2004;24:985–96.
2. Rizos H, McKenzie HA, Ayub AL, Woodruff S, Becker TM, Scurr LL, et al. Physical and functional interaction of the p14ARF tumor suppressor with ribosomes. J Biol Chem 2006;281:38080–8.
3. Andersen JS, Lyon CE, Fox AH, Leung AK, Lam YW, Steen H, et al. Directed proteomic analysis of the human nucleolus. Curr Biol 2002;12:1–11.
4. Andersen JS, Lam YW, Leung AK, Ong SE, Lyon CE, Lamond AI, et al. Nucleolar proteome dynamics. Nature 2005;433:77–83.
5. Kamijo T, Weber JD, Zambetti G, Zindy F, Roussel MF, Sherr CJ. Functional and physical interactions of the ARF tumor suppressor with p53 and Mdm2. Proc Natl Acad Sci U S A 1998;95:8292–7.
6. Weber JD, Taylor LJ, Roussel MF, Sherr CJ, Bar-Sagi D. Nucleolar Arf sequesters Mdm2 and activates p53. Nat Cell Biol 1999;1:20–6.
7. Pomerantz J, Schreiber-Agus N, Liegeois NJ, Silverman A, Alland L, Chin L, et al. The Ink4a tumor suppressor gene product, p19Arf, interacts with MDM2 and neutralizes MDM2's inhibition of p53. Cell 1998;92:713–23.
8. Zhang Y, Xiong Y, Yarbrough WG. ARF promotes MDM2 degradation and stabilizes p53: ARF-INK4a locus deletion impairs both the Rb and p53 tumor suppression pathways. Cell 1998;92:725–34.
9. Kamijo T, Zindy F, Roussel MF, Quelle DE, Downing JR, Ashmun RA, et al. Tumor suppression at the mouse INK4a locus mediated by the alternative reading frame product p19ARF. Cell 1997;91:649–59.
10. Kamijo T, Bodner S, van de Kamp E, Randle DH, Sherr CJ. Tumor spectrum in ARF-deficient mice. Cancer Res 1999;59:2217–22.
11. Weber JD, Jeffers JR, Rehg JE, Randle DH, Lozano G, Roussel MF, et al. p53-independent functions of the p19(ARF) tumor suppressor. Genes Dev 2000;14:2358–65.
12. Apicelli AJ, Maggi LB Jr, Hirbe AC, Miceli AP, Olanich ME, Schulte-Winkeler CL, et al. A non-tumor suppressor role for basal p19ARF in maintaining nucleolar structure and function. Mol Cell Biol 2008;28:1068–80.
13. Colombo E, Bonetti P, Lazzerini Denchi E, Martinelli P, Zamponi R, Marine JC, et al. Nucleophosmin is required for DNA integrity and p19Arf protein stability. Mol Cell Biol 2005;25:8874–86.
14. Korgaonkar C, Hagen J, Tompkins V, Frazier AA, Allamargot C, Quelle FW, et al. Nucleophosmin (B23) targets ARF to nucleoli and inhibits its function. Mol Cell Biol 2005;25:1258–71.
15. Brady SN, Yu Y, Maggi LB Jr, Weber JD. ARF impedes NPM/B23 shuttling in an Mdm2-sensitive tumor suppressor pathway. Mol Cell Biol 2004;24:9327–38.
16. Enomoto T, Lindstrom MS, Jin A, Ke H, Zhang Y. Essential role of the B23/NPM core domain in regulating ARF binding and B23 stability. J Biol Chem 2006;281:18463–72.
17. Rocak S, Linder P. DEAD-box proteins: the driving forces behind RNA metabolism. Nat Rev Mol Cell Biol 2004;5:232–41.
18. Fuller-Pace FV. DExD/H box RNA helicases: multifunctional proteins with important roles in transcriptional regulation. Nucleic Acids Res 2006;34:4206–15.
19. Yang Q, Del Campo M, Lambowitz AM, Jankowsky E. DEAD-box proteins unwind duplexes by local strand separation. Mol Cell 2007;28:253–63.
20. Bleichert F, Baserga SJ. The long unwinding road of RNA helicases. Mol Cell 2007;27:339–52.
21. Ruggero D, Pandolfi PP. Does the ribosome translate cancer? Nat Rev Cancer 2003;3:179–92.
22. Palmero I, Pantoja C, Serrano M. p19ARF links the tumour suppressor p53 to Ras. Nature 1998;395:125–6.
23. Zindy F, Eischen CM, Randle DH, Kamijo T, Cleveland JL, Sherr CJ, et al. Myc signaling via the ARF tumor suppressor regulates p53-dependent apoptosis and immortalization. Genes Dev 1998;12:2424–33.
24. de Stanchina E, McCurrach ME, Zindy F, Shieh SY, Ferbeyre G, Samuelson AV, et al. E1A signaling to p53 involves the p19(ARF) tumor suppressor. Genes Dev 1998;12:2434–42.
25. Bredemeyer AJ, Lewis RM, Malone JP, Davis AE, Gross J, Townsend RR, et al. A proteomic approach for the discovery of protease substrates. Proc Natl Acad Sci U S A 2004;101:11785–90.
26. Maggi LB Jr, Kuchenruether M, Dadey DY, Schwope RM, Grisendi S, Townsend RR, et al. Nucleophosmin serves as a rate-limiting nuclear export chaperone for the Mammalian ribosome. Mol Cell Biol 2008;28:7050–65.
27. Pelletier CL, Maggi LB Jr, Brady SN, Scheidenhelm DK, Gutmann DH, Weber JD. TSC1 sets the rate of ribosome export and protein synthesis through nucleophosmin translation. Cancer Res 2007;67:1609–17.
28. Ayrault O, Andrique L, Fauvin D, Eymin B, Gazzeri S, Seite P. Human tumor suppressor p14ARF negatively regulates rRNA transcription and inhibits UBF1 transcription factor phosphorylation. Oncogene 2006;25:7577–86.
29. Lessard F, Morin F, Ivanchuk S, Langlois F, Stefanovsky V, Rutka J, et al. The ARF tumor suppressor controls ribosome biogenesis by regulating the RNA polymerase I transcription factor TTF-I. Mol Cell 2010;38:539–50.
30. O'Sullivan AC, Sullivan GJ, McStay B. UBF binding *in vivo* is not restricted to regulatory sequences within the vertebrate ribosomal DNA repeat. Mol Cell Biol 2002;22:657–68.
31. Fukuda T, Yamagata K, Fujiyama S, Matsumoto T, Koshida I, Yoshimura K, et al. DEAD-box RNA helicase subunits of the Drosha complex are required for processing of rRNA and a subset of microRNAs. Nat Cell Biol 2007;9:604–11.
32. Jalal C, Uhlmann-Schiffler H, Stahl H. Redundant role of DEAD box proteins p68 (Ddx5) and p72/p82 (Ddx17) in ribosome biogenesis and cell proliferation. Nucleic Acids Res 2007;35:3590–601.
33. Bates GJ, Nicol SM, Wilson BJ, Jacobs AM, Bourdon JC, Wardrop J, et al. The DEAD box protein p68: a novel transcriptional coactivator of the p53 tumour suppressor. EMBO J 2005;24:543–53.
34. Suzuki HI, Yamagata K, Sugimoto K, Iwamoto T, Kato S, Miyazono K. Modulation of microRNA processing by p53. Nature 2009;460:529–33.
35. Sugimoto M, Kuo ML, Roussel MF, Sherr CJ. Nucleolar Arf tumor suppressor inhibits ribosomal RNA processing. Mol Cell 2003;11:415–24.
36. Murano K, Okuwaki M, Hisaoka M, Nagata K. Transcription regulation of the rRNA gene by a multifunctional nucleolar protein, B23/nucleophosmin, through its histone chaperone activity. Mol Cell Biol 2008;28:3114–26.
37. Grisendi S, Bernardi R, Rossi M, Cheng K, Khandker L, Manova K, et al. Role of nucleophosmin in embryonic development and tumorigenesis. Nature 2005;437:147–53.
38. Yu Y, Maggi LB Jr, Brady SN, Apicelli AJ, Dai MS, Lu H, et al. Nucleophosmin is essential for ribosomal protein L5 nuclear export. Mol Cell Biol 2006;26:3798–809.
39. Jensen ED, Niu L, Caretti G, Nicol SM, Teplyuk N, Stein GS, et al. p68 (Ddx5) interacts with Runx2 and regulates osteoblast differentiation. J Cell Biochem 2008;103:1438–51.
40. Luo J, Solimini NL, Elledge SJ. Principles of cancer therapy: oncogene and non-oncogene addiction. Cell 2009;136:823–37.

Downloaded from cancerres.aacrjournals.org on April 16, 2013. © 2011 American Association for Cancer Research.

Molecular and Cellular Biology

Identification of DHX33 as a Mediator of rRNA Synthesis and Cell Growth

Yandong Zhang, Jason T. Forys, Alexander P. Miceli, Abigail S. Gwinn and Jason D. Weber

Mol. Cell. Biol. **2011, 31(23):4676. DOI: 10.1128/MCB.05832-11.**
Published Ahead of Print 19 September 2011.

Updated information and services can be found at:
http://mcb.asm.org/content/31/23/4676

These include:

REFERENCES This article cites 52 articles, 21 of which can be accessed free at: http://mcb.asm.org/content/31/23/4676#ref-list-1

CONTENT ALERTS Receive: RSS Feeds, eTOCs, free email alerts (when new articles cite this article), more»

Information about commercial reprint orders: **http://journals.asm.org/site/misc/reprints.xhtml**
To subscribe to to another ASM Journal go to: **http://journals.asm.org/site/subscriptions/**

Journals.ASM.org

Downloaded from http://mcb.asm.org/ on April 16, 2013 by Washington University in St. Louis

MOLECULAR AND CELLULAR BIOLOGY, Dec. 2011, p. 4676–4691 Vol. 31, No. 23
0270-7306/11/$12.00 doi:10.1128/MCB.05832-11
Copyright © 2011, American Society for Microbiology. All Rights Reserved.

Identification of DHX33 as a Mediator of rRNA Synthesis and Cell Growth▽

Yandong Zhang, Jason T. Forys, Alexander P. Miceli, Abigail S. Gwinn, and Jason D. Weber*

BRIGHT Institute and Department of Internal Medicine, Division of Molecular Oncology, Siteman Cancer Center, Washington University School of Medicine, St. Louis, Missouri 63110

Received 20 June 2011/Returned for modification 8 July 2011/Accepted 10 September 2011

In this report, we employed a lentiviral RNA interference screen to discover nucleolar DEAD/DEAH-box helicases involved in RNA polymerase I (Pol I)-mediated transcriptional activity. Our screen identified DHX33 as an important modulator of 47S rRNA transcription. We show that DHX33 is a cell cycle-regulated nucleolar protein that associates with ribosomal DNA (rDNA) loci, where it interacts with the RNA Pol I transcription factor upstream binding factor (UBF). DHX33 knockdown decreased the association of Pol I with rDNA and caused a dramatic decrease in levels of rRNA synthesis. Wild-type DHX33 overexpression, but not a DNA binding-defective mutant, enhanced 47S rRNA synthesis by promoting the association of RNA polymerase I with rDNA loci. In addition, an NTPase-defective DHX33 mutant (K94R) acted as a dominant negative mutant, inhibiting endogenous rRNA synthesis. Moreover, DHX33 deficiency in primary human fibroblasts triggered a nucleolar p53 stress response, resulting in an attenuation of proliferation. Thus, we show the mechanistic importance of DHX33 in rRNA transcription and proliferation.

RNA is a highly structured macromolecule whose secondary and tertiary conformations facilitate an array of specific interactions with proteins. The DEAD/DEAH-box family of RNA helicases (here referred to as DDX/DHX) (3) is one such classification of RNA binding proteins that are capable of modifying the higher-ordered structures of RNA through the hydrolysis of ATP/nucleoside triphosphate (NTP) (41). DDX/DHX proteins often form large multiprotein complexes that participate in fundamental biological activities such as RNA transcription, RNA editing, pre-mRNA splicing, ribosome biogenesis, and RNA decay (3).

DDX/DHX helicases are named and characterized by the conserved DEAD/DEAH motif common among all family members. Through site-directed mutagenesis analysis, DEAD/DEAH along with seven conserved peptide motifs have been found to participate in ATP/NTP binding, hydrolysis, and substrate binding (28). Despite the conservation of these peptide motifs, the remaining sequences within each RNA helicase family member vary widely. Specifically, differences exist between the two categories of DDX and DHX proteins. DDX proteins contain a unique Q motif at their N termini that distinguishes them from DHX proteins. It was proposed previously that the Q motif might sense the state of ATP *in vivo* (40), given that DHX-box proteins are promiscuous in their ability to utilize NTP (16).

Ribosome biogenesis is a complex multistep process, the majority of which occurs in the nucleolus of the cell (24, 43). The transcription of ribosomal DNA (rDNA) is the initial and rate-limiting step in ribosome biogenesis, and as such, it is influenced by multiple levels of regulation (25). One of the key regulators of rDNA transcription is the upstream binding factor (UBF), a transcriptional transactivator that binds to the upstream core element of rDNA and subsequently bends rDNA (37). This change in the rDNA structure favors the binding of SL.1 as well as other associating factors to the rDNA locus (2). This allows for the recruitment of RNA polymerase I (Pol I) to initiate rDNA transcription (14, 23, 34). Recently, multiple functions have been found to be associated with UBF in rRNA transcription, including promoter clearance, the displacement of histone H1, and an enhancement of elongation (15, 27, 35). UBF also binds to rDNA regions outside transcribed regions, and its overexpression causes a global decondensation of rDNA chromatin structures (6). The activities of various transcription factors in rRNA transcription can be altered by posttranslational modifications involving the phosphorylation and acetylation of UBF, SL.1, and TIF-IA (25). In mammalian cells, a single precursor rRNA transcript, 47S rRNA (14.3 kb), is transcribed from rDNA by the RNA polymerase I complex. This large polycistronic transcript encompasses 18S, 5.8S, and 28S rRNAs and includes several spacer regions.

In the present report, we screened a group of nucleolar DDX/DHX-box proteins for their influence on pre-rRNA transcription by utilizing lentiviral RNA interference (RNAi) knockdown analysis. Various degrees of perturbation in rRNA transcription were observed by reducing the expression levels of numerous nucleolar DDX/DHX proteins. One of these nucleolar family members, DHX33, had a dramatic impact on pre-rRNA transcription and on nucleolar structure upon its knockdown, which could be rescued only by a helicase-competent and DNA binding-competent DHX33 protein. We found that DHX33 localized to nucleoli, where it associated with rDNA and UBF. The DHX33 knockdown caused a dramatic reduction of RNA polymerase I-mediated transcriptional activity. The overexpression of DHX33 stimulated rDNA transcription by promoting the rDNA occupancy of RNA polymerase I, all of which required NTPase activity and an rDNA binding capacity. Thus, DHX33 appears to be an intricate player in rRNA transcription and nucleolar organization.

* Corresponding author. Mailing address: BRIGHT Institute, Department of Internal Medicine, Division of Molecular Oncology, Washington University School of Medicine, 660 South Euclid Avenue, Campus 8069, St. Louis, MO 63110. Phone: (314) 747-3896. Fax: (314) 747-2797. E-mail: jweber@dom.wustl.edu.

▽ Published ahead of print on 19 September 2011.

Downloaded from http://mcb.asm.org/ on April 16, 2013 by Washington University in St. Louis

MATERIALS AND METHODS

Cell culture. Primary human BJ fibroblasts were cultured in Dulbecco's modified essential medium (DMEM) and M199 medium (4:1; Sigma) supplemented with 15% fetal bovine serum (FBS) and penicillin-streptomycin. HeLa cells, *p53*-null mouse embryonic fibroblast (MEF) cells, and BT549 breast cancer cells were cultured in complete DMEM supplemented with 10% FBS and penicillin-streptomycin. All cells were maintained at 37°C in 5% CO_2.

Antibodies. Anti-DHX33 antibody (rabbit polyclonal, catalog number NB100-2581) was obtained from Novus Biologicals. Anti-UBF mouse monoclonal (F-9, catalog number sc-13125), rabbit polyclonal (H-300, catalog number sc-9131), anti-phospho-UBF (pUBF) (Ser484) (catalog number sc-21638), anti-gamma-tubulin (catalog number sc-7396), anti-p21 (F-5, catalog number sc-6246), anti-p53 (DO-1, catalog number sc-126), anti-fibrillarin (H-140, catalog number sc-25397), anti-cyclin D1 (catalog number sc-450), anti-RPA194 (H-300, catalog number sc-28714), anti-RRN-3 (Y-23, catalog number sc-133978), anti-transcription termination factor (TTF) (24) (catalog number sc-136371), anti-TATA binding protein (TBP) (catalog number sc-204), and anti-epidermal growth factor receptor (EGFR) (catalog number sc-03) antibodies were obtained from Santa Cruz Biotechnology. Anti-glyceraldehyde-3-phosphate dehydrogenase (GAPDH) antibody (A300-641A) was obtained from Bethyl Laboratories. Anti-FLAG (M2) antibody was obtained from Sigma.

Immunoprecipitation and Western blots. Cells were lysed in buffer containing 1% NP-40, 50 mM Tris (pH 7.5), and 150 mM NaCl and supplemented with protease and phosphatase inhibitor cocktails (Sigma). After incubation on ice for 10 min, cell lysates were further sonicated to ensure complete disruption. Lysates were then centrifuged for 10 min at 13,000 rpm, and supernatants were subjected to a protein quantification assay. For Western blots, 50 μg of cell lysate was loaded onto a precast minigel (Bio-Rad), followed by transfer onto a polyvinylidene difluoride (PVDF) membrane. For immunoprecipitation, cell lysates were diluted to approximately 1 mg/ml with lysis buffer; 500 μg of the total cell lysate was incubated with 2 μg of the indicated antibody for 2 h at 4°C, followed by the addition of protein A/G-Sepharose beads, and further incubated for 1 h at 4°C. After centrifugation at 1,500 rpm for 2 min, the beads were washed 3 times with cell lysis buffer before analysis.

Plasmids. The full-length coding sequence for DHX33 (Mammalian Gene Collection [MGC]) was purchased from Open Biosystems. Primers were designed to clone the open reading frame (ORF) of DHX33 into p3XFLAG-CMV10.0 at HindIII/BamHI sites. To subclone DHX33 into pLVX-IRES-hygromycin, p3XFLAG-CMV10.0-DHX33 was further digested with SacI/BamHI to release the 3× FLAG-DHX33 fragment, treated with Klenow fragment, and then inserted into pLVX-IRES-hygromycin at the blunted XbaI site. A QuikChange site-directed mutagenesis kit (Stratagene) was used to carry out the mutation of K94N and K94R as well as the DNA binding box deletion mutants of DHX33 in plasmid pLVX-DHX33. The human UBF1 ORF with a Myc tag and a Flag tag (pCMV-6-UBF1) was purchased from Origene. To subclone UBF1-Myc into the pLVX vector, UBF1-Myc was cut by BamHI/EcoRV from pCMV6-UBF1, blunt ended by Klenow fragment, and then ligated into the pLVX vector at the blunt-ended XbaI site. The human UBF2 ORF was purchased from Origene and was subcloned into the pLVX vector at the XbaI/BamHI site. A QuikChange site-directed mutagenesis kit was used to carry out the mutation of S484D and S484A in UBF1/2. Five different pLKO.1 plasmids containing short hairpin RNA (shRNA) to target each of the indicated DEAD/DEAH-box proteins (human) were obtained from the Genome Sequencing Center at Washington University. A pLKO.1 scrambled shRNA control plasmid was purchased from Addgene.

Immunofluorescence microscopy. For 5-bromo-2-deoxyuridine (BrdU) analysis, cells were incubated with BrdU for 18 h, followed by 10% formalin–10% methanol fixation for 15 min at room temperature. Cells were blocked with 5% FBS and incubated with mouse anti-BrdU antibody (Clontech). Rhodamine-conjugated goat anti-mouse antibody was then applied and incubated for an additional 30 min at room temperature. Cell nuclei were counterstained with 4′,6-diamidino-2-phenylindole (DAPI). To analyze DHX33 localization, cells were transfected with p3XFLAG-CMV-DHX33. Transfected cells were fixed with 10% formalin–10% methanol. Cells were then incubated with mouse anti-FLAG (M2; Sigma) antibody at a 1:200 dilution. Goat anti-mouse antibody–fluorescein isothiocyanate (FITC) was applied to facilitate the visualization of the DHX33 protein. To mark cell nucleoli, rabbit antifibrillarin antibody was used at a dilution of 1:100, followed by incubation with goat anti-rabbit antibody–rhodamine.

47S rRNA synthesis analysis. Cells were pulsed with [^{3}H]uridine (Amersham) at a concentration of 2.5 μCi/ml for 30 min and chased with unlabeled uridine-containing medium at a concentration of 5 mM for the indicated time points. Cells were normalized based on equal cell numbers. Total RNA was isolated by using RNAsolv (Omega Biotek) according to the manufacturer's instructions. RNA was loaded onto 1% agarose-formaldehyde gels and was transferred onto a nylon Hybond membrane (Millipore). After UV cross-linking and spraying with Enhancer (Amersham), the membrane was exposed to film and subjected to autofluorography. For *in situ* run-on assays, the protocol was performed as previously described (18). Briefly, cells were incubated in complete medium containing 2 mM 5′-fluorouridine (FUrd) for 10 min at 37°C in 5% CO_2 and fixed in 10% formalin–10% methanol. The incorporated FUrd was visualized by incubating cells with monoclonal anti-BrdU antibody (Sigma) for 1 h and with goat anti-mouse antibody coupled to rhodamine for 30 min.

Pulse-chase with [*methyl*-^{3}H]methionine for rRNA processing. Cells were first incubated with methionine-cysteine-free medium for 30 min, and [*methyl*-^{3}H] methionine was then added at a concentration of 50 μCi/ml and incubated for 30 min at 37°C. Cells were chased with unlabeled medium containing 10 μM methionine and incubated at 37°C for various times. Approximately 1.0×10^6 cells were pelleted and dissolved in RNAsolv for RNA extraction. RNA was loaded onto a denaturing gel, transferred onto a nylon membrane, and subjected to autofluorography as described above.

Nucleolus fractionation. Approximately 10^8 cells were collected for cell fractionation. Cells were washed with phosphate-buffered saline (PBS) twice and resuspended in 1 ml buffer (10 mM HEPES-KOH [pH 7.9], 1.5 M $MgCl_2$, 10mM KCl, and 0.5 mM dithiothreitol [DTT]) for 30 min on ice. Phenylmethylsulfonyl fluoride (PMSF) was added to a final concentration of 0.2 mM, and the mixture was then Dounce homogenized until all cytoplasmic membranes were disrupted. For cytosolic isolation, cells were centrifuged at 1,190 rpm for 5 min at 4°C to obtain the supernatant. The resulting pellet was resuspended in 0.45 ml of 0.25 M sucrose–10 mM $MgCl_2$, layered onto 0.45 ml of 0.35 M sucrose–0.5 mM $MgCl_2$, and centrifuged at 2,790 rpm for 5 min at 4°C. Pelleted nuclei were then resuspended in 0.75 ml of 0.35 M sucrose–0.5 mM $MgCl_2$ with protease and phosphatase inhibitors (Sigma). Nuclei were sonicated to disrupt the nuclear membrane. The nuclear isolate was layered on top of 0.75 ml of 0.88 M sucrose–0.5 mM $MgCl_2$ and centrifuged at $2,800 \times g$ for 10 min at 4°C. The pellet was resuspended in 0.5 ml of 0.35 M sucrose–0.5 mM $MgCl_2$, and sucrose layering was repeated as described above. Nucleoli were fractionated as the subsequent pellet.

FACS analysis. Cells were trypsinized and washed with PBS. Cells were then resuspended in PBS, and 100% ethanol was added dropwise to obtain a final ethanol concentration of 75%. Cells were centrifuged at 2,000 rpm at 4°C for 2 min. Cells were then washed with PBS and resuspended in propidium iodide (PI) working solution (PBS containing 1% FBS, 250 μg/ml of RNase A, and 30 μg/ml of propidium iodide). Cells were filtered through a 35-μm strainer cap (Becton Dickinson) before being subjected to fluorescence-activated cell sorter (FACS) analysis.

qRT-PCR. The primers were all designed by use of Primer Express 2.0 software and purchased from Integrated DNA Technologies. Total RNA was extracted by use of a NucleoSpin II (Clontech) RNA isolation kit and was reverse transcribed into cDNA by use of a SuperScript III first-strand synthesis kit (Invitrogen). PCRs were performed with a Bio-Rad C1000 thermal cycler and managed with Bio-Rad CFX96 software. For analysis of 47S rRNA transcript levels, SYBR green FastMix (Quanta Biosciences) was used, and transcript quantification was performed by comparison with standard curves generated from dilution series of cDNA of human 47S rRNA (cloned into pCR2.1Topo). SYBR green mix from Bio-Rad was used for all other quantitative real-time PCR (qRT-PCR) analyses. Transcript quantification was calculated based on the $\Delta\Delta C_T$ value after normalization to GAPDH values. Melt curve analysis confirmed that single products were amplified.

Chromatin immunoprecipitation. Trypsinized cells were washed with PBS and fixed with 1% formaldehyde at room temperature for 10 min. To stop cross-linking, 1.25 M L-glycine was added to a final concentration of 0.125 M. After washing with 1× PBS, cells were resuspended in lysis buffer containing 1% SDS, 10 mM EDTA, and 50 mM Tris (pH 8.1) with protease and phosphatase inhibitors. To shear chromatin, cell lysates were sonicated extensively, centrifuged to pellet debris, and then diluted in buffer containing 0.5% NP-40, 50 mM Tris (pH 7.5), and 150 mM NaCl at a 1:5 ratio. Cell lysates were precleared by incubation with 2.5 μg of sheared salmon sperm DNA and 50 μl protein A/G beads for 30 min at 4°C. Following incubation with 5 μg of antibody overnight at 4°C, 2.5 μg sheared salmon sperm DNA and 50 μl of protein A/G beads were added and further incubated for 1 h. The beads were then washed twice in radioimmunoprecipitation assay (RIPA) buffer, twice in RIPA buffer containing 500 mM NaCl, and once with buffer containing 0.5% NP-40, 50 mM Tris (pH 7.5), and 150 mM NaCl. The beads were then extracted three times with a solution containing 1% SDS and 0.1 M $NaHCO_3$. To reverse the cross-linking, 6 M NaCl

Downloaded from http://mcb.asm.org/ on April 16, 2013 by Washington University in St. Louis

TABLE 1. DEAD/DEAH RNA helicase family

Human/mouse helicase	Yeast ortholog	Ribosome biogenesis
DDX1		
DDX3X	Dbp1p	+
DDX5	Dbp2p	
DHX8	Prp22p	
DHX9		
DDX10	Dbp4p	+
DHX16	Prp2p	
DDX17	Dbp2p	
DDX18	Has1p	+
DDX2		+
DDX23	Prp28p	
DDX24	Mak5p	+
DDX27	Drs1p	+
DDX31	Dbp7p	+
DHX33		
DDX37	Dhr1p	+
DDX39	Sub2p	
DDX41		
DDX46	Prp5p	
DDX47	Rrp3p	+
DDX48	Fal1p	+
DDX49	Dbp8p	+
DDX50		+
DDX51	Dbp6p	+
DDX52	Rok1p	+
DDX54	Dbp10p	+
DDX55	Spb4p	+
DDX56	Dbp9p	+

was added into the pooled extraction samples to a final concentration of 0.3 M, and samples were heated at 65°C for 5 h. DNA fragments were extracted by use of a Qiagen QuickSpin column and eluted. Quantitative PCR (qPCR) was performed with these purified DNA samples.

Cell size and volume. Primary human BJ fibroblasts (2×10^6 cells) were harvested by trypsinization, washed with 1× PBS, and resuspended in 10 ml DMEM. One milliliter of the cell suspension was mixed with 20 ml Isoton diluent (Beckman) and analyzed on a Multisizer III instrument according to the manufacturer's protocol (Beckman). Over 75,000 particles were analyzed in triplicate from three independent isolations using a 100-μm aperture.

Ag staining of nuclealar organizing region (AgNOR staining). Cells were seeded onto glass coverslips overnight and were fixed and stained the following day. Cells were fixed in 2% glutaraldehyde, followed by postfixation in a 3:1 ethanol-acetic acid solution. Cells were stained with a 0.33% formic acid–33.3% silver nitrate solution in 0.66% gelatin and mounted onto slides with Vectashield (Vector Labs).

Subcellular protein fractionation. Subcellular proteins were fractionated by use of a subcellular protein fractionation kit from Pierce. BJ cells (2×10^6 cells) were fractionated into cytosolic, membrane-bound, soluble nuclear, as well as chromatin-bound parts according to standard protocols.

RESULTS

Screening of nucleolar RNA helicases involved in rRNA synthesis. Ribosome biogenesis is an evolutionarily conserved cellular activity that is vital for normal cell growth and proliferation. Several nuclear/nucleolar DEAD/DEAH-box proteins (represented in Table 1, together with their orthologs in *Saccharomyces cerevisiae*) were chosen based on the human nucleolar proteome (http://www.lamondlab.com) (1). They have been shown to participate in various aspects of ribosome biogenesis, including rRNA processing and ribosome assembly (41). However, none of the currently characterized family members have been shown to participate in pre-rRNA transcription. We performed a lentiviral RNA interference screen in order to identify a set of nucleolar DDX/DHX RNA helicases that were necessary for RNA polymerase I-mediated pre-rRNA synthesis. First, five unique shRNAs for each DDX/DHX protein were screened to validate their knockdown efficiencies. Two validated shRNAs were then delivered into primary human fibroblast cells by lentiviral infection. The knockdown efficiency for each DDX/DHX mRNA was detected by quantitative real-time PCR (qRT-PCR) reactions, as shown in Fig. 1B. Pre-rRNA transcription was assayed by monitoring the production of the short-lived 47S rRNA precursor by qRT-PCR (7). Changes in 47S rRNA transcript levels correlated with the efficiency of each DDX/DHX helicase knockdown by qRT-PCRs. As shown in Fig. 1C, the knockdown of several DDX/DHX proteins correlated with decreased pre-rRNA synthesis although with various degrees of perturbation. A significant decrease in the rRNA transcription level (up to 10-fold) compared to that of the control was observed for DHX33, DHX9, and DDX46 following the shRNA delivery (Fig. 1C), while up to a 3-fold to 4-fold decrease was seen for DDX23, DDX48 (eukaryotic initiation factor 4A [eIF4A]), DDX18, DDX47, DDX56, DDX50, DDX51, DDX3X, and DDX48 (Fig. 1C). Table 2 shows the ratios between the change of 47S rRNA expression and the change of mRNA expression for each protein after small interfering RNA (siRNA) knockdown. Notably, although the DHX33 mRNA expression level was decreased by only 60%, we detected a tremendous 10-fold reduction of rRNA synthesis. Given the extreme sensitivity of rRNA synthesis to lower DHX33 expression levels, we chose to further explore the potential role of DHX33 in rRNA transcription.

DHX33 is essential for pre-rRNA synthesis and is a cell cycle-regulated protein. Given that the nucleolus is the site of rRNA synthesis, processing, and assembly (24), we monitored newly synthesized rRNA species in both control and DHX33 knockdown cells using a pulse-chase of [^{3}H]uridine (39). The DHX33 knockdown efficiency was verified by Western blots, as shown in Fig. 2A. Steady-state levels of rRNA harvested from equal numbers of control and DHX33 knockdown cells showed significant reductions of steady-state levels of mature 28S rRNA and 18S rRNA in DHX33 knockdown cells (Fig. 2A, middle and bottom). While there was a significant reduction in levels of all rRNA species, including 47S, 32S, 28S, and 18S rRNAs (Fig. 2B, top), we observed no accumulation of rRNA precursors (Fig. 2B, top), nor did we find any changes in the ratios of each rRNA species when we performed additional [*methyl*-^{3}H]methionine pulse-chase experiments (39) to label newly synthesized pre-rRNA (Fig. 2C and D), indicating that DHX33 is not involved in pre-rRNA processing. To dissect the mechanism of DHX33 in pre-rRNA synthesis, and to further exclude the possibility of rRNA processing defects due to the DHX33 knockdown, BJ fibroblasts were pretreated with 5-fluorouracil to halt rRNA processing for 15 min prior to a [^{3}H]uridine pulse to label newly synthesized 47S rRNA (9, 39). Using equal numbers of cells, we found that the synthesis of 47S rRNA was greatly diminished in DHX33 knockdown cells following a 30-min pulse with [^{3}H]uridine (Fig. 2E).

In addition, RNA polymerase I transcription was more directly assessed by using a 5-fluorouridine (FUrd) incorporation *in situ* run-on assay. In this assay, active RNA polymerase I transcription is correlated directly with the amount of incor-

Downloaded from http://mcb.asm.org/ on April 16, 2013 by Washington University in St. Louis

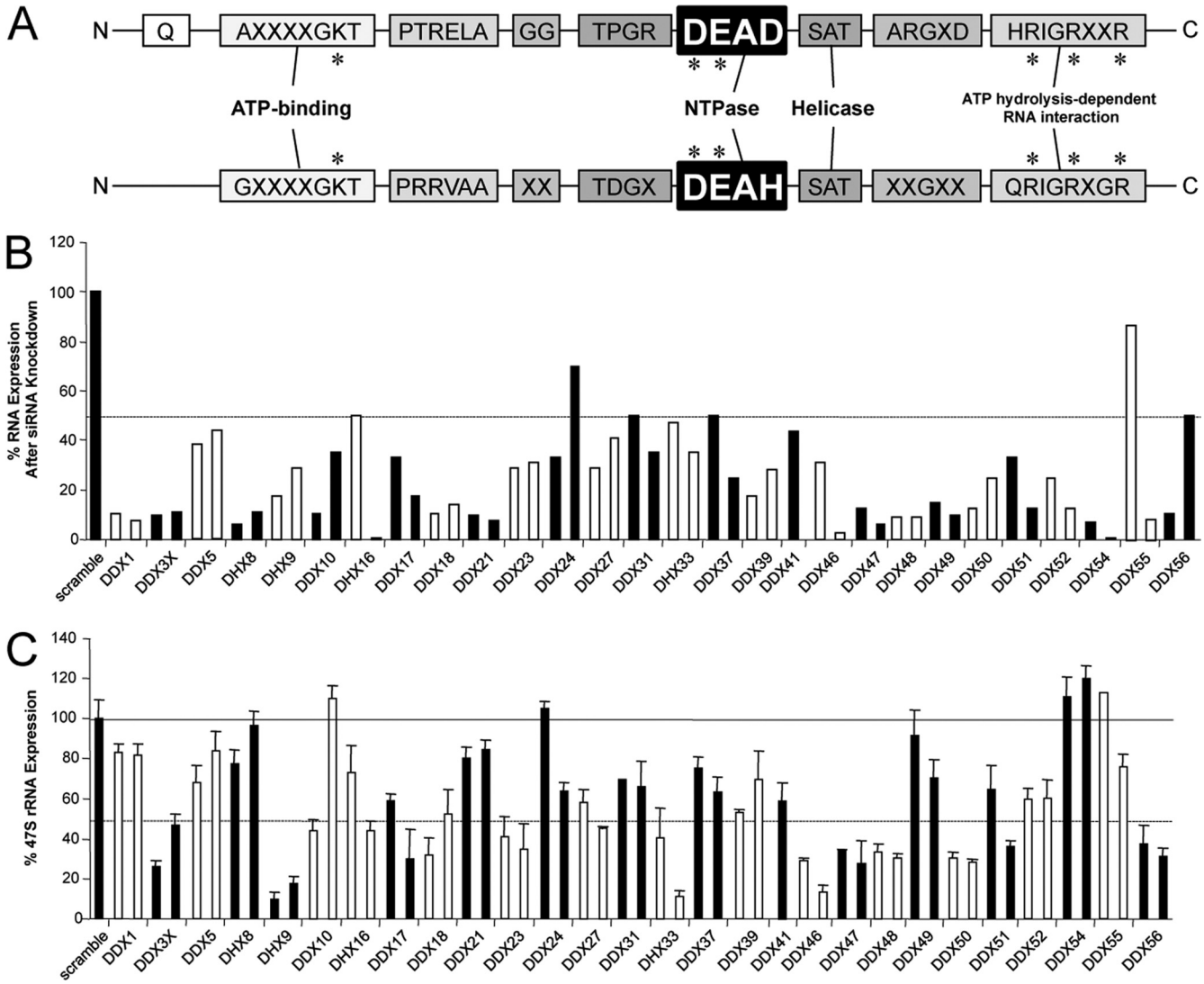

FIG. 1. Lentivirus-mediated RNAi screen of DDX/DHX-box proteins reveals a requirement for several helicases in RNA polymerase I-mediated transcription. (A) Schematic diagram for conserved peptide motifs of DDX and DHX proteins. Critical amino acids for helicase function are marked with an asterisk. (B) Total RNA extracted from human fibroblast BJ cells 4 days after lentiviral infection with each indicated shRNA. The knockdown efficiency of each shRNA for a specific DDX/DHX protein was analyzed by qRT-PCR using scrambled shRNA as a negative control. The dashed line marks 50% expression. (C) Total RNA from BJ cells analyzed by qRT-PCR for the 47S rRNA transcript copy number. The graph shows representative results of two independent screenings performed in triplicate. All values were normalized based on the scrambled control, which was set as 100%. Bars represent standard deviations for three separate qRT-PCR analyses. The solid line marks 100% expression, and the dashed line marks 50% expression.

porated FUrd in nucleoli (18). In control BJ cells, we observed high levels of FUrd incorporation at nucleolar sites using an anti-BrdU antibody recognizing incorporated FUrd (Fig. 2F). In contrast, the knockdown of DHX33 with two separate shRNAs elicited a pronounced decrease, based on equal exposure times of immunofluorescent signals, in levels of nucleolar FUrd incorporation (Fig. 2F).

DHX33, along with its conserved family members, is an NTP-dependent RNA helicase (32). To determine whether NTPase activity was required for DHX33's rRNA transcriptional regulation, we performed site-directed mutagenesis on a critical and conserved amino acid, K94, in the NTPase domain of DHX33; the resulting single point mutation is K94N. The mutation of this critical lysine residue was shown previously to severely cripple RNA NTPase activity among DHX family members (28). BJ fibroblasts were infected with shRNAs to reduce levels of DHX33 and were rescued with the lentiviral delivery of either wild-type or K94N mouse DHX33. Three base pair mismatches exist between the murine DHX33 sequence and the human-targeted shRNA sequence, making the murine overexpression construct moderately resistant to shRNA-directed knockdown. As shown in Fig. 3A, the overexpression of wild-type and K94N mutant DHX33 rescued DHX33 protein levels to approximately 50% of scrambled shRNA control levels. Importantly, the wild-type but not the NTPase-dead mutant DHX33 expression construct could res-

Downloaded from http://mcb.asm.org/ on April 16, 2013 by Washington University in St. Louis

TABLE 2. DDX/DHX knockdown efficiencies and 47S rRNA transcription ratios

Gene	Mean % mRNA	Mean % 47S rRNA	Ratio of 47S rRNA/mRNA
DDX1	7.69	81.4	10.58518
DDX3X	10	26.6	2.66
DDX5	38	68.3	1.797368
DHX8	6.2	77.2	12.45161
DHX9	18	9.6	0.533333
DDX10	10.5	44.4	4.228571
DHX16	1	43.8	43.8
DDX17	18	29.5	1.638889
DDX18	10.8	32.2	2.981481
DDX2	10	80.2	8.02
DDX23	30.7	34.8	1.13355
DDX24	33	105	3.181818
DDX27	35.3	66.4	1.88102
DDX31	29	58	2
DHX33	35	11.2	0.32
DDX37	25	63.6	2.544
DDX39	18	53.2	2.955556
DDX41	43.5	59.1	1.358621
DDX46	29	31	1.068966
DDX47	6.25	28	4.48
DDX48	9	30.8	3.422222
DDX49	10	70.5	7.05
DDX50	12.5	30.9	2.472
DDX51	13	36.4	2.8
DDX52	12.5	60.1	4.808
DDX54	7	111	15.85714
DDX55	8.24	76	9.223301
DDX56	10.8	37.7	3.490741

cue pre-rRNA synthesis to an appreciable degree (4-fold increase over DHX33 knockdown) (Fig. 3B).

Previous studies have shown that rRNA transcription is a growth factor-stimulated process (17). We observed a steady increase in 47S transcription levels as BJ cells reentered the cell cycle following serum stimulation (Fig. 3C). Additionally, expression levels of DHX33 increased upon serum stimulation and reached maximal levels concomitant with maximum phosphorylated UBF Ser484 and 47S rRNA transcription levels (Fig. 3C), indicating that DHX33 responds to growth stimuli in a manner similar to that of the canonical rRNA transcriptional apparatus.

DHX33 localizes to the cell nucleolus and associates with NORs during mitosis. Although DHX33 is an uncharacterized member of the DEAH-box family, a previous proteomic analysis of HeLa cells identified DHX33 as a nucleolar protein (1). To verify the nucleolar localization of endogenous human DHX33, cellular fractionation was performed on two different human cell lines: BT549 breast cancer cells and diploid BJ fibroblasts. We found that DHX33 localized to cell nucleoli in both BT549 and BJ cells, although it was not entirely excluded from the nucleoplasm (Fig. 4A). The nucleolar localization of DHX33 was further confirmed by the costaining of BT549 cells that transiently overexpress FLAG-DHX33 with fibrillarin (Fig. 4B). Colocalization between UBF and DHX33 was detected in both murine *p53*-null MEFs and human BJ fibroblasts (Fig. 4B). As cells progress through the G_2/M border, nucleoli disassemble, with only a few proteins that are critical for RNA polymerase I transcription remaining associated with nucleolar organizing regions (NORs). UBF1 is one of these proteins (51). To check the localization of DHX33 in mitosis, cells were treated with nocodazole for 18 h to arrest the cell cycle at prometaphase. Under this cell cycle setting, we found that DHX33 and UBF1 again colocalized at the NOR (Fig. 4C).

DHX33 associates with rDNA and UBF. To further dissect the mechanism of DHX33's role in RNA polymerase I transcription, chromatin immunoprecipitation (ChIP) was performed with BT549 human breast cancer cells that overexpressed the FLAG epitope-tagged DHX33 protein. Figure 5A depicts the position of the primer sets used for ChIP analysis along the rDNA locus. We observed a 2- to 7-fold increase in the association between DHX33 and the transcribed/promoter rDNA regions, demonstrating an association between DHX33 and the rDNA locus (Fig. 5B). As two positive controls, we also compared DHX33 with SL.1 and the RNA Pol I large subunit RPA194. SL.1 displayed an interaction only with the promoter region, with enrichment up to 8-fold, while RPA194 showed enrichment up to 40-fold at both promoter and transcribed regions (Fig. 5B). The fact that DHX33 associated with rDNA across the entire promoter and transcribed regions implies that its function may not be confined to transcriptional initiation. To further confirm the interaction between DHX33 and rDNA, we performed a cell fractionation analysis of BJ fibroblast cells. DHX33 was released only by micrococcal nuclease, and this occurred predominantly in chromatin-bound fractionation (Fig. 5C), indicating that DHX33 could be an architecture protein that associates with rDNA chromatin and modulates its function. In addition, we found that overexpressed FLAG-tagged DHX33 interacted with endogenous UBF, as demonstrated by the coimmunoprecipitation of UBF with FLAG antibodies (Fig. 5D). To examine this property more closely, we generated a deletion mutant of DHX33 that lacks 15 amino acids (Δ536-550). The fragment (positions 536 to 550) was found to be fairly similar to a conserved DNA binding box shared by several DEAH DNA helicases (Fig. 5E). The subcellular localization of this deletion mutant still remained in the nucleolus but with diffuse staining apparent in the nucleoplasm (Fig. 5E). Protein expression levels of mutant and wild-type DHX33 are shown in Fig. 5F. We found that the deletion mutant severely crippled its DNA binding activity, as detected by ChIP analysis (Fig. 5F). Taken together, these findings demonstrate the association of DHX33 with rDNA loci, through a critical 15-amino-acid motif, and UBF, a known rDNA binding protein.

DHX33 deficiency reduces RPA194 recruitment to the rDNA locus. UBF is a critical player in the transcription of pre-rRNA. Its phosphorylation has been shown to be required for its activation and participation in RNA polymerase I transcription (38, 42, 45). We found that the DHX33 knockdown significantly reduced the phosphorylation of UBF on Ser484 without affecting the total cellular expression levels of UBF (Fig. 6A). Moreover, the phosphorylation of UBF on Ser484 was shown previously to be required for the recruitment of RNA polymerase I proteins to the rDNA locus (44). In DHX33 knockdown cells, RPA194, a core component of RNA polymerase I (11), displayed no reduction in expression levels (Fig. 6A). However, RPA194 exhibited more than a 50% reduction in its rDNA binding activity, as measured by chromatin immunoprecipitation (Fig. 6B), implying that in the absence of DHX33, the UBF phosphorylation level was reduced, with a

Downloaded from http://mcb.asm.org/ on April 16, 2013 by Washington University in St. Louis

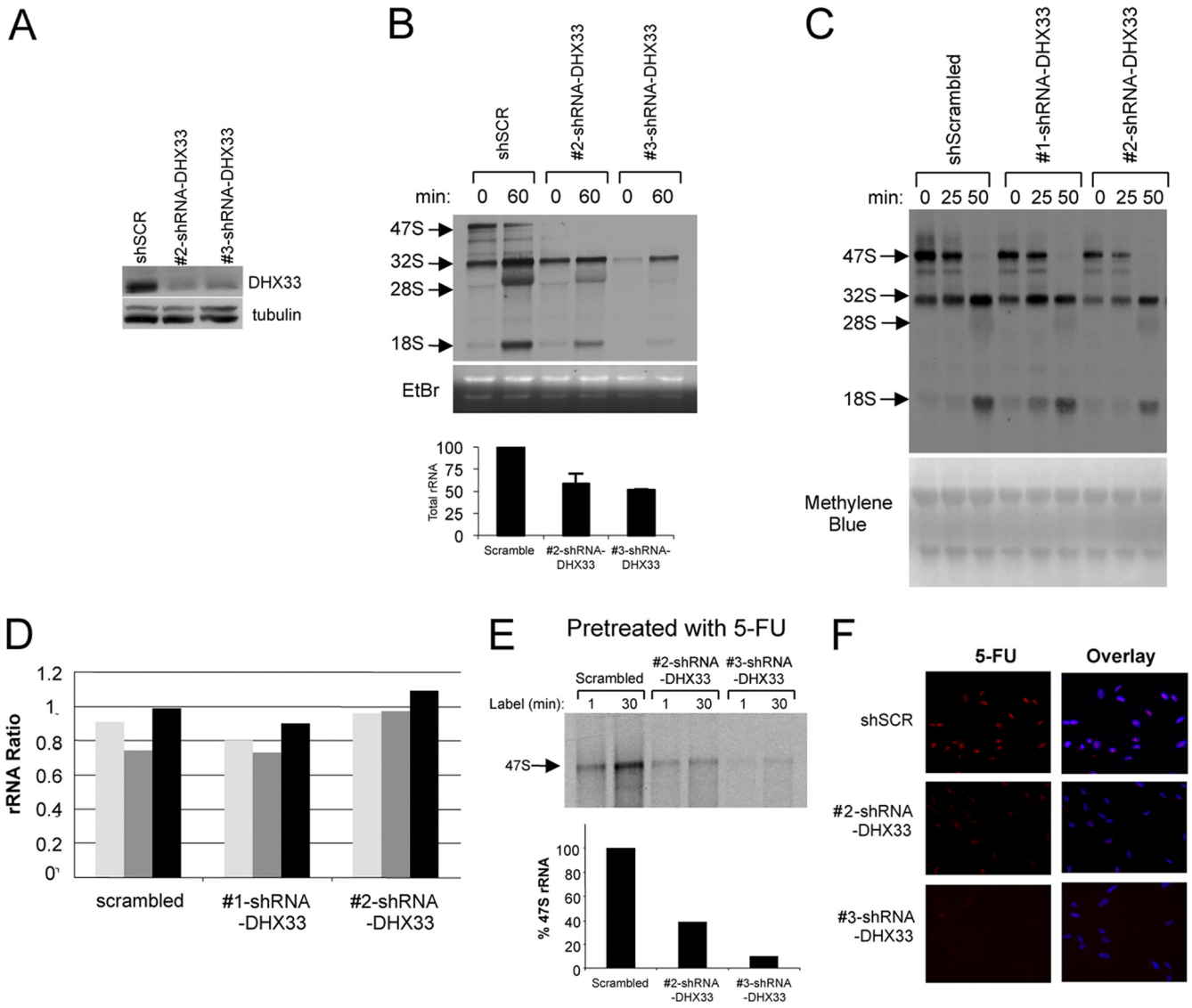

FIG. 2. DHX33 is essential for pre-rRNA synthesis but not processing. (A) BJ cells were infected with scrambled or DHX33 shRNAs. Total cell lysates from each were prepared at 4 days postinfection and subjected to Western blot analysis with the indicated antibodies. (B) From the above-mentioned infected cells, equal numbers of BJ cells (2×10^6 cells) were pulsed with [^{3}H]uridine and then chased with unlabeled uridine and harvested at the indicated times. Total RNA was extracted, separated, transferred onto membranes, and subjected to autofluorography. Newly synthesized 47S, 32S, 28S, and 18S rRNAs are shown (top). Ethidium bromide (EtBr)-stained agarose gels show overall 28S and 18S rRNAs in these samples (middle). Quantification of mature rRNAs is shown in the bottom panel. Bars represents standard deviations from 3 independent experiments. (C) BJ cells infected with the 2 different shRNA-DHX33-encoding lentiviruses were labeled with [*methyl*-^{3}H]methionine and chased with cold methionine for the indicated times. Total RNA was extracted from equal numbers of cells, separated, transferred onto membranes, and subjected to autoradiography. Newly synthesized and labeled rRNA species are indicated by arrows. The bottom panel shows the methylene blue-stained membrane to show the loading of each sample. (D) Densitometry quantitation of ratios between different rRNA species in each BJ cell sample depicted in a bar graph. (E) The BJ cells described above (2×10^6 cells) were pretreated with 5-fluorouracil (5-FU) to halt rRNA processing and then pulse-chased with [^{3}H]uridine to monitor the total levels of 47S rRNA over a 30-min period. Total RNA was extracted, separated, transferred onto membranes, and subjected to autoradiography. Newly synthesized 47S rRNA is shown. (F) The BJ cells described above were pulsed with 5-fluorouridine (5-FUrd), fixed, and stained with an anti-BrdU antibody recognizing incorporated 5-FUrd (red). Nuclei were demarcated with DAPI, and an overlay of the signals is shown. Representative images from three independent experiments are shown.

concomitant failure to recruit RPA194 to rDNA loci. As parallel controls in the analysis, we also analyzed rDNA occupancy for UBF and SL.1 across the promoter/transcribed region. We found no significant change for UBF and SL.1 rDNA occupancy between scrambled control and DHX33 knockdown cells, indicating that the DHX33 knockdown specifically reduced RNA Pol I loading at rDNA (Fig. 6B).

To further explore the mechanism for the reduced pre-rRNA synthesis in DHX33 knockdown BJ cells, we hypothesized that the phosphorylation of UBF resided downstream of DHX33 and upstream of efficient rDNA transcription. Thus, we rescued levels of phosphorylated UBF at Ser484 with phosphomimetic mutants of both UBF1 and UBF2 in DHX33 knockdown cells. UBF2 is a splice variant of UBF1 but has a

Downloaded from http://mcb.asm.org/ on April 16, 2013 by Washington University in St. Louis

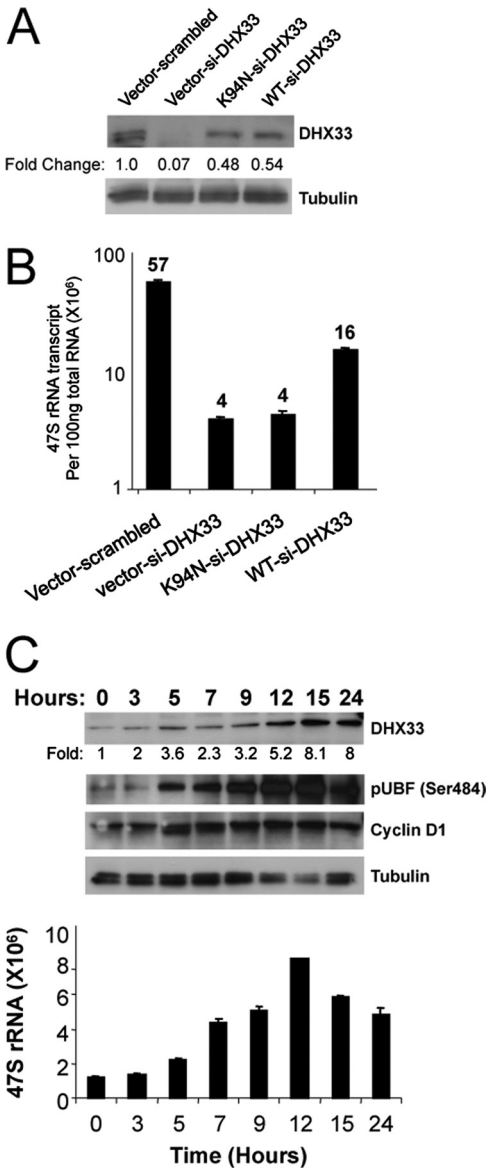

FIG. 3. DHX33 helicase activity is required for pre-rRNA synthesis. (A and B) BJ cells were first infected with wild-type (WT) or helicase-dead K94N DHX33 mutant constructs, followed by a secondary infection with lentiviruses containing the indicated siRNA knockdown constructs (scrambled or DHX33 specific). Cells were then selected in both puromycin- and hygromycin-containing media and analyzed by Western blotting for DHX33 and tubulin (A) and by qRT-PCR for 47S rRNA transcript levels (B) of BJ cells ($n = 3$). Numbers of 47S rRNA transcripts appear above each bar. (C) BJ cells were grown arrested in serum-free medium for 48 h and stimulated with 15% serum for the indicated times. Whole-cell lysates were subjected to Western blot analysis using antibodies recognizing DHX33, pUBF (Ser484), cyclin D1, and tubulin. Total RNA from the same samples was subjected qRT-PCR analysis for 47S pre-rRNA levels and is reported per 100 ng RNA.

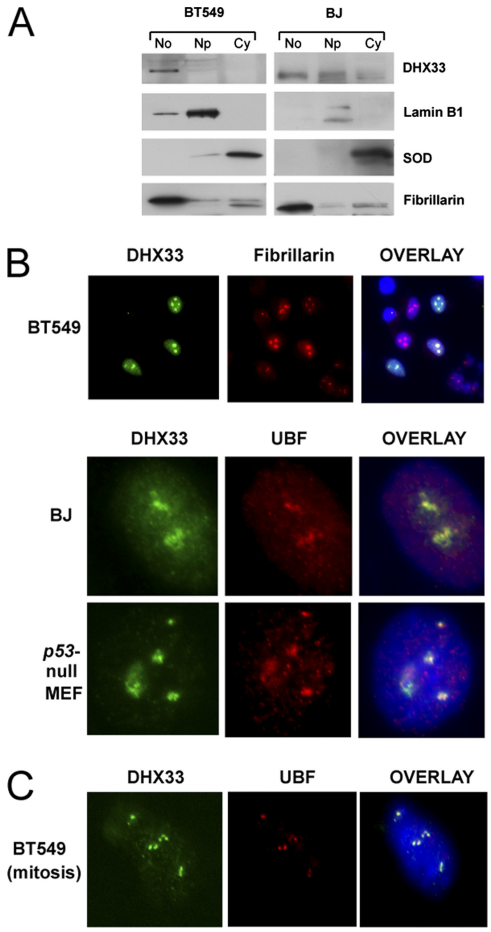

FIG. 4. DHX33 localizes to cell nucleoli. (A) Equal numbers of BT549 cells and BJ human primary fibroblasts (1×10^8 cells) were separated into nucleolar (No), nucleoplasmic (Np), and cytoplasmic (Cy) fractions. Proteins isolated from each fraction were analyzed by Western blotting using antibodies recognizing DHX33, cytosolic superoxide dismutase (SOD), nucleolar fibrillarin, and nuclear lamin B1. (B) BT549 cells, BJ cells, or *p53*-null MEFs were infected with a lentivirus encoding FLAG-tagged DHX33. At 4 days postinfection, transduced cells were fixed and stained with antibodies recognizing FLAG (DHX33) (green), fibrillarin (red), or UBF (red). Nuclei were demarcated with DAPI. Transfected BT549 cells showed an overexpression of FLAG-DHX33 in the nucleoli, as marked by fibrillarin at a ×20 magnification. An overlay of signals (yellow) is also shown for DHX33-UBF colocalization at a ×100 magnification for BJ cells and *p53*-null MEFs. (C) The BT549 cells described above were treated with nocodazole at 1 μM for 18 h, and cells were then fixed and costained with anti-UBF (red) and anti-FLAG (green) antibodies as described above. DHX33 and UBF colocalized at the NOR, as shown by the overlaid yellow signal at a ×100 magnification.

truncated second high-mobility-group (HMG) box and has a decidedly weaker activity than UBF1 in bending DNA (19, 36). Knockdown levels for DHX33 were precisely evaluated by qPCR analysis after normalization with GAPDH mRNA (Fig. 7A). Overexpression levels of UBF were analyzed by Western blotting (Fig. 7B and D). We found that in DHX33 knockdown cells, the weaker UBF2 (S484D) mutant did not restore rRNA transcription (Fig. 7E). However, the overexpression of UBF1 (wild type and S484D) was able to restore 47S rRNA levels approximately 70 to 80% in DHX33 knockdown cells (Fig. 7C). When both UBF1 and UBF2 (wild type and S484D) were transduced into DHX33 knockdown cells, Pol I transcription was restored (Fig. 7C) to a level comparable to that of the scrambled shRNA control, indicating that saturating the system with large amounts of UBF overcomes the deleterious effects of the DHX33 knockdown.

Downloaded from http://mcb.asm.org/ on April 16, 2013 by Washington University in St. Louis

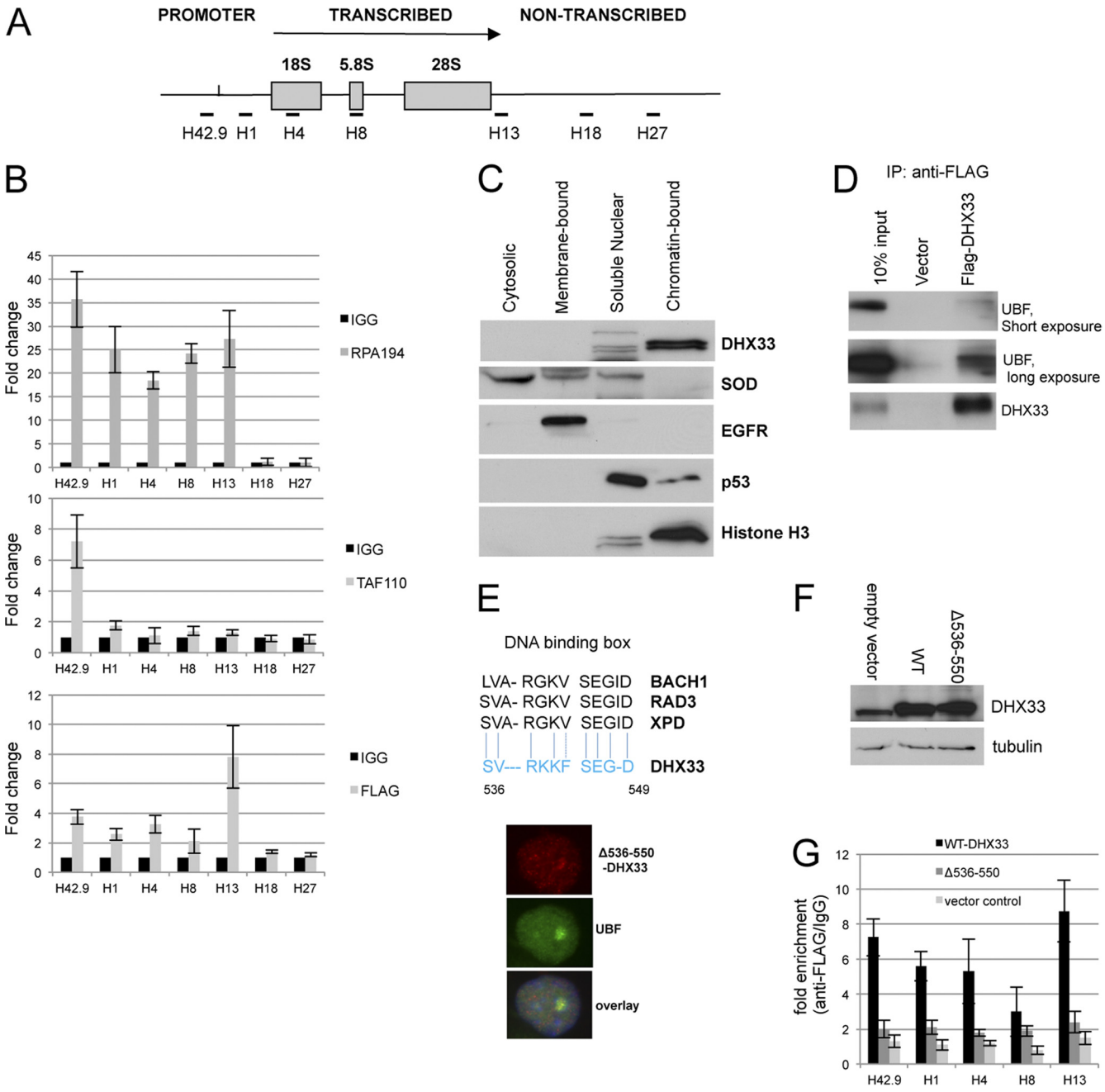

FIG. 5. DHX33 associates with rDNA and UBF. (A) Diagram depicting rDNA transcribed, nontranscribed, and promoter regions and the location for primer sets used for chromatin immunoprecipitation (ChIP). (B) BT549 cells transduced with FLAG-tagged DHX33 were lysed and incubated with nonimmune mouse IgG or antibodies recognizing the FLAG epitope, RPA194, as well as TAF110. PCR analysis using the above-mentioned rDNA primers was used to detect DNA sequences associated with immunoprecipitation. (C) BT549 cells were fractionated, and equal amounts of protein lysates were analyzed by Western blotting with the indicated antibodies. (D) BT549 cells stably expressing either FLAG-tagged DHX33 or an empty vector were immunoprecipitated (IP) with anti-FLAG antibody and immunoblotted with the indicated antibodies. (E) Alignment of DHX33 amino acids 536 to 550 with the DNA binding boxes of several known DEAH DNA helicases. BT549 cells were infected by a lentivirus encoding a DHX33 deletion mutant (Δ536-550). Cells were fixed and stained with anti-FLAG antibody for the detection of the localization of the DHX33 deletion mutant (red) and anti-UBF antibody (green) as a nucleolar marker by immunofluorescence. (F) BT549 cells were infected by a lentivirus encoding either wild-type (WT) DHX33 or its deletion mutant (Δ536-550). Whole-cell lysates were prepared at 4 days postinfection and analyzed by Western blotting with the indicated antibodies. (G) The above-mentioned cells were fixed and subjected to ChIP analysis. Equal amounts of cell lysate were immunoprecipitated with either anti-FLAG antibody or mouse IgG. (Error bars are taken from data from 2 independent experiments.)

DHX33 overexpression increases RNA polymerase I-mediated transcription, a process that requires DHX33 rDNA binding activity. To more directly determine the involvement of DHX33 in RNA polymerase I-mediated transcription, we utilized lentiviral infection to overexpress DHX33 in human BT549 cells. Western blot analysis showed the overexpression of both wild-type DHX33 and its NTPase-dead mutant (K94N) (Fig. 8A). However, only wild-type DHX33 stimulated 47S

Downloaded from http://mcb.asm.org/ on April 16, 2013 by Washington University in St. Louis

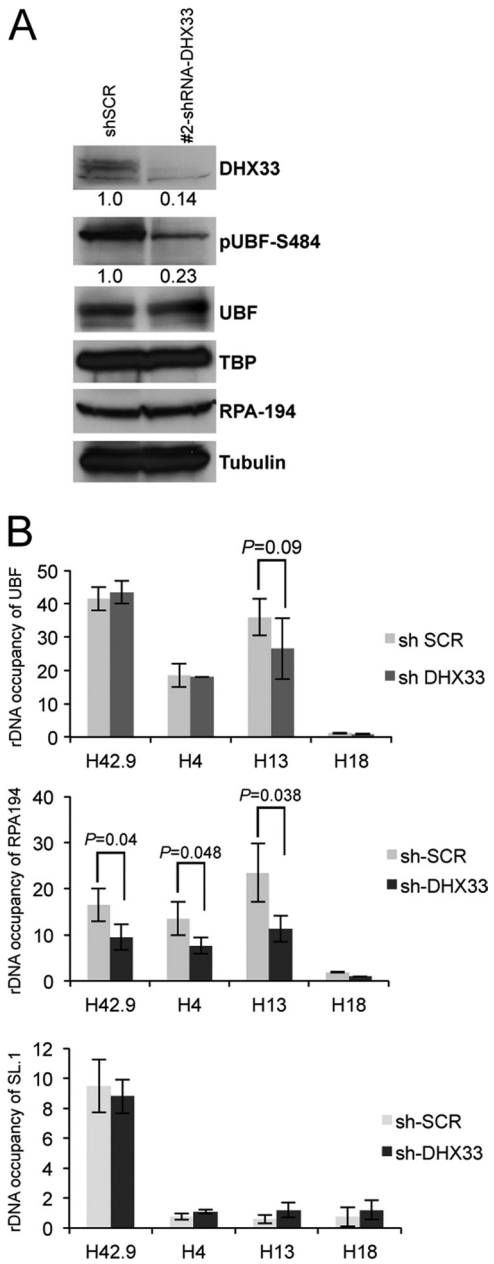

FIG. 6. DHX33 deficiency reduces RPA194 recruitment to the rDNA locus. (A) BJ cells were infected with the indicated lentiviruses, and whole-cell lysates were subjected to Western blot analysis using antibodies recognizing the indicated proteins. (B) Equal amounts of the cell lysates described above were subjected to ChIP analysis using anti-RPA194 or anti-SL.1 and anti-UBF antibodies, IgG, and the indicated rDNA primer sets (H42.9, H4, H13, and H18). The fold change for each antibody or IgG is shown across the rDNA locus. Bars represent standard deviations from 3 independent experiments.

rRNA synthesis (3-fold) (Fig. 8B), further demonstrating the positive role of DHX33 and its NTPase activity in rRNA transcription. To study the mechanism of the DHX33-mediated enhancement of rRNA synthesis, we performed ChIP analyses for cells overexpressing wild-type DHX33, an empty vector, or K94N mutant DHX33. Wild-type but not K94N mutant DHX33 increased the rDNA occupancy of RNA Pol I 2-fold (Fig. 8C). Additionally, we measured the rDNA occupancy of Rrn-3, a transcription-competent subunit of the RNA polymerase I complex, and transcription termination factor (TTF) and found that the rDNA occupancy of RRN-3 was also increased by 2-fold in the presence of wild-type DHX33 but not the K94N mutant. We found no significant change of rDNA occupancy for TTF-1 in the presence of either wild-type or K94N mutant DHX33 (Fig. 8C).

The overexpression of the DHX33 Δ536-550 DNA binding mutant caused a significant reduction in rRNA synthesis compared to that of the wild-type DHX33 control (Fig. 8D), which correlated with a severe inhibition of RNA polymerase I recruitment to rDNA loci (Fig. 8E). This further supports the idea that DHX33 binds to the rDNA locus through its DNA binding domain to recruit RNA Pol I and promote rRNA transcription.

An NTPase-defective mutant of DHX33 (K94R) acts in a dominant negative manner to inhibit rRNA synthesis. To provide more evidence for the participation of DHX33 and the importance of its NTPase activity in rRNA transcription, we generated an additional NTPase-defective mutation of DHX33, K94R. The DHX33 K94R mutant localized properly to nucleoli (Fig. 9A). BT549 cells were transduced with a lentivirus expressing either the wild type or the DHX33 K94R mutant (Fig. 9B) and were assayed for rRNA transcription. We found that wild-type DHX33 was able to enhance rRNA synthesis by more than 2-fold, while the K94R mutant inhibited rRNA synthesis by 2-fold compared to cells transduced with an empty vector (Fig. 9C), indicating that endogenous DHX33 was competitively inhibited by the overexpressed DHX33 K94R mutant. We hypothesized that mutant DHX33 might therefore bind equally well to UBF. Indeed, the coimmunoprecipitation of UBF with FLAG-tagged wild-type and mutant DHX33 showed that the K94R mutant of DHX33 bound to UBF as well as wild-type DHX33 (Fig. 9D), providing further mechanistic evidence that the NTPase activity of DHX33 is critical for its function in rRNA synthesis.

DHX33 is required for maintenance of nucleolar integrity. Previous studies have shown that the transcriptional repression of rRNA synthesis alters the normal nucleolar structure (33). To establish the consequences of the DHX33 knockdown on nucleolar morphology, two different nucleolar markers, nucleophosmin (NPM) and fibrillarin, were used to mark the nucleolus after DHX33 knockdown in BJ fibroblasts. NPM- and fibrillarin-marked nucleoli became less distinct and much smaller following the DHX33 knockdown (Fig. 10A). We verified that the contraction of nucleoli was not due to decreased protein expression levels for either NPM or fibrillarin (Fig. 10B). Furthermore, silver staining for nucleolar organizing regions (30) was also performed on both control and DHX33 knockdown cells to further document changes in nucleolar morphology. Following the DHX33 knockdown (Fig. 10C), the nuclear area occupied by AgNOR staining was significantly reduced (Fig. 10D), consistent with previous studies linking changes in pre-rRNA transcription with nucleolar morphology (5).

DHX33 is essential for cell growth, with a DHX33 deficiency inducing p53-dependent cell cycle arrest. During our initial RNA interference screening, we observed changes in cellular morphology in BJ cells transduced with shRNAs targeting

Downloaded from http://mcb.asm.org/ on April 16, 2013 by Washington University in St. Louis

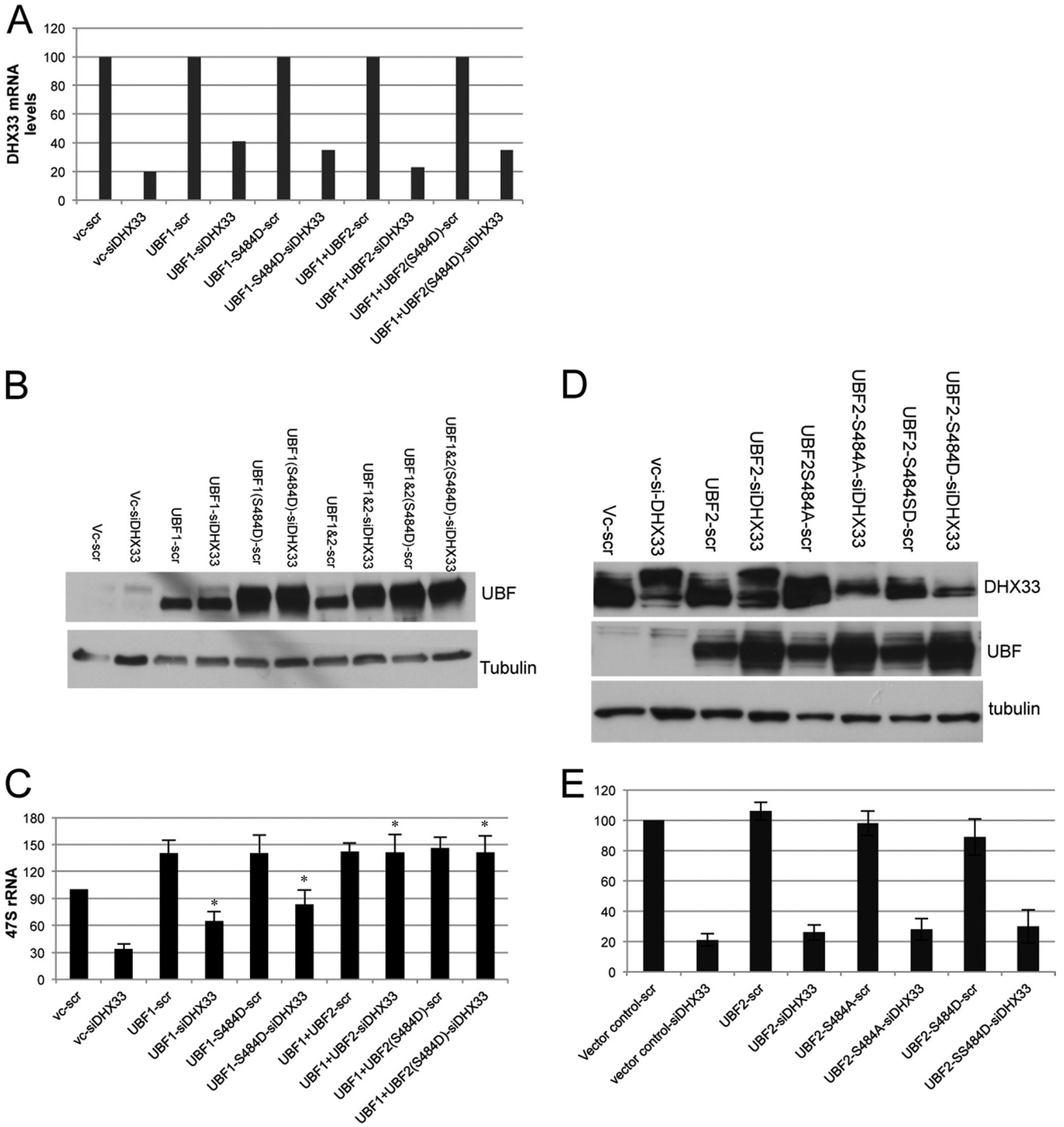

FIG. 7. Overexpression of UBF restores 47S rRNA levels in the absence of DHX33. (A) BJ cells were first infected with the indicated lentiviruses encoding the empty vector or UBF1/UBF2 (wild type or S484 mutant) and then infected with a lentivirus encoding either scrambled or shRNA-DHX33 lentivirus. Total RNA was prepared 4 days after the last infection, and the total mRNA level of DHX33 is shown after normalization to GAPDH mRNA levels. vc, vector control. (B) Whole-cell lysates were prepared from the above-mentioned cells and were subjected to Western blot analysis with anti-UBF and anti-tubulin antibodies. (C). RNA polymerase I transcriptional activity was detected by qRT-PCR analysis of human 47S rRNA transcripts from equal amounts of total RNA samples (*, $P \leq 0.01$ for $n = 3$). (D) BJ cells were first infected with the indicated lentiviruses encoding the empty vector or UBF2 (wild type or S484 mutants) and then infected with a lentivirus encoding either scrambled or shRNA-DHX33 lentivirus. Whole-cell lysates were prepared 4 days after the second infections and were subjected to Western blotting with the indicated antibodies. (E) RNA polymerase I transcriptional activity was detected by qRT-PCR analysis of human 47S rRNA transcripts from equal amounts of total RNA samples.

Downloaded from http://mcb.asm.org/ on April 16, 2013 by Washington University in St. Louis

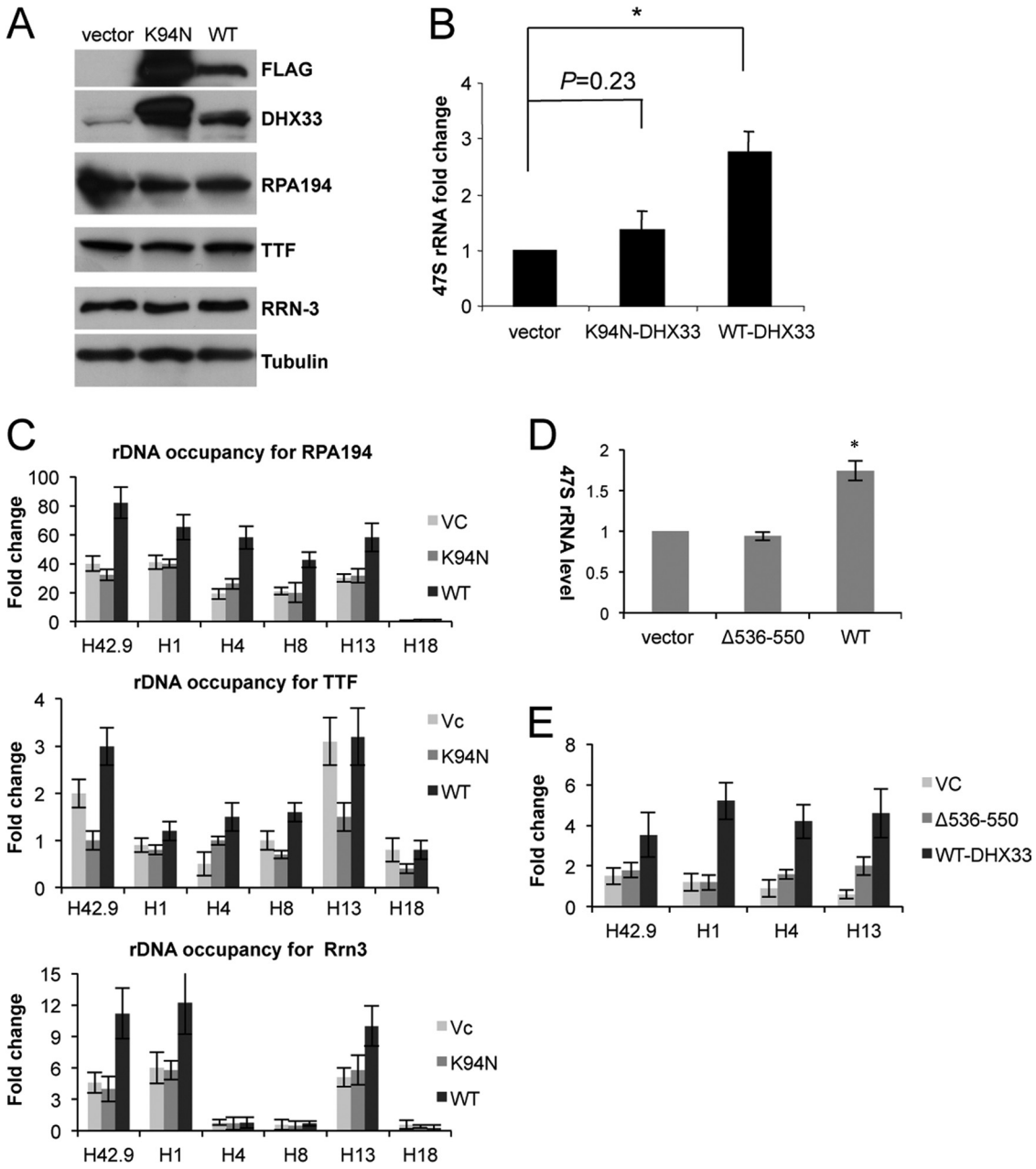

FIG. 8. DHX33 overexpression increases rRNA transcription. (A) BT549 cells were infected with lentiviruses encoding FLAG-tagged wild-type (WT) DHX33, K94N mutant DHX33, or an empty vector. Cell lysates were analyzed for DHX33 expression by Western blot analysis using antibodies recognizing the FLAG epitope, DHX33, RPA194, TTF, Rrn-3, and tubulin. (B) BT549 cells were selected in hygromycin for 3 days and harvested 48 h after selection for total RNA extraction. RNA polymerase I transcriptional activity was detected by qRT-PCR analysis of human 47S rRNA transcripts (*, $P \leq 0.01$ for $n = 3$). (C) The BT549 cells described above were fixed and immunoprecipitated for ChIP analysis with anti-RPA194, anti-Rrn, and anti-TTF antibodies and IgG. The indicated primer sets (H42.9, H1, H4, H8, H13, and H18) were used for PCR amplifications. Error bars are taken from 2 independent experiments. (D) BT549 cells were infected with lentiviruses encoding FLAG-tagged wild-type (WT) DHX33 or Δ536-550 mutant DHX33. Total RNA was extracted. RNA polymerase I transcriptional activity was detected by qRT-PCR analysis of human 47S rRNA transcripts from equal amounts of total RNA samples (*, $P \leq 0.01$ for $n = 3$). (E) The above-mentioned cells were fixed and subjected to ChIP analysis with anti-RPA194 antibody. Equal amounts of cell lysates were used for immunoprecipitation, and data presented are fold enrichments of anti-RPA194/IgG across the indicated rDNA loci. Error bars are taken from data from 3 independent experiments.

DHX33. Moreover, previous studies have shown clear links between nucleolar integrity and p53 activation, with altered nucleoli resulting in a p53-dependent stress response (31). Compared to control cells, DHX33 knockdown cells were significantly smaller (Fig. 11A). This diminished size was further verified by measuring the diameter of individual cells. BJ cells transduced with scrambled control shRNAs measured 19.6 μm in diameter, while transduction with shRNA 2 and shRNA 3

Downloaded from http://mcb.asm.org/ on April 16, 2013 by Washington University in St. Louis

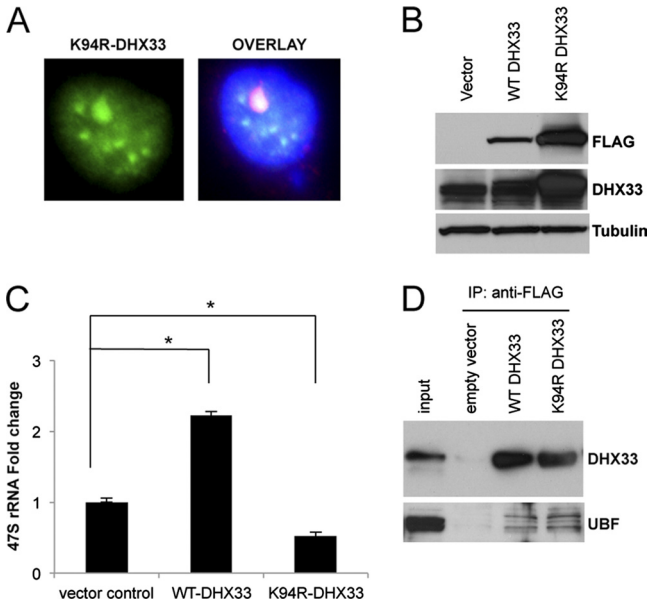

FIG. 9. A helicase-defective mutant of DHX33 inhibits endogenous rRNA synthesis in a dominant negative manner. (A) BT549 cells were infected with a lentivirus encoding either wild-type DHX33, the K94R DHX33 mutant, or an empty vector. Cells that were infected with the K94R DHX33 mutant were fixed and stained with anti-FLAG antibody to check for the localization of mutant DHX33 (green) and UBF (red). Nuclei were demarcated with DAPI, and the overlaid image is shown. The DHX33 K94R mutant colocalized with UBF, as shown in yellow in the nucleolus. (B) The BT549 cells described above were harvested for whole-cell extraction. Equal amounts of protein lysate were analyzed by Western blotting to detect the expression of the wild type or the DHX33 K94R mutant with the indicated antibodies. (C) The BT549 cells described above were harvested as described above for total RNA extraction. Endogenous rRNA transcription was monitored by qPCR analysis of human 47S rRNA transcript levels ($P < 0.001$ [$n = 3$]). (D) The BT549 cells described above were immunoprecipitated with anti-FLAG tag antibody and immunoblotted with the indicated antibodies.

targeting DHX33 resulted in cell diameters of 18.1 and 17.9 μm, respectively ($P \leq 0.05$) (Fig. 11B). These findings correlate with our initial screen, which identified DHX33 expression as a requirement for maintaining 47S rRNA transcript levels (Fig. 11C); reduced levels of rRNA transcripts would predict a commensurate reduction in the overall cell size.

Recent studies have emphasized a new role for the nucleolus as a sensor of cellular stress (21, 22, 31, 50). In this context, a disruption of rRNA synthesis results in a prototypical p53 response, often triggering cell cycle arrest (29, 31). We sought next to determine whether the loss of DHX33 would trigger a similar response. Proliferation curves of human primary fibroblast cells were generated following infection with lentiviruses encoding shRNAs targeting DHX33 (Fig. 11C). Cell proliferation was reduced upon the DHX33 knockdown (Fig. 11C). The DHX33 reduction also induced a significant G_1 cell cycle arrest following FACS analysis of transduced BJ cells (Fig. 11D).

The reduction in DHX33 expression levels in BJ fibroblasts resulted in a significant induction of both p53 and p21 protein expression (Fig. 11E). To determine whether the cell cycle arrest following the DHX33 loss was solely p53 dependent, we infected *p53*-null mouse embryonic fibroblasts (MEFs), compared to wild-type MEFs, with lentiviruses encoding shRNAs targeting DHX33. For *p53*-null MEFs, we did not observe any significant differences in the cell cycle profiles between scrambled and DHX33 shRNA-infected cells (Fig. 11F) despite our ability to knock down DHX33 by 50% (Fig. 11H). Additionally, we did not observe a decrease in UBF Ser484 phosphorylation in *p53*-null MEFs exhibiting a reduction in DHX33 protein expression levels (Fig. 11H), suggesting that the inhibition of UBF phosphorylation upon the loss of DHX33 is p53 dependent and is an indirect result of cell cycle arrest following the depletion of DHX33. This further supports the notion that DHX33 is essential for pre-rRNA synthesis regardless of the UBF phosphorylation status. Previous reports have shown that p53 induction can repress RNA polymerase I-mediated transcription under certain conditions (4, 52). However, in *p53*-null MEFs, the synthesis of 47S rRNA was still decreased by up to 75% upon the DHX33 knockdown (Fig. 11G), indicating that the attenuation of 47S rRNA synthesis following the loss of DHX33 is p53 independent.

DISCUSSION

The DEAD/DEAH-box protein family consists of 57 members; family members are encoded as relatively large proteins of more than 400 amino acids in length. In addition to a core helicase domain, there are also extending N-terminal and C-terminal domains that are thought to be involved in protein-protein/RNA interactions (20). Although generally believed to contain probable RNA helicase/unwindase activity, some members of the DDX/DHX family, such as DHX9 (also called RNA helicase A), have also been shown to bind DNA and function as a DNA helicase (53). In fact, DEAH RNA helicases contain some degree of structural homology to DNA helicases (13). Other than their functions in general RNA metabolism, including RNA splicing, translation, rRNA processing, and mRNA decay, some DDX/DHX proteins, including DHX9 (26), DDX5/DDX17 (46, 48), DHX20 (49), and DDX21 (47), have been found to play important roles in transcriptional regulation (8). Specifically, DHX9 has been shown to bind directly to RNA polymerase II through the concerted efforts of its helicase core domain and N-terminal domain (26). Other DDX proteins, such as DDX5, DDX20, and DDX21, can function as transcriptional coactivators or repressors through direct protein-protein interactions (8). Our large-scale screen in this study focused on important players in RNA polymerase I transcription in the nucleolus, a cellular activity which none of the DDX/DHX family of proteins had been associated with to date. Within the entire DEAD/DEAH-box protein family, over half of all DDX/DHX proteins localize to the nucleolus, making them prime candidates for RNA polymerase I-mediated transcriptional regulation.

The regulation of RNA polymerase I transcription succumbs to multiple forms of intracellular stress or perturbations in signaling events involved in cell growth (10). Additionally, the nucleolus can act as a sensor of DNA damage, nutrient availability, and stress signals to shut down rRNA synthesis (10, 21, 31). In this report, we observed decreases in levels of rRNA synthesis after knocking down many members of the nucleolar DEAD/DEAH-box protein family. Whether all of these pro-

Downloaded from http://mcb.asm.org/ on April 16, 2013 by Washington University in St. Louis

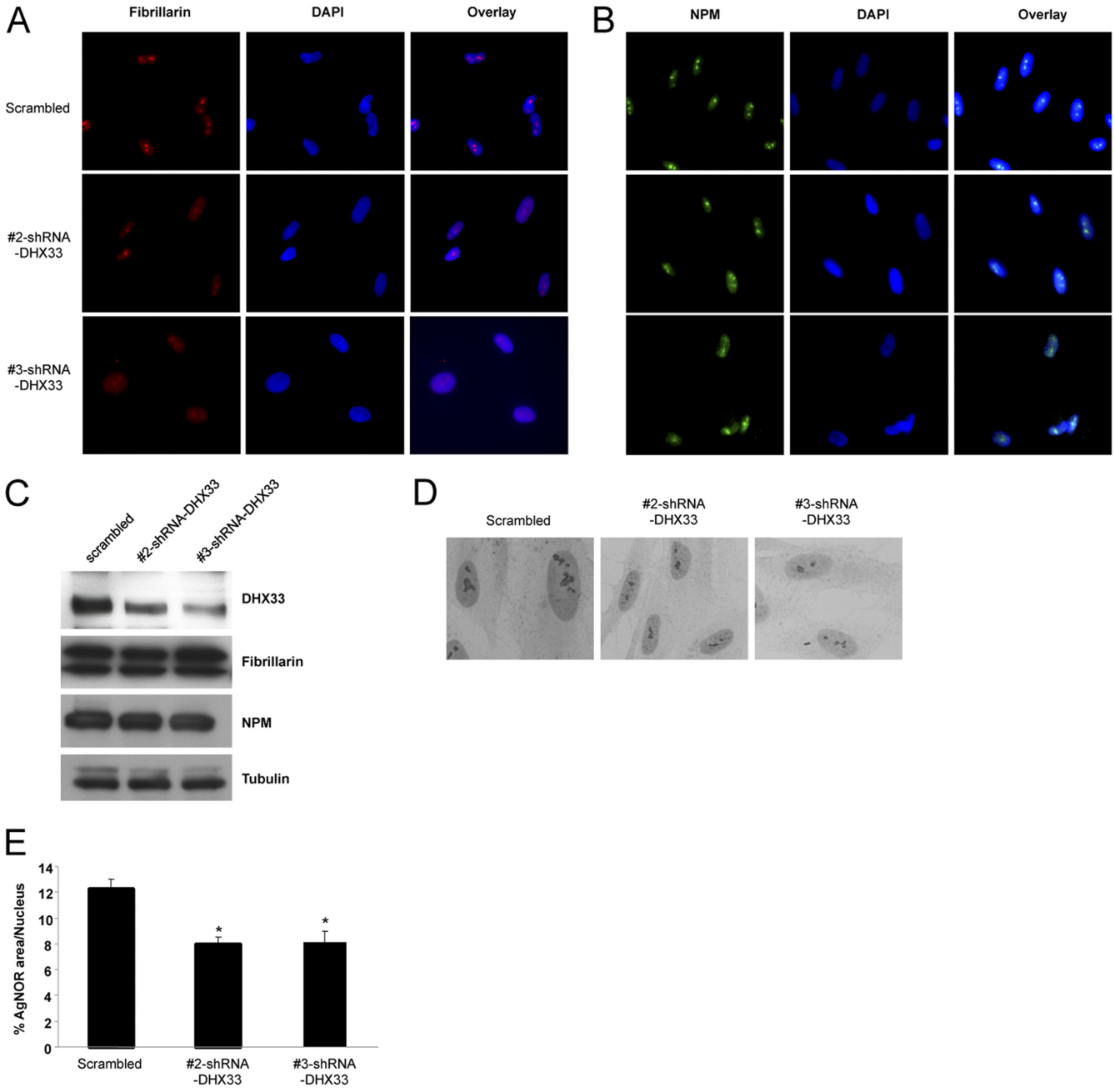

FIG. 10. Altered nucleolar morphology in the absence of DHX33. (A and B) BJ cells infected with the indicated shRNA-encoding lentiviruses were subjected to immunofluorescence microscopy with either antifibrillarin (A) or anti-NPM (B) antibody. A typical image is shown for each sample. (C) The above-mentioned cells were harvested, and whole-cell lysates were analyzed by Western blotting using antibodies recognizing DHX33, fibrillarin, NPM, and tubulin. (D) Infected BJ cells were fixed and stained with silver. Silver-stained nucleoli were visualized by phase-contrast microscopy. (E) Quantitation of silver-stained nucleolar area versus total nuclear area for >100 cells, given as percentages by use of MetaMorph software (*, $P \leq 0.001$ for $n = 3$).

teins are directly required for RNA polymerase I-mediated transcription remains a critical question. Given the feedback loop between cellular stress and reduced nucleolar function, it is possible that a reduced expression level of DEAD/DEAH proteins elicits a stress signal that ultimately reduces rRNA synthesis and cell growth.

Our findings provide a direct link between critical roles of DHX33 in cell growth and rRNA synthesis. The DHX33 knockdown exhibited a great degree of rRNA synthesis inhibition (10-fold) in relation to the extent of the knockdown achieved for the entire nucleolar helicase family screened. This drastic degree of reduction of rRNA synthesis upon a DHX33 deficiency implicates its pivotal role in RNA polymerase I-mediated transcription. We have shown that DHX33 participates in rRNA transcription through its interaction with one of the key players in RNA polymerase

Downloaded from http://mcb.asm.org/ on April 16, 2013 by Washington University in St. Louis

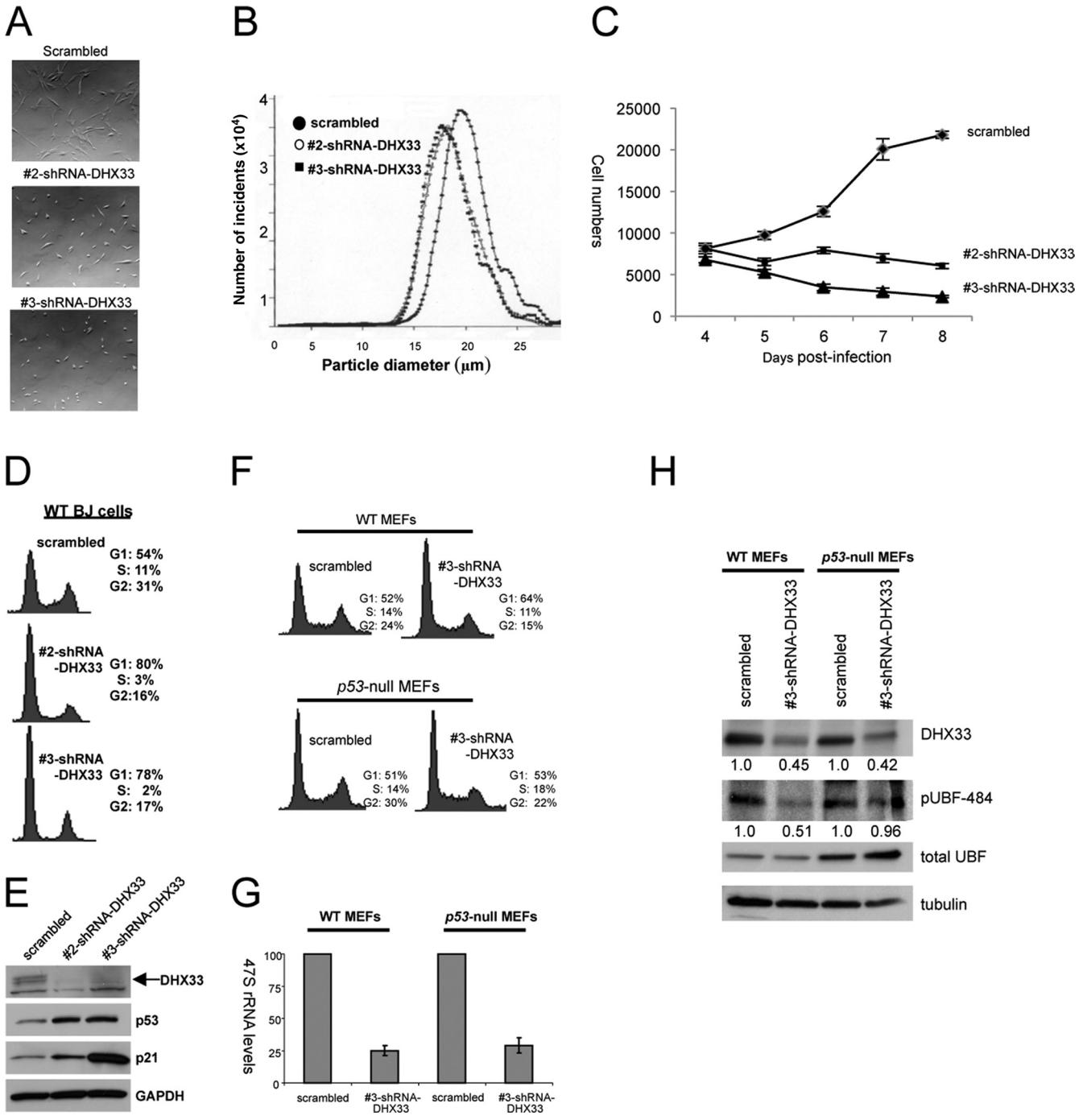

FIG. 11. DHX33 is essential for cell growth, and DHX33 deficiency induces cell cycle arrest. (A) BJ cells were infected with lentiviruses encoding scrambled or two DHX33 short hairpins. Live cells were visualized 5 days after lentiviral infection. (B) The infected cells described above were trypsinized and subjected to size analysis using the Coulter method. (C) BJ cells were infected with two different shRNA-DHX33 lentiviruses, selected for 3 days, replated (7.5×10^3 cells), and manually counted daily for 5 days. (D) The BJ cells described above were trypsinized and fixed with 75% ethanol. Cell cycle analysis were performed with a FACSCalibur instrument after propidium iodide staining. (E) Whole-cell lysates from the above-mentioned BJ cells were subjected to Western blot analysis using antibodies recognizing DHX33, p53, p21, and tubulin. (F) Wild-type MEFs (WT MEFs) or *p53*-null MEFs were infected with lentiviruses encoding scrambled or DHX33 short hairpin RNA. Cells were trypsinized and subjected to cell cycle analysis at 5 days postinfection. (G) Total RNAs were extracted from the above-described infected cells and analyzed for 47S pre-rRNA by qRT-PCR based on 100 ng of total RNA and normalized to the scrambled control of wild-type MEFs. Bars represent standard deviations from 3 separate experiments. (H) Total cell lysates were prepared from the above-mentioned BJ cells and subjected to Western blot analysis using antibodies recognizing DHX33, phospho-UBF (Ser484), UBF, and tubulin.

Downloaded from http://mcb.asm.org/ on April 16, 2013 by Washington University in St. Louis

I-mediated transcription, UBF, an rDNA architectural protein.

Ser484 of UBF is phosphorylated by two G_1-specific protein kinase holoenzymes, cyclin D1-CDK4 and cyclin E-CDK2 (44). We originally postulated that the loss of DHX33, which induced a significant G_1 cell cycle arrest in wild-type cells, might result in a loss of UBF phosphorylation through an indirect means. Specifically, G_1-arrested DHX33 knockdown cells should exhibit decreased CDK4 and CDK2 activities, thus reducing UBF Ser484 phosphorylation. Moreover, we showed that the loss of DHX33 triggered a potent p53 response with a rapid induction of p21, a well-known inhibitor of CDK2 activity (12). However, we demonstrated that the DHX33 loss in *p53*-null MEFs did not cause a reduction of UBF Ser484 phosphorylation but still diminished rRNA transcription levels without cell cycle arrest. Thus, it appears more likely that DHX33 exerts a more direct effect on rRNA transcription through influencing the rDNA occupancy of RNA polymerase I, an effect that we have also shown requires DHX33's NTPase activity.

Our data have identified a novel protein, DHX33, as a critical player in ribosome RNA transcription. We have shown that DHX33 is a nucleolar chromatin binding protein, where it associates with UBF and rDNA loci. UBF, as an rDNA chromatin-modulating protein, binds across the entire rDNA promoter and the transcribed as well as the nontranscribed regions to facilitate changes in the rDNA conformation in order to fully activate rRNA transcription. Our findings are consistent with the idea that DHX33, through both its NTPase activity and DNA binding, might facilitate the conformational change of rDNA through the hydrolysis of ATP. Thus, DHX33 would act as a crucial interaction partner for UBF during this essential process in order to promote rDNA transcription. Further elucidation of the extent of the regulation imposed on the cell by this family of RNA helicases could deepen our understanding of several essential biological processes.

ACKNOWLEDGMENTS

We thank the members of the Weber laboratory for their advice and technical assistance. The Genome Institute and Children's Discovery Institute at Washington University provided lentiviral RNAi library constructs.

J.T.F. was supported by NIH grant 5T32 GM007067. A.P.M. was supported by Department of Defense Breast Cancer Research Program award X81XWH-08-BCRP-PREDOC. This work was supported by NIH grant CA120436 and an Era of Hope scholar award in breast cancer research (BC007304) to J.D.W.

REFERENCES

1. **Andersen, J. S., et al.** 2002. Directed proteomic analysis of the human nucleolus. Curr. Biol. **12:**1–11.
2. **Bell, S. P., R. M. Learned, H. M. Jantzen, and R. Tjian.** 1988. Functional cooperativity between transcription factors UBF1 and SL1 mediates human ribosomal RNA synthesis. Science **241:**1192–1197.
3. **Bleichert, F., and S. J. Baserga.** 2007. The long unwinding road of RNA helicases. Mol. Cell **27:**339–352.
4. **Budde, A., and I. Grummt.** 1999. p53 represses ribosomal gene transcription. Oncogene **18:**1119–1124.
5. **Caperta, A. D., N. Neves, W. Viegas, C. S. Pikaard, and S. Preuss.** 2007. Relationships between transcription, silver staining, and chromatin organization of nucleolar organizers in Secale cereale. Protoplasma **232:**55–59.
6. **Chen, D., A. S. Belmont, and S. Huang.** 2004. Upstream binding factor association induces large-scale chromatin decondensation. Proc. Natl. Acad. Sci. U. S. A. **101:**15106–15111.
7. **Cui, C., and H. Tseng.** 2004. Estimation of ribosomal RNA transcription rate in situ. Biotechniques **36:**134–138.
8. **Fuller-Pace, F. V.** 2006. DExD/H box RNA helicases: multifunctional proteins with important roles in transcriptional regulation. Nucleic Acids Res. **34:**4206–4215.
9. **Ghoshal, K., and S. T. Jacob.** 1994. Specific inhibition of pre-ribosomal RNA processing in extracts from the lymphosarcoma cells treated with 5-fluorouracil. Cancer Res. **54:**632–636.
10. **Grummt, I.** 2003. Life on a planet of its own: regulation of RNA polymerase I transcription in the nucleolus. Genes Dev. **17:**1691–1702.
11. **Grummt, I.** 1999. Regulation of mammalian ribosomal gene transcription by RNA polymerase I. Prog. Nucleic Acid Res. Mol. Biol. **62:**109–154.
12. **Harper, J. W., G. R. Adami, N. Wei, K. Keyomarsi, and S. J. Elledge.** 1993. The p21 Cdk-interacting protein Cip1 is a potent inhibitor of G1 cyclin-dependent kinases. Cell **75:**805–816.
13. **He, Y., G. R. Andersen, and K. H. Nielsen.** Structural basis for the function of DEAH helicases. EMBO Rep. **11:**180–186.
14. **Jantzen, H. M., A. M. Chow, D. S. King, and R. Tjian.** 1992. Multiple domains of the RNA polymerase I activator hUBF interact with the TATA-binding protein complex hSL1 to mediate transcription. Genes Dev. **6:**1950–1963.
15. **Kermekchiev, M., J. L. Workman, and C. S. Pikaard.** 1997. Nucleosome binding by the polymerase I transactivator upstream binding factor displaces linker histone H1. Mol. Cell. Biol. **17:**5833–5842.
16. **Kim, S. H., J. Smith, A. Claude, and R. J. Lin.** 1992. The purified yeast pre-mRNA splicing factor PRP2 is an RNA-dependent NTPase. EMBO J. **11:**2319–2326.
17. **Klein, J., and I. Grummt.** 1999. Cell cycle-dependent regulation of RNA polymerase I transcription: the nucleolar transcription factor UBF is inactive in mitosis and early G1. Proc. Natl. Acad. Sci. U. S. A. **96:**6096–6101.
18. **Kruhlak, M., et al.** 2007. The ATM repair pathway inhibits RNA polymerase I transcription in response to chromosome breaks. Nature **447:**730–734.
19. **Kuhn, A., et al.** 1994. Functional differences between the two splice variants of the nucleolar transcription factor UBF: the second HMG box determines specificity of DNA binding and transcriptional activity. EMBO J. **13:**416–424.
20. **Linder, P.** 2006. Dead-box proteins: a family affair—active and passive players in RNP-remodeling. Nucleic Acids Res. **34:**4168–4180.
21. **Maggi, L. B., Jr., and J. D. Weber.** 2005. Nucleolar adaptation in human cancer. Cancer Invest. **23:**599–608.
22. **Mayer, C., H. Bierhoff, and I. Grummt.** 2005. The nucleolus as a stress sensor: JNK2 inactivates the transcription factor TIF-IA and down-regulates rRNA synthesis. Genes Dev. **19:**933–941.
23. **McStay, B., M. W. Frazier, and R. H. Reeder.** 1991. xUBF contains a novel dimerization domain essential for RNA polymerase I transcription. Genes Dev. **5:**1957–1968.
24. **Melese, T., and Z. Xue.** 1995. The nucleolus: an organelle formed by the act of building a ribosome. Curr. Opin. Cell Biol. **7:**319–324.
25. **Moss, T., and V. Y. Stefanovsky.** 2002. At the center of eukaryotic life. Cell **109:**545–548.
26. **Nakajima, T., et al.** 1997. RNA helicase A mediates association of CBP with RNA polymerase II. Cell **90:**1107–1112.
27. **Panov, K. I., J. K. Friedrich, J. Russell, and J. C. Zomerdijk.** 2006. UBF activates RNA polymerase I transcription by stimulating promoter escape. EMBO J. **25:**3310–3322.
28. **Pause, A., and N. Sonenberg.** 1992. Mutational analysis of a DEAD box RNA helicase: the mammalian translation initiation factor eIF-4A. EMBO J. **11:**2643–2654.
29. **Pestov, D. G., Z. Strezoska, and L. F. Lau.** 2001. Evidence of p53-dependent cross-talk between ribosome biogenesis and the cell cycle: effects of nucleolar protein Bop1 on G(1)/S transition. Mol. Cell. Biol. **21:**4246–4255.
30. **Roussel, P., and D. Hernandez-Verdun.** 1994. Identification of Ag-NOR proteins, markers of proliferation related to ribosomal gene activity. Exp. Cell Res. **214:**465–472.
31. **Rubbi, C. P., and J. Milner.** 2003. Disruption of the nucleolus mediates stabilization of p53 in response to DNA damage and other stresses. EMBO J. **22:**6068–6077.
32. **Schwer, B.** 2001. A new twist on RNA helicases: DExH/D box proteins as RNPases. Nat. Struct. Biol. **8:**113–116.
33. **Shav-Tal, Y., et al.** 2005. Dynamic sorting of nuclear components into distinct nucleolar caps during transcriptional inhibition. Mol. Biol. Cell **16:**2395–2413.
34. **Smith, S. D., et al.** 1990. Interaction of RNA polymerase I transcription factors with a promoter in the nontranscribed spacer of rat ribosomal DNA. Nucleic Acids Res. **18:**1677–1685.
35. **Stefanovsky, V., F. Langlois, T. Gagnon-Kugler, L. I. Rothblum, and T. Moss.** 2006. Growth factor signaling regulates elongation of RNA polymerase I transcription in mammals via UBF phosphorylation and r-chromatin remodeling. Mol. Cell **21:**629–639.
36. **Stefanovsky, V. Y., and T. Moss.** 2008. The splice variants of UBF differentially regulate RNA polymerase I transcription elongation in response to ERK phosphorylation. Nucleic Acids Res. **36:**5093–5101.
37. **Stefanovsky, V. Y., G. Pelletier, D. P. Bazett-Jones, C. Crane-Robinson, and T. Moss.** 2001. DNA looping in the RNA polymerase I enhancesome is the

Downloaded from http://mcb.asm.org/ on April 16, 2013 by Washington University in St. Louis

result of non-cooperative in-phase bending by two UBF molecules. Nucleic Acids Res. **29:**3241–3247.
38. **Stefanovsky, V. Y., et al.** 2001. An immediate response of ribosomal transcription to growth factor stimulation in mammals is mediated by ERK phosphorylation of UBF. Mol. Cell **8:**1063–1073.
39. **Sugimoto, M., M. L. Kuo, M. F. Roussel, and C. J. Sherr.** 2003. Nucleolar Arf tumor suppressor inhibits ribosomal RNA processing. Mol. Cell **11:**415–424.
40. **Tanner, N. K.** 2003. The newly identified Q motif of DEAD box helicases is involved in adenine recognition. Cell Cycle **2:**18–19.
41. **Tanner, N. K., and P. Linder.** 2001. DExD/H box RNA helicases: from generic motors to specific dissociation functions. Mol. Cell **8:**251–262.
42. **Tuan, J. C., W. Zhai, and L. Comai.** 1999. Recruitment of TATA-binding protein-TAFI complex SL1 to the human ribosomal DNA promoter is mediated by the carboxy-terminal activation domain of upstream binding factor (UBF) and is regulated by UBF phosphorylation. Mol. Cell. Biol. **19:**2872–2879.
43. **Venema, J., and D. Tollervey.** 1999. Ribosome synthesis in Saccharomyces cerevisiae. Annu. Rev. Genet. **33:**261–311.
44. **Voit, R., M. Hoffmann, and I. Grummt.** 1999. Phosphorylation by G1-specific cdk-cyclin complexes activates the nucleolar transcription factor UBF. EMBO J. **18:**1891–1899.
45. **Voit, R., A. Kuhn, E. E. Sander, and I. Grummt.** 1995. Activation of mammalian ribosomal gene transcription requires phosphorylation of the nucleolar transcription factor UBF. Nucleic Acids Res. **23:**2593–2599.
46. **Watanabe, M., et al.** 2001. A subfamily of RNA-binding DEAD-box proteins acts as an estrogen receptor alpha coactivator through the N-terminal activation domain (AF-1) with an RNA coactivator, SRA. EMBO J. **20:**1341–1352.
47. **Westermarck, J., et al.** 2002. The DEXD/H-box RNA helicase RHII/Gu is a co-factor for c-Jun-activated transcription. EMBO J. **21:**451–460.
48. **Wilson, B. J., et al.** 2004. The p68 and p72 DEAD box RNA helicases interact with HDAC1 and repress transcription in a promoter-specific manner. BMC Mol. Biol. **5:**11.
49. **Yan, X., J. F. Mouillet, Q. Ou, and Y. Sadovsky.** 2003. A novel domain within the DEAD-box protein DP103 is essential for transcriptional repression and helicase activity. Mol. Cell. Biol. **23:**414–423.
50. **Yao, Z., et al.** 2010. B23 acts as a nucleolar stress sensor and promotes cell survival through its dynamic interaction with hnRNPU and hnRNPA1. Oncogene **29:**1821–1834.
51. **Young, D. W., et al.** 2007. Mitotic occupancy and lineage-specific transcriptional control of rRNA genes by Runx2. Nature **445:**442–446.
52. **Zhai, W., and L. Comai.** 2000. Repression of RNA polymerase I transcription by the tumor suppressor p53. Mol. Cell. Biol. **20:**5930–5938.
53. **Zhou, K., et al.** 2003. RNA helicase A interacts with dsDNA and topoisomerase IIalpha. Nucleic Acids Res. **31:**2253–2260.

Downloaded from http://mcb.asm.org/ on April 16, 2013 by Washington University in St. Louis

Molecular and Cellular Biology

$p19^{ARF}$ and Ras^{V12} Offer Opposing Regulation of DHX33 Translation To Dictate Tumor Cell Fate

Yandong Zhang, Anthony J. Saporita and Jason D. Weber
Mol. Cell. Biol. **2013, 33(8):1594. DOI: 10.1128/MCB.01220-12.**
Published Ahead of Print 11 February 2013.

Updated information and services can be found at:
http://mcb.asm.org/content/33/8/1594

These include:

REFERENCES

This article cites 43 articles, 16 of which can be accessed free at: http://mcb.asm.org/content/33/8/1594#ref-list-1

CONTENT ALERTS

Receive: RSS Feeds, eTOCs, free email alerts (when new articles cite this article), more»

Information about commercial reprint orders: **http://journals.asm.org/site/misc/reprints.xhtml**
To subscribe to to another ASM Journal go to: **http://journals.asm.org/site/subscriptions/**

Journals.ASM.org

Downloaded from http://mcb.asm.org/ on April 16, 2013 by Washington University in St. Louis

MCB
Journals.ASM.org

p19^{ARF} and Ras^{V12} Offer Opposing Regulation of DHX33 Translation To Dictate Tumor Cell Fate

Yandong Zhang, Anthony J. Saporita, Jason D. Weber

BRIGHT Institute and Department of Internal Medicine, Division of Molecular Oncology, Siteman Cancer Center, Washington University School of Medicine, St. Louis, Missouri, USA

DHX33 is a pivotal DEAH-box RNA helicase in the multistep process of RNA polymerase I-directed transcription of the ribosomal DNA locus. We explored the regulation of DHX33 expression by Ras^{V12} and ARF to determine DHX33's role in sensing these opposing signals to regulate ribosome biogenesis. In wild-type primary fibroblasts, Ras^{V12} infection induced a transient increase in DHX33 protein level, as well as an rRNA transcriptional rate that was eventually suppressed by a delayed activation of the ARF/p53 pathway. DHX33 expression was exclusively controlled at the level of translation. ARF caused a dramatic reduction in polysome-associated DHX33 mRNAs, while Ras^{V12} led to a complete shift of existing DHX33 mRNAs to actively translating polysomes. The translation of DHX33 by Ras^{V12} was sensitive to inhibitors of phosphatidylinositol 3-kinase, mTOR, and mitogen-activated protein and was pivotal for enhanced rRNA transcription and enhanced overall cellular protein translation. In addition, DHX33 knockdown abolished Ras^{V12}-induced rRNA transcription and protein translation and prevented both the *in vitro* and *in vivo* transforming properties of oncogenic Ras^{V12}. Our results directly implicate DHX33 as a crucial player in establishing rRNA synthesis rates in the face of Ras^{V12} or ARF signals, adjusting ribosome biogenesis to match the appropriate growth or antigrowth signals.

Cancers frequently harbor genetic mutations that activate oncogenes or inactivate tumor suppressors, leading to uncontrolled cell growth, evasion of apoptosis, and other enhanced cellular properties (1). To accommodate the rapid proliferation of cancer cells, several associated biological activities are also augmented in cancer cells (2). Recently, increasing evidence has shown that cancer cells often increase ribosome production to improve protein translation and cell growth (3–7). Ribosome biogenesis is frequently targeted by activated oncogenes and repressed by tumor suppressors (as reviewed in references 3 and 8). In fact, the link between nucleolar hypertrophy and tumorigenesis was recognized more than 100 years ago (8, 9). More recent data indicate that a marked increase in rRNA synthesis is a general attribute of many cancers (9, 10), which is consistent with the idea that changes in rRNA synthesis may be prerequisite alteration in the progression to cellular transformation. The rate of cancer cell proliferation in tumors is directly proportional to nucleolar size and RNA polymerase I (Pol I) activity, with overexpression of pre-rRNA correlating with poor prognosis in many cancers (10–13).

Ribosome biogenesis largely occurs in the nucleolus and is a highly coordinated biological process that includes rRNA synthesis, modification, processing, and assembly into ribosome subunits (10, 14–16). It is tightly controlled and directly linked to cell cycle events; defects in ribosome biogenesis often lead to apoptosis or cell cycle arrest (17–19). The initial step of ribosome biogenesis, ribosomal DNA (rDNA) transcription, is subject to numerous layers of regulation (20–22). Human rDNA contains >400 copies of the rRNA genes, organized in tandem arrays on five different human chromosomes. Initiation of rDNA transcription requires assembly of a specific multiprotein complex including Pol I and numerous associated proteins (3, 10). Two of these proteins are upstream binding factor (UBF) and the promoter selectivity factor, SL1/TIF-IB. Interaction of these two proteins at rDNA promoter leads to assembly of the preinitiation complex and subsequent transcriptional activation at the promoter (15, 23). Given its extreme importance in initiating ribosome biogenesis, rDNA transcription is greatly influenced by the Ras, Myc, and NPM oncogenes, as well as the ARF, p53, and PTEN tumor suppressors (14, 16, 24–29).

We previously identified the nucleolar DHX33 DEAH-box RNA helicase as an important mediator of RNA Pol I transcription through its interaction with UBF at rDNA loci following serum stimulation (30). In the present study, we explored the mechanism underlying DHX33 regulation. We now report that DHX33 is positioned at the crossroads of opposing Ras and ARF activities; oncogenic Ras^{V12} stimulates but ARF represses translation of existing DHX33 mRNAs. In this manner we show that, DHX33 is used as an endpoint of contrasting signals to set ribosome biogenesis rates. Using xenograft models and established Ras mutant cancer cell lines, we demonstrate that DHX33 accumulation is pivotal for Ras^{V12} to initiate tumor formation.

MATERIALS AND METHODS

Cell culture. Wild-type mouse embryonic fibroblasts (MEFs), $Arf^{-/-}$ ear fibroblasts, $Arf^{-/-}$ MEFs, $p53^{-/-}$ MEFs, $p53^{-/-}$; $Mdm2^{-/-}$ MEFs, and $p53^{-/-}$; $Mdm2^{-/-}$; $Arf^{-/-}$ MEFs were isolated from C57BL/6/Sv129 mixed mice. BxPC-3, Capan-2, Miapaca-2, and Panc-1 pancreatic cancer cell lines were kindly provided by Andrea Wang-Gillam (Washington University), BeaS2B cells were provided by Gregory Longmore (Washington University), and H441 and A549 lung cancer cells were provided by Steven Brody (Washington University). BxPC-3 and H441 cells were

Received 27 November 2012 Returned for modification 2 January 2013
Accepted 3 February 2013
Published ahead of print 11 February 2013
Address correspondence to Jason D. Weber, jweber@dom.wustl.edu.
Copyright © 2013, American Society for Microbiology. All Rights Reserved.
doi:10.1128/MCB.01220-12

Downloaded from http://mcb.asm.org/ on April 16, 2013 by Washington University in St. Louis

grown in RPMI 1640 containing 10% fetal bovine serum (FBS) with antibiotics and supplements (10 mmol of HEPES, 4.5 g of glucose, 2 mmol of L-glutamine, and 1 mmol of sodium pyruvate/liter). A549 cells were grown in F-12 medium supplemented with 10% FBS and 1% penicillin-streptomycin. All other cells were maintained in Dulbecco modified Eagle medium (DMEM) supplemented with 10% FBS and 1% penicillin-streptomycin. All cell lines were incubated at 37°C with 5% CO_2 in a humidified incubator. U0126 and LY294002 were purchased from Sigma. Rapamycin was purchased from LC laboratories.

Western blotting and antibodies. Whole-cell lysates were prepared by incubation with 1× NP-40 buffer that included 0.5% NP-40 and 1% sodium dodecyl sulfate (SDS) supplemented with HALT protease and phosphatase inhibitors (Sigma). Lysates were cleared by centrifugation and protein concentration was tested by DC assay (Bio-Rad). Lysates were boiled with SDS sample buffer, separated by SDS-PAGE, and transferred to polyvinylidene difluoride membrane (Millipore). Membranes were blocked in 5% nonfat dry milk TBS-T buffer (10 mmol of Tris-HCl [pH 7.4]/liter, 150 mmol of NaCl/liter, 0.1% Tween 20) and incubated in primary antibodies diluted in blocking buffer at 4°C overnight. Blots were washed with TBS-T buffer and incubated with horseradish peroxidase-conjugated secondary antibodies (1:10,000; GE Healthcare) in blocking buffer at room temperature. Immune complexes were visualized with an enhanced chemiluminescence kit (GE Healthcare). Primary antibodies for immunodetection were sourced as follows: anti-ARF (rat; Santa Cruz), antitubulin (goat; Santa Cruz), anti-DHX33 (Novus), anti-S6 (Cell Signaling), anti-pS6 (Cell Signaling), anti-NF1 (Santa Cruz), anti-Ras (Santa Cruz), anti-p53 (Cell Signaling), anti-AKT (Cell Signaling), and anti-pS473-AKT (Cell Signaling).

Quantitative reverse transcription-PCR (qRT-PCR). Primers were all designed by Primer Express 2.0 software and purchased from Integrated DNA technologies. Total RNA was extracted by NucleoSpin II (Clontech) RNA isolation kit and was reverse transcribed into cDNA by SuperScript III first-strand synthesis kit (Invitrogen). PCRs were performed on Bio-Rad C1000 thermal cycler and managed with Bio-Rad CFX96 software. For analysis of 47S rRNA transcript levels, SYBR green FastMix (Quanta Biosciences) was used and transcript quantification was performed by comparison with standard curves generated from dilution series of cDNA of human 47S rRNA (cloned in pCR2.1Topo). SYBR green mix from Bio-Rad was used for all other qRT-PCR analysis. Transcript quantification was calculated based on the value of $\Delta\Delta C_T$ after normalization to GAPDH (glyceraldehyde-3-phosphate dehydrogenase) values. Melting curve analysis confirmed that single products were amplified.

Focus assay. Human cancer cell lines were infected by pLKO.1 lentivirus encoding shScrambled RNA or shRNA to knockdown DHX33, and cells were selected by puromycin for 2 days. Cells were then plated at a density of 10^4 per 100-mm dish and grown for 10 to 20 days. Colonies were washed with cold phosphate-buffered saline twice and fixed with 100% methanol for 10 min at room temperature. Colonies were then stained with Giemsa stain for 1 h at room temperature and washed with water before air-dried and photographed.

Soft agar assay. A total of 10^4 cells were mixed in 4.0 ml of 0.3% agar–1× DMEM–10% FBS as the top agar and plated into 60-mm plates with 4.0 ml of 0.6% agar–1× DMEM–10% FBS as the base agar. Plates were incubated at 37°C and checked every 3 days, and the cells were fed with 2.0 ml of 0.3% agar–1× DMEM–10% FBS every week. The colonies were photographed and counted 2 to 3 weeks later.

Polysome profiles. Cells (3×10^6) after transduction with the indicated virus for 96 h were treated with 10 μg of cycloheximide/ml prior to harvesting and counting. Cells were subjected to cytoplasmic ribosome fractionation as described previously using a sucrose density gradient system ranging from 7 to 47% (Teledyne ISCO). Fractions were collected, and RNA was extracted with TRIzol and converted into cDNA with superscript reverse transcriptase III (Invitrogen) before quantitative PCR analysis with the appropriate primers.

[^{3}H]uridine pulse-chase labeling. Cells were first infected with the indicated virus. At 3 days postinfection, the cells were replated at a confluence of 60 to 70% per plate. On the following day, the cells were then pulsed with [^{3}H]uridine at a concentration of 2.5 μCi/ml for 30 min and chased with unradiolabeled uridine at a concentration of 5 mM for the indicated time points. Approximately 2×10^6 cells were pelleted, and the total RNA was isolated after dissolving cells in RNAsolv (Omega Biotek, Norcross, GA). Formaldehyde RNA denaturing gel was run to separate different species of rRNA and then transferred to nylon Hybond+ membrane. After UV cross-linking and spraying with Enhancer (Perkin Elmer), the membrane was exposed to film and subjected to autoradiography.

[^{35}S]methionine incorporation. Cells were starved in cysteine-methionine-free medium for 4 h and then pulsed with [^{35}S]methionine (50 μCi/ml)-containing medium for 30 min before being harvested. The cells were lysed, and supernatants were precipitated with trichloroacetic acid at a concentration of 10%. Protein pellets were subsequently dissolved by 1% SDS and analyzed for protein concentration. The samples were then analyzed for radioactivity by liquid scintillation counting. The data presented were normalized based on equal amount of protein in each sample.

Mouse xenografts. Animals were handled according to protocols approved by the Washington University Animal Studies Committee. Nude mice were purchased from Jackson laboratories. *Arf*-null cells after transduction with the indicated virus were injected subcutaneously with 10^6 cells into the flanks of mice. Tumors were dissected after 2 weeks and photographed.

RESULTS

p19^{ARF} induction during oncogenic stress lowers DHX33 protein levels. ARF is the principal tumor surveillance protein charge with preventing aberrant cell growth and proliferation during oncogenic insult (18, 31). In wild-type primary fibroblasts, oncogenic Ras^{V12} induces ARF protein expression, resulting in subsequent p53 activation and cell cycle arrest. Numerous tumor suppressers and oncogenes are known to influence the levels and activities of key molecules involved in rDNA transcription, suggesting that rRNA transcription might be a focal point of opposing signaling moieties (3). Previously, we have shown that the DHX33 DEAH RNA box helicase is a novel regulator of rRNA transcription (30). To test whether p19^{ARF} and Ras^{V12} could affect DHX33 expression, wild-type (WT) MEFs were infected with either control, Ras^{V12}, or ARF-expressing retroviruses. DHX33 protein levels were analyzed at 2, 3, or 5 days postinfection. As shown, the ectopic expression of ARF resulted in a significant decrease in the DHX33 protein expression 2 days postinfection (Fig. 1A). Reduction of DHX33 by ARF continued through 3 days postinfection, when the DHX33 protein levels decreased 10-fold (Fig. 1B). In contrast, oncogenic stress by Ras^{V12} infection resulted in slightly more DHX33 protein than control cells at 2 and 3 days postinfection (Fig. 1A and B). Noticeably, upregulation of ARF and p53 were only modest at these early time points following ectopic Ras^{V12} expression. However, after 5 days of Ras^{V12} infection, wild-type primary cells expressed significant levels of ARF with a resultant decrease in DHX33 protein (2-fold reduction) compared to control cells (Fig. 1C). These results indicate that two major pathways might regulate DHX33: ARF/p53 and oncogenic Ras^{V12}. The opposing activities from these two pathways caused DHX33 levels to be transiently increased and then significantly decreased. In accordance with this hypothesis, Ras^{V12} infection of fibroblasts deficient in ARF (*Arf*-null MEFs) resulted in a robust increase in DHX33 levels from 2 days until 6 days postinfection (Fig. 1D). This is in contrast to a 2-fold reduction of DHX33 in WT MEFs in

Downloaded from http://mcb.asm.org/ on April 16, 2013 by Washington University in St. Louis

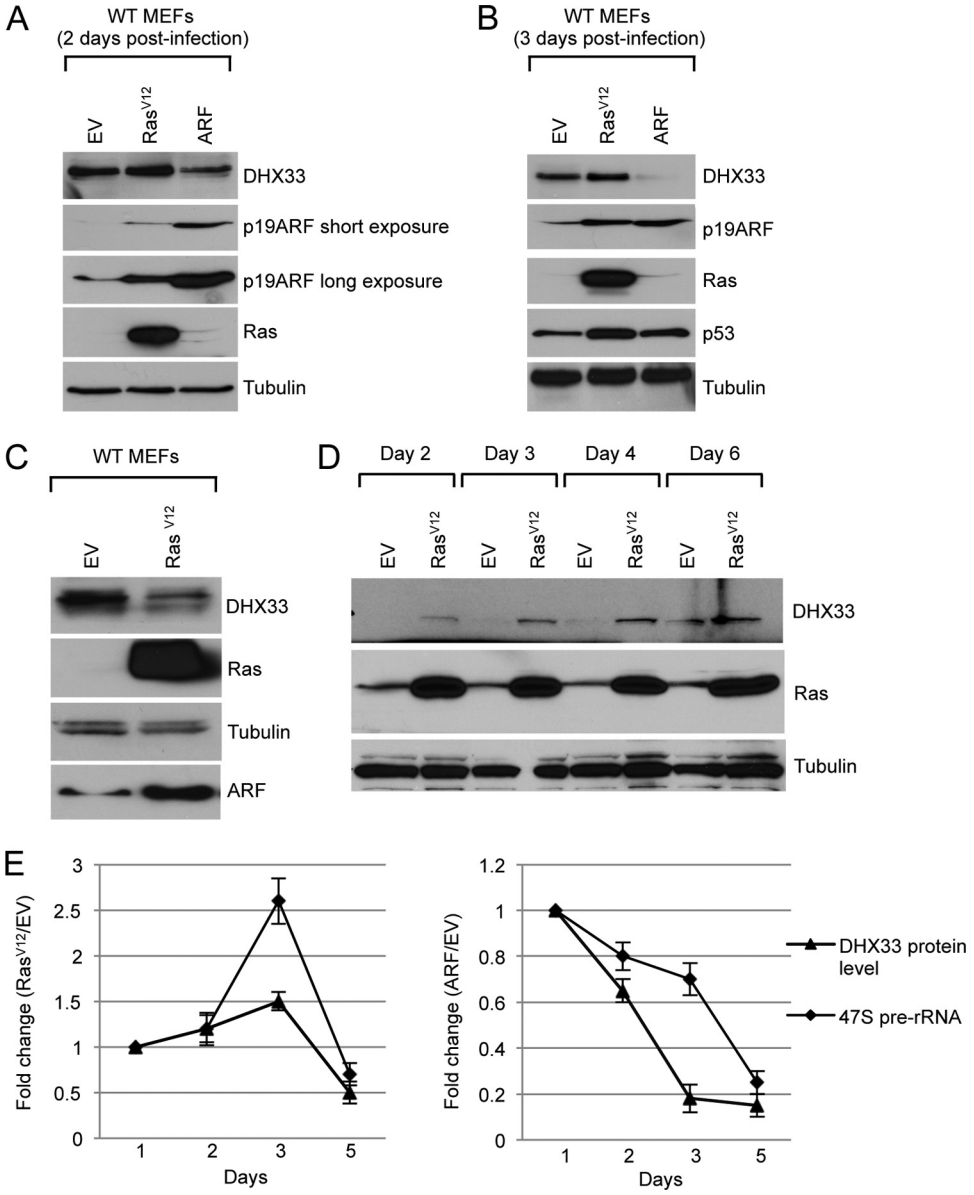

FIG 1 Regulation of DHX33 during oncogenic stress. (A) Wild-type MEFs were infected with retroviruses encoding Ras^{V12}, $p19^{ARF}$, or empty vector, whole-cell lysates were prepared at 2 days postinfection and were subjected to Western blot analysis with the indicated antibodies. (B) The above-mentioned cells were harvested 3 days postinfection, and whole-cell extracts were subjected to Western blot analysis with the indicated antibodies. (C) Wild-type MEFs were infected with retroviruses encoding Ras^{V12} or empty vector, whole-cell extracts were prepared 5 days postinfection and were subjected to Western blot analysis with the indicated antibodies. (D) *Arf*-null MEFs were infected with retroviruses encoding Ras^{V12} or empty vector, whole-cell extracts were prepared from 2 days till 6 days postinfection and were subjected to Western blot analysis with the indicated antibodies. (E) Wild-type MEFs were infected with the above-mentioned retroviruses, and total RNA was extracted at 2, 3, or 5 days postinfection. Mouse 47S pre-rRNA levels were analyzed by real-time PCR and graphed in a time-dependent manner. Changes in DHX33 protein levels in the time course were also graphed after quantitation of DHX33 signals in panels A to C after normalization to the empty vector control. Error bars were taken from three independent experiments.

which endogenous ARF function is intact and induced during Ras^{V12} infection. Thus, our results indicate that endogenous ARF is a key regulator of DHX33 expression during oncogenic stress.

We next performed quantitative real-time PCR (qRT-PCR) to determine ribosome RNA transcriptional rates by analyzing 47S pre-rRNA transcript levels in both Ras^{V12} and ARF-infected wild-type MEFs. As shown in Fig. 1E, ARF infection resulted in the downregulation of rRNA transcription in a time-dependent manner. At 5 days postinfection, 47S rRNA levels dropped to 30% of that in the control sample. Moreover, Ras^{V12} infection first resulted in a transient increase in pre-rRNA synthesis at 2 and 3 days postinfection (up to 2.5-fold), but after 5 days postinfection, after endogenous ARF induction, the pre-rRNA levels dropped to 70% of empty vector control (Fig. 1E). This trend is in agreement with the increase in DHX33 followed by its decrease over time after Ras^{V12} infection.

ARF regulation of DHX33 is dependent on Mdm2 and p53. The ARF tumor suppresser has p53-dependent and -independent

Downloaded from http://mcb.asm.org/ on April 16, 2013 by Washington University in St. Louis

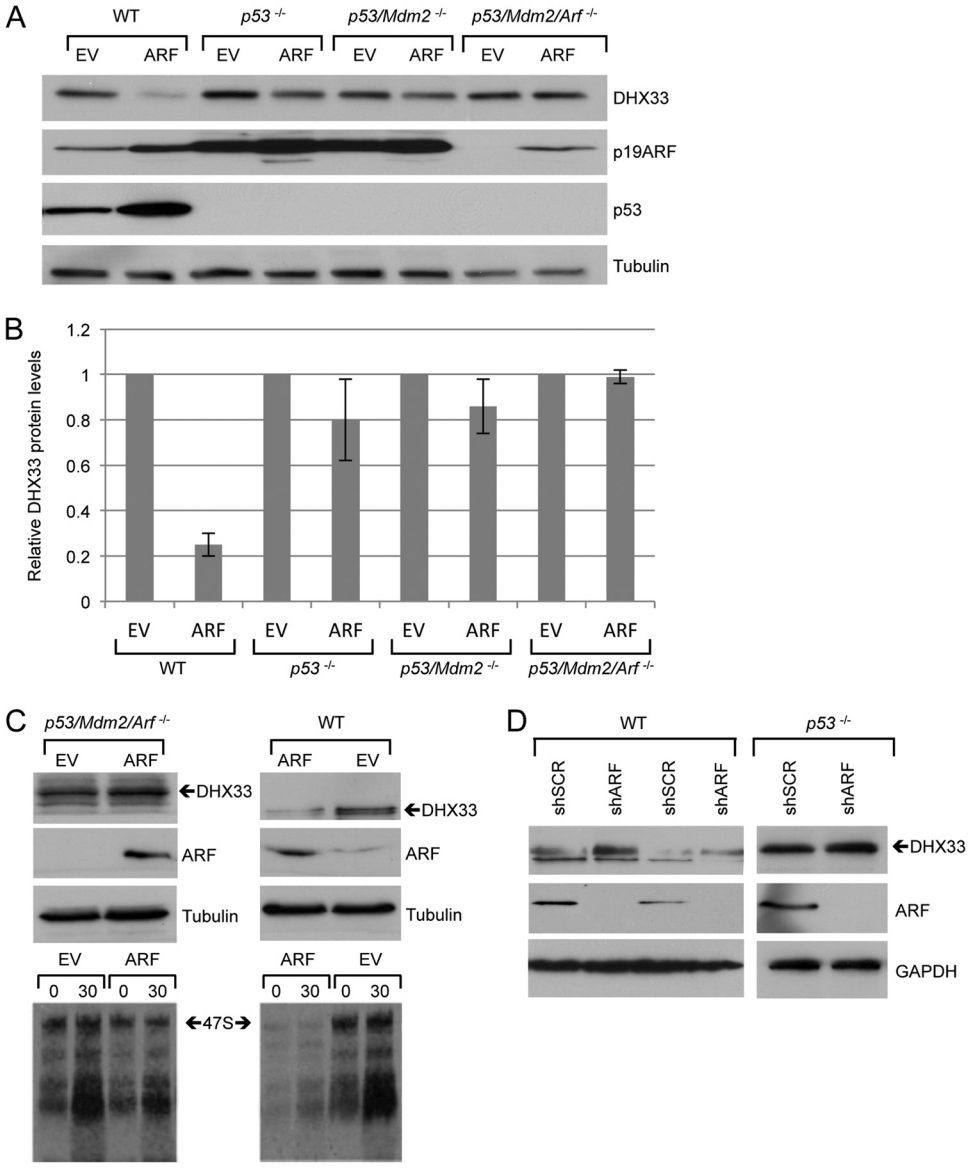

FIG 2 Reduction of DHX33 by ARF infection is dependent on p53 and Mdm2. (A) Wild-type MEFs, *p53*-null MEFs, $p53^{-/-}$; $Mdm2^{-/-}$ MEFs, and $p53^{-/-}$; $Mdm2^{-/-}$; $Arf^{-/-}$ MEFs were infected with retroviruses encoding either pBABE empty vector or pBABE-HA-ARF. Whole-cell lysates were prepared 5 days postinfection and were subjected to Western blot analysis by the indicated antibodies. (B) Quantitation of the DHX33 protein levels after normalization to empty vector in each group, error bars were taken from three independent experiments. (C) MEFs were infected by retrovirus encoding pBABE empty vector or pBABE-HA-ARF. At 4 days postinfection, cells were harvested and analyzed by Western blotting with the indicated antibodies. At 4 days postinfection, cells were also pulsed by [^{3}H]uridine and chased at the indicated time points. Total RNA were analyzed for 47S pre-rRNA levels. (D) WT MEFs or *p53*-null MEFs were infected with lentivirus encoding either shSCR or shARF. At 4 days postinfection, the cells were harvested and subjected to Western blot analysis with the indicated antibodies.

functions (32). Wild-type MEFs maintain an intact p53 pathway downstream of ARF, suggesting that regulation of DHX33 by ARF in WT MEFs could be p53 dependent. To study whether this regulation occurs in a p53-dependent manner, we infected $p53^{-/-}$ MEFs, $p53^{-/-}$; $Mdm2^{-/-}$ (DKO) MEFs, and $p53^{-/-}$; $Mdm2^{-/-}$; $Arf^{-/-}$ (TKO) MEFs with ARF-expressing retroviruses. As shown in Fig. 2, ARF overexpression in WT MEFs resulted in a significant reduction in DHX33 levels. However, the reduction of DHX33 was far less significant in *p53*-null MEFs and DKO MEFs. In TKO MEFs, we observed no reduction in DHX33 protein levels, indicating that reduction of DHX33 by ARF requires p53 (Fig. 2B). In addition, we found that the infection of ARF in wild-type MEFs resulted in a much greater inhibition of ribosome RNA synthesis than in TKO MEFs (Fig. 2C). Our results indicate that ARF inhibits ribosome biogenesis not only in a p53-independent manner but also in a p53-dependent manner. Knockdown of endogenous ARF only mildly enhanced DHX33 protein expression in $p53^{-/-}$ MEFs (Fig. 2D), suggesting that p53 is required for DHX33 induction following loss of ARF.

ARF reduces DHX33 protein levels through a translational control mechanism. To dissect the mechanism of DHX33 reduction by ARF, we first analyzed DHX33 mRNA levels. qRT-PCR

Downloaded from http://mcb.asm.org/ on April 16, 2013 by Washington University in St. Louis

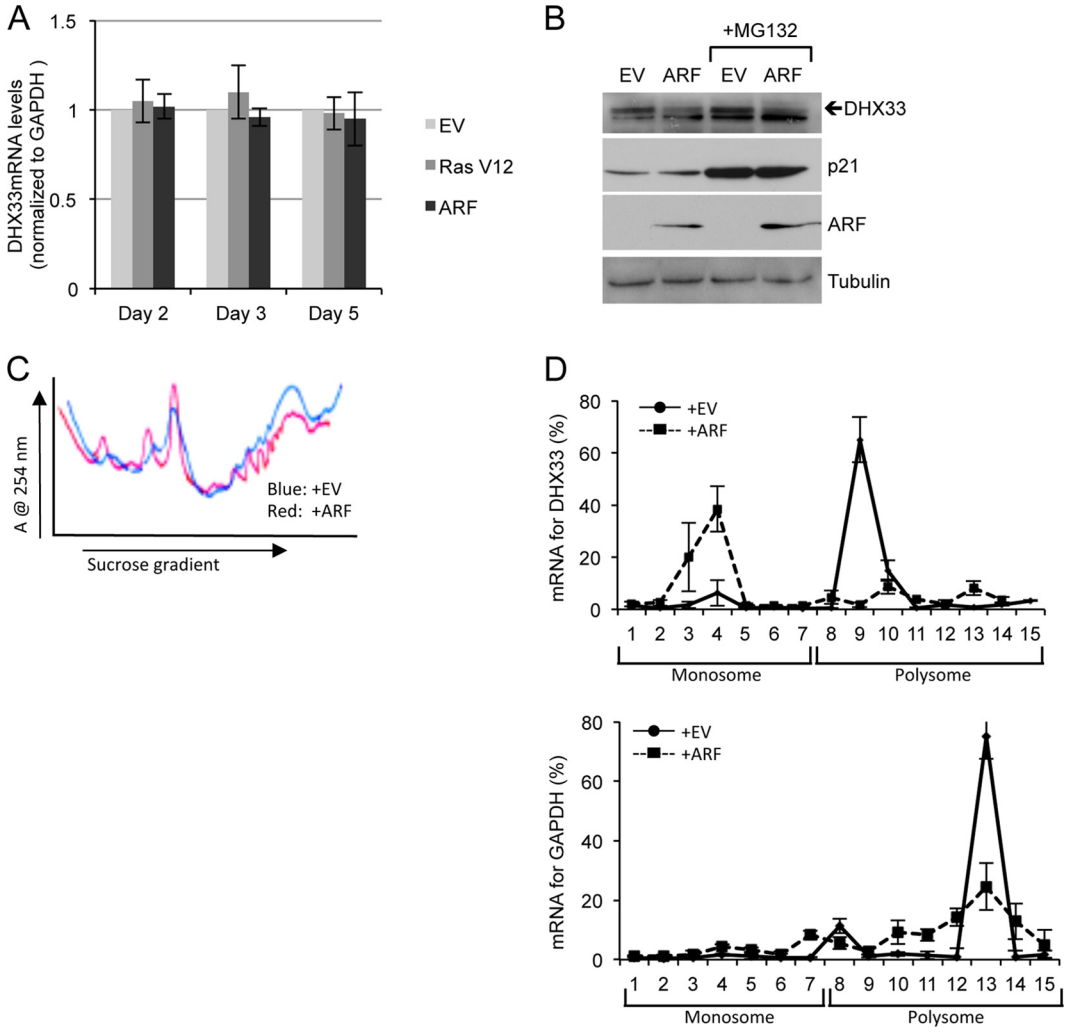

FIG 3 Induction of ARF inhibits DHX33 translation. (A) Wild-type MEFs were infected with retroviruses encoding empty vector, $p19^{ARF}$, or Ras^{V12}, and the total RNA was extracted from each sample at 2, 3, or 5 days postinfection. DHX33 mRNA levels were analyzed by qPCR with GAPDH as an internal control. Bars represent the standard deviation taken from three separate experiments. (B) Wild-type MEFs were infected with retroviruses encoding empty vector (EV) or $p19^{ARF}$. At 3 days postinfection, the cells were treated with 50 μM MG132 for 6 h, and total cell lysates were prepared and subjected to Western blot analysis with the indicated antibodies. p21 protein stabilization was used as a positive control to monitor MG132 function. (C) A total of 1.5×10^6 wild-type cells infected with retroviruses encoding empty vector or $p19^{ARF}$ at 3 days postinfection were subjected to cytosolic polysome fractionation. The absorbance was monitored at 254 nm, and resultant ribosome profiles are shown for each sample. (D) The above-mentioned fractions from monoribosomes or polysomes were subjected to total RNA isolation and qPCR analysis to detect DHX33 mRNA levels. GAPDH mRNA levels were used as a control. The data presented are the percentages of mRNA from each fraction calculated from a standard curve generated by a series of diluted DHX33 plasmid. Error bars were taken from two independent experiments.

was performed on total RNAs isolated from ARF- and Ras^{V12}-infected cells at 2, 3, and 5 days postinfection. Both GAPDH mRNA and actin mRNAs were used as internal controls. We observed no significant change in DHX33 mRNA expression at each time point after ARF or Ras^{V12} infection of WT MEFs compared to the empty vector control (Fig. 3A). These results indicate that reduction of DHX33 by ARF does not occur by transcriptional regulation. ARF has been previously shown to influence the stability of several proteins (33, 34). To determine whether DHX33 protein reduction was due to accelerated protein degradation upon ARF induction, cells were treated with MG132, a 26S proteasome inhibitor, for 6 h. As shown in Fig. 3B, we found that DHX33 was not stabilized in the presence of MG132. As a positive control, $p21^{CIP1}$ was stabilized to a significant degree with MG132 treatment, demonstrating that MG132 is functioning as expected to inhibit 26S proteasome. These results imply that reduction of DHX33 in the presence of ARF is not due to accelerated protein degradation.

To determine whether DHX33 reduction was due to translational repression of existing DHX33 mRNAs, we chose to analyze polysome-associated DHX33 mRNAs. We performed a polysome fractionation by sucrose gradient after lysis of WT MEFs that were either transduced with vector control or ARF overexpressing retroviruses (Fig. 3C). We analyzed the mRNA distribution of DHX33 in monosome and polysome fraction by qRT-PCR. As shown in Fig. 3D, we found that in ARF-infected WT MEFs, a large portion of DHX33 mRNAs (up to 60% of total mRNA) had moved into the monoribosome fractions. Conversely, empty vector-infected WT MEFs exhibited a majority of their DHX33 mRNAs associated with polysomes (70%). These data clearly in-

Downloaded from http://mcb.asm.org/ on April 16, 2013 by Washington University in St. Louis

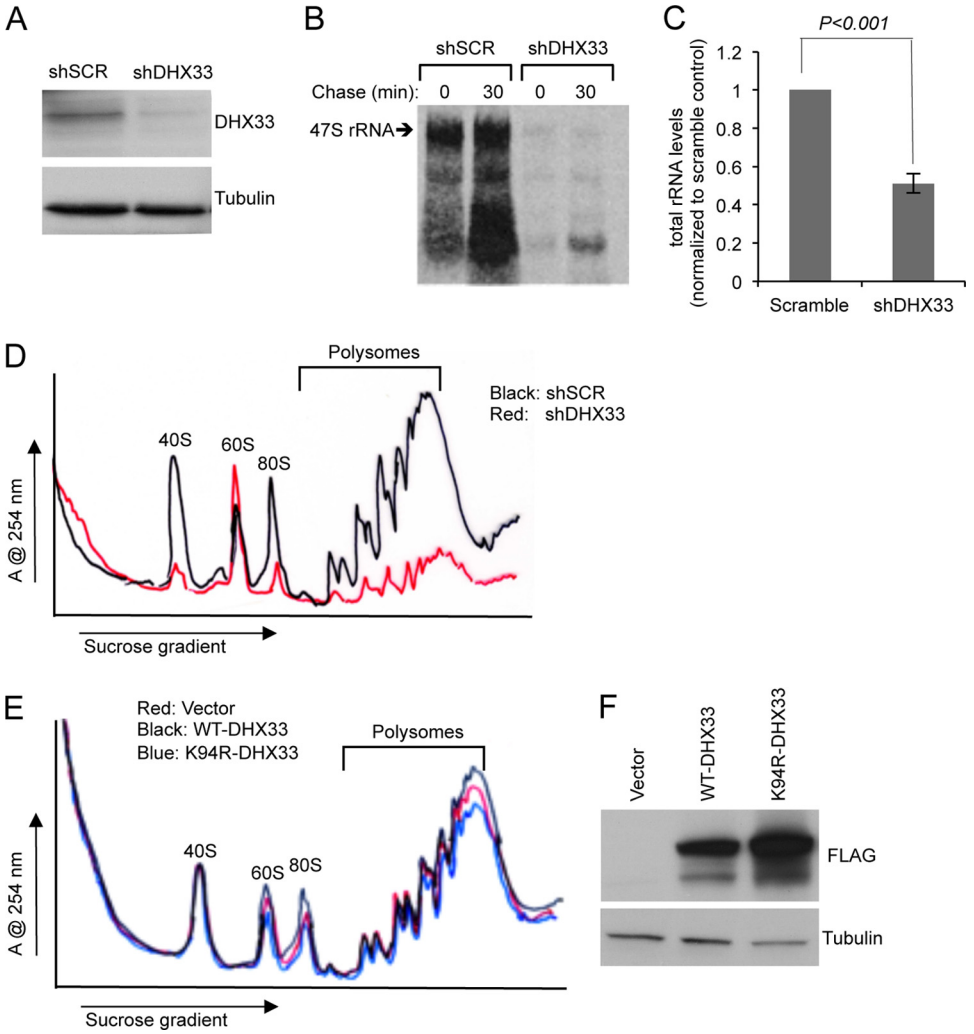

FIG 4 DHX33 protein knockdown or overexpression influences ribosome biogenesis and protein translation. (A) *Arf/p53/Mdm2*$^{-/-}$ MEFs were infected by lentivirus encoding shRNA-DHX33 or shScrambled (shSCR). At 3 days after infection, the cell lysates were subjected to Western blot analysis with anti-DHX33 and tubulin antibodies. (B) Infected cells from above were pulsed with [^{3}H]uridine and chased for the indicated time points to monitor newly synthesized rRNA. Equal numbers of cells were pelleted for total RNA extraction. RNA was separated and transferred onto nylon membranes for autoradiography. (C) Equal numbers of the above-mentioned cells were subjected to total RNA isolation and then isolated by formaldehyde RNA denaturing gel. 28S and 18S rRNA were visualized by ethidium bromide staining and quantified. Bars were taken from three different experiments. (D) Equal numbers of *Arf/p53/Mdm2*$^{-/-}$ MEFs infected by the indicated short-hairpin lentiviruses were subjected to cytosolic ribosome profile analysis at 4 days postinfection. (E and F) *Arf/p53/Mdm2*$^{-/-}$ MEFs were infected with lentiviruses encoding empty vector, DHX33 (wild type) or mutant DHX33 (K94R). At 4 days postinfection, infected cells were subjected to cytosolic polysome profile analysis (E) and Western blot analysis with the indicated antibodies (F).

dicate that ARF induction causes a translational repression of DHX33 in the cytoplasm.

DHX33 protein reduction decreases protein translation, while DHX33 overexpression enhances protein translation. Our previous data has shown that DHX33 is an important regulator of rRNA transcription; DHX33 knockdown reduced rRNA production, while DHX33 overexpression enhanced rRNA synthesis (30). In TKO MEFs, we manipulated DHX33 levels by utilizing lentivirus infection to knockdown (Fig. 4A) or overexpress (Fig. 4E) DHX33 protein. As shown in Fig. 4B, knockdown of DHX33 nearly abolished all rRNA production. Since rRNA is the key component for ribosome assembly, we hypothesized that DHX33 knockdown should result in less available ribosomes and thus decrease overall protein translation. mRNAs undergoing active translation are bound to multiple ribosomes, forming polysomes. The level of polysomes is widely regarded as an indicator of overall protein translational activity. Therefore, we performed cytosolic ribosome fractionation using sucrose gradients to monitor polysome levels. Strikingly, we noted a significant reduction of polysomes in TKO MEFs infected with DHX33 knockdown lentiviruses (Fig. 4D). The cytosolic 40S and 80S ribosomes were also decreased dramatically. Interestingly, the 60S ribosome peak was enhanced, indicating a different dynamic regulation of 40S and 60S, even though all of the rRNA species were decreased significantly (Fig. 4C).

Previously, we have found that wild-type DHX33 overexpression enhanced rRNA synthesis, while helicase-defective mutant of DHX33 (K94R) inhibited it (30). To determine the effect of DHX33 overexpression on cell growth, we transduced wild-type DHX33 and helicase-dead K94R mutant of DHX33 in TKO MEFs

Downloaded from http://mcb.asm.org/ on April 16, 2013 by Washington University in St. Louis

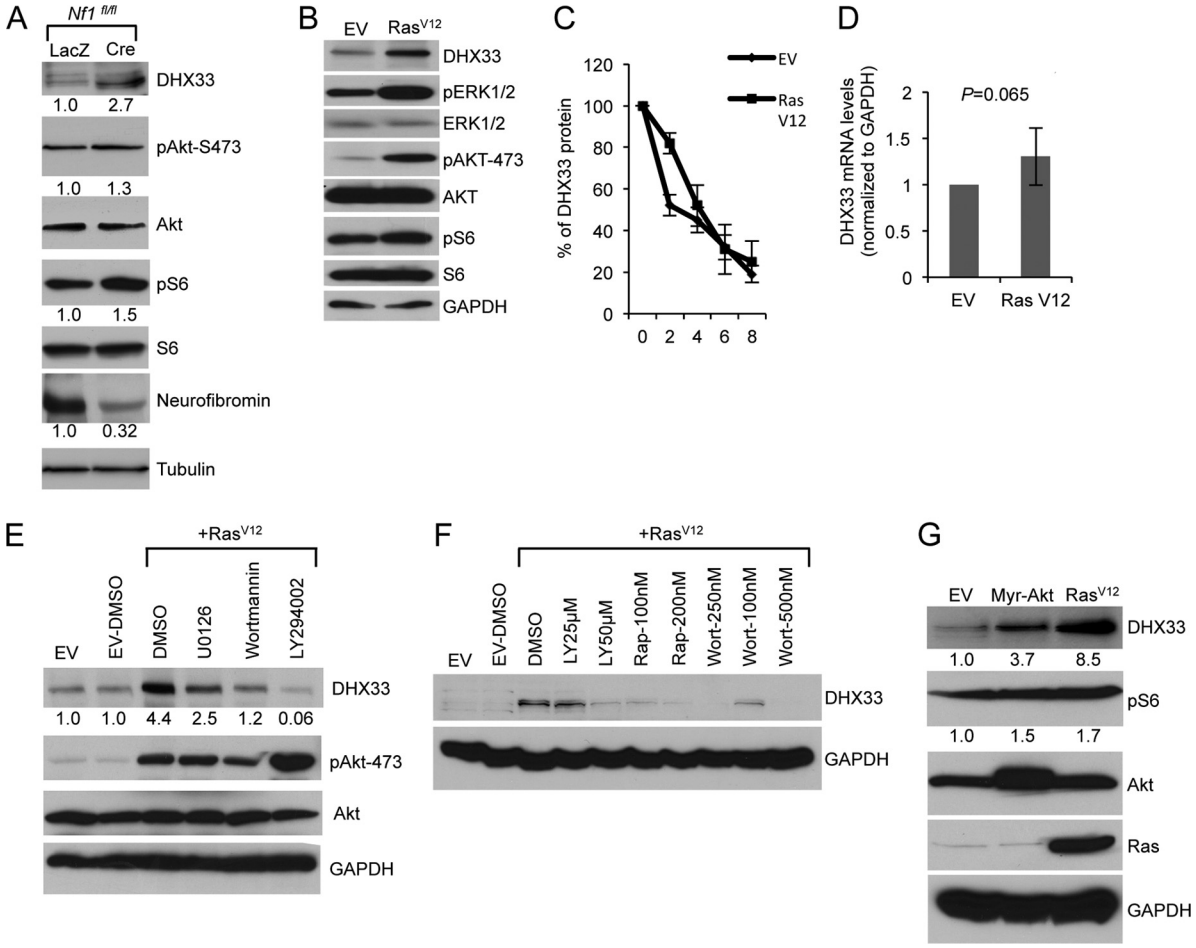

FIG 5 Ras activity induces DHX33 protein expression. (A) *Nf1*$^{fl/fl}$ MEFs were infected with adenoviruses encoding either LacZ or Cre recombinase at a multiplicity of infection of 200. At 2 days postinfection, the cells were then serum starved for 72 h. Equal amount of cell lysates were subjected to Western blot analysis with the indicated antibodies. (B) *Arf*-null ear fibroblasts from 2-month-old mice were infected with retroviruses encoding either pBABE empty vector (EV) or pBABE-Ras^{V12}. At 3 days postinfection, infected cells were subjected to Western blot analysis with the indicated antibodies. (C) The above-mentioned cells were treated with cycloheximide at a concentration of 80 μg/ml for the indicated times. Protein extracts from the cells pelleted from the indicated time points was subjected to Western blot analysis. Signals of DHX33 protein was graphed after normalization to GAPDH control. Bars represent errors from two independent experiments. (D) Total RNA was isolated from the above-mentioned cells and changes of DHX33 mRNA levels were analyzed by qPCR with GAPDH as a control. *P* is derived from five separate experiments. (E) *Arf*-null ear fibroblasts were infected with empty vector or Ras^{V12}. At 3 days postinfection, the cells were treated with U0126 (20 μM), wortmannin (100 nM), or LY294002 (50 μM) for 24 h. Cell lysates were subjected to Western blot analysis with the indicated antibodies. (F) *Arf*-null cells infected with empty vector or Ras^{V12} were treated with rapamycin, wortmannin, or LY294002 as indicated for 24 h. Cell lysates were prepared and analyzed for DHX33 protein levels with GAPDH as a loading control. (G) *Arf*-null MEFs were infected with retroviruses encoding myristoylated Akt (Myr-Akt), Ras^{V12}, or empty vector. Cell lysates were prepared at 4 days postinfection after puromycin selection and analyzed by Western blotting for DHX33, pAkt-473, Akt, and GAPDH protein levels. The fold change is indicated below identified blots.

by lentivirus infection. Wild-type DHX33 only slightly enhanced 80S formation and polysome formation, whereas the K94R DHX33 mutant resulted in decreased levels of polysomes (Fig. 4E). This suggests that DHX33 is important for translation, but its overexpression might not be sufficient to significantly enhance protein synthesis. Western blot analysis showed levels of overexpressed wild-type and K94R mutant DHX33 (Fig. 4F).

Ras^{V12} stimulates DHX33 mRNA translation. We previously showed that Ras^{V12} expression caused a significant increase in DHX33 protein expression in *Arf*-null MEFs, implying that Ras hyperactivation regulates DHX33 levels in the absence of *Arf*. The neurofibromin (*Nf1* gene) tumor suppressor protein is an upstream regulator of Ras signaling; loss of *Nf1* results in irreversible activation of Ras and results in subsequent heightened growth and proliferation *in vitro* and *in vivo* tumor formation (35–37). We isolated MEFs from *Nf1*$^{fl/fl}$ mice and used adenovirus to overexpress Cre recombinase, resulting in the successful deletion of *Nf1* alleles (Fig. 5A). Compared to the control Lac Z adenovirus-infected *Nf1*$^{fl/fl}$ MEFs, we found that DHX33 was upregulated 2.7-fold following *Nf1* loss (Fig. 5A). As a confirmation for the activation of Ras signaling, we also detected increased levels of phospho-S6 and phospho-AKT (Fig. 5A).

In order to dissect the mechanism of DHX33 induction by Ras signaling, we first confirmed the activation of several conserved signaling events downstream of Ras. As shown in Fig. 5B, Ras^{V12} expression in *Arf*-null cells induced activation of the mitogen-activated protein kinase (MAPK) pathway as indicated by increased phospho-ERK1/2 and activation of phosphatidylinositol

Downloaded from http://mcb.asm.org/ on April 16, 2013 by Washington University in St. Louis

3-kinase (PI3K)/AKT pathway as indicated by phospho-AKT-S473, as well as activation of mTOR pathway by increased phospho-S6. To check whether upregulation of DHX33 in this setting was due to protein stability or mRNA level changes, we performed protein half-life assays. As shown in Fig. 5C, there was no significant change in DHX33 stability in empty vector or Ras^{V12}-transduced cells. Next, we analyzed mRNA levels of DHX33 by RT-PCR and found no significant change in DHX33 mRNA in Ras^{V12}-infected cells (Fig. 5D). To dissect the mechanism of DHX33 induction by Ras, we treated Ras^{V12}-infected *Arf*-null cells with PI3K/AKT or MAPK pathway inhibitors. Upregulation of DHX33 was completely abolished by the PI3K pathway inhibitors wortmannin and LY294002 but only partially by MEK inhibitor U0126 (Fig. 5E), demonstrating that Ras/PI3K is the main signaling pathway that regulates DHX33 protein induction. To determine whether DHX33 upregulation was controlled by mTOR activation, we treated cells with rapamycin. As shown in Fig. 5F, rapamycin inhibited the induction of DHX33 in a dose-dependent manner to a similar extent as wortmannin and LY294002, indicating that the Ras/PI3K/mTOR pathway is primarily responsible for upregulating DHX33 translation. To further confirm these results, we infected *Arf*-null MEFs with a constitutively active myristoylated Akt (Myr-Akt) retrovirus and found that activation of Akt alone was able to induce DHX33 protein levels but not to the levels seen in Ras^{V12}-infected cells (Fig. 5G).

We also analyzed DHX33 mRNA distribution on polysomes. As expected, Ras^{V12} infection significantly enhanced production of cytosolic ribosomes and polysome formation (Fig. 6A). Approximately 70% of DHX33 mRNA was not associated with polysomes in *Arf*-null cells (Fig. 6B). In contrast, a majority (75%) of DHX33 mRNAs associated with polysomes in *Arf*-null cells that were infected with Ras^{V12} retroviruses (Fig. 6B). As a control, GAPDH mRNA distribution was also analysis and showed no significant difference between empty vector and Ras^{V12} infection (Fig. 6B). This significant difference shows that DHX33 mRNAs are selectively translated upon Ras^{V12} infection in the absence of *Arf*. To confirm that the Ras/PI3K/mTOR pathway indeed translationally regulates DHX33, we further treated the cells with rapamycin and analyzed DHX33 mRNA distribution on polysomes. As shown in Fig. 6C and D, rapamycin treatment resulted in a reduction of DHX33 protein levels and global protein translational repression. A significant proportion of DHX33 mRNA was shifted from polysomes to monoribosomes following rapamycin treatment (Fig. 6E).

DHX33 upregulation is required for enhanced rRNA transcription during Ras activation. We have previously reported that DHX33 is an important factor in rRNA transcription (30). We hypothesized that elevated levels of DHX33 during Ras activation are important for Ras to promote rRNA synthesis. To test this hypothesis, we first detected pre-rRNA transcript levels by qRT-PCR in both empty vector and Ras^{V12}-infected *Arf*-null cells and saw a 2- to 3-fold increase in 47S rRNA levels (Fig. 7A). To test whether DHX33 was required for this observed increase in pre-rRNA levels, *Arf*-null fibroblasts were first infected with Ras^{V12} retroviruses, followed by a second infection with lentiviruses expressing knockdown shRNAs for DHX33 (Fig. 7B). We performed pulse-chase labeling with [^{3}H]uridine to detect ongoing rRNA synthesis. We found that reduction in DHX33 resulted in significantly lower 47S rRNA transcript levels that mirrored those seen in uninfected *Arf*-null cells (Fig. 7C). We also measured global protein synthesis by [^{35}S]methionine incorporation into newly synthesized proteins for Ras^{V12} transformed *Arf*-nulls cells after DHX33 knockdown and found that DHX33 knockdown caused a significant reduction in protein synthesis (Fig. 7D).

DHX33 is required in Ras^{V12}-initiated tumor formation. Given that we have shown a requirement for DHX33 in Ras^{V12}-initiated 47S rRNA transcription, we next sought to determine the contribution of DHX33 to Ras^{V12}-driven cellular transformation. *Arf*-null MEFs infected with Ras^{V12} retroviruses were subjected to a second infection with shSCR or shDHX33 lentiviruses. DHX33 protein knockdown efficiency was analyzed by Western blotting (Fig. 8A). Importantly, DHX33 knockdown did not reduce DHX33 levels below those seen in control cells (Fig. 8A, lanes 1 and 4). After DHX33 knockdown, cells were plated in soft agar and grown for 2 weeks and resultant transformed cell colonies were counted. We observed a significant decrease in soft agar colonies in Ras^{V12}+shDHX33-infected cells, underscoring the importance of heightened DHX33 expression in Ras^{V12}-mediated cellular transformation (Fig. 8B). We next determined whether DHX33 knockdown influenced Ras^{V12}-initiated mRNA translation. Again, *Arf*-null MEFs were infected with Ras^{V12} retroviruses and subjected to a second infection with lentiviruses encoding shRNAs for DHX33. Western blot analysis confirmed successful overexpression of Ras^{V12} and knockdown of DHX33 (Fig. 8C). We measured significant decreases in cytosolic ribosome subunits and actively translating polysomes in the Ras^{V12}+shDHX33 cells (Fig. 8D), indicating that elevated DHX33 expression is required for enhanced ribosome production and mRNA translation following ectopic Ras^{V12} expression. To assess the impact of DHX33 knockdown on Ras^{V12}-initiated tumor formation, we injected 10^6-infected cells into the flanks of immunocompromised mice. At 2 weeks postinjection, we detected significant tumor cell growth of the cells infected with Ras^{V12}+shSCR, while cells infected with Ras^{V12}+shDHX33 did not exhibit any measurable tumor formation (Fig. 8E). This striking difference indicates that DHX33 is a crucial target of oncogenic Ras^{V12} and is required to enhance Ras^{V12}-mediated cell growth and tumor formation.

Correlation between DHX33 protein levels, 47S rRNA levels, and cell proliferation in K-Ras mutated human cancer cell lines. Ras gene mutation has been frequently observed in human cancers (23). To determine whether endogenous DHX33 is upregulated in human cancers harboring mutant Ras alleles, we performed Western blot analysis for endogenous DHX33 protein levels on a panel of human cancer cell lines. As shown in Fig. 9A, we found elevated DHX33 protein levels in three of five K-Ras mutant cancer cell lines using wild-type K-Ras cell lines as a comparison. DHX33 protein levels were significantly upregulated in Miapaca-2, PANC-1, and A549 cells compared to wild-type K-Ras human cancer cell line, BxPC-3 or normal immortalized human lung epithelial cell line, BeaS-2B (Fig. 9A). Due to the pivotal role of DHX33 in rRNA transcription, we also measured 47S rRNA levels by qRT-PCR in a panel of K-Ras mutated cancer cell lines. We discovered that 47S rRNA transcript levels correlated with DHX33 protein levels (Fig. 9B). For example, 47S rRNA transcript levels were the highest in Miapaca-2 cells, where DHX33 protein level was also the highest. Although in Capan-2, where DHX33 levels were the lowest, 47S rRNA level were also the lowest (Fig. 9B). Moreover, we also noticed that cell proliferation rates were tightly correlated with DHX33 protein levels and 47S rRNA levels in these K-Ras mutated human cancer cell lines (Fig. 9C).

Downloaded from http://mcb.asm.org/ on April 16, 2013 by Washington University in St. Louis

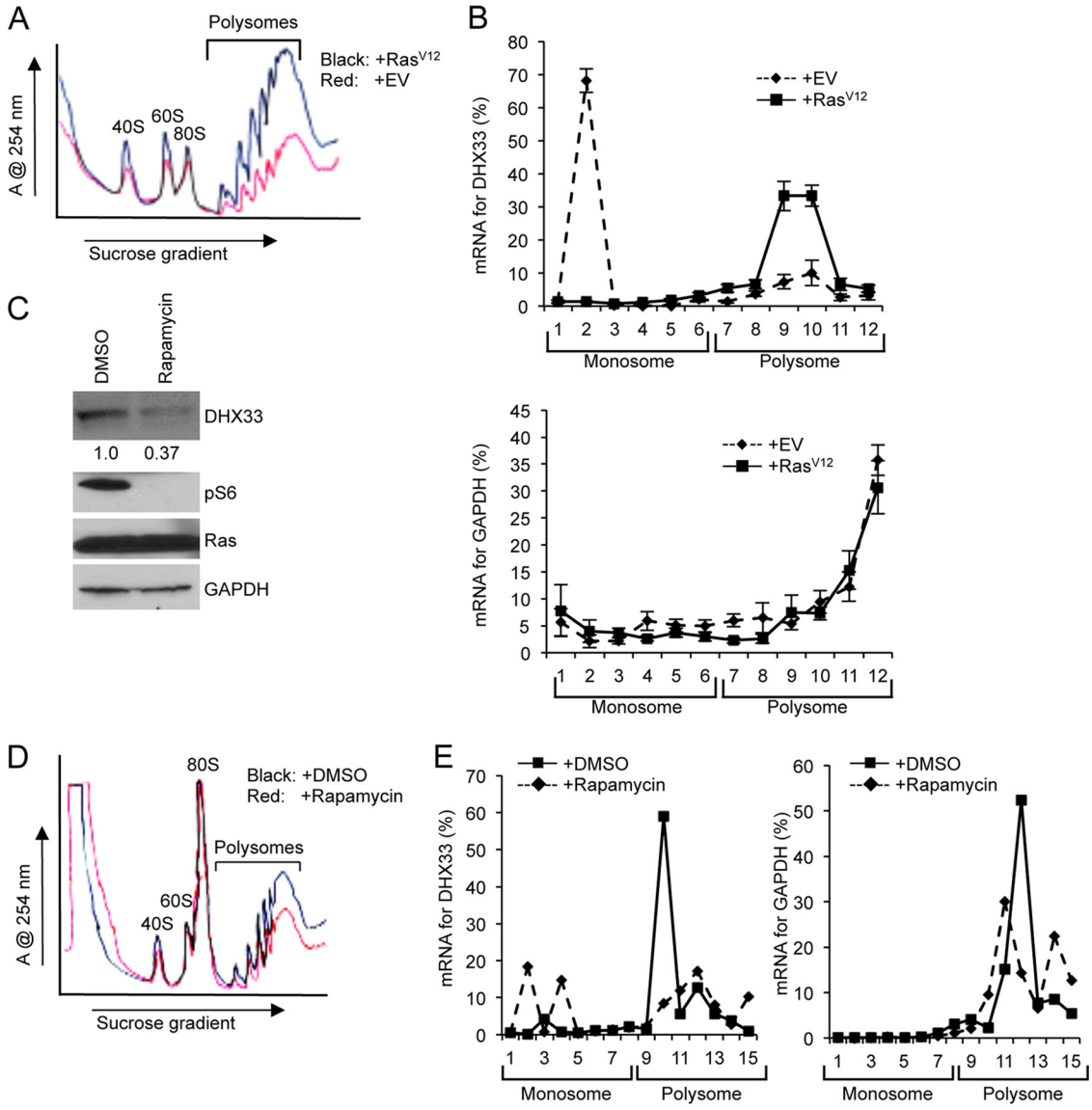

FIG 6 DHX33 protein induction is under translational control. (A) A total of 3×10^6 *Arf*-null cells infected with retroviruses encoding empty vector or Ras^{V12} at 4 days postinfection were subjected to cytosolic ribosome profiling. (B) The resultant fractionations from above were analyzed by RT-PCR for DHX33 mRNA distribution on ribosomes. GAPDH was used as a negative control. Bar data were taken from three independent experiments. (C) Ras^{V12}-infected *Arf*-null cells at 4 days postinfection were treated with rapamycin at 100 nM for 24 h. Whole-cell extracts were then subjected to total protein analysis by Western blotting with the indicated antibodies. The fold change is indicated underneath the blots. (D) A total of 3×10^6 of Ras^{V12}-infected *Arf*-null cells after rapamycin treatment (100 nM) were subjected to cytosolic ribosome profiling. (E) The resultant fractions from above were analyzed by RT-PCR for DHX33 mRNA distribution on ribosomes. GAPDH was used as a negative control. The data represents a typical result from three independent experiments.

To study the importance of DHX33 protein upregulation in K-Ras mutated human cancer cells, we utilized two unique shRNAs to knock down endogenous human DHX33 protein levels and measured cell growth over time. The knockdown efficiency of DHX33 for all five different cancer cell lines is shown in Fig. 9D. All cells exhibited some dependency on DHX33 for sustained proliferation (Fig. 9E). However, the negative impact of DHX33 on long-term proliferation was the most dramatic in the highly proliferative Miapaca-2 and A549 cells. The p53 mutational status might influence the different outcomes we observed for DHX33 knockdown. DHX33 knockdown in Miapaca-2 (mutant p53) resulted in significant cell death, while in p53 wild-type A549 cells, DHX33 knockdown resulted in a G_2/M arrest (Fig. 9F). Taken together, our results show that elevated DHX33 protein expression in mutant K-Ras cancer cell lines is pivotal in enhancing rRNA transcription and proliferation.

DISCUSSION

Ras is one of the most frequently mutated oncogenes in human cancers. Three members of the Ras family, sharing 85% primary sequence identity, have been found to be activated in human cancers: H-Ras, N-Ras, and K-Ras (25). Up to 30% of human lung cancers harbor K-Ras mutations and, in pancreatic cancers, the K-Ras mutation rate is >90% (25). Ras signaling is a complex

Downloaded from http://mcb.asm.org/ on April 16, 2013 by Washington University in St. Louis

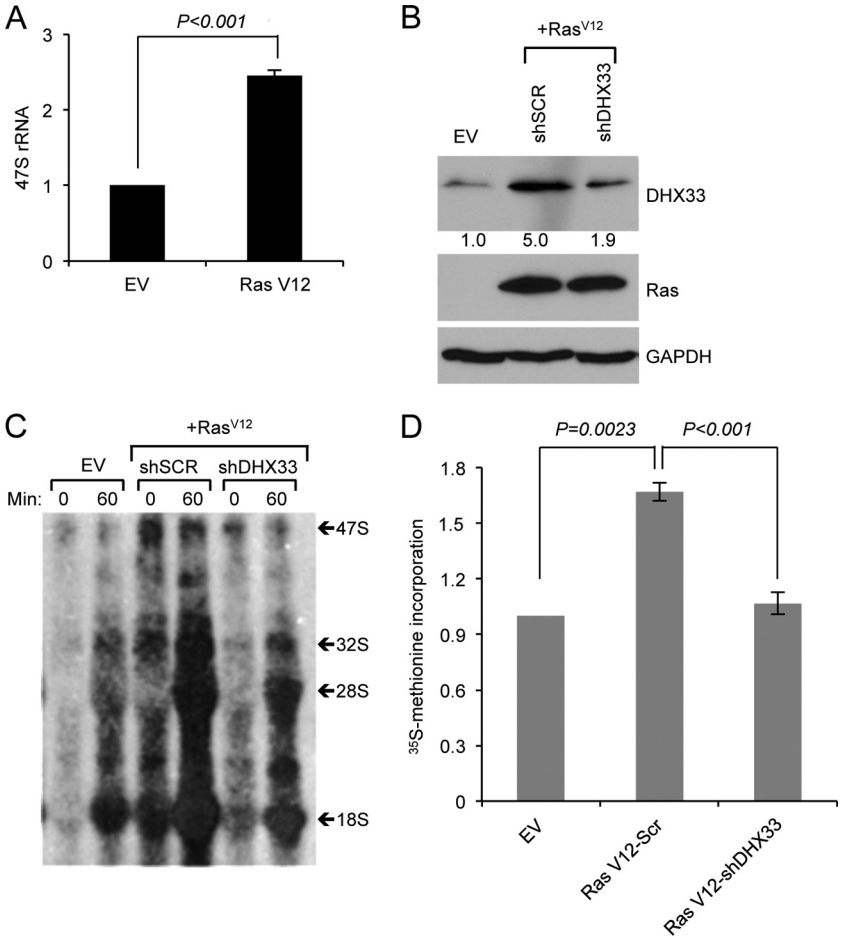

FIG 7 DHX33 protein induction plays a crucial role in Ras^{V12}-enhanced rRNA transcription. (A) *Arf*-null ear fibroblasts from 2-month-old mice were infected with either empty vector or Ras^{V12}-encoding retroviruses. Total RNA was extracted and analyzed by RT-PCR for 47S pre-rRNA levels. Error bars indicate standard deviation from three independent experiments. (B, C, and D) *Arf*-null ear fibroblasts were infected with retroviruses encoding empty vector or Ras^{V12}. At 2 days postinfection, the cells were then infected with lentiviruses encoding shScrambled (SCR) or shRNA-DHX33 for 3 days. Cells were then subjected to Western blot analysis for DHX33 protein levels (B). Equal numbers of cells were pulsed with [^{3}H]uridine and chased at the indicated time points, the total RNA was isolated and separated for rRNA synthesis analysis, and a representative result from three independent experiments is shown (C). The cells were then pulse-labeled with [^{35}S]methionine incorporation and ^{35}S-labeled proteins were measured. Error bars represent the standard deviation from three independent experiments (D). **, $P < 0.001$.

network whose downstream components play multiple roles in cell growth and cell proliferation. In its active, GTP-bound state, Ras is able to activate two major oncogenic signaling cascades: Raf/MEK/ERK and PI3K/AKT pathway (28). Aside from its role in promoting cell proliferation and cell survival, cell invasiveness and enhanced production of angiogenic factors, Ras activation also causes a significant elevation in the production of rRNA and increases in mRNA translation. Ras enhanced ribosome RNA synthesis are due to a variety of contributions from several Ras downstream effectors such as ERK (38–40), cyclin D1 (41, 42), and mTOR (43, 44), all of which can promote RNA Pol I transcription through different mechanisms. However, these enhancements and gains were observed in cells lacking an intact ARF/p53 pathway. The canonical roles of the ARF tumor suppressor reside in its ability to sense activated Ras alleles and prevent downstream cellular processes normally augmented by oncogenic Ras. Thus, it seems that proteins central to these processes must be under the control of both ARF and Ras regulators. Identifying these key players was our focus.

In this report, we identified a new downstream target of Ras, the DHX33 DEAH-box RNA helicase. DHX33 plays as an important role in promoting rRNA synthesis and ribosome biogenesis (30). In cells that maintain an intact *Arf* locus, oncogenic Ras^{V12} overexpression resulted in a significant reduction in DHX33 protein expression without any lowering of DHX33 mRNA. The timing of DHX33 downregulation coincided with the classical induction of ARF expression by oncogenic *Ras^{V12}* alleles. This negative regulation was not observed in cells lacking *p53*, arguing that the attenuation of DHX33 protein expression relied on the canonical ARF/p53 tumor suppressor pathway. Our results support the notion that other than cell cycle regulation, a p53-dependent role of ARF might also reside in inhibiting ribosome biogenesis. The ARF tumor suppressor has been found to inhibit rRNA synthesis (14, 24) through its ability to prevent UBF phosphorylation (24) and by translocating TTF-I, a RNA polymerase I termination factor, from the nucleolus into the nucleus (31). Nonetheless, in the absence of *Arf*, Ras^{V12} was quite capable of dramatically increasing DHX33 protein expression, squarely placing DHX33 in the nexus

Downloaded from http://mcb.asm.org/ on April 16, 2013 by Washington University in St. Louis

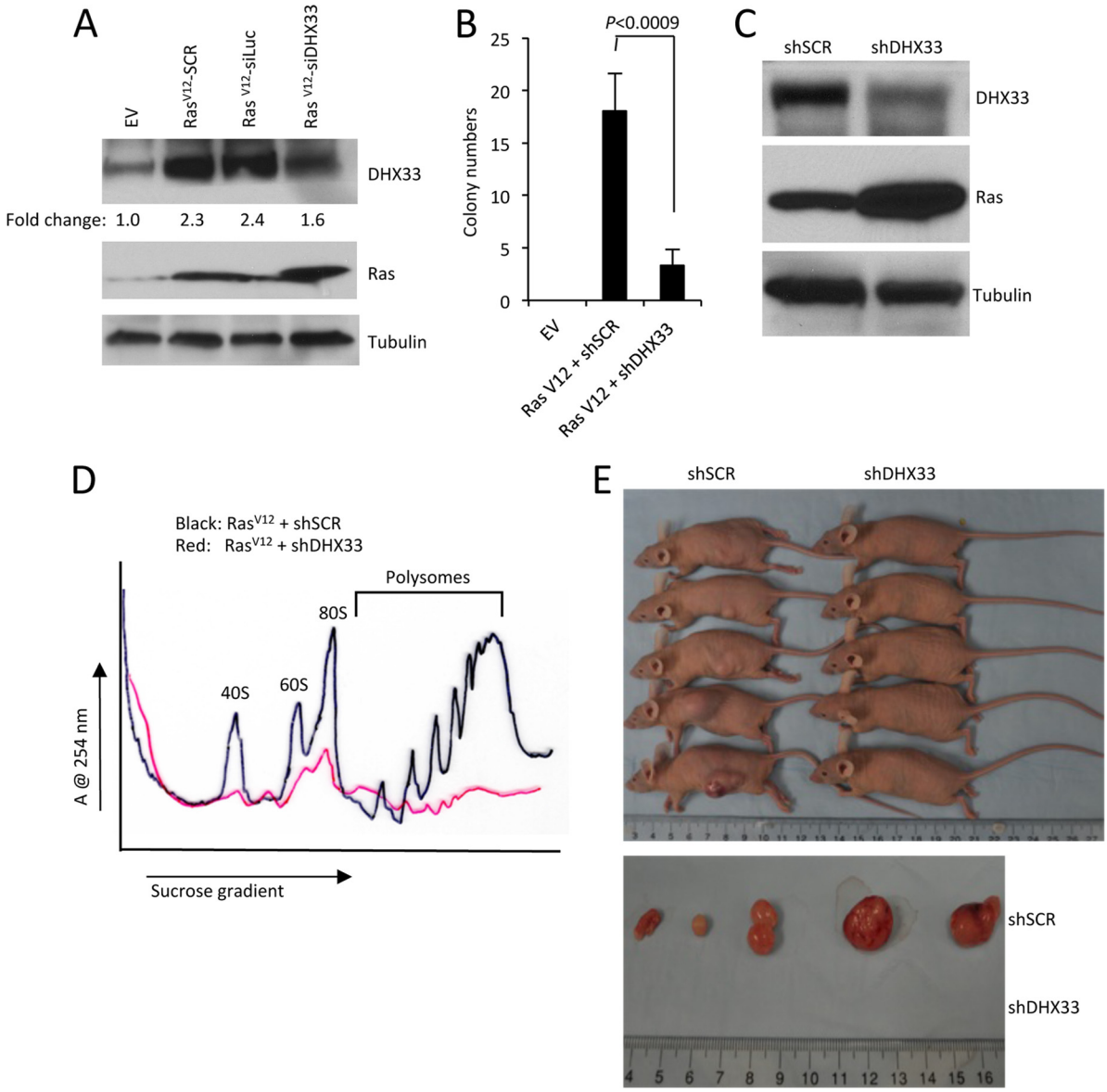

FIG 8 DHX33 induction is required for Ras^{V12}-initiated tumor formation. (A) *Arf*-null ear fibroblasts from 2-month-old mice were infected with retroviruses encoding pBABE-empty vector (EV) or pBABE-Ras^{V12}. Cells were then infected with lentiviruses encoding shScrambled (shSCR), shLuciferase (shLuc), or shDHX33. Whole-cell lysates were extracted and analyzed by Western blotting with Ras, DHX33, and tubulin antibodies. (B) A total of 5×10^3 infected cells were plated onto soft agar 60-mm plates in triplicate to measure anchorage-independent cell growth after 14 days. Quantitation of the colony numbers is presented from three representative fields under ×4 magnification. Error bars represent the standard deviation calculated from three different fields of colonies on triplicate plates. (C) *Arf*-null NIH 3T3 cells were infected with retroviruses encoding Ras^{V12}, followed by infection with lentiviruses encoding shScrambled (shSCR) or shDHX33. Whole-cell lysates were subjected to Western blot analysis with Ras, DHX33, and tubulin antibodies. (D) A total of 3×10^6 infected NIH 3T3 cells were subjected to cytosolic ribosome profiles. (E) The upper panel shows NIH 3T3 cells infected with retroviruses encoding Ras^{V12} that were then infected with shSCR or shDHX33 lentiviruses. A total of 10^6 infected NIH 3T3 cells were injected into the flanks of nude mice. Tumor formation was visualized and photographed after 14 days. For the lower panel, mice were sacrificed at day 14 postinjection, and tumors were excised and photographed.

of ARF and Ras regulation. In contrast to ARF, Ras^{V12} considerably shifted existing DHX33 mRNAs onto translating polysomes. Thus, we have identified a new route through which ARF inhibits rRNA synthesis.

We have provided evidence that elevated expression of DHX33 is critical for Ras^{V12}-induced cellular transformation. Importantly, our experiments utilized shRNAs that target and reduce DHX33 expression back to just above baseline. As such, we are not entirely removing DHX33 from these cells. Reduction of DHX33 in Ras^{V12}-expressing *Arf*-null cells resulted in a return of 47S rRNA and mRNA translation back to levels normally seen in *Arf*-null cells. These cells no longer grow in soft agar and do not form tumors in immunocompromised mice. Much of the focus on ARF tumor biology has been on its ability to respond to oncogenic signals, such as those emanating from Ras^{V12}, to induce a potent p53-dependent cell cycle arrest. Even more recently, a significant amount of interest has also shifted to ARF's ability to directly inhibit ribosome biogenesis independent of p53. Our new find-

Downloaded from http://mcb.asm.org/ on April 16, 2013 by Washington University in St. Louis

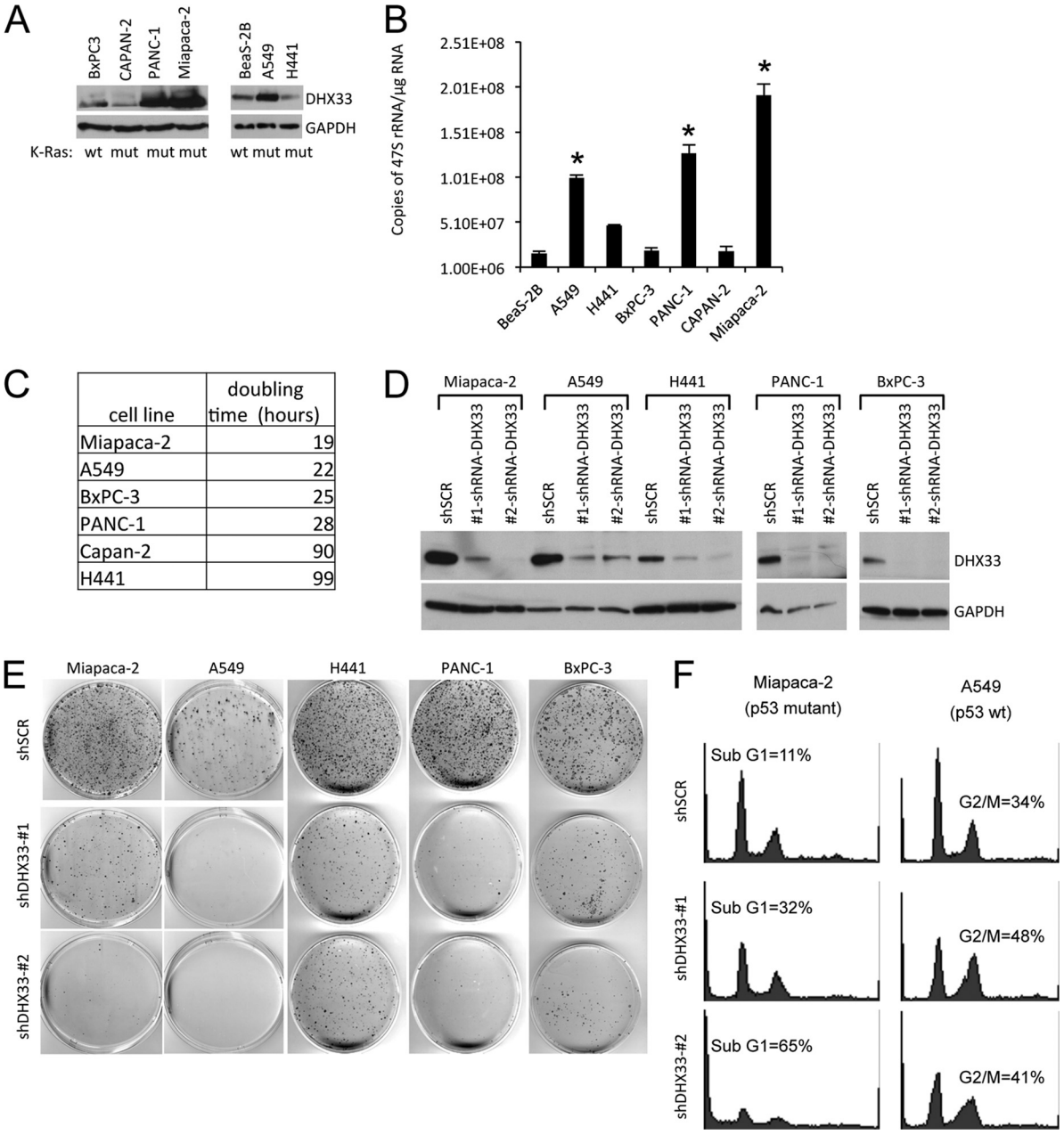

FIG 9 DHX33 is overexpressed in Ras-mutated cancer cell lines and is required for their efficient growth and proliferative properties. (A) A panel of K-Ras mutated or wild-type cancer cell lines (mutation status is shown at the bottom) were screened for total DHX33 protein expression, p14ARF status is also shown at the bottom. (B) 47S rRNA was measured by RT-PCR and normalized to total RNA levels. Error bars represent the standard deviation from three separate experiments. *, $P < 0.001$. (C) A total of 5×10^4 cells were plated onto six-well culture plates. Cell numbers were counted daily and graphed. The doubling time was calculated based on growth curves and is shown in the table. (D) The indicated cell lines were infected with lentiviruses encoding shScrambled (shSCR) or shDHX33. Whole-cell lysates were extracted 4 days postinfection and subjected to Western blot analysis with antibodies recognizing DHX33 and tubulin. (E) shSCR or shDHX33-infected cells (10^4) from indicated cancer cell lines were plated onto 100-mm culture dishes. The cells were fixed 10 or 20 days later with 100% methanol and incubated with Giemsa stain for 1 h. Stained colonies were air dried and photographed. (F) shSCR or shDHX33-infected cells (10^4) from Miapaca-2 and A549 cancer cells were subjected to cell cycle analysis by flow cytometry after propidium iodide staining.

ings herein imply that ARF and Ras are in a constant struggle for downstream target activation/inactivation. Normal cells harboring activated *Ras* alleles in the face of wild-type ARF are unable to gain access to critical downstream targets, such as DHX33, to fully activate critical processes required for tumorigenesis. ARF effectively eliminates these proteins by removing their mRNAs from actively translating polyribosomes. When *Arf* is lost, Ras gains access to these targets, and active translation of them ensues. How ARF might selectively repress mRNA translation remains to be investigated, but our findings with DHX33 are reminiscent of ARF's regulation of VEGFA translation (45).

Enhanced ribosome biogenesis is tightly correlated with enhanced cell proliferation in human cancers. Targeting RNA Pol I transcription has been regarded as a potential treatment for cancer

Downloaded from http://mcb.asm.org/ on April 16, 2013 by Washington University in St. Louis

patients (3). Several drugs, including actinomycin D, cisplatin, 5-fluorouracil, and camptothecin have been shown to inhibit RNA Pol I transcription (46–48). However, this field is still at the early stage and will require more selective targets in order to develop efficient therapeutic drugs that preferentially inhibit tumor growth while sparing normal cells. Recently, selective drugs that target rRNA synthesis have been developed, shedding a more positive light onto our ability to target rRNA synthesis as a way of treating cancers. One of the latest compounds, CX-3543, is a small molecule nucleolus-targeting agent that selectively disrupts nucleolin/rDNA G-quadruplex complexes in the nucleolus (49). CX-3543 inhibited Pol I transcription and induced apoptosis in cancer cells and is currently in phase II clinical trials. Another compound, CX-5461, selectively inhibits Pol I-driven relative to Pol II-driven transcription, DNA replication, and mRNA translation (50). CX-5461 inhibits the initiation stage of rRNA synthesis and induces both senescence and autophagy through a p53-independent process in solid tumor cell lines. Although more work needs to be done in order to develop efficient and more specific drugs to target RNA Pol I transcription as a way for cancer treatment, the validity of the approach itself has proven fruitful.

It seems uncertain whether other consensus targets of both ARF and oncogenic Ras^{V12} exist. However, given the pleiotropic effects of ARF and Ras, identification of other common proteins seems likely. In fact, given the large number of RNA helicases in the DEAD/DEAH-box family, DHX33 may signal the first of many dually regulated helicases. Given our findings that the helicase activity of DHX33 was required for the Ras^{V12}-driven phenotype, generating novel compounds that inhibit its helicase activity seems a viable approach to prevent Ras^{V12}-induced transformation, especially in clinically relevant settings where Ras mutants, and thus aberrant DHX33 expression, drive the disease.

ACKNOWLEDGMENTS

We thank the members of the Weber laboratory for their advice and technical assistance. Lian-Fai Yee provided *Arf*-null ear fibroblasts. The Genome Institute and Children's Discovery Institute at Washington University provided lentiviral RNAi library constructs.

A.J.S. was supported by Komen for the Cure. This study was supported by National Institutes of Health grant CA120436 and by an Era of Hope Scholar Award in Breast Cancer Research (BC007304) to J.D.W.

REFERENCES

1. **Hanahan D, Weinberg RA.** Hallmarks of cancer: the next generation. Cell **144**:646–674.
2. **Luo J, Solimini NL, Elledge SJ.** 2009. Principles of cancer therapy: oncogene and non-oncogene addiction. Cell **136**:823–837.
3. **Drygin D, Rice WG, Grummt I.** The RNA polymerase I transcription machinery: an emerging target for the treatment of cancer. Annu. Rev. Pharmacol. Toxicol. **50**:131–156.
4. **Maggi LB, Jr, Weber JD.** 2005. Nucleolar adaptation in human cancer. Cancer Invest. **23**:599–608.
5. **Montanaro L, Trere D, Derenzini M.** 2008. Nucleolus, ribosomes, and cancer. Am. J. Pathol. **173**:301–310.
6. **White RJ.** 2008. RNA polymerases I and III, non-coding RNAs and cancer. Trends Genet. **24**:622–629.
7. **White RJ.** Transcription by RNA polymerase III: more complex than we thought. Nat. Rev. Genet. **12**:459–463.
8. **Pianese G.** 1896. Beitrag zur Histologie und Aetiologie der Carcinoma Histologische und experimentelle Untersuchungen. Beitr. Pathol. Anat. Allgem. Pathol. **142**:1–193.
9. **Williamson D, Lu YJ, Fang C, Pritchard-Jones K, Shipley J.** 2006. Nascent pre-rRNA overexpression correlates with an adverse prognosis in alveolar rhabdomyosarcoma. Genes Chromosomes Cancer **45**:839–845.
10. **Grummt I.** 2003. Life on a planet of its own: regulation of RNA polymerase I transcription in the nucleolus. Genes Dev. **17**:1691–1702.
11. **Derenzini M, Trere D, Pession A, Govoni M, Sirri V, Chieco P.** 2000. Nucleolar size indicates the rapidity of cell proliferation in cancer tissues. J. Pathol. **191**:181–186.
12. **Derenzini M, Trere D, Pession A, Montanaro L, Sirri V, Ochs RL.** 1998. Nucleolar function and size in cancer cells. Am. J. Pathol. **152**:1291–1297.
13. **Trere D, Ceccarelli C, Montanaro L, Tosti E, Derenzini M.** 2004. Nucleolar size and activity are related to pRb and p53 status in human breast cancer. J. Histochem Cytochem. **52**:1601–1607.
14. **Ayrault O, Andrique L, Fauvin D, Eymin B, Gazzeri S, Seite P.** 2006. Human tumor suppressor p14ARF negatively regulates rRNA transcription and inhibits UBF1 transcription factor phosphorylation. Oncogene **25**:7577–7586.
15. **Learned RM, Learned TK, Haltiner MM, Tjian RT.** 1986. Human rRNA transcription is modulated by the coordinate binding of two factors to an upstream control element. Cell **45**:847–857.
16. **Zhai W, Comai L.** 2000. Repression of RNA polymerase I transcription by the tumor suppressor p53. Mol. Cell. Biol. **20**:5930–5938.
17. **Rubbi CP, Milner J.** 2003. Disruption of the nucleolus mediates stabilization of p53 in response to DNA damage and other stresses. EMBO J. **22**:6068–6077.
18. **Sherr CJ.** 1998. Tumor surveillance via the ARF-p53 pathway. Genes Dev. **12**:2984–2991.
19. **Yuan X, Zhou Y, Casanova E, Chai M, Kiss E, Grone HJ, Schutz G, Grummt I.** 2005. Genetic inactivation of the transcription factor TIF-IA leads to nucleolar disruption, cell cycle arrest, and p53-mediated apoptosis. Mol. Cell **19**:77–87.
20. **Chedin S, Laferte A, Hoang T, Lafontaine DL, Riva M, Carles C.** 2007. Is ribosome synthesis controlled by pol I transcription? Cell Cycle **6**:11–15.
21. **Laferte A, Favry E, Sentenac A, Riva M, Carles C, Chedin S.** 2006. The transcriptional activity of RNA polymerase I is a key determinant for the level of all ribosome components. Genes Dev. **20**:2030–2040.
22. **Palmero I, Pantoja C, Serrano M.** 1998. $p19^{ARF}$ links the tumour suppressor p53 to Ras. Nature **395**:125–126.
23. **Fernandez-Medarde A, Santos E.** Ras in cancer and developmental diseases. Genes Cancer **2**:344–358.
24. **Ayrault O, Andrique L, Larsen CJ, Seite P.** 2004. Human Arf tumor suppressor specifically interacts with chromatin containing the promoter of rRNA genes. Oncogene **23**:8097–8104.
25. **Downward J.** 2003. Targeting RAS signalling pathways in cancer therapy. Nat. Rev. Cancer **3**:11–22.
26. **Grandori C, Gomez-Roman N, Felton-Edkins ZA, Ngouenet C, Galloway DA, Eisenman RN, White RJ.** 2005. c-Myc binds to human ribosomal DNA and stimulates transcription of rRNA genes by RNA polymerase I. Nat. Cell Biol. **7**:311–318.
27. **Grewal SS, Li L, Orian A, Eisenman RN, Edgar BA.** 2005. Myc-dependent regulation of rRNA synthesis during *Drosophila* development. Nat. Cell Biol. **7**:295–302.
28. **Shields JM, Pruitt K, McFall A, Shaub A, Der CJ.** 2000. Understanding Ras: 'it ain't over 'til it's over'. Trends Cell Biol. **10**:147–154.
29. **Zhang C, Comai L, Johnson DL.** 2005. PTEN represses RNA Polymerase I transcription by disrupting the SL1 complex. Mol. Cell. Biol. **25**:6899–6911.
30. **Zhang Y, Forys JT, Miceli AP, Gwinn AS, Weber JD.** 2011. Identification of DHX33 as a mediator of rRNA synthesis and cell growth. Mol. Cell. Biol. **31**:4676–4691.
31. **Lessard F, Morin F, Ivanchuk S, Langlois F, Stefanovsky V, Rutka J, Moss T.** The ARF tumor suppressor controls ribosome biogenesis by regulating the RNA polymerase I transcription factor TTF-I. Mol. Cell **38**:539–550.
32. **Weber JD, Jeffers JR, Rehg JE, Randle DH, Lozano G, Roussel MF, Sherr CJ, Zambetti GP.** 2000. p53-independent functions of the $p19^{ARF}$ tumor suppressor. Genes Dev. **14**:2358–2365.
33. **Itahana K, Bhat KP, Jin A, Itahana Y, Hawke D, Kobayashi R, Zhang Y.** 2003. Tumor suppressor ARF degrades B23, a nucleolar protein involved in ribosome biogenesis and cell proliferation. Mol. Cell **12**:1151–1164.
34. **Zhang Y, Xiong Y, Yarbrough WG.** 1998. ARF promotes MDM2 degradation and stabilizes p53: ARF-INK4a locus deletion impairs both the Rb and p53 tumor suppression pathways. Cell **92**:725–734.
35. **Basu TN, Gutmann DH, Fletcher JA, Glover TW, Collins FS, Downward J.** 1992. Aberrant regulation of ras proteins in malignant tumour cells from type 1 neurofibromatosis patients. Nature **356**:713–715.

Downloaded from http://mcb.asm.org/ on April 16, 2013 by Washington University in St. Louis

36. **Dasgupta B, Yi Y, Chen DY, Weber JD, Gutmann DH.** 2005. Proteomic analysis reveals hyperactivation of the mammalian target of rapamycin pathway in neurofibromatosis 1-associated human and mouse brain tumors. Cancer research. **65**:2755–2760.
37. **Johannessen CM, Reczek EE, James MF, Brems H, Legius E, Cichowski K.** 2005. The NF1 tumor suppressor critically regulates TSC2 and mTOR. Proc. Natl. Acad. Sci. U. S. A. **102**:8573–8578.
38. **Stefanovsky V, Langlois F, Gagnon-Kugler T, Rothblum LI, Moss T.** 2006. Growth factor signaling regulates elongation of RNA polymerase I transcription in mammals via UBF phosphorylation and r-chromatin remodeling. Mol. Cell **21**:629–639.
39. **Stefanovsky VY, Pelletier G, Hannan R, Gagnon-Kugler T, Rothblum LI, Moss T.** 2001. An immediate response of ribosomal transcription to growth factor stimulation in mammals is mediated by ERK phosphorylation of UBF. Mol. Cell **8**:1063–1073.
40. **Zhao J, Yuan X, Frodin M, Grummt I.** 2003. ERK-dependent phosphorylation of the transcription initiation factor TIF-IA is required for RNA polymerase I transcription and cell growth. Mol. Cell **11**:405–413.
41. **Voit R, Grummt I.** 2001. Phosphorylation of UBF at serine 388 is required for interaction with RNA polymerase I and activation of rDNA transcription. Proc. Natl. Acad. Sci. U. S. A. **98**:13631–13636.
42. **Voit R, Hoffmann M, Grummt I.** 1999. Phosphorylation by G1-specific cdk-cyclin complexes activates the nucleolar transcription factor UBF. EMBO J. **18**:1891–1899.
43. **Hannan KM, Brandenburger Y, Jenkins A, Sharkey K, Cavanaugh A, Rothblum L, Moss T, Poortinga G, McArthur GA, Pearson RB, Hannan RD.** 2003. mTOR-dependent regulation of ribosomal gene transcription requires S6K1 and is mediated by phosphorylation of the carboxy-terminal activation domain of the nucleolar transcription factor UBF. Mol. Cell. Biol. **23**:8862–8877.
44. **Mayer C, Zhao J, Yuan X, Grummt I.** 2004. mTOR-dependent activation of the transcription factor TIF-IA links rRNA synthesis to nutrient availability. Genes Dev. **18**:423–434.
45. **Kawagishi H, Nakamura H, Maruyama M, Mizutani S, Sugimoto K, Takagi M, Sugimoto M.** ARF suppresses tumor angiogenesis through translational control of VEGFA mRNA. Cancer Res. **70**:4749–4758.
46. **Ghoshal K, Jacob ST.** 1997. An alternative molecular mechanism of action of 5-fluorouracil, a potent anticancer drug. Biochem. Pharmacol. **53**:1569–1575.
47. **Jordan P, Carmo-Fonseca M.** 1998. Cisplatin inhibits synthesis of rRNA in vivo. Nucleic Acids Res. **26**:2831–2836.
48. **Pondarre C, Strumberg D, Fujimori A, Torres-Leon R, Pommier Y.** 1997. In vivo sequencing of camptothecin-induced topoisomerase I cleavage sites in human colon carcinoma cells. Nucleic Acids Res. **25**:4111–4116.
49. **Drygin D, Siddiqui-Jain A, O'Brien S, Schwaebe M, Lin A, Bliesath J, Ho CB, Proffitt C, Trent K, Whitten JP, Lim JK, Von Hoff D, Anderes K, Rice WG.** 2009. Anticancer activity of CX-3543: a direct inhibitor of rRNA biogenesis. Cancer Res. **69**:7653–7661.
50. **Drygin D, Lin A, Bliesath J, Ho CB, O'Brien SE, Proffitt C, Omori M, Haddach M, Schwaebe MK, Siddiqui-Jain A, Streiner N, Quin JE, Sanij E, Bywater MJ, Hannan RD, Ryckman D, Anderes K, Rice WG.** Targeting RNA polymerase I with an oral small molecule CX-5461 inhibits rRNA synthesis and solid tumor growth. Cancer Res. **71**:1418–1430.

Downloaded from http://mcb.asm.org/ on April 16, 2013 by Washington University in St. Louis